β_1-adrenoceptor blockade treatment of right ventricular dysfunction caused by pulmonary hypertension

Ewan Douglas Fowler BSc, MRes

Submitted in accordance with the requirements for the degree of
Doctor of Philosophy

University of Leeds
Faculty of Biological Sciences
School of Biomedical Sciences
Multidisciplinary Cardiovascular Research Centre

October, 2015

The candidate confirms that the work submitted is his/her own, except where work which has formed part of jointly authored publications has been included. The contribution of the candidate and the other authors to this work has been explicitly indicated below. The candidate confirms that appropriate credit has been given within the thesis where reference has been made to the work of others.

Acknowledgements

I am most grateful to my supervisor, Prof Ed White, with whom I have thoroughly enjoyed working during my 4 years at Leeds. I am incredibly appreciative of your excellent guidance and willingness to allowing me the academic freedom to pursue my own interests. I'm extremely grateful for the opportunities you afforded me including Amsterdam, New Zealand and the US.

Thanks to my co-supervisor Prof Derek Steele for your insight and opinions on my results and hypotheses over the years. Dr Sarah Calaghan who was so welcoming when I arrived at Leeds, I hope we can work together on more projects in the future. Prof John Colyer for invaluable scientific discussions and his opinions on my work, and also great conversations at the pub. Dr Rachel Stones made a vital contribution to this project with your expertise in molecular biology. Dr Mark Drinkhill who performed all the *in vivo* pressure-volume measurements, including many that didn't make it into this thesis. Prof Stuart Egginton and Dr David Hauton for their role in developing and implementing the oxygen modelling software, and in particular to Dr Hauton for discussions on this topic and histology advice. Thanks to Prof Chris Peers and Dr John Boyle for allowing me time on the oxygraph recorders and for discussion of the results.

Thanks to Prof Ger Stienen for allowing me to spend six weeks in his lab in Amsterdam performing the stretch experiments and to Dr Rob Wüst for helping organise my visit (and for letting me crash on his sofa when the money ran out!). I am particularly grateful to Dr Michiel Helmes who taught me the difficult cell stretching technique and also for excellent scientific discussions. 'Dank je wel!' to Vasco Sequeira and everyone at the VU who made me feel so welcome and introduced me to kroketten, bitterballen and Brouwerij 't IJ.

I'm also incredibly privileged to have worked with such great friends as David, Ruth, Emma, Sabine and Matt. David you have been most influential in shaping my outlook on science and beyond through our often heated discussions. Ruth you've kept me balanced on a knife edge between athleticism and full blown beer belly through our early morning bike rides, afternoons of coffee and cake, and evenings in the Faversham – I dread to think what will happen when I leave! Emma, Sie gewesen sind eine Freude, neben sitzen und ich wünschen könnte nicht für eine besser Nachbarn! Sabine it's been great to have someone to go to UNOD and Subdub with – next time it

will be OBF in France! Matt you taught me loads in the lab and were always up for a much needed pint after work in the early days – sorry to be leaving just as you return to Leeds!

Most importantly I thank my family: Mum, Dad, Lindsay, Lauren and Laura. Mum and Dad for their unwavering support and encouragement throughout my many years of higher education. Linny and Lauren for helping me keep one foot in Glasgow and not cocooned away as I'd no doubt otherwise be. And finally Laura, who knows better than anyone exactly what the last 4 years have involved and what this means to me – thank you all for being so supportive.

Author publications

Research papers

Work directly attributable to the author and presented in this thesis has featured in joint-author publications which are listed below. An echocardiographic estimate of ventricle wall stress calculated using data in Chapter 3 was included in Benoist *et al*. (2014). Passive ventricle stretch in isolated hearts was included in Sequeira *et al*. (2015) and is included as Appendix B. I contributed to Natali *et al*. (2015) in part by helping with and maintaining the monocrotaline heart failure model. Figures from Chapter 6 were included in Fowler et al. (2015) as Figures 3&8. Co-authors contributed to these publications by performing and planning experiments and by revising manuscripts.

Benoist D, Stones R, Benson AP, **Fowler ED**, Drinkhill MJ, Hardy MEL, Saint DA, Cazorla O, Bernus O & White E. (2014) Systems approach to the study of stretch and arrhythmias in right ventricular failure induced in rats by monocrotaline. *Progress in Biophysics and Molecular Biology*, **115**, 162-172.

Sequeira V, Najafi A, McConnell M, **Fowler ED**, Bollen IAE, Wüst RCI, dos Remedios C, Helmes M, White E, Stienen GJM, Tardiff J, Kuster DWD & van der Velden J. (2015) Synergistic role of ADP and Ca^{2+} in diastolic myocardial stiffness. *Journal of Physiology*, **593**(17), 3899-916.

Natali, AJ, **Fowler ED**, Calaghan SC & White E. (2015) Voluntary exercise delays heart failure onset in rats with pulmonary artery hypertension. *American Journal of Physiology – Heart and Circulatory Physiology,* **309,** 421-4.

Fowler ED, Benoist D, Drinkhill MJ, Stones R, Helmes M, Wüst RCI, Stienen GJM, Steele DS & White E. (2015). Decreased creatine kinase is linked to diastolic dysfunction in rats with right heart failure induced by pulmonary artery hypertension. *Journal of Molecular and Cellular Cardiology* **86,** 1-8.

Published abstracts

Fowler ED, Stones R, Steele DS & White E. (2013). Reduced expression of creatine kinase and diastolic dysfunction in failing rat ventricular myocytes *37th Congress of IUPS (Birmingham, UK)* **Proc 37th IUPS,** PCB057.

Norman R, Hardy M, **Fowler ED**, White E & Calaghan S. (2013). Remodelling of the caveolar domain in right ventricular failure in rats. *37th Congress of IUPS (Birmingham, UK)* **Proc 37th IUPS,** PCB044.

Fowler ED, Stones R, Benoist D, Drinkhill MJ & White E. (2014). Reduced expression of creatine kinase in rat failing right ventricle causes diastolic dysfunction in ventricular myocytes. *J Muscle Res Cell Motil* **35,** 90.

Fowler ED, Drinkhill M, Steele D & White E. (2014). Passive stiffness in the failing right ventricle: contribution of collagen and creatine kinase. *Proc Physiol Soc* **31**

Fowler ED, Drinkhill MJ, Wust RC, Helmes M, Stienen GJM, Steele DS & White E. (2015). Workloop Contractions in Isolated Cardiac Myocytes Reflect in vivo Pressure-Volume Dysfunction in Rat Right Heart Failure. *Biophysical journal* **108,** 294a.

Fowler ED, Norman R, Steer E, Pervolaraki E, Stones R, Drinkhill M, Calaghan SC, Steele DS & White E. (2015). The β_1 adrenergic receptor blocker metoprolol improves survival and partially restores Ca^{2+} handling abnormalities in rat pulmonary artery hypertension. *Proc Physiol Soc* **34,** C03.

Norman R, **Fowler ED**, Stones R, White E & Calaghan S. (2015). Reverse-remodelling of cardiac β-adrenergic responsiveness in metoprolol-treated pulmonary hypertensive rats. *Proc Physiol Soc* **34,** PC019.

Communications

Oral

Reduced expression of creatine kinase in rat failing right ventricle causes diastolic dysfunction in ventricular myocytes. May 2013. *The 42nd European Muscle Conference*, Amsterdam, The Netherlands.

Diastolic dysfunction in rat pulmonary arterial hypertension studied at the cellular, whole organ and *in vivo* level. September 2014. *Early Career Research Conference in Cardiovascular and Diabetes Research*. Leeds, UK.

Workloop contractions in isolated cardiac myocytes reflect *in vivo* pressure-volume dysfunction in rat right heart failure. November 2014. *Alternative Muscle Club*, Leeds, UK. **Oral communication prize**

β_1-adrenergic receptor block improves survival and Ca^{2+} handling in right ventricle failure. March 2015. *Multidisciplinary Cardiovascular Research Centre Annual Retreat*, Derwent water, UK.

The β_1 adrenergic receptor blocker metoprolol improves survival and partially rescues Ca^{2+} handling abnormalities in right ventricle failure. April 2015. *Northern Cardiovascular Research Group Meeting*, Newcastle, UK.

The β_1 adrenergic receptor blocker metoprolol improves survival and partially restores Ca^{2+} handling abnormalities in rat pulmonary artery hypertension. July 2015. *The Physiological Society Annual Meeting*, Cardiff, UK. **Oral communication prize**

Improved survival and Ca^{2+} handling in rat pulmonary arterial hypertension following β_1 adrenergic blockade. September 2015. *Alternative Muscle Club*, Canterbury, UK.

Posters

The 37th Congress of IUPS, Birmingham, UK. July 2013.
Multidisciplinary Cardiovascular Research Centre Retreat. Leeds, UK. March 2014.
Northern Cardiovascular Research Group meeting, Manchester, UK. April 2014.
The Physiological Society Annual Meeting, London, UK. July 2014.
The Biophysical Society Annual Meeting, Baltimore, MA. February 2015.

Abstract

Failure of the right ventricle (or ventricular) (RV) is the leading cause of death in patients with pulmonary arterial hypertension (PAH), however no treatments specifically target the failing RV. β_1-adrenoceptor blockers (β-blockers, BB) reduce mortality in left heart failure but current clinical guidelines caution against their use in PAH. Recent studies suggest β-blockers may be beneficial in PAH however the mechanisms remain unknown. The present study sought to establish whether the β_1-blocker metoprolol (10 mg/kg/day) improved survival and function in a rat model of PAH induced by monocrotaline (60 mg/kg, MCT), and to elucidate the mechanisms responsible.

Daily metoprolol or placebo was administered 15 days post-monocrotaline injection. PAH resulted in severe RV hypertrophy, dysfunction and heart failure by median day 23 in placebo treated rats (FAIL), whereas metoprolol extended the median survival to day 31 (MCT+BB). RV function measured by echocardiography and catheterisation was severely impaired in FAIL, but was partially restored in MCT+BB on day 23±1. Metoprolol appeared to act primarily on the myocardium and not the vasculature.

Contractile abnormalities in isolated FAIL RV cardiomyocytes included increased cell volume, negative force and Ca^{2+} transient response to faster pacing, increased stiffness to stretch and shorter resting sarcomere length. Reduced creatine kinase activity was found in FAIL; creatine kinase inhibition reproduced characteristics of FAIL in healthy cells, whereas exogeneous creatine kinase reversed the shorter sarcomere length in FAIL cells. Contractile and Ca^{2+} handling properties of MCT+BB cells were partially or fully restored relative to healthy cells. Capillary density was reduced in FAIL and partially restored in MCT+BB; computer modelling indicated fewer areas of hypoxia in MCT+BB RV. Assessment of FAIL RV mitochondria revealed reduced creatine-coupled respiration but no other detectable defects.

Metoprolol improved survival, Ca^{2+}-handling, contractility, oxygen delivery and diastolic properties of PAH rats. β-blockers represent a novel myocardium-specific therapy to target the failing RV in PAH.

Contents

Figures

Chapter 1

Chapter 2

Chapter 3

Chapter 4

Chapter 5

Chapter 6

Chapter 7

Appendix A

Appendix B

Tables

Main Abbreviations and agents

2,3-BDM	2,3-butanedione monoxime
AC	adenylyl cyclase
ACR	acceptor control ratio
ADP	adenosine diphosphate
AKAP	A kinase anchoring protein
AMP	adenosine monophosphate
ANOVA	analysis of variance
ANT	adenine nucleotide translocase
AP	action potential
AR	adrenoceptor
Asc	ascorbate
atenolol	β_1 adrenoceptor-specific antagonist
ATP	adenosine triphosphate
AV	atrioventricular
BAPTA	1,2-bis(o-aminophenoxy)ethane-N,N,N',N'-tetraacetic acid, fast calcium buffer
BIN-1	bridging integrator-1 (amphyphysin 2)
bisoprolol	β_1 adrenoceptor-specific antagonist
BLEB	Tyrode's solution plus blebbistatin
BMPRII	bone morphogenetic protein receptor type II
cAMP	cyclic adenosine monophosphate
carvedilol	non-selective $\alpha_1/\beta_1/\beta_2$ adrenoceptor antagonist
CD	capillary density
CF	capillary to fibre ratio
CI	mitochondrial respiratory complex I
CICR	calcium-induced calcium release
CII	mitochondrial respiratory complex II
CIII	mitochondrial respiratory complex III
CIV	mitochondrial respiratory complex IV
CK	creatine kinase
CK-B	brain isoform creatine kinase
CK-M	muscle isoform creatine kinase
CK-mt	mitochondrial creatine kinase

CON	control (saline treated rats)
COPD	chronic obstructive pulmonary disease
CoQ	oxidized coenzyme Q
$CoQH_2$	reduced coenzyme Q
Cr	creatine
CRU	calcium release unit
CS	citrate synthase
CV	mitochondrial respiratory complex V
DAD	delayed afterdepolarization
di-8-ANEPPS	voltage-sensitive lipophilic membrane dye
DNFB	1-fluoro-2,4-dinitrobenzene
Ea	arterial elastance
EC	excitation-contraction
ECM	extracellular matrix
EDFLR	end-diastolic force-length relationship
EDPVR	end-diastolic pressure-volume relationship
EGTA	ethyleneglycol bis(β-aminoethyl ether) N,N,N,N'-tetraacetic acid, slow calcium buffer
Em	membrane potential
ESFLR	end-systolic force-length relationship
ESPVR	end-systolic pressure-volume relationship
ESPVR/Ea	a measure of coupling between ventricle contractility and arterial compliance
ET-1	endothelin-1
ETS	electron transport system
FAD^+	oxidized flavin adenine dinucleotide
$FADH_2$	reduced flavin adenine dinucleotide
FAIL	monocrotaline-treated rats at the point of manifest heart failure
FAIL+BB	monocrotaline and metoprolol treated rats at the point of manifest heart failure
FCCP	Carbonyl cyanide-4-(trifluoromethoxy)phenylhydrazone
FCR	flux control ratio
FDA	United States Food and Drug Administration
FFT	fast-Fourier transform
Fluo-4-AM	cell-permeant non-ratiometric fluorescent calcium indicator
FPGA	field-programmable gate array

FRET	Förster resonance energy transfer
FSG	Frank-Starling gain index
Fura-4F-AM	cell-permeant ratiometric fluorescent calcium indicator
GDP	Guanosine diphosphate
GPCR	G-protein coupled receptor
GRK	G-protein coupled receptor kinases
GTP	Guanosine triphosphate
HEPES	4-(2-hydroxyethyl)-1-piperazineethanesulfonic acid, pH buffer
HIF-1α	hypoxia-inducible factor 1α
HW:BW	heart weight to body weight ratio
ICa	L-type calcium current
IFM	interfibrillar mitochondria
JP2	junctophillin 2
$K_{CAFFEINE}$	rate constant of calcium removal via NCX and slow pathways
KmADP	apparent Michaelis-Menten constant for ADP
K_{SERCA}	rate constant of calcium removal via SERCA
$K_{SYSTOLIC}$	rate constant of systolic calcium removal
LEAK	non-phosphorylating leak respiration
Liver:BW	liver to body weight ratio
Lung:BW	lung to body weight ratio
LV	left ventricle
LVSCI	left ventricle systolic circularity index
MCT	monocrotaline
MCT+BB	monocrotaline and metoprolol treated rats taken on the median survival of FAIL rats
metoprolol	β_1 adrenoceptor-specific antagonist
MHC	myosin heavy chain
MI	myocardial infarction
MIM	mitochondrial inner membrane
MiR05	mitochondrial respiration medium 05
MMP	matrix metalloproteinase
MOM	mitochondrial outer membrane
mRNA	messenger ribonucleic acid
MyoTak	collagen-based biological glue
NAD^+	oxidized nicotinamide adenine dinucleotide
NADH	reduced nicotinamide adenine dinucleotide

NCX	sodium-calcium exchanger
nebivolol	β_1 adrenoceptor-specific antagonist with β_2/β_3 agonist properties
NMR	nuclear magnetic resonance
NO	nitric oxide
NOS	nitric oxide synthase
NYHA	New York Heart Association
OCT	optimal cutting temperature compound
OXPHOS	oxidative phosphorylation
PA	pulmonary artery
PAB	pulmonary artery banding
PAD	pulmonary artery diameter
PAH	pulmonary arterial hypertension
PBS	phosphate-buffered saline
PCr	phosphocreatine
PCWP	pulmonary capillary wedge pressure
PDE	phosophodiesterase
PGC-1α	Peroxisome proliferator-activated receptor gamma coactivator 1-alpha
PKA	protein kinase A
PKC	protein kinase C
PKG	protein kinase G
PLB	phospholamban
PMCA	plasma membrane Ca^{2+} ATPase
propranolol	non-selective β_1/β_2 adrenoceptor antagonist
PSAX	parasternal short-axis view
PVR	pulmonary vascular resistance
ROS	reactive oxygen species
ROX	residual oxygen consumption
RV	right ventricle
RV:LV+S	ratio of RV weight to LV+S weight (Fulton's Index of RV hypertrophy)
SAN	sinoatrial node
SERCA	sarco(endo)plasmic reticulum ATPase
sGC	soluble guanylyl cyclase
SL	sarcomere length
SR	sarco(endo)plasmic reticulum

SSM	subsarcolemma mitochondria
SUIT	substrate-uncoupler-inhibitor titration protocol
SV	stroke volume
TAPSE	tricuspid annular plane excursion
TCA	tri-carboxylic acid cycle
TMPD	N,N,N',N'-Tetramethyl-p-phenylenediamine dihydrochloride
TNF-α	tumour necrosis factor alpha
t-tubule	transverse tubule
TYR	Tyrode’s solution
VDAC	voltage-dependent anion channel
VEGF	vascular endothelial growth factor
VTI	velocity-time integral
XSA	cross-sectional area

Chapter 1 General introduction

1.1 General introduction

The most recent statistics from the British Heart Foundation reveal diseases of the cardiovascular system affected 1.6 million people in the UK in 2012/13, at an estimated cost to the NHS in excess of £8.5 billion per annum (Bhatnagar *et al.*, 2015). Of these patients, 3.9% were afflicted by diseases of the pulmonary circulation or right heart, such as pulmonary arterial hypertension (PAH), chronic obstructive pulmonary disease and pulmonary thromboembolism, often leading to right heart failure. Heart failure can be defined as the pathological inability of the heart to supply the body's demand for oxygen, or to do so at the expense of increased filling pressure. Patients are usually graded according to their functional capacity using the New York Heart Association Functional Classification, which defines heart failure along a spectrum from no limitation to physical activity, to severe symptoms of heart failure even at rest which are exacerbated by even light activity. The impairment of mobility has a profoundly negative impact on quality of life and without early diagnosis and treatment early mortality is inevitable (McKee *et al.*, 1971).

Progress in diagnosing and treating heart failure has benefitted patient survival and quality of life immensely, however the majority of new treatments have been for left heart failure and comparatively little is known regarding the specific nature of right ventricular (RV) failure. RV failure is the leading cause of death in patients with PAH (Delcroix & Naeije, 2010) and poor RV function is an important risk factor in left heart failure (Kjaergaard *et al.*, 2007; Szwejkowski *et al.*, 2012). Despite the clinical importance no treatments are currently available which specifically target the failing RV, leading some to propose trialling existing drugs used in left heart failure as 'novel' treatments for RV failure (Handoko *et al.*, 2010). One such class of drug gaining interest are β-adrenoceptor blockers (β-blockers) which have been a mainstay of therapy in left heart failure for several decades as they offer long-term benefits to morbidity and mortality (Waagstein *et al.*, 1989; Waagstein *et al.*, 1993; Poole-Wilson *et al.*, 2003), but are currently contraindicated in PAH (Provencher *et al.*, 2006b; Galiè *et al.*, 2015b). Recent clinical (Thenappan *et al.*, 2014; Bandyopadhyay *et al.*, 2015) and preclinical studies (Bogaard *et al.*, 2010; de Man *et al.*, 2011; Perros *et al.*, 2015) have found no deleterious effects of β-blockers in PAH and actually reported improvements in survival and RV function, although the mechanisms responsible are still unclear. Therefore the purpose of this study was first to establish whether β-

blockers improved survival and RV function in a rat model of PAH, and secondly to identify the mechanisms responsible for RV dysfunction and subsequent rescue with β-blockers.

1.2 Structure and function of the heart

1.2.1 Anatomy

The heart is located in the chest immediately posterior to the sternum. The free end of the heart points down and towards the left whereas the base containing the great arteries and veins is at the top at the level of the third costal cartilage. The superficial anatomy of the heart consists of two thin-walled atria separated by an interatrial septum sitting on top of two thicker walled muscular ventricles (Martini, 2006). The atria and ventricles are divided into a right and left side and the 4 chambers of the heart are enclosed by serous membranes which adhere to the epicardial surface of the heart and secrete pericardial fluid which acts as a lubricant reducing friction during contraction. These membranes and fluids are enclosed by the fibrous pericardium which stabilizes and constrains the heart.

The function of the right and left atria is broadly similar, in that they both receive blood returning from the systemic and pulmonary circulation, respectively, and deliver it to the ventricles. They are thin walled allowing them to cope with sudden changes in venous return. The superior and inferior vena cava supply deoxygenated blood from the systemic circulation to the right atrium whereas two right and two left pulmonary veins supply oxygenated blood returning from the pulmonary circulation to the left atrium. The right atrium is further supplied by the cardiac veins which return blood via the coronary sinus inferior to the superior vena cava. The right and left atrium are divided from the ventricles by the fibrous tricuspid and mitral valves, respectively.

The ventricles are more muscular than the atria and the LV is approximately 6 times the mass of the RV (Lorenz *et al.*, 1999). The shortening and thickening of muscle fibres in the walls of the ventricles reduces the chamber volume forcing blood out during ejection.

1.2.2 Left ventricle and systemic circulation

The geometry of the LV is that of an ellipsoidal thick walled chamber. LV diastolic pressure is typically around 8 mmHg and rises to around 130 mmHg in healthy

individuals (Sengupta *et al.*, 2008). Two thick papillary muscles anchor the chordae tendinae to the two flaps of the mitral valve which prevents backflow of blood into the atrium during systole.

Ventricular myocytes in the LV are predominantly arranged parallel to the surrounding cells forming fibres which arrange into a helix with a prevailing orientation which can be described in terms of its angle. In the LV the fibre angle changes counter clockwise from around -60° in the subepicardium, to circumferential in the midmyocardium, to +90° in the subendocardium (Jiang *et al.*, 2004). When the heart contracts during systole the apex is pulled towards the base while simultaneously sheets of fibres slide past each other in a 'wringing' motion due to muscle fibre orientation which thickens the ventricle wall reducing the chamber lumen further and efficiently ejecting blood (Hales *et al.*, 2012).

The systemic circulation is a high resistance circuit (around 1100 dyne.s.cm^{-5}) with typical systolic and diastolic pressures around 120 mmHg and 80 mmHg, respectively (Stamler *et al.*, 1994). These pressures are necessary to allow blood to be delivered against gravity and to the most distal parts of the body.

1.2.3 Right ventricle and pulmonary circulation

The RV pumps blood through the short and normally low resistance pulmonary circulation (around 50 dyne.s.cm^{-5}) which is the site of gas exchange (Stamler *et al.*, 1994). The RV can be described anatomically in terms of its inlet through the tricuspid valve with its associated chordae tendinae and three papillary muscles, the highly trabeculated RV free wall, and the smooth infundibulum of the outflow tract region. Viewed in cross section the RV is a crescent shaped thin walled chamber contiguous with the interventricular septum at its anterior and posterior aspects. The interventricular septum normally bulges convex into the RV chamber reflecting the transseptal pressure gradient (Portman *et al.*, 1987). A longitudinal section through the 4 chambers reveals the RV to be triangular with papillary muscles attaching to the chordae tendinae ready to contract and resist retrograde flow during RV contraction. The pressure required to perfuse the pulmonary circulation is much lower than the systemic circulation and the RV has approximately one sixth of the muscle mass but a larger end diastolic volume than the LV (75 vs 66 mL per body surface area (m^2) in humans), however as the two chambers are connected in series the stroke volume is generally equal (Lorenz *et al.*, 1999). The systolic RV pressures in healthy individuals

is typically around 25 mmHg whereas diastolic pressure is around 4 mmHg (Chemla *et al.*, 2002).

RV contraction begins with the papillary muscles followed by the inflow region and ends with contraction of the infundibulum which produces a sustained ejection of blood even as RV pressure is rapidly falling, possibly due to the momentum of blood and the low pulmonary artery (PA) diastolic pressure (Dell'Italia, 1991). Contraction occurs predominantly through longitudinal shortening and movement of the tricuspid annulus relative to the apex of the heart, with comparatively less concentric movement of the RV free wall compared to the LV. Ejection is further assisted by the LV pulling on the RV at the points of attachment to the interventricular septum (Starr *et al.*, 1943).

Under normal circumstances the RV ejects blood into a highly compliant and distensible pulmonary arterial system. Pulmonary artery systolic and diastolic blood pressures are typically around 18-25 and 8-12 mmHg respectively, though these can transiently rise for instance at the onset of exercise before additional vessels are recruited by vasodilation.

1.2.3.1 Examining cardiac function *in vivo*

Echocardiography and ventricular pressure-volume measurements using conductance catheters are two major techniques used in the characterisation of *in vivo* cardiac function.

Echocardiography

Echocardiography is a widely used tool to examine cardiac function *in vivo* as it is non-invasive and carries minimal risk, reveals a great deal of information which can be extracted fairly rapidly, and is low cost so can be repeatedly performed. Consequently it is an ideal technique for monitoring the progression of heart failure and the efficacy of treatments allowing interventions to be adjusted if necessary.

In echocardiography an ultrasound signal is generated by passing an alternating current through piezoelectric crystals in the head of a transceiver which deform depending on the polarity (Feigenbaum, 2004). Similarly, when returning sound waves strike the crystals they generate an electric current which is recorded by the transceiver. The transceiver alternates between transmitting (usually around 1% of the time) and recording (99% of the time). When the transceiver is placed against the body

sound travels through the tissue, generally in straight lines until it encounters an interface with a tissue of different acoustic properties. When this happens some of the wave is reflected back to the transceiver at the incident angle while the rest is refracted and continues to propagate through the tissue or is absorbed. The velocity of sound through a medium depends on its density, as sound travels more quickly through denser objects, but in most soft tissue in the body the velocity is a fairly constant 1540 m/s. Thus the presence of a reflected wave identifies the boundaries of different tissues, while the delay between the outgoing and returning wave is determined by the distance between the object and the transceiver. This information is processed online by the ultrasound machine and displayed as a two-dimensional representation of the underlying tissue.

It is also possible to detect blood flow through vessels using a kind of echocardiography which capitalises on the shift in wavelength which occurs when sound travels through a medium moving towards or away from the observer, in the so called Doppler shift. A classic example of this is the siren of an ambulance travelling towards an observer sounds higher pitched due to the waves being compressed, whereas when the ambulance drives in the opposite direction the waves are stretched and sound lower pitched (a description of how velocity can be mathematically deduced from the Doppler shift is given in Section 2.3.2). Doppler echocardiography can be performed with one set of continually transmitting crystals and a second set of receiving crystals, however this cannot discriminate where the returning signal comes from. The great advancement in clinical Doppler echocardiography was the advent of 'pulsed mode' Doppler which allows the measurement of velocity and depth by alternately transmitting and receiving and adjusting the duty cycle to restrict the recording to a set depth.

There are limitations to what can be studied using echocardiography. For instance, certain tissues such as bone which is very dense and the lungs which contain a lot of air, transmit sound poorly and therefore almost all of the sound is reflected. This may restrict access to deeper tissues (e.g. the ribs and lungs can limit the view of the heart) and may necessitate the use of alternative viewing windows such as transoesophageal echocardiography. A wave can reflect off an object whose thickness is at least one quarter of its wavelength, thus the ability to resolve small objects requires high wave frequencies typically in the MHz range (Feigenbaum, 2004). This means low frequency waves penetrate deep into tissue but have poor resolution, whereas high frequency

waves give greater detail but have little penetration because the signal is reflected by more objects. The orientation of tissue relative to the wave also affects the quality of image as wave reflections from boundaries at 90° to the transceiver produce the greatest reflections, whereas those parallel to the wave produce minimal reflections. This has implications in the heart with its round chambers where typically the anterior and posterior walls can be visualised but the lateral walls can suffer from image dropout.

Cardiac pressure-volume loops

The cardiac cycle can be conceptualized as consisting of four phases of changing pressure and volume, depicted as a loop (Figure 1.1). Phase 1, isovolumic contraction, consists of a rise in ventricular pressure due to contraction of the ventricle at the onset of systole without a change in volume due to closure of the aortic or PA valves. Phase 2 occurs between aortic or PA valve opening and closing and therefore represents the ejection of blood under quasi-isotonic conditions. The transition to Phase 3 corresponds to end systole when ejection stops, the valves close and pressure declines under isovolumic conditions. Phase 4 begins with mitral or tricuspid valve opening and represents ventricle refilling with blood due to passive and active filling during diastole. The effect of inotropic or lusitropic factors such as altered filling pressures, vascular resistance, or catecholamines on the ventricle and vasculature can easily be visualised as a change in the shape of the PV loop. PV loops allow a greater insight into ventricle contractility as they permit load-independent parameters of contractility to be calculated which are not affected by heart rate or vascular resistance (Figure 1.2) (Champion *et al.*, 2009; Naeije & Manes, 2014).

RV and LV PV loops differ in their normal shape which reflects differences in arterial diastolic pressure (afterload) and isovolumic contraction and relaxation times (Burkhoff *et al.*, 1987). The LV exhibits a pronounced isovolumic contraction Phase 1 due to the time it takes for ventricular pressure to exceed arterial afterload, similarly there is a long isovolumic relaxation as ventricular pressure falls after aortic valve closure. In contrast the RV PV loop is normally triangular due to the smaller difference between ventricular diastolic pressure and afterload (Redington *et al.*, 1988) (Figure 1.1), although pathological changes due to pressure or volume overload can reduce the differences as both ventricles develop pronounced isovolumic contraction and relaxation phases (Redington *et al.*, 1990). For this reason some parameters commonly used to describe LV function such as the highly load-dependent dP/dt_{max} are

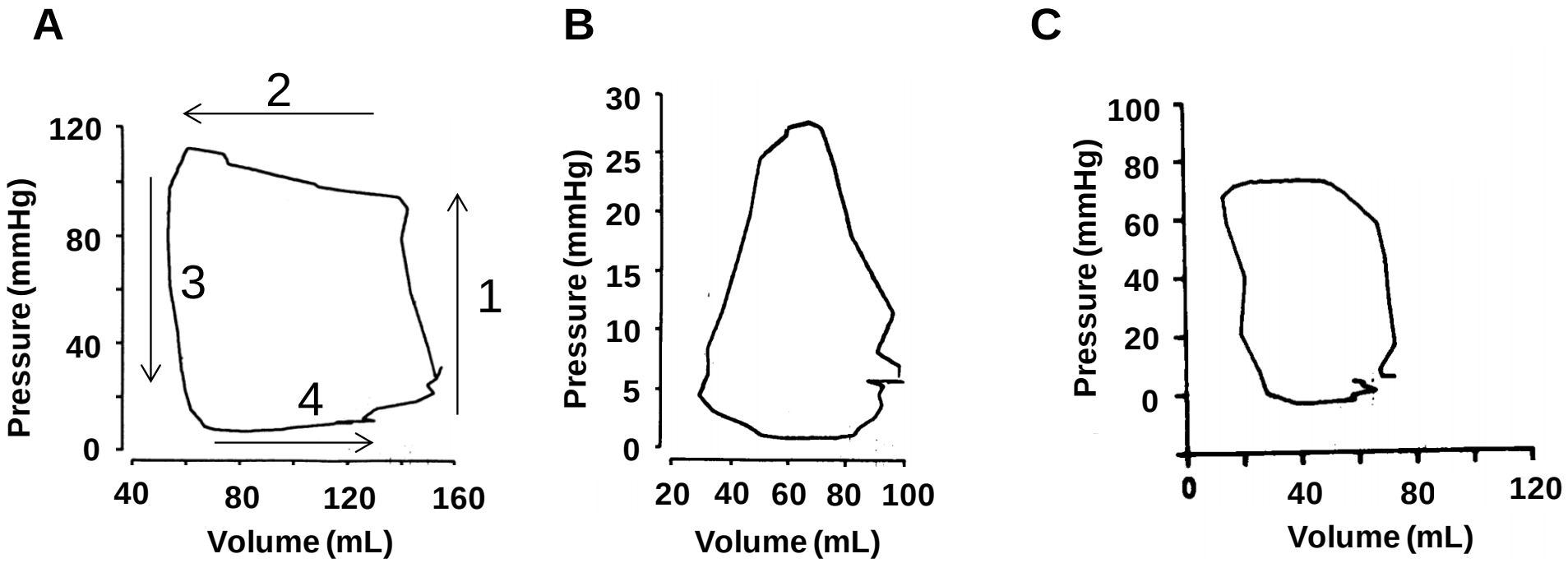

Figure 1.1 Cardiac pressure-volume loops

A Human LV PV loop showing the four phases of contraction: 1) isovolumic contraction, 2) ejection, 3) isovolumic relaxation, and 4) refilling. **B** Healthy RV PV loop with no discernible isovolumic contraction and relaxation and low systolic pressure. **C** RV PV loop from a patient with pulmonary stenosis showing a more rectangular loop with high systolic pressure. Figure adapted from Redington *et al.* (1990)

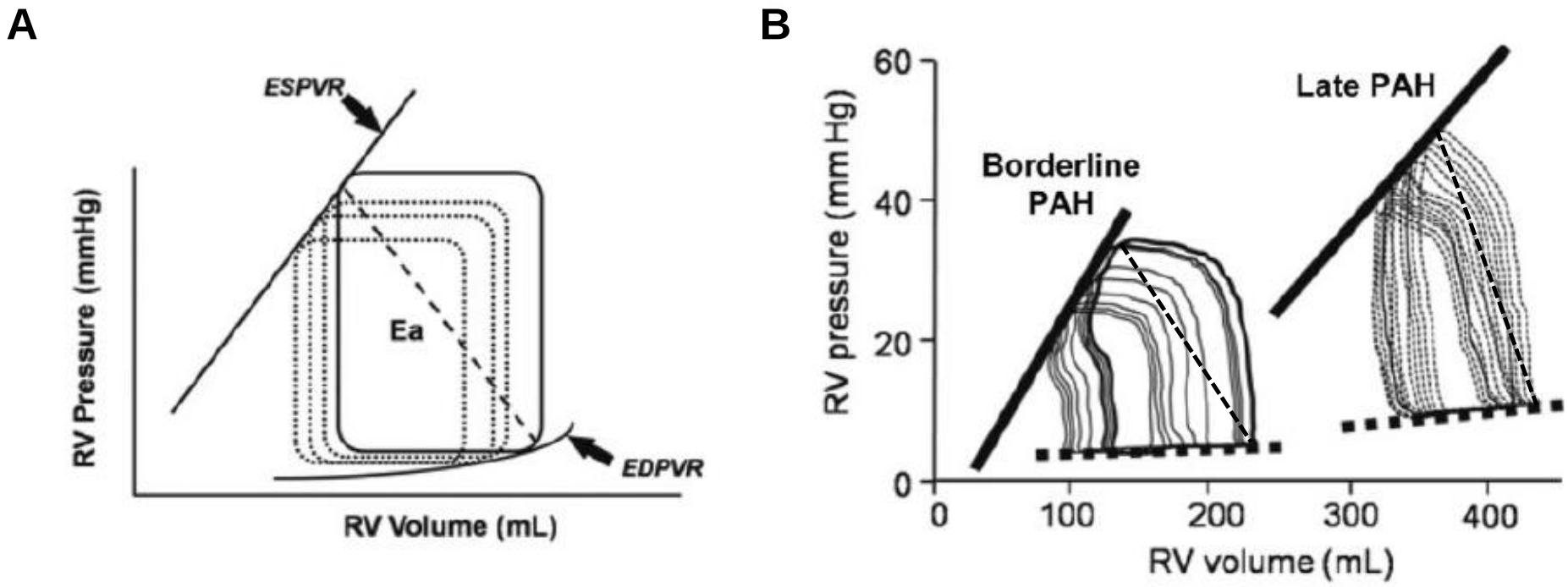

Figure 1.2 Ventriculo-arterial coupling measured by pressure-volume analysis

A Diagram of pressure-volume (PV) measurements during progressive preload reduction. Arterial elastance (Ea) reflects the relationship between stroke volume and systolic pressure. **B** RV PV loops in compensated and decompensated PAH. Ea steepens in late PAH due to continued vascular remodelling, however ESPVR decreases as RV contractility progressively worsens. Consequently, ventriculo-arterial coupling is initially preserved (ESPVR ≈ Ea) but then declines (ESPVR < Ea) . Figure adapted from Champion *et al*. (2009).

of questionable value in the RV, as the short isovolumic contraction time leads to low values of dP/dt_{max} which can increase even in a severely compromised RV as the afterload and therefore isovolumic contraction time increases (Gleason & Braunwald, 1962).

1.2.4 Electrical conduction

Cardiomyocytes in the heart are electrically connected and function as a syncytium, meaning every cell should depolarize during every heartbeat, however the order in which they depolarize is critical to ensure the ventricles fill and eject blood efficiently; uncontrolled activation can rapidly lead to pump failure and death. To this end a specialised conduction system in the heart carries the depolarization wavefront to regions of the heart at different rates and ensures a synchronized contraction.

The heart generates its own electrical impulse originating in specialized pacemaker cells which display intrinsic automaticity and set a basal heart rate of around 100 beats per minute in humans, though at rest this is reduced by parasympathetic nervous activity to 60-80 beats per minute. Pacemaker cells are situated in the sinoatrial node (SAN) which is located near the inflow of the superior vena cava into the right atrium and automaticity of SAN cells is critical to their function. Automaticity is shared with other cells such as atrioventricular (AV) node cells, however as the firing rate of SAN cells is faster than AV node cells they normally determine the minimum heart rate. SAN cells undergo spontaneous diastolic depolarization under the control of a 'membrane clock' regulated by channels which carry inward currents and reduce outward repolarizing currents, and also possibly through an independent mechanism of spontaneous Ca^{2+} release from the sarcoplasmic reticulum ('calcium clock') which generates inward current through Ca^{2+} efflux from the cell (Honjo *et al.*, 2003; Monfredi *et al.*, 2013).

The action potential (AP) wavefront spreads from the SAN to the AV node though internodal pathways and during the process spreads to activate atrial cardiomyocytes. At this point the activity is confined to the atria due to the fibrous atrioventricular valves which do not conduct. The AV node sits near the coronary sinus in the right atrium and connects with specialized conducting fibres in the interventricular septum called the bundle of His which divides to separately supply the RV and LV. The AV node slows the propagation of the AP into the ventricles allowing time for the atria to contract and fill the ventricles with blood. The right and left bundle branches travel towards the

apex, then turn and divide to supply the papillary muscles and Purkinje fibres. The papillary muscles contract first due to direct innervation by the bundle branches, applying tension to the AV valves preventing retrograde blood flow into the atria during ventricular contraction. Purkinje fibres then activate the remaining myocardium starting from the endocardium and apex and travelling towards the epicardium and base of the heart.

The action potential (AP) propagates between cardiomyocytes through intercellular coupling at the ends of cells (Veeraraghavan *et al.*, 2014). Gap junctions form from hemi-channels of hexamers of connexin proteins (Cx43 being the primary cardiac isoform) expressed in opposing membranes at the intercalated disk. These pores connect the cytosol of neighbouring cells as a syncytium allowing electrotonic diffusion of Na^+ ions during an AP (Söhl & Willecke, 2004). This organisation results in anisotropic conduction through the myocardium which is faster parallel than transverse to muscle fibres (Kanai & Salama, 1995).

1.2.5 Coronary blood supply

The coronary circulation begins with a right and left coronary artery originating at the aortic sinuses at the base of the ascending aorta. The right coronary artery supplies most of the RV and right atrium except the posterior wall and inferoseptal region which are supplied by the left anterior descending artery. The left coronary artery supplies the LV, interventricular septum and left atrium. Gas and solute exchange between the blood and myocardium occurs via capillaries which generally run parallel to muscle fibres. Blood is collected from the capillary bed in venules which feed into the cardiac veins which either return blood to the right atrium via the coronary sinus or drain directly into the RV via the Thebesian system of small veins (von Ludinghausen, 2003).

The RV and LV differ in their normal coronary perfusion, as the LV experiences phasic perfusion mainly during diastole due to compression of vessels resulting from the high intramural stress generated during systole whereas the RV with its smaller muscle mass experiences more continual flow throughout systole and diastole. Elevated RV pressures in PAH stops RV coronary flow during systole resulting in perfusion mainly during diastole (Lowensohn *et al.*, 1976).

1.2.6 Extracellular matrix

The extracellular matrix (ECM) is the acellular component of tissues consisting of proteins such as collagens, fibronectin, glycoproteins and proteases. It serves as a scaffold to interconnect cells and distribute the mechanical forces generated by the heart during contraction and diastolic filling (Souders *et al.*, 2009). Frank and Langer (1974) showed using electron microscopy that collagen constituted 4% of the extracellular matrix. Collagen forms triple helical strands comprised of $(X\text{-}Y\text{-}Glycine)_n$ repeating units, where X and Y are predominantly proline and 4-hydroxyproline (Bella *et al.*, 1994). The predominant collagen isoform in the rodent heart is Type I which forms large well organised fibre strands which are stiff and resist stretching (Ishikawa *et al.*, 1992a). Type III collagen is the other main cardiac isoform which forms a fine reticular network surrounding cells and is more compliant.

A significant proportion of the ECM is synthesized by fibroblasts which comprise 55-70% of all cells in the adult LV (Zak, 1974; Nag, 1980; Banerjee *et al.*, 2007). Fibroblasts also secrete protease enzymes (matrix metalloproteinases; MMPs) which degrade the ECM allowing fibrous scars to form around injured tissue such as a myocardial infarction (MI). The secretion and activation of MMPs occurs in response to growth factor and cytokine signalling through interleukins and tumour necrosis factor (TNF)-α and is important in facilitating the remodelling process.

1.2.7 Cardiomyocyte structure

Ventricular cardiomyocytes are generally rectangular ellipsoids in shape with a long axis of 100-150 µm and short axis of 15-25 µm. A plasma membrane (sarcolemma) encloses the cell which is relatively impermeable to ions and charged molecules except through specific channels and ion transporters expressed on the cell surface allowing the establishment of an electrochemical gradient of ions. The sarcolemma of ventricular myocytes is highly invaginated and forms tubules (t-tubules) which travel deep inside the cell which have a distinct ion channel composition to the surface sarcolemma. Atrial myocytes contain a sparser tubule network (Dibb *et al.*, 2013). At the ends of cardiomyocytes are specialized regions called the intercalated disks which form end-to-end connections which couple cells both mechanically and electrically. Immediately below the sarcolemma is a dense population of mitochondria which power the energy-dependent processes of ion exchange and contraction and occupy around 30% of total cell volume. Adult cardiomyocytes are typically binucleate and terminally

differentiated. The remaining ~70% of cardiomyocyte volume is occupied by an interdigitating array of myofilament proteins which contain the contractile elements necessary for cell shortening; certain cell types specialized for generating or conducting electrical waves are nearly devoid of this contractile apparatus. An internal Ca^{2+} store (sarcoplasmic reticulum) encircles the myofilaments and forms close connections with t-tubules. A dense cytoskeleton permeates throughout cells forming connections between membranes and internal structures giving structural support, as well as acting as a scaffold for cytosolic protein binding and trafficking.

1.2.8 Myofilament structure

The sarcomere is the fundamental unit of muscle contraction and is composed of interdigitating arrays of actin and myosin filaments which give rise to the striated appearance of cardiac muscle under a light microscope. The Z-lines demarcate the boundaries of the sarcomere and are maintained by α-actinin which forms connections between thin filaments and has both a structural and signaling role (Bers, 2001). The Z-disk is important in maintaining the interfilament spacing of myocytes which is critical to crossbridge formation. When viewed in cross-section, muscle cells appear as a hexagonal lattice with the globular heads of central thick filaments projecting out towards thin actin filaments at a regular distance of around 43 nm at resting length (Figure 1.3) (Konhilas *et al.*, 2002). The terminal Z-disk also contains signaling complexes such as desmosomes and fascia adherens which anchor the intracellular myofilaments and cytoskeleton to the sarcolemma and extracellular matrix and are involved in the activation of transcription factors in response to mechanical stress.

The actin thin filament is composed of repeating units of globular actin which forms a double stranded filamentous actin polymer. One end of the actin thin filament anchors to the Z-disk while the other end extends about 1 μm towards the centre of the sarcomere. Tropomyosin is another doubled stranded helix which binds in the groove of the actin filament and extends for about 7 actin monomers. The troponin (Tn) complex comprising the tropomyosin binding TnT, Ca^{2+} binding TnC, and inhibitory subunit TnI, binds to tropomyosin and regulates its position within the actin groove.

The myosin thick filament is held halfway between Z-lines and contains the proteins responsible for shortening the sarcomere during contraction. The thick filament extends perpendicular to the M-line for 0.8 μm in each direction and is composed of around 300 myosin heavy chains (MHC). Each MHC is composed of an α-helical tail

about 130 nm in length and a globular head containing the ATP and actin binding domains. Myosin can be proteolytically divided into most of the tail region (light meromyosin) and the remaining tail and head region (heavy mereomyosin). Heavy meremyosin can further be digested into an S1 region containing the flexible neck and globular head, and an S2 region which contains the remaining α-helical tail. Point mutations in either the S1 or S2 region are strongly associated with cardiomyopathies (Colegrave & Peckham, 2014). Each MHC also has an essential and a regulatory light chain associated with its S1 region which confer stability and influence crossbridge cycling kinetics when phosphorylated. In the centre of the A-band is the M-line which contains no myosin heads but does contain proteins such as myomesin which anchor myosin, titin and creatine kinase (Auerbach *et al.*, 1999).

Titin is the largest protein in the body (3-3.3 MDa) spanning the half sarcomere from Z-disk to M-line by more than 1 μm when a cell is stretched. It is a bidirectional spring which determines the slack sarcomere length in unloaded cardiomyocytes by exerting a passive force when cells are stretched and a restoring force when cells are shortened (King *et al.*, 2011) and is thought to be the main determinant of passive stiffness in the healthy myocardium at physiological sarcomere lengths (Wu *et al.*, 2000; Chung & Granzier, 2011). The extensible region of titin occurs in the I-band of the sarcomere and consists of three regions: 1) a PEVK (proline, glutamate, valine, lysine) rich region 2) a highly folded Ig repetition domain and 3) a cardiac isoform-specific N2B or N2BA element. The N2BA isoform of titin contains a longer PEVK region (600-800 residues) and is therefore more compliant and has a higher molecular mass than the shorter stiffer N2B isoform (163 residues). The spring elements unfold according to their entropic state (Ig domains unfold first, followed by the PEVK and N2B/N2BA domains) then refold when the cell shortens (Watanabe *et al.*, 2002; Nedrud *et al.*, 2011). Titin-based stiffness depends on isoform expression and post-translational modification of residues in the spring elements by phosphorylation and oxidation (Borbély *et al.*, 2009; Grutzner *et al.*, 2009; Hidalgo *et al.*, 2013). A restoring force is generated by titin when sarcomeres shorten below ~1.97 μm which is important during the early phase of diastole as it returns the cell to its resting length (King *et al.*, 2011). Titin may also have a signalling role in response to stretch as it binds to proteins such as telethonin in the Z-disk, thought to be important in t-tubule stability, and also contains a

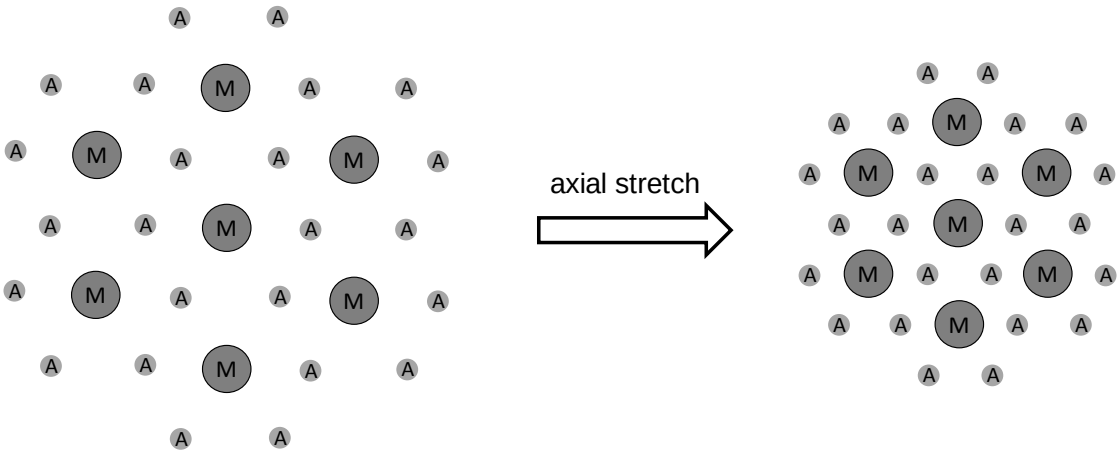

Figure 1.3 Myofilament lattice spacing

Thin actin filaments (A) are arranged in a hexagonal array surrounding thick myosin filaments (M). Axial stretch of a cardiomyocyte leads to a decrease in lattice spacing. Redrawn from Shiels & White (2008).

serine/threonine kinase domain which is activated by stretch (Puchner *et al.*, 2008; Candasamy *et al.*, 2014).

A dense cytoskeleton composed of filaments of actin and tubulin monomers facilitate trafficking of proteins around the cell and provides structural support to cardiomyocytes (Rogers & Gelfand, 2000; Nishimura *et al.*, 2005). Other roles include internalization of receptors on the cell membrane (Limas & Limas, 1990), remodelling cell membrane morphology (Zhang *et al.*, 2014), stretch induced reactive oxygen species production (Prosser *et al.*, 2011) and modulation of energy metabolism (Maldonado *et al.*, 2010).

1.3 Energy metabolism in the heart

1.3.1 Mitochondria: structure and function

Mitochondria are essential subcellular organelles found in the vast majority of cell types in the body which harness the energy liberated by the oxidation of substrates to generate ATP which powers energy-demanding cellular processes. There are 10000 to 20000 mitochondria in every cardiomyocyte which account for 30% of total cell volume (Williams *et al.*, 2015). Two populations of mitochondria are found in cardiomyocytes either in the immediate subsarcolemma (SSM) or between rows of myofilaments (interfibrillar mitochondria; IFM) (Figure 1.4). IFM are thought to normally exhibit higher maximal oxidative capacity (Palmer *et al.*, 1977), although this may change in a diseased state (Rosca *et al.*, 2008; Vazquez *et al.*, 2015). In addition transmural variation in mitochondrial function is thought to occur which may also be differentially affected by disease (Sharov *et al.*, 2000; MacDonald *et al.*, 2011).

The function of muscle mitochondria is assisted by their highly organised structure consisting of an outer membrane (MOM) separated from an inner membrane (MIM) by the intermembrane space (Scheffler, 2008). The MIM contains lipid soluble respiratory complexes and is highly folded to increase surface area. Enclosed by the MIM is the matrix which contains water soluble enzymes of the tri-carboxylic acid (TCA) cycle and enzymes responsible for β-oxidation of fatty acids (Figure 1.5). In the adult heart 60-90% of energy is supplied by fatty acid oxidation, while most of the remaining 10-30% comes from glucose oxidation (Neely & Morgan, 1974); a small proportion of energy can come from glycolysis but normally the heart is a net consumer of lactate and not a producer. Glycolysis in the cytosol produces pyruvate which is converted to acetyl-CoA in the matrix under the control of pyruvate dehydrogenase. Acetyl-CoA is also

produced through β-oxidation of fatty acids in the matrix (Tzagoloff, 1982). The first step of the TCA cycle is catalyzed by the enzyme citrate synthase which reacts acetyl-CoA with the four carbon oxaloacetate forming citric acid. Through a series of seven reactions the two carbons from acetyl-CoA are oxidized to reduce NAD^+ forming a pool of NADH and produce CO_2 as a waste product. The other high energy intermediate formed during the TCA cycle is $FADH_2$ which is produced from FAD^+ during the oxidation of succinate to fumarate by the enzyme succinate dehydrogenase which is a component of Complex II of the electron transport system (Complex II) and the only membrane bound enzyme of the TCA cycle.

1.3.2 Electron transport system

The electron transport system uses NADH and $FADH_2$ produced by the TCA cycle as a source of electrons to power the pumping of H^+ ions across the MIM to generate a large membrane potential (-180 mV). The controlled dissipation of this membrane potential through influx of H^+ drives the final complex of the respiratory system (F_1F_0-ATP synthase) which synthesises ATP from ADP. This process is facilitated by the presence of four respiratory complexes which facilitate electron transport and proton pumping, and the fifth ATP synthase (Scheffler, 2008).

In Complex I (NADH dehydrogenase) NADH is oxidised to NAD^+ with the transfer of two electrons to the lipid soluble carrier Coenzyme Q (CoQ) forming $CoQH_2$ and in the process four H^+ are exported into the intermembrane space (Tzagoloff, 1982). Complex II (succinate dehydrogenase) catalyses the oxidation of succinate to fumarate producing $FADH_2$ which is immediately oxidized to FAD^+ with the transfer of electrons to CoQ but no pumping of H^+ occurs at this step. Thus CI and CII share a common pathway for electron flow via CoQ, or the 'Q-junction', which converge into Complex III (cytochrome c reductase). Complex III transfers electrons from $CoQH_2$ to the water soluble carrier cytochrome c (cyt c) with the transport of a further four H^+ across the MIM. The final respiratory complex to establish the H^+ gradient is cytochrome c oxidase (complex IV) which transfers 4 electrons from cyt c to molecular O_2 producing water. The final complex in the ETS is also the ATP generating step which utilises the electrochemical gradient established by the preceding steps to drive the catalytic subunit of the F_1F_0 ATP synthase which phosphorylates low energy ADP to the high energy ATP.

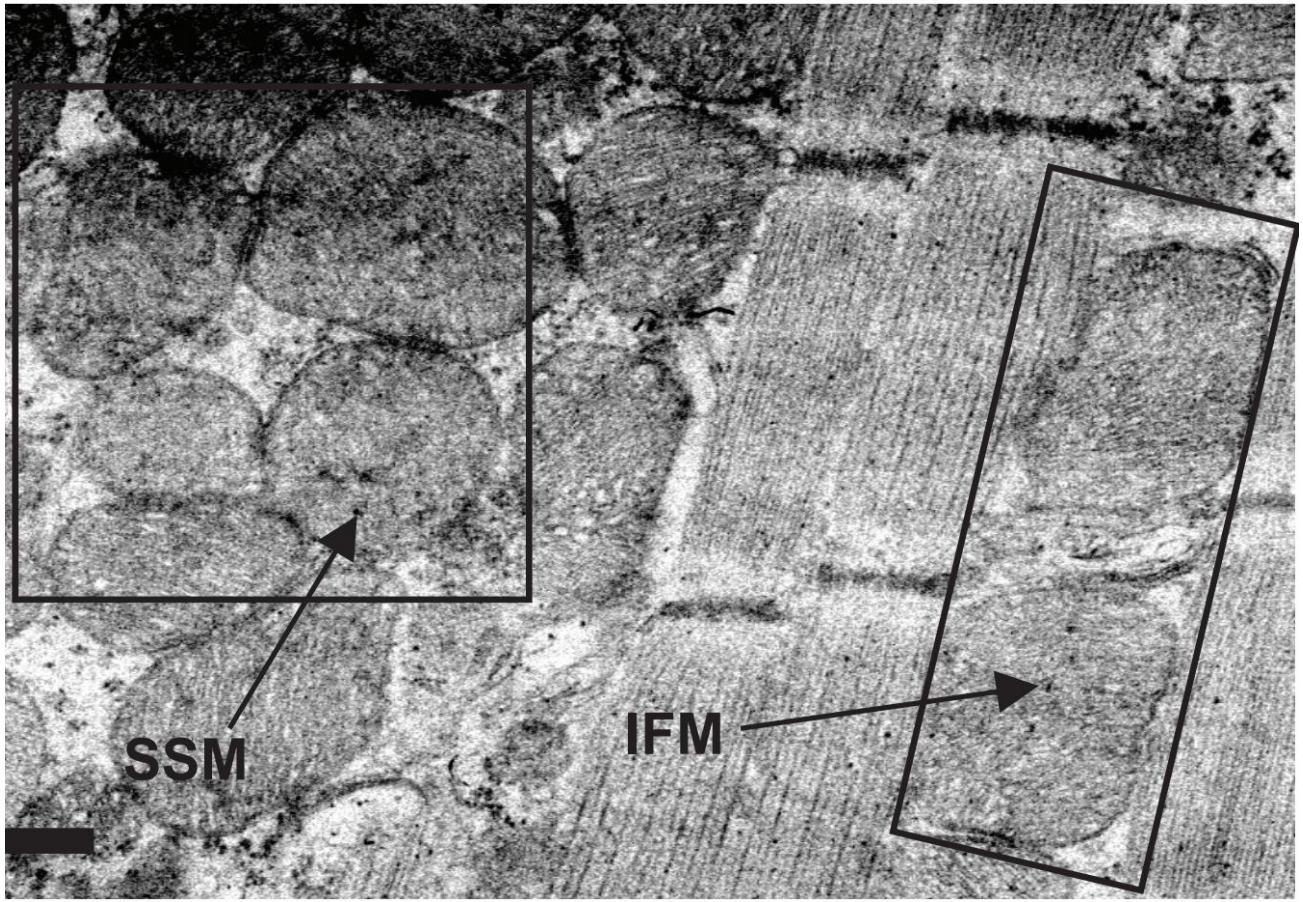

Figure 1.4 Subcellular distribution of mitochondria

Electron micrograph image of mouse LV imaged at ×10,000. Mitochondria are located in the immediate subsarcolemma (SSM) and interspersed between myofilaments (IFM). Bar shows 0.5 µm. Figure adapted from Hollander *et al.* 2014.

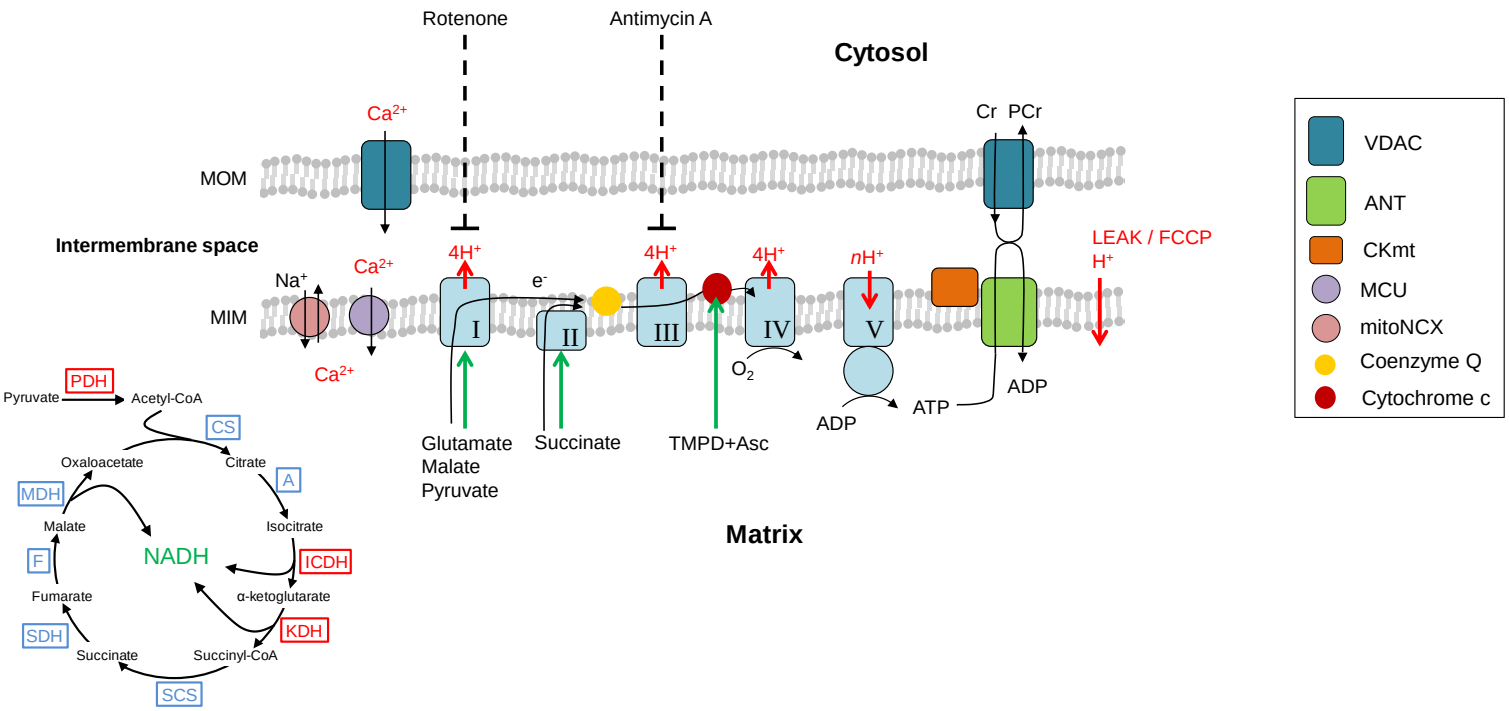

Figure 1.5 Electron transport system

Schematic diagram of production of electron donors in the TCA cycle and sources of electron flow into the electron transport system. ATP produced by mitochondria is immediately used by CK-mt to generate PCr which diffuses into the cytosol via VDAC. Ca^{2+} released during systole activates Ca^{2+}-dependent dehydrogenases (*red boxes*). Leak of H^+ across the MIM decreases mitochondrial efficiency. Rotenone and antimycin A block electron transport through complex I and III, respectively. PDH, pyruvate dehydrogenase; CS, citrate synthase; A, aconitase; ICDH, isocitrate dehydrogenase; KDH, α-ketoglutarate dehydrogenase; SCS, succinyl-CoA synthetase; SDH, succinate dehydrogenase; F, fumarase; MDH, malate dehydrogenase; MCU, mitochondrial Ca^{2+} uniporter. Figure adapted from Kilbaugh *et al*. (2015) and Williams *et al*. (2015).

1.3.3 Regulation of mitochondrial respiration

Mitochondria respond to changing energy requirements by increasing or decreasing the ATP synthesis in response to feedback from factors such as the availability of adenylates and ions such as Ca^{2+}. The addition of ADP to isolated mitochondria in the presence of substrates immediately increases respiration through a process of phosphate acceptor control (Chance & Williams, 1955). The large ADP and ATP molecules are impermeable to the mitochondrial outer membrane (MOM) and therefore enter and leave mitochondria through the voltage dependent anion channel (VDAC). VDAC is a 19 stranded β-barrel with an effective pore size of 14 Å (Ujwal *et al.*, 2008). VDAC is perhaps a misnomer, as even in the voltage dependent closed state VDAC is still permeable to cations such as Ca^{2+}, however the pore size and therefore permeability of VDAC to adenylates is reduced in intact cells by the binding of negatively charged free tubulin to the pore channel (Rostovtseva *et al.*, 2008; Maldonado *et al.*, 2010).

The adenine nucleotide translocase (ANT) situated in the inner mitochondrial membrane exchanges ATP produced in the matrix for ADP in the intermembrane space. The activity of the ANT and therefore the stimulation of respiration is greatly facilitated by its functional coupling to octameric mitochondrial creatine kinase (CK-mt) (Bessman & Fonyo, 1966). CK-mt rapidly hydrolyses ATP and transfers P_i to the small molecule creatine producing phosphocreatine (PCr) which easily diffuses through VDAC into the cytosol (Guzun *et al.*, 2009), while the product ADP is immediately transported back into the matrix via the ANT in exchange for further ATP. This mechanism permits a small pool of adenylates to be retained and continually cycled without needing to enter the bulk cytosol.

The cytosolic concentration of ATP and ADP measured using ^{31}P-NMR changes little in the heart during abrupt increases in work, suggesting they are not the main stimulus for increased respiration during periods of demand (Balaban *et al.*, 1986). In contrast, Ca^{2+} enters and leaves mitochondria on a beat by beat basis through VDAC then into the matrix via the Ca^{2+} uniporter (Lu *et al.*, 2013). This activates Ca^{2+}-sensitive pyruvate, α-ketoglutarate and isocitrate dehydrogenases of the TCA cycle thus stimulating mitochondrial respiration (Figure 1.5) (McCormack *et al.*, 1990). Ca^{2+} entry occurs on the same time scale as the systolic Ca^{2+} transient but removal from the matrix happens over a longer time due to exchange of Ca^{2+} and Na^{+} (and Li^{+}) via the mitochondrial NCX; the stoichiometry of mitochondrial Ca^{2+} and Na^{+} exchange remains

to be demonstrated conclusively (Boyman *et al.*, 2013; Lu *et al.*, 2013). The difference in entry and exit kinetics means mitochondrial Ca^{2+} can accumulate when heart rate is high and therefore modulate energy production according to demand.

Electron transfer is normally tightly coupled to ATP synthesis through one-electron reduction of carrier proteins down the electrochemical gradient with greater than 98% of electrons resulting in the reduction of molecular O_2 to water. However some respiration occurs due to leak of H^+ across the MIM via endogenously expressed uncoupling proteins or the ANT, or slippage of electrons from electron carriers. Dedicated uncoupling proteins are expressed in some tissues such as the brown fat of infants and allow the translocation of H^+ directly across the MIM which uncouples electron transport from ATP production for the purpose of generating heat. Leak of electrons can occur if CI or CIII are inhibited or impaired by disease resulting in direct reduction of O_2 to the superoxide radical (Turrens & Boveris, 1980; Ide *et al.*, 1999).

1.3.4 Creatine kinase system

The rapid and reversible formation of ATP or PCr through the creatine kinase (CK) reaction was discovered by Lohmann (1934) and was initially considered as a temporal energy buffer during periods of high energy turnover. The discovery of the mitochondrial isoform (CK-mt) and its ability to exert acceptor control over respiration spurred on the development of the 'phosphocreatine energy-shuttle' hypothesis (Jacobs *et al.*, 1964; Bessman & Fonyo, 1966). This hypothesis postulates the reversible CK reaction allows the transport of high energy phosphates around the cell in the form of small easily diffusible PCr while simultaneously removing lower energy ADP and its inhibitory effect on ATPases. The compartmentation of adenylates and preferential ability of PCr over solely ATP to sustain muscle contraction has since been thoroughly demonstrated (Ventura-Clapier *et al.*, 1987a; Kaasik *et al.*, 2001; Kuum *et al.*, 2009; Birkedal *et al.*, 2014).

Cardiomyocytes contain a mixture of 4 CK isoenzymes which all catalyze the reversible reaction with equal activity:

$$MgADP^- + PCr^{2-} + H^+ \leftrightarrow MgATP^{2-} + Cr$$

CK-mt accounts for 20-30% of total CK activity and is found exclusively in the intermembrane space of mitochondria as an octamer or dimer functionally coupled to

the ANT through binding with cardiolipin (Khuchua *et al.*, 1998). Cytosolic isoforms consist either of 86 kDa homodimers of muscle (CK-M) or brain isoforms (CK-B), or heterodimers (CK-MB). CK-M is the most abundant isoform in adult cardiomyocytes accounting for around 70% of total CK (Younes *et al.*, 1985). CK-MB and CK-B constitute a small proportion of total activity in healthy adult cardiomyocytes, though during early development and in disease their absolute and relative abundance increases (Ingwall, 1984).

The dense myofilament lattice, t-tubule and SR networks represent a significant barrier to diffusion of adenylates through cardiomyocytes (Sokolova *et al.*, 2009), therefore the much smaller molecule PCr forms an energy shuttle between sites of ATP production and utilisation through the colocalisation of CK with ATPases. This ensures a high ATP/ADP ratio in the vicinity of ATPases and prevents product inhibition by ADP. Around 10-30% of CK-M is bound to myomesin in the M-line of sarcomeres where it is functionally coupled to myosin (Ventura-Clapier *et al.*, 1987a; Hornemann *et al.*, 2003). CK-M is also functionally coupled to SERCA (Kuum *et al.*, 2009) and at the sarcolemma to the Na^+/K^+ ATPase (Grosse *et al.*, 1980) and ATP-sensitive I_{KATP} channels (Crawford *et al.*, 2002). CK-B loosely associates with the I-band of myofilaments in complexes of glycolytic enzymes (Kraft *et al.*, 2000). The targeting of different CK isoforms to the M-band or glycolytic complexes is thought to occur exclusively through the affinity of their N-terminal domain to their respective binding partners (Stolz & Wallimann, 1998)

1.4 Excitation-contraction coupling

Excitation-contraction (EC) coupling in ventricular myocytes is the process through which a change in the membrane potential of the sarcolemma leads to a small influx of Ca^{2+} to the cell which leads to a larger release of Ca^{2+} from the sarcoplasmic reticulum (SR) activating myofilament proteins resulting in the generation of force or shortening. Cytosolic Ca^{2+} is returned to resting levels by efflux from the cell or sequestering into the SR which causes dissociation of actin-myosin crossbridges and muscle relaxation (Figure 1.6) (Bers, 2002).

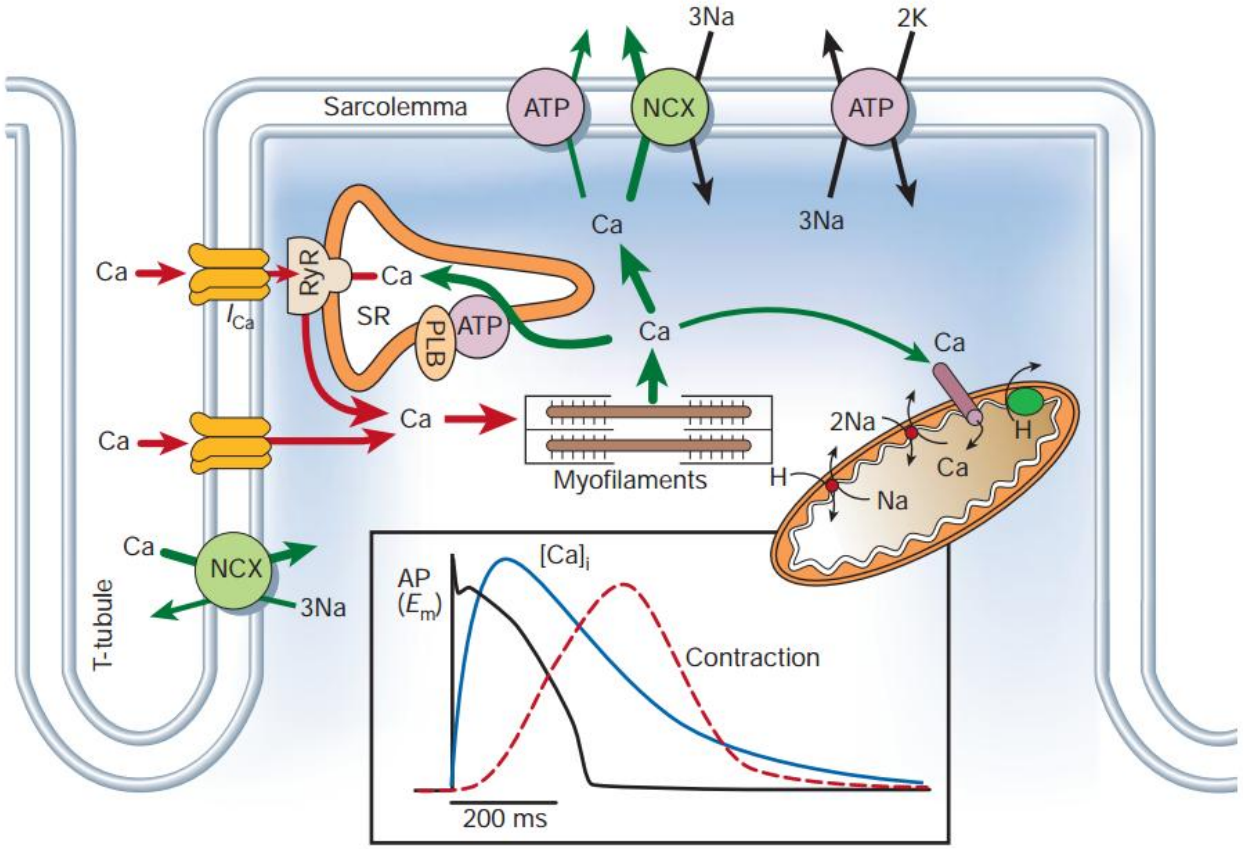

Figure 1.6 Cardiac excitation-contraction coupling

Ca^{2+} transport pathways activated in response to electrical activation. Inset shows the different time course of the action potential, Ca^{2+} transient, and contraction in a rabbit ventricular myocyte at 37°C. Figure from Bers (2002).

1.4.1 Ventricular action potential

At rest Na^+ and K^+ ions are pumped across the sarcolemma generating a membrane potential (E_m) between the inside of the cell membrane which is negatively charged and the outside which is positively charged. The ventricular AP arises due to the opening and closing of channels in the sarcolemma which allow the passage of ions carrying an electric current. The AP morphology varies depending on species, cell type and region of the heart (both base-apex and transmural) due to differential expression of ion channels (Akar & Rosenbaum, 2003), and has an important role in determining the refractory period which coordinates contraction across the heart (Schram *et al.*, 2002). The AP can be divided into 5 phases whose morphology is shaped by the presence and conductance of different ion channels which can activate and inactivate depending on voltage, time and ions present (Nerbonne & Kass, 2005). A model of an idealised human ventricular AP is illustrated in Figure 1.7.

During diastole E_m is in a hyperpolarized resting state (Phase 4) maintained between -90 to -70 mV by the inwardly rectifying potassium current (I_{K1}) (Dhamoon & Jalife, 2005). The channels which carry I_{K1} (K_{ir} 2.1) activate at E_m negative of -40 mV and carry an outward current making the cytosolic side of the membrane more negative up to the point at which E_m equals the reversal potential of potassium (E_k, around -80 mV). I_{K1} carries an inward current at membrane potentials more negative than E_K, thus stabilizing the resting membrane potential. During depolarization I_{K1} is inhibited by Ca^{2+} and Mg^{2+} ions and polyamides (Nerbonne & Kass, 2005) thus reducing the repolarizing effect and allowing the membrane potential to rapidly rise.

The rapid upstroke of the action potential occurs during Phase 0. An initial rise in E_m to around -70 mV due to the electrical coupling to neighbouring cells via gap junctions triggers the opening of voltage-gated sodium channels (primarily Na_v 1.5) carrying the inward I_{Na} current which further depolarizes the membrane to around +40 mV. The rapid onset of I_{Na} is followed by an equally rapid decrease in I_{Na} due to voltage- and time-dependent closure of channels which allows repolarisation to begin.

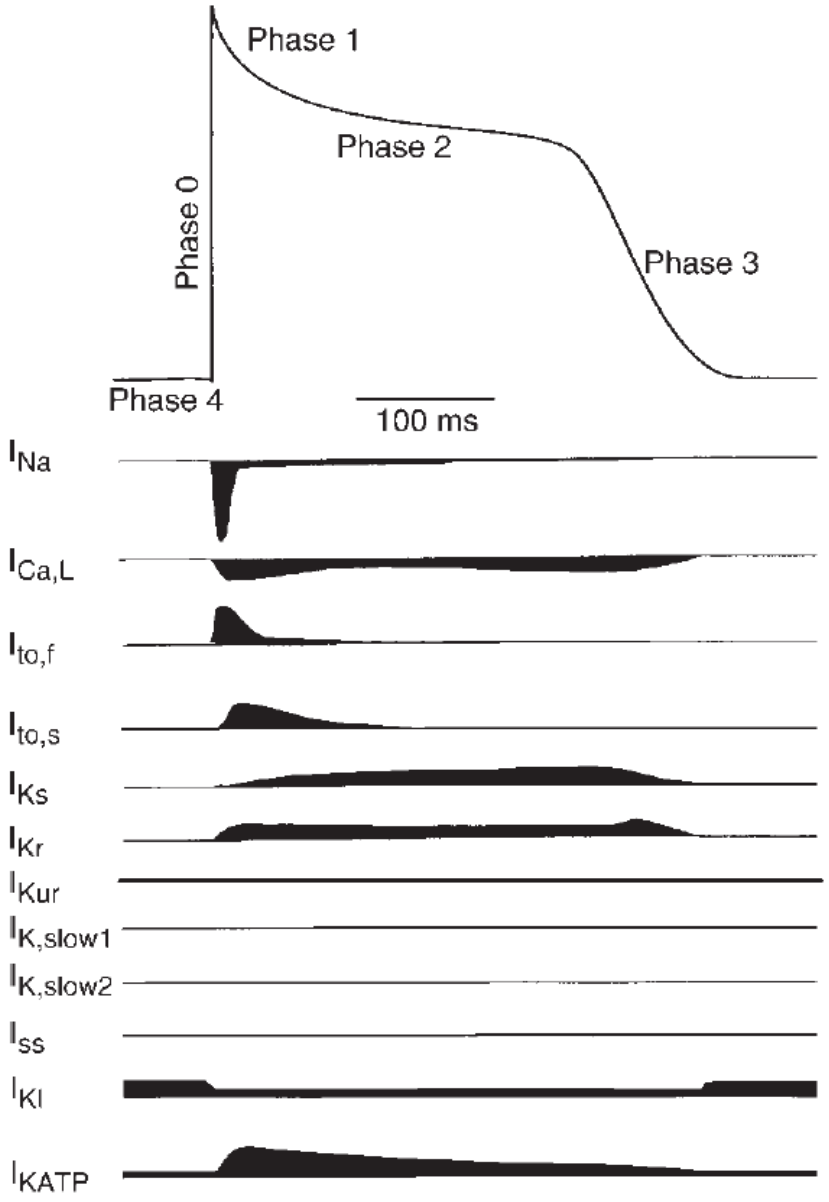

Figure 1.7 Ventricular cardiomyocyte action potential

Time course of inward (downward deflections) and outward (positive deflections) currents which are active during the human ventricular action potential (top). Not shown is I_{NCX}, which carries outward current early during the action potential then reverses and carries inward current as Ca^{2+} is removed from then cell. Rat ventricular action potentials are shorter and more triangular due to I_{Kr} and I_{Ks} being low or absent. Figure from Nerbonne and Kass (2005).

The initial repolarisation of the cell during Phase 1 occurs due to inactivation of I_{Na} with simultaneous activation of the transient outward potassium current (I_{to}). I_{to} is carried by three channels with similar rapid activation kinetics but have different time-dependent inactivation kinetics. K_v 4.2 and 4.3 channels inactivate rapidly and carry the $I_{to,fast}$ current, whereas K_v 1.4 channels deactivate slowly and carry the $I_{to,slow}$ current (Apkon & Nerbonne, 1991). During this time E_m approaches 0 mV which is the peak of the I_{Ca} activation curve, allowing influx of Ca^{2+} to the cell.

In human ventricular action potentials Phase 2 is typified by a pronounced plateau following early repolarisation representing the opposing influences of inward current generated by entry of Ca^{2+} to the cell (I_{Ca}) through voltage dependent long lasting calcium channels (Ca_v 1.2) and repolarising influence of delayed K channels. I_{Ca} begins to activate at around -30 mV and reaches its peak around 0 mV. The inactivation of I_{Ca} occurs through voltage, Ca^{2+} and time-dependent mechanisms (Benitah *et al.*, 2010). A fast (I_{Kr}) and slowly activating (I_{Ks}) repolarising outward K current begin to activate during Phase 2 (Sanguinetti & Jurkiewicz, 1990). I_{Kr} inactivates rapidly, shows inward rectification, and recovers quickly from inactivation, whereas I_{Ks} shows outward rectification and does not inactivate. Rabbits have a similar AP morphology to humans, however small rodents such as rats and mice have a very short Phase 2 due to species differences in ion channel densities (Nerbonne, 2000).

Final repolarisation to the resting membrane potential during Phase 3 is achieved by the voltage-, time- and Ca^{2+}-dependent inactivation of I_{Ca} and the remaining current generated by I_{Kr} and I_{Ks} which repolarises the cell.

1.4.1 Transverse-axial tubule system

A dense tubule network formed by invaginations of the sarcolemma occurring primarily at the Z-line of sarcomeres is present in adult ventricular myocytes from most mammalian species and in some other cell types including skeletal myocytes and atrial myocytes of large animals (Dibb *et al.*, 2013). T-tubules are approximately 200 nm in diameter and make up around 1% of the total cell volume (Page *et al.*, 1971) but due to their large surface area account for 25-30% of total cell membrane (Kawai *et al.*, 1999; Bryant *et al.*, 2015). They project radially into the interior of the cell at the Z-lines of sarcomeres giving rise to the name ‘transverse’ tubule (t-tubule), where they co-localize with the junctional SR forming a functional unit called a dyad. Ca_v 1.2 channels are expressed at a 3- to 9-fold greater abundance in t-tubules compared to

the surface sarcolemma (Kawai *et al.*, 1999; Bryant *et al.*, 2015), thus placing them immediately opposite the junctional SR which is densely populated with ryanodine receptors (RYR2). This arrangement facilitates the primary role of t-tubules in ensuring uniform Ca^{2+} entry throughout the cell which potentiates SR release and ensures a rapid upstroke of the systolic Ca^{2+} transient.

The close apposition (12-15 nm) with the terminal cisternae of the SR arises due to stabilization by scaffolding proteins such as junctophilin-2 (JP2) which forms a microdomain called the dyadic cleft in which ion concentrations change rapidly and of greater magnitude than in the bulk cytosol (Dries *et al.*, 2013). This activates Ca^{2+} dependent protein kinases in the dyadic cleft which can phosphorylate RYR2 sensitizing it to further Ca^{2+} release (Maier & Bers, 2007). Other ion channels and receptors highly expressed in t-tubules compared to the surface sarcolemma include NCX and the sarcolemmal Ca^{2+} ATPase (Scriven *et al.*, 2000; Yang *et al.*, 2002; Chase & Orchard, 2011), whereas others such as Na_v 1.5 appear to be more evenly distributed throughout the sarcolemma (Yang *et al.*, 2002). β_2 adrenoceptors are also primarily localised to t-tubules by the scaffolding protein caveolin-3, resulting in a compartmented cAMP response to selective stimulation β_2-AR (Nikolaev *et al.*, 2010).

The structural integrity and localisation of ion channels and receptors to t-tubules is maintained by scaffolding proteins thought to include bridging integrator-1 (BIN-1) (also called amphiphysin II), JP2, caveolin-3 and telethonin (t-cap). BIN-1 has a positively charged concave surface with a high affinity for phospholipid membranes (Peter *et al.*, 2004). Expression of BIN-1 in cell types normally devoid of membrane invaginations is sufficient to induce tubule formation, whereas knockdown of BIN-1 in cardiomyocytes reduces overall tubule density suggesting it has an important role in the formation of membrane invaginations (Hong *et al.*, 2014). JP2 tethers the sarcolemma to the junctional SR maintaining the 12-15 nm cleft through its 8 lipophillic N-terminus domains which associate with the t-tubule sarcolemma, α-helical domain spanning the dyadic cleft, and C-terminus transmembrane domain embedded into the SR (Takeshima *et al.*, 2000). Knockdown of JP2 in mice reduces the proportion of transverse but not longitudinal tubules, suggesting it is important in maintaining the dyads (Chen *et al.*, 2013). T-tubule formation may also be helped by the association of caveolin-3, highly expressed in cholesterol-rich rafts in the sarcolemma, with α-actinin found in the Z-disk of sarcomeres (Parton *et al.*, 1997; Ueda *et al.*, 2004).

A smaller network of axial (or longitudinal) tubules spanning between half and one full sarcomere (1-2 μm) form connections between the sarcolemma and longitudinal SR with the generic name 'couplons'. Their role in EC coupling in health has received less attention than the more prolific t-tubule network, however up to 20% of RYR2 may be associated with axial tubules in the form of couplons and the association between sarcolemma and SR is indistinguishable from that of dyads suggesting they may also play a role in EC coupling (Asghari *et al.*, 2009).

1.4.2 Calcium-induced calcium release

Ca^{2+}-induced Ca^{2+}-release (CICR) in cardiac muscle was described by Fabiato and Fabiato (1975) in a series of seminal papers as the process through which a small amount of Ca^{2+} activates RYR2 Ca^{2+} release channels on the SR thus amplifying the signal and raising cytosolic Ca^{2+} from around 100 nM at rest to ~1 μM at the peak of the Ca^{2+} transient. The fundamental units of Ca^{2+} release were shown by Cheng *et al.* (1993) to be Ca^{2+} sparks. The spatial and temporal summation of around 10000 Ca^{2+} sparks produces the systolic Ca^{2+} transient (Cheng *et al.*, 1993; Shang *et al.*, 2014).

RYR2 are arranged in quatrefoil clusters of Ca^{2+} release units (CRU) in cardiac muscle consisting of around 14 RyR per CRU primarily located at the junctional SR, with a smaller proportion of CRU on the longitudinal SR (Chen-Izu *et al.*, 2006; Soeller *et al.*, 2007; Baddeley *et al.*, 2009; Soeller & Baddeley, 2013). Interactions within CRU confer stability and allow coupled gating of the channels, making the whole unit open and close in unison. Ca^{2+} is thought to activate RYR2 by first binding to a low affinity site with a fast association constant (Fabiato, 1985). Termination of Ca^{2+} release occurs due to inactivation of I_{Ca} and Ca^{2+} dependent inactivation of RYR2 as well as depletion of junctional SR stores (Bers *et al.*, 1990). At high cytosolic Ca^{2+} concentrations a high affinity inactivation site on RYR2 with a slow association becomes occupied thus inactivating the channel and giving rise to a refractory period which prevents uncontrolled self-activation (Fabiato, 1985). SR depletion of Ca^{2+} may also contribute to the refractory period between Ca^{2+} release events (Sham *et al.*, 1998).

Under normal circumstances Ca^{2+} sparks also occur in the absence of an action potential through the stochastic opening of RYR2 (Cheng *et al.*, 1993). Factors which destabilize CRU such as increased SR load, RYR2 sensitization by phosphorylation or oxidation, dissociation of accessory proteins, and increased cytosolic Ca^{2+} tend to

increase spark frequency (Loughrey *et al.*, 2004; Zima & Blatter, 2006; Zima *et al.*, 2010; Bovo *et al.*, 2011). Ca^{2+} spark diffusion is limited due to rapid reuptake by SERCA in the junctional SR meaning they normally fail to activate CRU on adjacent sarcomeres across the ~2 µm gap between Z-disks. However if this does happen an iterative saltatory process of CICR occurs resulting in a Ca^{2+} wave which propagates along the cell at around 70 µm/s (Lukyanenko & Györke, 1999).

1.4.3 Myofilament activation

Muscle shortening occurs due to the cycling of myosin heads in the thick filament which bind to actin thin filaments causing a conformational change in myosin which pulls actin along the filament before detaching ready to repeat the cycle; in striated muscle this process is mostly regulated at the level of the thin filament (Figure 1.8) (de Tombe, 2003; Kobayashi *et al.*, 2008). In diastole TnI binds to actin and sterically hinders crossbridge formation and the first step of myofilament activation involves Ca^{2+} relieving this inhibition through inducing a conformational change in the tropomyosin complex. Ca^{2+} binding to the N terminus of TnC causes a conformational shift which exposes a previously hidden hydrophobic region of the protein which is attracted to and binds TnI. This destabilizes TnI causing it to switch binding from actin to TnC which further stabilizes Ca^{2+} binding to TnC. The release of actin by TnI results in tropomyosin shifting deeper into the groove of the actin filament and changes from a blocked state to a closed state. This is relayed through tropomyosin causing the complex to shift deeper within the groove of the actin helix thus exposing further actin binding sites on the thin filament. A 5-10 amino acid overlap between the carboxy and amino ends of tropomyosin imparts a stiffness which means neighbouring tropomyosin also shift deeper into the actin groove cooperatively activating further myosin binding. Strongly bound myosin further activates the thin filament by maintaining tropomyosin in the open state and promoting the TnC-TnI interaction even in the absence of Ca^{2+} (Li *et al.*, 2014). Phosphorylation by protein kinases of troponins and regulatory proteins such as myosin binding protein-C on the thick filament influences myofilament Ca^{2+} sensitivity and therefore force and kinetics of contraction (Kooij *et al.*, 2010; Walker *et al.*, 2011a).

The S1 region of MHC contains the ATP binding pocket which hydrolyses ATP. Inorganic phosphate (P_i) is released upon actin binding causing the myosin head to rotate, thus translating the two filaments past each other during the powerstroke. For the cycle to continue ADP must dissociate (the rate limiting step in the crossbridge

cycle) to allow more ATP to bind, which releases actin from myosin. ATP is hydrolysed to ADP and P_i which remain bound to myosin, causing the head to straighten having moved along the actin filament by 5-10 nm. The steps involved, as proposed by Goldman and Brenner (1987) are illustrated in Figure 1.9.

1.4.4 Mechanical function

The Frank-Starling law of the heart as it is now know, was established through the work of Otto Frank (1865-1944) and Ernest H. Starling (1866-1927) who working independently built on the work of those at Carl Ludwig's Physiological Institute in Leipzig in describing the process by which an increase in end-diastolic volume immediately increases the force of contraction to maintain stroke volume (Zimmer, 2002). The same effect can be seen in isolated muscle cells and tissue as an inverted U-shape isometric length-tension relationship as described by Grimm and Whitehorn (1968), which reaches a maximum at sarcomere lengths (SL) between 2-2.2 µm.

The shape of the SL-tension relationship was initially attributed to the degree of actin and myosin overlap affecting the availability of crossbridge binding (Gordon *et al.*, 1966). Overlap increases as sarcomeres are stretched from slack length but then decreases beyond the optimal length due to reduced overlap and fewer attached crossbridges. Conversely force is impaired at short SL due to collision of actin filaments below 2 µm, while further shortening below 1.6 µm causes myosin to collide with the Z-disk greatly reducing the force generating ability. This explains much of the Frank-Starling mechanism, however cannot fully account for why force continues to increase in cardiac muscle stretched from SL 2.0 to 2.2 µm when the number of available crossbridges does not change, therefore further contributory mechanisms are likely.

An increase in Ca^{2+} sensitivity is widely recognised to contribute to the increased force produced at longer SL, however the precise mechanisms through which this occurs are not entirely understood (Shiels & White, 2008). Acute stretch of intact cardiomyocytes increases the developed force without an increase in the systolic Ca^{2+} transient (Allen & Kurihara, 1982; White *et al.*, 1993; Yasuda *et al.*, 2003), in fact the peak of the Ca^{2+} transient measured using a fluorescent dye may actually be reduced and the rate of decay slowed during stretch. Conversely, unloaded shortening increases the peak of the Ca^{2+} transient (Janssen & de Tombe, 1997). This indicates loading increases TnC affinity for Ca^{2+} and therefore retains it for longer during the contraction. This causes

the rate of tension decay to be slower at longer sarcomere lengths (de Tombe, 2003; Li *et al.*, 2014).

An ongoing focus has been on the mechanisms which regulate cooperative activation of the thin filament. This occurs when strongly bound crossbridges shift the tropomyosin complex deeper into the groove of the actin filament and into the open state thus exposing and increasing the affinity of further actin binding sites in a process of positive feedback (de Tombe, 2003). Kurihara *et al.* (1990) showed Ca^{2+} was released from the myofilaments of ferret papillary muscles injected with aequorin when quickly shortened, whereas when the muscles were incubated with 2,3-BDM this effect was absent, indicating the length-dependent increased affinity of TnC requires strong myosin attachment. This could be due to allosteric feedback from tropomyosin causing greater excursion of the hydrophobic TnI binding patch of TnC thus increasing the TnC-TnI interaction, as was shown by Li *et al.* (2014) using a FRET tagged TnC N-terminal.

Crossbridge attachment is a stochastic process therefore decreasing the interfilament spacing increases the likelihood of actin-myosin interaction. Stretching cardiac muscle from SL 1.9 to 2.3 µm decreases muscle width by around 13% which compresses the myofilament lattice spacing (Figure 1.3) (Fukuda *et al.*, 2000). Decreasing lattice spacing using Dextran beads in chemically permeabilized cardiomyocytes increases Ca^{2+} sensitivity at short SL (Fuchs & Wang, 1996). Titin may reduce interfilament spacing during stretch through its association with the Z-disk, as rats expressing a giant N2BA-G titin isoform have reduced length-dependent activation (Patel *et al.*, 2012). However not all studies support interfilament spacing as a primary cause of length-dependent activation as Konhilas *et al.* (2002) found a poor correlation between Ca^{2+} sensitivity and lattice spacing caused by stretch and osmotic compression.

Even unloaded cells must shorten against an internal load and a viscous component thought to be due to the cytoskeleton (Zile *et al.*, 1999). An elastic element due to the giant protein titin acts as a brake at end systole and exerts a restoring force returning the cell to resting length (Helmes *et al.*, 1996). Titin may also be involved in the process of 'shortening deactivation' in which Ca^{2+} sensitivity is reduced at short SL by exerting a radial strain on the Z-disk increasing myofilament lattice spacing.

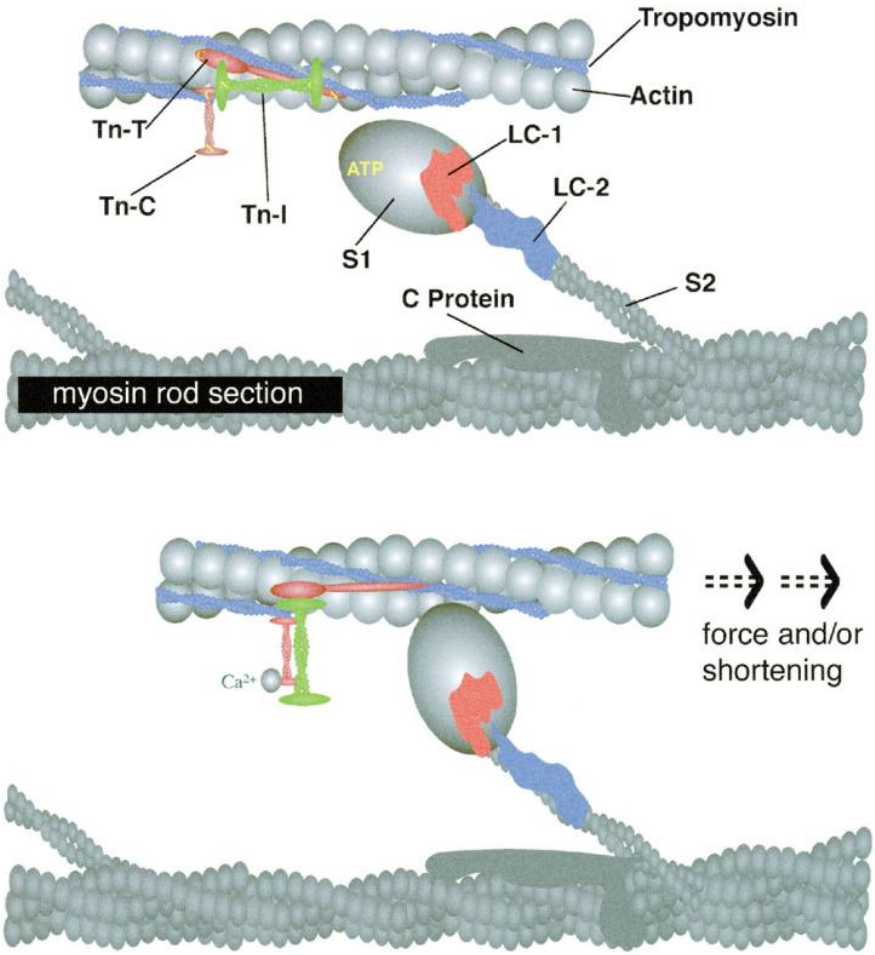

Figure 1.8 Regulation of crossbridge formation

Schematic representation of myofilaments in diastole (*top*) and systole (*bottom*). In the absence of Ca^{2+} tropomyosin inhibits crossbridge formation. Ca^{2+} binding to TnC during systole causes a conformational change in the inhibitory TnI leading to movement of tropomyosin deeper into the actin helix and exposure of the thin filament to the actin binding site on myosin heads. Energy stored from the hydrolysis of ATP in the myosin neck region is used to generate force or shortening. Figure adapted from de Tombe (2003).

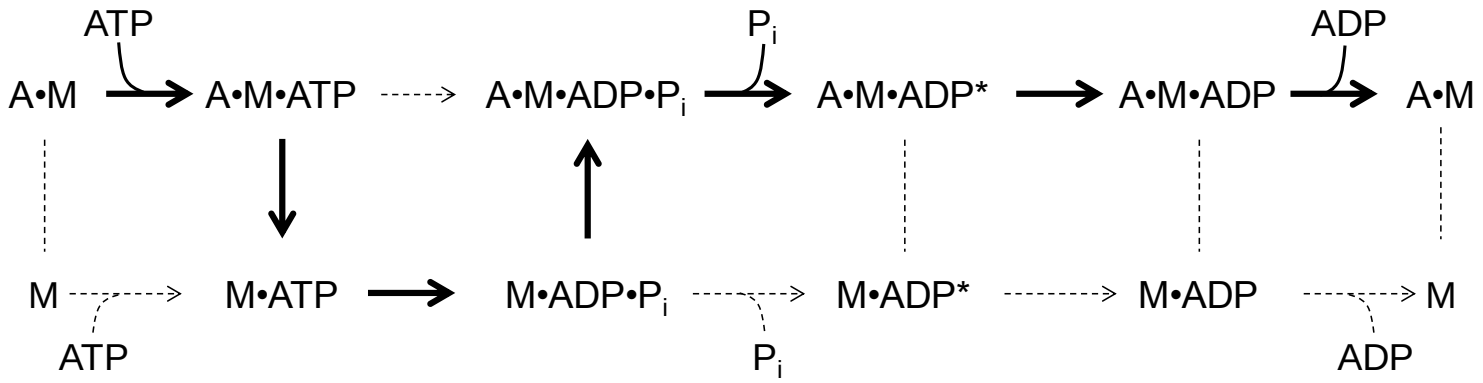

Figure 1.9 Steps of the crossbridge cycle

Model of the steps of the crossbridge cycle. The main order of the cycle is indicated by thick black arrows, although each step is possible. M, myosin; A, actin. Figure redrawn from Bers (2003).

The aforementioned mechanisms of length-dependent activation responsible for the Frank-Starling mechanism have all been acute (within one activation cycle) effects, however a slow force response to stretch also occurs. The Anrep effect is an increase in the force of contraction due to elevated afterload lasting more than a few minutes causing an increase in the end-systolic volume. The effect is mediated by an increase in the systolic Ca^{2+} transient amplitude and can be blocked by inhibiting stretch-activated channels permeable to Na^{+} and/or Ca^{2+} with streptomycin, inhibiting angiotensin and endothelin receptors, preventing Na^{+}/H^{+} exchange across the sarcolemma, or by blocking NCX (Cingolani *et al.*, 2003; Calaghan & White, 2004; Luers *et al.*, 2005; Kockskämper *et al.*, 2008). Thus the slow force response seems to be due to intracellular accumulation of Ca^{2+} via reverse mode NCX and increased myofilament sensitivity, secondary to intracellular accumulation of Na^{+} via stretch-activated channels and Na^{+}/H^{+} exchanger.

The mechanical properties of cardiomyocytes have primarily been elucidated through isometric or loaded contractions in chemically skinned cells and unloaded cell shortening, however neither of these can reproduce the forces experienced during the cardiac cycle. Early attempts at stretching electrically-excitable cells were cumbersome or unreliable, for instance embedding cells in gel matrices, trapped between coverglass slides, or using suction micropipettes (Garnier, 1994). A breakthrough came from the laboratory of Didier Garnier in the 1990s with the use of compliant carbon fibres which could stick to cell membranes by electrostatic forces and allowed the force of auxotonic contractions to be measured from the displacement of the fibre (Le Guennec *et al.*, 1990; White *et al.*, 1993).

The first physiological workloop style contractions in isolated cardiomyocytes were conducted by Yasuda *et al.* (2001) and Nishimura *et al.* (2004) using feedforward control of a piezo motor to clamp carbon fibre bending either by stretching or shortening the cell, however these were limited by the relatively low force needed for the cell to detach (~ 5.7 µN). This problem has been aided recently by the development of a biological glue consisting of extracellular matrix proteins, which enhances the attachment between cell and fibre allowing greater stretch and larger forces to be measured (Prosser *et al.*, 2011). Further recent advances include fast high resolution optical force transducers based on atomic force microscopy technology which are essentially isometric (Helmes *et al.*; Tasche *et al.*, 1999).

1.4.5 Cytosolic Ca^{2+} removal

The termination of I_{Ca} and cessation of Ca^{2+} release from the SR starts the process of removal of Ca^{2+} from the cytosol and cell relaxation. The primary Ca^{2+} removal pathways are SERCA and the sarcolemma NCX; the plasma membrane Ca^{2+} ATPase (PMCA) and mitochondrial Ca^{2+} uniporter also have a small contribution to Ca^{2+} removal.

The SR is the intracellular Ca^{2+} store in myocytes and encircles the myofilaments occupying around 5% of total cell volume (Page *et al.*, 1971). The SR can be divided morphologically into a junctional region, which contains most of the CRU and a substantial amount of SERCA, and the longitudinal SR which also contains SERCA but minimal RYR2. The junctional SR forms close connections with t-tubules and is the source of the vast majority of Ca^{2+} released during an action potential. The SR is refilled by SERCA which hydrolyses one ATP molecule to power the pumping of two Ca^{2+} ions into the SR against an approximately 1000 fold concentration gradient (~100 nM in cytosol, 100 µM in SR) (Vangheluwe *et al.*, 2003). Of all ATPases, SERCA requires the greatest free energy of ATP hydrolysis to function normally (Tian *et al.*, 1998). Inside the SR calsequestrin chelates free Ca^{2+} greatly reducing the concentration gradient and free energy requirement of SERCA. SERCA activity is controlled by its endogenous inhibitor phospholamban (PLB) which is incorporated into the SR membrane. PLB binds to and inhibits SERCA when unphosphorylated but relieves its inhibition when phosphorylated at Ser^{16} by PKA or Thr^{17} by CaMKII (Mattiazzi *et al.*, 2005). SR Ca^{2+} release is highly dependent on SR content, therefore factors which increase SR content tend to increase the systolic Ca^{2+} transient and developed force (Shannon *et al.*, 2000).

NCX is the main Ca^{2+} efflux pathway and is distributed primarily in the t-tubules (Despa *et al.*, 2003; Chase & Orchard, 2011; Bovo *et al.*, 2014). NCX in forward mode utilizes the electrochemical gradient to pump 1 Ca^{2+} ion out of the cell in exchange for 3 Na^+ ions into the cell, thus slightly depolarizing the cell. NCX is energetically less efficient than SERCA as only one Ca^{2+} ion is removed from the cytosol per ATP (indirectly via the Na^+/K^+ ATPase). A fast heart rate or pacing rate in myocytes increases intracellular Na^+ reducing forward-mode NCX and resulting in cytosolic accumulation of Ca^{2+} which is sequestered in the SR (Harrison & Boyett, 1995). This increases total SR content and is primarily responsible for the positive force-frequency relationship in most mammals (Endoh, 2004). NCX flux can also reverse depending on membrane

potential and the concentration of ions across the membrane, for instance a small amount of Ca^{2+} enters the cell via reverse-mode NCX during the early action potential, and NCX is responsible for the transient inward current generated by spontaneous Ca^{2+} release (Berlin *et al.*, 1989; Grantham & Cannell, 1996).

The PMCA is located exclusively in the t-tubules of cardiomyocytes and transports 1 Ca^{2+} per ATP hydrolysed (Chase & Orchard, 2011). It is slow and therefore contributes little to Ca^{2+} removal under normal circumstances. It maximally removes Ca^{2+} from the cytosol by <1 µM/s, in comparison to SERCA (200 µM/s) and NCX (30 µM/s). A small amount (~1%) of the systolic Ca^{2+} transient is also taken into the mitochondrial matrix through the Ca^{2+} uniporter on the MIM (Lu *et al.*, 2013). Mitochondrial Ca^{2+} is slowly released back into the cytosol via the mitochondrial NCX.

The relative contribution of each pathway to Ca^{2+} removal in rat ventricular myocytes is around 90% SERCA, 7-9% NCX and <2% slow pathways, whereas in rabbit and humans the proportional contribution of NCX is greater (70% SERCA, 28% NCX and <2% slow pathways) (Negretti *et al.*, 1993; Bassani *et al.*, 1994). This means species such as rabbit tend to deplete their SR stores when left unstimulated, whereas species with high SERCA activity such as mice and rats tend to accumulate SR Ca^{2+} at rest (Bassani & Bers, 1994; Bers *et al.*, 1998; Hobai & O'Rourke, 2001).

1.4.6 Adrenergic system

The β-adrenergic system is one of the main neural/hormone-regulated mechanisms through which the heart increases cardiac output during periods of demand, such as during exercise. Noradenaline is released from sympathetic nerves which directly innervate the myocardium and adrenaline is released into circulation from the adrenal glands on the kidneys in response to decreased output from baroreceptors in the aortic arch and carotid arteries activated by stretch. Agonist binding to β-adrenoceptors (βAR) on the cell membrane initiates a cascade of intracellular signalling events which mediate the chronotropic (increased heart rate), inotropic (increased force of contraction) and lusitropic (faster relaxation) response.

βAR exist in an equilibrium between active (R*) and inactive (R) forms. The presence of an agonist stabilizes the receptor in its active conformation increasing downstream signalling events, however even in the absence of agonist, intrinsic receptor activity contributes to a basal level of cAMP within cardiomyocytes. This constitutive receptor

activity is important for maintaining a basal level of phosphorylation of key intracellular targets, including PLB and myofilament proteins such as MyBP-C and TnI, which are important for normal systolic and diastolic function (Gresham & Stelzer, 2015). Neutral antagonists compete with agonists for binding thus preventing the stabilization of the receptor in its active conformation. Reverse agonists possess a further ability to reduce the intrinsic activity of receptors by stabilizing them in the inactive R conformation (Bond *et al.*, 1995). Metoprolol, but not carvedilol, exhibits reverse agonist properties and as such may be superior at preventing βAR desensitization by preventing receptor phosphorylation. Some β-blockers such as carvedilol are also partial agonists, meaning they can stabilize the receptor in its R* conformation, but do so less well than a full agonist. This property of carvedilol means it may actually contribute to receptor desensitization through recruitment of β-arrestins targeting the receptor for internalization (Wisler *et al.*, 2007). Likewise, carvedilol failed to increase or even decreased β_1AR expression in ventricular samples from human heart failure, whereas chronic metoprolol treatment resulted in increased β_1AR density, (Gilbert *et al.*, 1996; Böhm *et al.*, 1998). Increased β_1AR sensitivity is potentially dangerous if patient adherence to β-blockers is poor or if treatment is suddenly withdrawn as this can lead to a rebound hypersensitivity, as shown by increased heart rate, susceptibility to arrhythmias and angina (Ross *et al.*, 1981; Morimoto *et al.*, 1999).

There are three isoforms (β_1, β_2 & β_3) which are all members of the G-protein coupled receptor (GPCR) family. The predominant cardiac isoform responsible for enhancing cardiac output and also the receptor most strongly implicated in adverse remodelling in heart failure is the β_1AR (Bristow, 2000).

1.4.6.1 β_1-adrenoceptor signalling

The β_1AR shares with all GPCRs a conserved 7 transmembrane α-helical domain and an intracellular domain which binds heterotrimeric guanine-nucleotide binding regulatory proteins (G proteins) (Rockman *et al.*, 2002). Upon agonist binding the receptor undergoes a conformational change causing GDP bound to stimulatory $G_{\alpha s}$ to be replaced by GTP which dissociates the different G proteins into the subunits $G_{\alpha s}$ and $G_{\beta\gamma}$ which bind to and regulate the activity of effector enzymes including adenylyl cyclase (AC). Different isoforms of AC are expressed throughout the body, of which AC5 and AC6 are the predominant isoforms in cardiomyocytes (Vatner *et al.*, 2013). $G_{\alpha s}$ binding causes dissociation of the AC regulatory subunit, increasing its enzymatic activity, and the production of the intracellular second messenger molecule cyclic AMP

(cAMP) from ATP. β_1AR stimulation leads to a cell-wide increase in cAMP which binds the regulatory subunit of protein kinase A (PKA) activating the enzyme to phosphorylate serine or threonine residues on proteins (Gorelik *et al.*, 2013). Phosphorylation of proteins is an important post-translational regulatory modification allowing fine control over cell function in seconds. β_1AR stimulation in sinoatrial node cells leads to phosphorylation of Ca^{2+} cycling and membrane channels increasing the firing frequency of the cells, therefore increasing heart rate (Lakatta *et al.*, 2010; Liao *et al.*, 2010). The archetypal inotropic effect of PKA activation in ventricular myocytes is mediated through phosphorylation of the L-type Ca^{2+} channel at Ser^{1928} and Ser^{1700} (Lemke *et al.*, 2008; Fuller *et al.*, 2010), RYR2 at Ser^{2808} and Ser^{2030} (Xiao *et al.*, 2006), and PLB at Ser^{16} (Sande *et al.*, 2002), which increases Ca^{2+} entry to the cell and uptake into the SR thus increasing the systolic Ca^{2+} transient amplitude and contraction (Weiss *et al.*, 2013). Phosphorylation of TnI reduces the affinity of TnC for Ca^{2+} which decreases myofilament sensitivity, which combined with faster Ca^{2+} removal via SERCA causes the cell to relax more quickly (Kentish *et al.*, 2001).

Compartmentation of cAMP means PKA preferentially targets proteins within a signalling domain thus preventing phosphorylation of every possible target every time β_1AR are activated. This is achieved in part through co-localization of AC and PKA to their targets via scaffolding proteins and by degradation of cAMP by phosphodiesterases (PDEs) (Steinberg & Brunton, 2001). PKA can bind to scaffolding proteins such as A kinase anchoring protein (AKAP) and caveolin-3 which also bind other proteins such as the L-type Ca^{2+} channel, allowing preferential phosphorylation of these targets (Bryant *et al.*, 2014). In cardiac myocytes the major constituent PDE isoforms are PDE3 and PDE4 whereas in vascular smooth muscle cells PDE5 is the major isoform (Omori & Kotera, 2007). PDEs are expressed in discrete subcellular locations, for instance in lipid rafts in the cell membrane and bound to the cytoskeleton in the cytosol, limiting the spread of the cAMP signal.

1.4.6.2 β_2-adrenoceptors

β_2AR are expressed at a much lower level than β_1AR in the myocardium with a relative ratio of approximately 20:80 in rat and human (Bristow, 2000; Leineweber *et al.*, 2003). β_2AR are three times more prevalent in the vasculature and bronchioles than β_1AR and mediate smooth muscle cell relaxation (O'Donnell & Wanstall, 1981). In cardiomyocytes under resting conditions β_2AR are located predominantly in t-tubules where they are targeted to caveolae through association with caveolin-3, whereas

β_1AR are distributed evenly throughout the sarcolemma (Rybin *et al.*, 2000; Nikolaev *et al.*, 2010). β_2AR stimulation normally has little lusitropic effect on cardiomyocytes as the cAMP signal is highly localized to the t-tubule. This is sufficient to promote L-type Ca^{2+} channel phosphorylation which increases the amplitude of the Ca^{2+} transient (Kuschel *et al.*, 1999). Uncoupling β_2AR from the t-tubules by disrupting caveolae with the cholesterol-scavenging methyl-β-cyclodextrin switches the cAMP response from a local to a global signal similar to β_1 stimulation (MacDougall *et al.*, 2012).

As well as $G_{\alpha s}$, β_2AR can also couple to the inhibitory $G_{\alpha i}$ protein following phosphorylation by PKA or GRK2 at high concentrations of agonist which activates protein phosphatase 1 and inhibits PKA thus limiting the global response to adrenergic stimulation (Liu *et al.*, 2009). This endows β_2AR with cardioprotective properties against apoptosis during catecholamine stimulation (Communal *et al.*, 1999).

1.4.6.3 β_3-adrenoceptors

The β_3AR is expressed at low levels in human heart, it is thought to mediate a negative inotropic response to catecholamine stimulation associated with nitric oxide (NO) production coupled to $G_{\alpha i}$ activation (Gauthier *et al.*, 1996; Gauthier *et al.*, 1998). This is mediated by protein kinase G phosphorylation of L-type Ca^{2+} channel (Méry *et al.*, 1991; Schröder *et al.*, 2003), TnI (Shah *et al.*, 1994), and activation of PDE2 which enhances cAMP degradation (Méry *et al.*, 1993).

1.4.6.4 α-adrenoceptors

α_1 receptors are also present in cardiomyocytes, however the proportion of αAR is only around 10% that of βAR in humans and rodents (Rockman *et al.*, 2002). The primary isoforms expressed in ventricular myocytes are α_{1A} and α_{1B} which couple with $G_{\alpha q}$. Unusually and in contrast to βAR, up to 80% of α_1AR are expressed on the nuclear membrane (Wright *et al.*, 2008). Their activation leads to diacyl glycerol and IP_3 release which in conjunction with Ca^{2+} activates protein kinase C (PKC) to phosphorylate targets such as the myosin light chain which increases Ca^{2+} sensitivity (Andersen *et al.*, 2002). α_1AR are also expressed in the pulmonary vasculature where they mediate vasconstriction via PKC mediated Ca^{2+} entry to smooth muscle cells, however this is normally antagonized by activation of β_1 and β_2 receptors which increase levels of cAMP and Ca^{2+} uptake into the SR.

PKC is a potent stimulus for hypertrophy and therefore α_1ARs are generally considered to contribute to pathological remodelling in heart failure, however there is evidence α_1AR activation may actually be cardioprotective in heart failure. Clinical trials of α_1AR blockers to treat hypertension have been stopped early due to a doubling of the risk of mortality, possibly due to preventing the inotropic effects of α_1AR activation (Furberg *et al.*, 2001). There is substantial heterogeneity in the response to α_1AR stimulation between cells from different regions of a ventricle, or between RV and LV cells, with some showing a positive and others a negative inotropic response. Healthy mouse RV cells tend to exhibit a negative response compared to LV cells (68 vs 36%) which is mediated by Ca^{2+} handling alterations (Chu *et al.*, 2013). Interestingly, this overall negative response of RV cells was switched to a positive response in a mouse model of RV failure, suggesting α_1AR may play different roles in health and disease (Cowley *et al.*, 2015).

1.4.6.5 Autoinhibition and desensitization

β-AR undergo desensitization which reduces receptor activity temporarily, or can cause internalization of the receptor and degradation reducing the responsiveness to future stimulation. Non-agonist specific desensitization occurs within seconds and results from phosphorylation of β-AR by PKA (Gardner *et al.*, 2004). When receptors are occupied with agonists a further process of homologous desensitization can occur through phosphorylation by G-protein coupled receptor kinases (GRKs). There are 6 members of the GRK family, of which GRK2 is most highly expressed in the myocardium (Sato *et al.*, 2015). Phosphorylation by GRKs increases the affinity of β-AR to binding by β-arrestin proteins which uncouple the receptor from its G-proteins and thus prevent signalling. β-arrestins also act as scaffolds for further proteins such as clathrin which target the receptor for endocytosis (Zhang *et al.*, 1997). Internalized receptors either undergo dephosphorylation in the acidic vesicles to be recycled to the surface membrane or are degraded (Marchese & Trejo, 2013). Long term desensitization occurs through decreased transcription or degradation of β-AR mRNA and increased degradation of internalized receptors.

1.5 Heart failure

1.5.1 Structural remodelling

Cardiomyocytes are terminally differentiated cells which cannot proliferate in adulthood and therefore must adapt to the increased mechanical stress of heart failure by

remodelling their geometry to maintain ventriculo-arterial coupling. Loading conditions are partly responsible for orchestrating the remodelling process by promoting lengthening or widening the cells depending on whether the ventricle is pressure or volume overloaded (Tamura *et al.*, 1998). Pressure overload is thought to increase myocyte cross-sectional area which helps normalize systolic wall stress, whereas volume overload leads to myocyte elongation which initially maintains stroke volume; however remodelling cannot continue indefinitely and if the underlying pathology is not extirpated pump failure will eventually result (Grossman *et al.*, 1975; Gerdes & Capasso, 1995). For instance, in spontaneously hypertensive rats at 5 months of age cardiomyocyte volume increases primarily due to increased cross sectional area, however during the transition to dilated systolic heart failure over 12-24 months myocyte growth is primarily driven by the addition of sarcomeres in series (Gerdes *et al.*, 1996; McCrossan *et al.*, 2004). Similar patterns of remodelling also occur in myocardial infarction and dilated cardiomyopathies (Gerdes *et al.*, 1992; Tamura *et al.*, 1998). Catecholamines are also a potent stimulus for hypertrophy as overexpressing β_1AR in mice or continually infusing isoprenaline into rats leads to concentric LV hypertrophy (Engelhardt *et al.*, 1999; McMartin & Summers, 1999). Similarly the hypertrophy associated with chronic β-AR activation in heart failure can be ameliorated with β-blockers (Bogaard *et al.*, 2010), or reduced by knocking out β_1 and β_2AR (Kiriazis *et al.*, 2008).

As the heart undergoes hypertrophy the diffusion distance between the cores of muscle fibres and capillaries increases. This could lead to a mismatch between O_2 supply and demand and the development of hypoxic and inexcitable regions of myocardium unable to contribute to contraction. Cardiomyocyte hypertrophy without an increase in capillary angiogenesis will reduced the capillary density (CD) of a tissue and thus increase the area supplied by each capillary. An excellent example of this was reported by Roberts and Wearn (1941) who showed CD decreased in hypertrophied LV from donated human hearts. In the early compensated stages of heart failure CD may be preserved by an increase in capillary number through angiogenesis in response to signalling factors such as VEGF and HIF-1α produced by hypoxic tissue (Shipley *et al.*, 1937; Sano *et al.*, 2007; Sutendra *et al.*, 2013), however in decompensated RV failure VEGF expression decreases which may result in capillary rarefaction (Kobayashi *et al.*, 1994; Bogaard *et al.*, 2010). The resultant tissue hypoxia is thought to promote apoptosis which has been reported in the failing RV in the rat monocrotaline (MCT) model of PAH (Campian *et al.*, 2009). The primary enzyme responsible for proteolysis

in apoptosis is caspase-3 which is produced as a 37 kDa full length protein and undergoes cleavage into the 17-19 kDa active 'executioner' isoenzyme by caspase 9 (Nicholson *et al.*, 1995), and both caspase 3 and 9 are increased in the failing RV of rat PAH (Mouchaers *et al.*, 2009; Okumura *et al.*, 2015). If apoptosis occurs the entire stress of contraction is distributed between fewer cardiomyocytes which respond by increasing cross-sectional area thus fuelling the viscous cycle. Myocardial fibrosis replaces lost cardiomyocytes and maintains the structural integrity of the heart (Cingolani *et al.*, 2004), however excessive fibrosis is frequently reported in failing human RV and LV (Chaturvedi *et al.*, 2010; Rain *et al.*, 2013) and in animal models of RV failure (Mouchaers *et al.*, 2009) which may impair pump function by reducing diastolic filling. Collagen also decreases the diffusion of O_2 in the interstitial space and thus may reduce oxygenation of muscle fibres (Sabbah *et al.*, 1995).

1.5.2 Metabolic derangement

Failing human and animal hearts have reduced PCr/ATP ratio which is associated with worse prognosis leading to the suggestion the heart is energy starved (Neubauer *et al.*, 1997; Ingwall & Weiss, 2004; Bottomley *et al.*, 2013). Mitochondrial mass has been found to increase during the early compensated phase of LV failure in rat (Kindo *et al.*, 2012) but then return to normal or decrease at more advanced stages of disease (De Sousa *et al.*, 2002), whereas in failing human hearts mitochondrial mass is usually preserved (Rosca *et al.*, 2008; Stride *et al.*, 2013) although occasionally small reductions have been reported (Lemieux *et al.*, 2011a). Reduced expression of the master activator of mitochondrial protein synthesis, PGC-1α, may be responsible as this was shown to decrease in rat LV and RV failure coinciding with reduced mitochondrial mass and CK-mt expression (Garnier *et al.*, 2003; Enache *et al.*, 2013). Maximal respiration is often decreased in animal models of LV failure (De Sousa *et al.*, 2002; Kindo *et al.*, 2012) and was found to progressively decrease over time in RV failure (Daicho *et al.*, 2009). This finding has also been reported in failing human myocardium in some (Sharov *et al.*, 2000; Lemieux *et al.*, 2011a; Stride *et al.*, 2013) but not all studies (Cordero-Reyes *et al.* (2014). The source of dysfunction is often attributed to decreased Complex I driven respiration, possibly due to decreased expression of Complex I proteins (Stride *et al.*, 2013), however this could also be due to damage to Complex I in the absence of altered expression (Kuznetsov *et al.*, 2004). Some studies have also reported decreased Complex II activity in human LV failure (Stride *et al.*, 2013) or even increased activity in RV failure in rats (Redout *et al.*, 2007). Decreased Complex I could result in a functional block the ETS leading to increased

ROS production (Ide *et al.*, 1999). Overexpression of CK-M in mice with transverse aortic constriction improves survival and function (Gupta *et al.*, 2012) and the contractility of the myocardium following ischaemia (Akki *et al.*, 2012) whereas absence of a functioning CK system greatly reduces the ability of rats to survive myocardial infarction (93% mortality vs 46% mortality with a functioning CK system) (Lorentzon *et al.*, 2007).

A shift from primarily fatty acid oxidation in health towards a greater reliance on glucose utilization also occurs in human and experimental models of heart failure and PAH (Oikawa *et al.*, 2005; Piao *et al.*, 2010). Carbohydrate oxidation yields more ATP per mole O_2 suggesting substrate use by mitochondria may adapt to optimize the efficiency of ATP production. Increased glycolysis and glycolytic enzyme expression is also frequently reported in failing hearts which may indicate the mitochondria are hypoxic (Champion *et al.*, 2009; Balestra *et al.*, 2015).

1.5.3 β-adrenergic signalling

Chronic reliance on the β adrenergic system to augment contractility in LV failure leads to desensitization of β_1-ARs in part due to receptor phosphorylation by PKA and GRK2 (recently reviewed by Sato *et al.* (2015)) and also due to increased GRK2 and β-arrestin expression which promotes receptor internalisation and degradation (Luttrell & Lefkowitz, 2002). Reduced β_1AR mRNA and protein have been reported in the RV of human and animal models of PAH along with reduced stimulatory $G_{\alpha s}$ subunit and adenylyl cyclase expression (Seyfarth *et al.*, 2000; Piao *et al.*, 2012). Loss of constitutive βAR activity may impair normal contractile function by causing hypophosphorylation of, for instance, Ca^{2+} handling proteins. Furthermore, these changes in βAR signalling will blunt the responsiveness to catecholamines and reduce the contractile reserve of the myocardium when challenged by an acute stress, for instance exercise. This loss of βAR-mediated inotropy was found in human failing RV and LV muscle samples and trabeculae and in RV muscle samples from animals models of PAH in response to isoprenaline (Holubarsch *et al.*, 1996; Quaile *et al.*, 2007; Milani-Nejad *et al.*, 2015). This may explain the apparent paradox between the detrimental effects of chronic β-adrenergic activation and the beneficial effects of β-blockers which could *increase* β-AR signalling by preserving β_1AR density, i.e., by preventing chronic excessive cAMP production βAR density and sensitivity is preserved, thus maintaining a basal level of cAMP for normal cell function while ensuring a dynamic response range is available during acute periods of high demand.

Hypophosphorylation of TnI increases myofilament Ca^{2+} sensitivity and impairs diastolic relaxation and has been reported in rat RV failure (Lamberts *et al.*, 2007a; de Man *et al.*, 2011). However other studies have instead found Ca^{2+} sensitivity decreases in skinned RV cells from rat PAH induced by pulmonary artery banding (Fan *et al.*, 1997) or remains the same in MCT (Benoist *et al.*, 2014) and in human PAH compared to donor hearts (Rain *et al.*, 2013). Differences in disease severity or sample preparation may account for these discrepancies.

Slower Ca^{2+} uptake into the SR has been reported in failing MCT RV cells which may be due to decreased expression of SERCA and reduced phosphorylation of PLB at Ser^{16} (Xie *et al.*, 2012; Benoist *et al.*, 2014), as Reilly *et al.* (2001) found transfecting failing cells with adenoviral constructs of SERCA2a restored the rate of Ca^{2+} uptake. Decreased SR content has been reported in human LV failure (Pieske *et al.*, 1999) and also in MCT RV cells and PAB feline models of PAH which would be expected to decrease the Ca^{2+} transient amplitude (Quaile *et al.*, 2007; Xie *et al.*, 2012). The Ca^{2+} transient amplitude has also been found elevated during the development of RV and LV failure suggesting Ca^{2+} handling changes during the natural progression of disease (Mørk *et al.*, 2007; Benoist *et al.*, 2012).

In mammals, a heart-rate dependent increase in contractility is one of the mechanisms which ensures adequate delivery of blood to the body during periods of increased metabolic demand. In healthy rat ventricular myocytes the relationship between twitch force and contraction rate is triphasic: initially large at low pacing frequencies 0.2-1 Hz due to diastolic Ca^{2+} loading of the SR, then lower around 1-2 Hz, then increasing up to 7 Hz, before decreasing beyond 7 Hz (Kassiri *et al.*, 2000). This overall positive response to pacing can switch to a negative force-frequency in human LV failure (Holubarsch *et al.*, 1996; Brixius *et al.*, 2001) and animal models of RV failure secondary to PAH (Lamberts *et al.*, 2007a; Quaile *et al.*, 2007). This is likely due to detrimental alterations in Ca^{2+} handling which impair systolic Ca^{2+} release. Reduced SERCA activity could impair Ca^{2+} reuptake and deplete the SR in a rate-dependent manner which would both reduce the amplitude of the systolic contraction and lead to accumulation of diastolic Ca^{2+} which would impair diastolic relaxation. Increased refractoriness of RYR2 Ca^{2+} release could reduce the amplitude of the systolic Ca^{2+} transient at faster pacing despite maintained SR Ca^{2+} content due to hypophosphorylation of RYR2 (Maier *et al.*, 2000; Poláková *et al.*, 2015).

A progressive loss of t-tubules occurs in ventricular myocytes during the transition from compensated hypertrophy to decompensated heart failure which strongly correlates with deterioration of cardiac function (Wei *et al.*, 2010). Expression of the t-tubule scaffolding proteins JP2 and BIN-1 are notably decreased in advanced experimental RV failure (Wei *et al.*, 2010; Xie *et al.*, 2012) and human LV failure (Hong *et al.*, 2012). This results in a slowing of Ca^{2+} release in MCT RV cells and a loss of spatial synchrony in LV cells from chronically ischaemic pig myocardium (Heinzel *et al.*, 2008; Xie *et al.*, 2012), which would delay and reduce the force of contraction (Ferrantini *et al.*, 2014). A slight reduction in Ca^{2+} release synchrony was seen in human LV cardiomyocytes from chronic ischaemia, although there was relatively little t-tubule disruption observed in this study possibly due to humans having a less dense t-tubule network compared to rats and mice (Louch *et al.*, 2004). Ca_v 1.2 expression and I_{Ca} density are usually not changed in heart failure as might be expected given the loss of t-tubules (Lee *et al.*, 1997), suggesting there may be redistribution of channels from t-tubules to the surface sarcolemma or enhanced activity of existing channels, as was recently reported in a rat model of myocardial infarction (Bryant *et al.*, 2015). JP2 and BIN-1 act as scaffolding proteins for Ca_v 1.2 therefore their loss during heart failure may influence the redistribution of I_{Ca} from the t-tubules to the surface sarcolemma (Hong *et al.*, 2010; Bennett *et al.*, 2015).

The most consistent electrophysiological finding in failing hearts is a prolongation of the action potential at low pacing rates (Janse, 2004), however in failing human, rabbit and rat myocardium a decrease in the cycle length leads to a sharp fall in AP duration (Vermeulen *et al.*, 1994; Benoist *et al.*, 2012). This steep AP duration restitution may be a trigger for the initiation of alternating long and short APs which can degenerate into ventricular fibrillation (Rosenbaum *et al.*, 1994). Reduced I_{to} is thought to play a major role in delaying repolarization in failing RV cells from MCT rats and may be due to reduced mRNA expression of the subunits which compose the channel (Benoist *et al.*, 2011). The role of I_{to} in humans and other large mammals may be less important due to the longer Phase 2 (Kääb *et al.*, 1996), however reduced I_{to} could slow repolarization during Phase 1 and thereby reduce I_{Ca} and thus the amplitude of the Ca^{2+} transient (Tomaselli & Marbán, 1999; Workman *et al.*, 2003). Reduced I_{K1} in failing hearts may also destabilize the resting membrane potential and make failing hearts more prone to delayed after depolarizations by transient inward currents generated by NCX (Kääb *et al.*, 1996; Benoist *et al.*, 2011).

Increased diastolic SR Ca^{2+} leak in the form of sparks and waves is thought to trigger arrhythmias in heart failure. Ca^{2+} waves propagate through pairs of isolated cells (Eisner *et al.*, 2012), in trabeculae (Miura *et al.*, 1993) and in Langendorff-perfused rat hearts (Minamikawa *et al.*, 1997; Kaneko *et al.*, 2000) and have been shown to trigger ectopic APs (Fujiwara *et al.*, 2008) and could contribute to the emergence of sustained ventricular fibrillation following burst pacing (Benoist *et al.*, 2011). Likely causes of increased Ca^{2+} leak in heart failure include increased SR content, phosphorylation and oxidation of RYR2, and dissociation of FKBP12.6 from RyR2. The emphasis placed on each of these mechanisms seems to vary depending on the laboratory and some results are conflicting. RYR2 has been found to be hyperphosphorylated by PKA and CaMKII in human failing hearts, possibly due to decreased RYR2-bound protein phosphatase 1 and 2 or increased β-AR activation. This caused dissociation of FKBP12.6 which could destabilize RYR2 (Marx *et al.*, 2000; Respress *et al.*, 2012). However PKA phosphorylation does not necessarily lead to FKBP12.6 dissociation (Xiao *et al.*, 2004), and FKBP12.6 dissociation is not always required for increased Ca^{2+} leak (Eschenhagen, 2010). Disulphide formation between thiol residues in RYR2 was reported to increase leak in cardiomyocytes isolated from a canine tachypacing model, which was reversed following acute incubation of cells with a reducing agent, indicating ROS-induced leak from the SR may further impair diastolic Ca^{2+} handling (Terentyev *et al.*, 2008).

1.6 Pulmonary arterial hypertension

1.6.1 Epidemiology

Pulmonary hypertension is a condition in which the normally low pressure, high compliance pulmonary circulation becomes increasingly resistant to blood flow requiring higher pulmonary artery systolic pressures to maintain adequate perfusion of the lungs. The clinical definition of pulmonary hypertension is a resting mean PA pressure ≥25 mmHg, compared to the normal range of 11-17 mmHg (Galiè *et al.*, 2015b). The clinical manifestation of PAH consists primarily of exercise intolerance, dyspnoea and systemic congestion due to raised right atrial filling pressure (Vonk-Noordegraaf *et al.*, 2013). Patients with pulmonary hypertension are currently classified into one of 5 groups depending the apparent etiology of disease: 1) idiopathic pulmonary arterial hypertension (PAH) 2) pulmonary hypertension secondary to left heart failure 3) pulmonary hypertension secondary to lung disease 4) pulmonary

hypertension due to chronic thromboembolism 5) pulmonary hypertension due to undefined or multifarious reasons (Simonneau *et al.*, 2009).

Group 2 pulmonary hypertension is the most common form as nearly all patients with LV failure will have some degree of pulmonary hypertension, defined as a mean PA pressure ≥25 mmHg with a pulmonary capillary wedge pressure (PCWP) >15 mmHg (an indicator of increased left atrial pressure) (Guazzi & Borlaug, 2012; Hoeper *et al.*, 2013). The raised PCWP is what separates Group 2 from Group 1, as in PAH patients the left atrial pressure is normal but the precapillary arterial pressure is elevated. Group 3 PAH includes patients with connective tissue disease such as scleroderma as well as chronic obstructive pulmonary disease (COPD). In these patients alveolar hypoxia is detected by the pulmonary vasculature which constricts to divert blood to better ventilated regions of the lung. Ascent to altitude also causes pulmonary hypertension through the same mechanism although this is transient and reverses upon returning to lower altitudes.

Group 1 consists of patients with pulmonary arterial hypertension (PAH) (formerly called primary or idiopathic PAH). This is a relatively rare condition affecting between 5 and 50 people per 1 million adults (Humbert *et al.*, 2010; Ling *et al.*, 2012), in comparison the annual incidence of LV failure is around 1400-2300 per 1 million adults (McKee *et al.*, 1971). PAH affects more women than men, with estimates ranging between 1.7 and 4.1 females affected per male (Humbert *et al.*, 2010; Ling *et al.*, 2012). This may be due to prevalent cases of PAH as women survive with the condition for significantly longer than men; in the UK, females make up 70% of incident cases of PAH (Jacobs *et al.*, 2014). Survival in PAH is extremely poor and left untreated the 1, 3 and 5 year survival in patients is 68%, 48% and 34%, respectively (D'Alonzo *et al.*, 1991). This is worse than the survival of patients with *prevalent* LV failure found in the Framingham study (79%, 55%, 38% at 1, 3, 5 years) (McKee *et al.*, 1971). Treatment with the most effective current PAH therapies modestly improves survival to 83% and 58% at 1 and 3 years respectively (Humbert *et al.*, 2010).

1.6.2 Vascular remodelling in pulmonary arterial hypertension

Narrowing of the pulmonary arterioles due to vasoconstriction, hypertrophy and proliferation of smooth muscle cells increases pulmonary vascular resistance over time (Humbert *et al.*, 2004; Haddad *et al.*, 2008a). Excessive smooth muscle cell remodelling can eventually lead to fully muscularized vessels in which flow is

completely obstructed. Disorganized proliferation of monoclonal populations of endothelial cells creates plexiform lesions in patients with severe PAH (Stacher *et al.*, 2012) and occurs in some preclinical hypoxic models of PAH (Gomez-Arroyo *et al.*, 2011). Plexiform lesions seem to precede concentric luminal obliteration and while their direct haemodynamic effect is not known their presence may reflect a serious underlying fault in the endothelium. The causes of this can be multifactorial and can arise from one or a combination of genetic, neurohormonal, inflammatory, and acquired alterations to the pulmonary arterioles (Humbert *et al.*, 2004).

Vasoconstriction is thought to influence the early stages of PAH and has been related to impaired production of vasodilators such as nitric oxide (NO) and prostacyclin. NO is produced in endothelial cells from L-arginine via the action of endothelial NO synthase (eNOS). Activation of soluble guanylyl cyclase (sGC) by NO results in the production of cGMP from GTP which activates PKG resulting in downstream phosphorylation of Ca^{2+} handling proteins which decrease cytosolic Ca^{2+}. NO mediated vasodilation is reduced in pulmonary arteries of PAH patients due to decreased expression and activity of NO synthase, increased cGMP degradation by PDE5, and increased ROS which degrades NO reducing its bioavailability (Giaid & Saleh, 1995; Friebe & Koesling, 2003; Landmesser *et al.*, 2003).

The prostacyclin pathway is another potent stimulus for vasodilation of the pulmonary and systemic vasculature. Prostacyclin is primarily produced in vascular endothelial cells from arachidonic acid by the enzyme cyclooxygenase (Brock *et al.*, 1999). Upon release from endothelial cells it binds to prostacyclin receptors which are a type of GPCR on vascular smooth muscle cells resulting in the activation of PKA and increased Ca^{2+} removal from the cytosol. Expression of prostacyclin synthase is reduced in the endothelial cells of PAH patients which coincides with reduced circulating levels of prostacyclin metabolites (Humbert *et al.*, 2004).

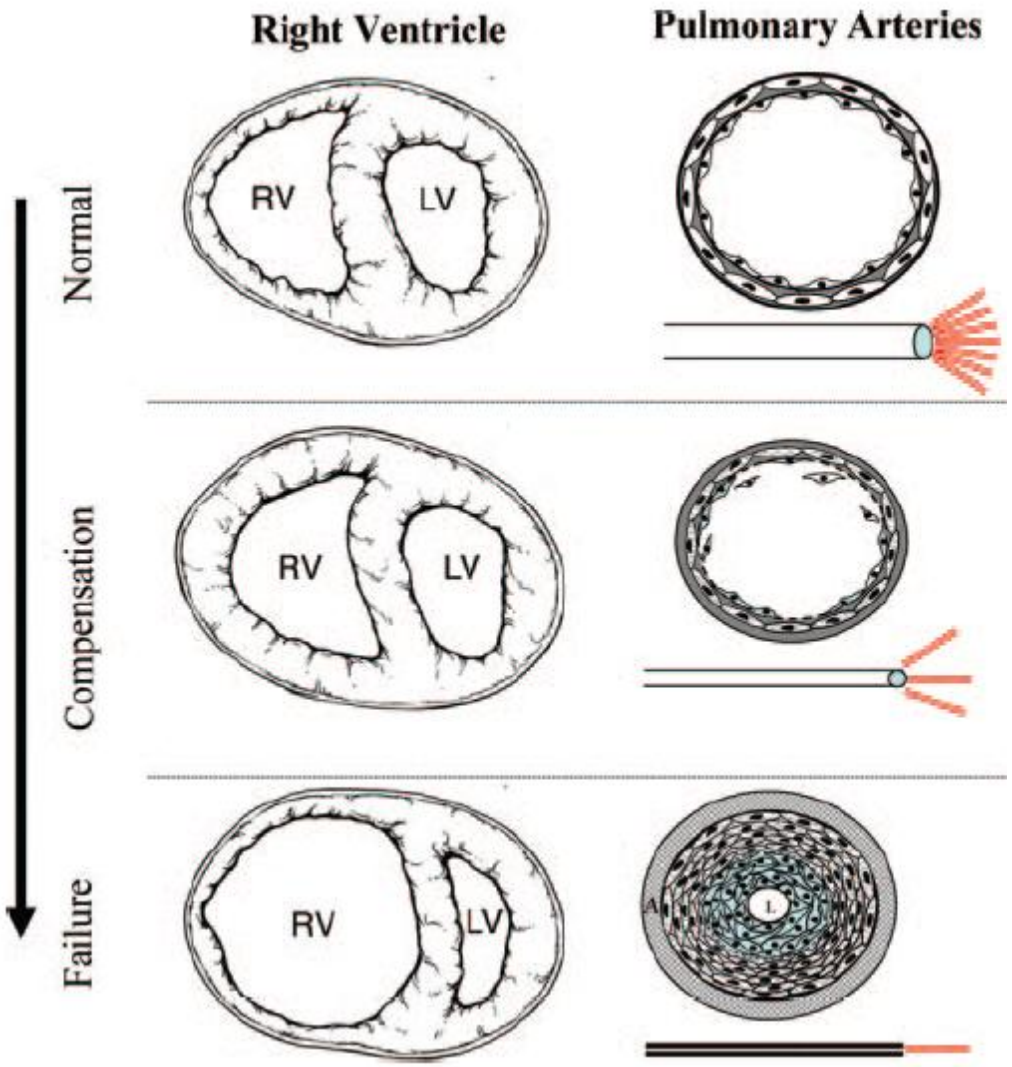

Figure 1.10 Progression of PAH and RV failure

The healthy RV pumps blood into compliant pulmonary arteries at low pressure. Dysfunctional pulmonary arteries are stiffer with a narrower lumen which increases resistance to blood flow. This is compensated for by RV hypertrophy to maintain cardiac output with raised systolic pressures. The RV eventually fails to cope with the worsening resistance and dilates into a low cardiac output state. Figure adapted from Champion *et al*. (2009).

Concomitant with reduced vasodilation is a rise in vasoactive peptides which induce constriction such as endothelin-1 (ET-1). ET-1 is a peptide produced by the vascular endothelium in response to diverse stimuli including angiotensin II, ROS and shear stress. ET-1 release from endothelial cells in the proximity of vascular smooth muscle cells binds to ET_A or ET_B receptors coupled to $G_{\alpha q}$ causing PKC activation and Ca^{2+} release from the SR (Wagner-Mann & Sturek, 1991). ET-1 and its receptors are upregulated in the vasculature of the MCT rat model and human PAH (Price *et al.*, 2012).

High circulating levels of noradrenaline have been reported in PAH patients which could initiate remodelling in the pulmonary vasculature through activation of α_1AR causing vasoconstriction and hypertrophy of smooth muscle cells through PKC. This is normally antagonized by β_1 and β_2AR however chronic activation of βAR leads to receptor internalization and downregulation (Faber *et al.*, 2006a). Mutations in the bone morphogenetic protein receptor 2 (BMPR2) gene which causes a truncation in the protein have been identified in 10-30% of patients with idiopathic PAH (Deng *et al.*, 2000), and BMPR2 protein is also decreased in PAH patients without mutations (Atkinson *et al.*, 2002). BMPs are part of the transforming growth factor-β1 family of proteins and inhibit pulmonary artery derived smooth muscle cell proliferation, therefore reduced signalling through this pathway could contribute to the concentric obliteration of arterioles (Yang *et al.*, 2005).

1.6.3 Right ventricle failure

Most research on remodelling in heart failure has been conducted in the LV and while there are certainly correlates with RV failure a direct extrapolation cannot be assumed due to the different normal physiology of the two chambers as well as the distinct embryological origin of the constituent cells (Haddad *et al.*, 2008b). A 2006 report from the US National Heart, Lung and Blood Institute recognized that experiments specifically on the failing RV were needed (Voelkel *et al.*, 2006). The thin-walled and highly compliant RV which supplies the pulmonary circulation responds poorly to increased afterload and SV suffers as a consequence (Abel & Waldhaus, 1967). The response of the RV to chronically elevated afterload is to undergo a complex process of structural, excitation-contraction coupling, and metabolic remodelling which are initially compensatory but ultimately become pathological (Figure 1.10). These changes are promoted partly through mechanical stresses experienced by cardiomyocytes but also through increasing reliance on catecholamines to provide the

inotropic support needed to maintain ventriculo-arterial coupling (Handoko *et al.*, 2010; Naeije & Manes, 2014).

It was initially thought the RV was merely a passive receptacle of blood as the heart can function normally for a short time without a working RV when unstressed (Starr *et al.*, 1943), however RV function becomes critical when load is increased (Lowensohn *et al.*, 1976). Accordingly, RV failure is the leading cause of death in PAH patients (Delcroix & Naeije, 2010), and is also a key determinant of survival in LV failure (Kjaergaard *et al.*, 2007; Szwejkowski *et al.*, 2012; Ghio *et al.*, 2013). For instance, increased RV end-diastolic diameter and decreased ejection fraction measured using echocardiography are associated with significantly worse survival in patients with PAH and chronic LV failure (Ghio *et al.*, 2010; Ghio *et al.*, 2011; Ghio *et al.*, 2013). Similarly, Rain *et al.* (2013) found that in PAH patients decreased RV diastolic compliance was closely associated with markers of disease severity (exercise capacity and stroke volume) which are associated with worse survival (van de Veerdonk *et al.*, 2011). Therefore there is great interest in identifying the cellular causes of RV dysfunction and failure and possible therapies which prevent or reverse these changes.

1.7 Therapies for pulmonary arterial hypertension

There is currently no cure for PAH except a lung or heart-lung transplant which immediately lowers vascular resistance removing the excess load on the heart and allows RV structure and function to return to normal (Katz *et al.*, 1996; Perrin *et al.*, 2015). This is clearly not an option in most patients due to scarcity of donor organs and recipient compatibility, therefore most patients receive one or a combination of drugs which target the vasculature and aim to improve vasodilation and reduce the afterload on the RV (Figure 1.11) (Perrin *et al.*, 2015). Currently approved specific therapies include prostanoids, endothelin (ET) receptor antagonists and phosphodiesterase-5 (PDE-5) inhibitors which target three separate pathways to induce vasodilation or prevent vasoconstriction. Treatment with any one of these therapies reduces the risk of mortality by around 40%, but there is little difference in efficacy between treatments (Galiè *et al.*, 2009), and combination therapy with two or all three treatments does not consistently improve morbidity or mortality beyond that achieved by monotherapy (Ghofrani *et al.*, 2003; McLaughlin *et al.*, 2014; Sitbon *et al.*, 2014). Patients who respond positively to treatment and show decreased vascular resistance may still deteriorate and RV function seems to be a more important determinant of outcome (van de Veerdonk *et al.*, 2011). New drugs have come on the

market in recent years however these have all been refinements of existing drugs which act on the same three pathways; with this in mind it is clear more therapeutic options are needed if progress is to be made in the treatment of PAH patients. The clear prognostic relevance of RV function and lack of therapies which target the RV in PAH has led to calls for further research into therapies which target the failing RV (Naeije, 2010); β-blockers in particular have garnered interest due to their beneficial effect in slowing maladaptive remodelling and reducing mortality in LV failure (Handoko *et al.*, 2010; Andersen *et al.*, 2015).

1.7.1 General therapies

Ca^{2+} channel blockers reduce the entry of Ca^{2+} into smooth muscle cells in the pulmonary arterioles causing vasodilation. Some studies have found the Ca^{2+} channel blockers diltiazem and nifedipine improve function in a subset of patients who are responsive to other vasodilating therapies (Sitbon *et al.*, 2005; Montani *et al.*, 2010), however no long term randomized controlled trials have demonstrated a survival benefit to Ca^{2+} channel blockers and bradycardia and systemic hypotension can occur as side effects. Anti-coagulants may be prescribed due to the increased risk of thrombi forming in inactive patients, particularly those receiving prostacyclins via an indwelling cannula. Diuretics may relieve some symptoms of systemic congestion and peripheral oedema, however large studies have not consistently found a survival benefit resulting from such therapy. No large scale randomized controlled trials have investigated the effect of exercise in PAH, unlike LV failure where moderate or intense exercise is safe and actively encouraged (Rognmo *et al.*, 2012). Small studies have found improvements in fatigue severity in PAH patients undergoing 10 weeks of low intensity exercise (Weinstein *et al.*, 2013) and a recent preclinical study found improved survival in MCT rats given access to running wheels (Natali *et al.*, 2015), and exercise has recently become encouraged within symptom limits (Galiè *et al.*, 2015b).

1.7.2 Prostacyclin analogues

Prostacyclin analogues bind directly to prostacyclin receptors initiating vasodilation of the pulmonary and systemic vascular beds. Intravenous infusion of epoprostenol, a synthetic mimetic of prostacylin, was shown to lower pulmonary arterial pressure in patients with PAH in a randomized control trial over 18 months (Rubin *et al.*, 1990), and became the first FDA-approved therapy for PAH in 1995. Tachyphylaxis is reported to

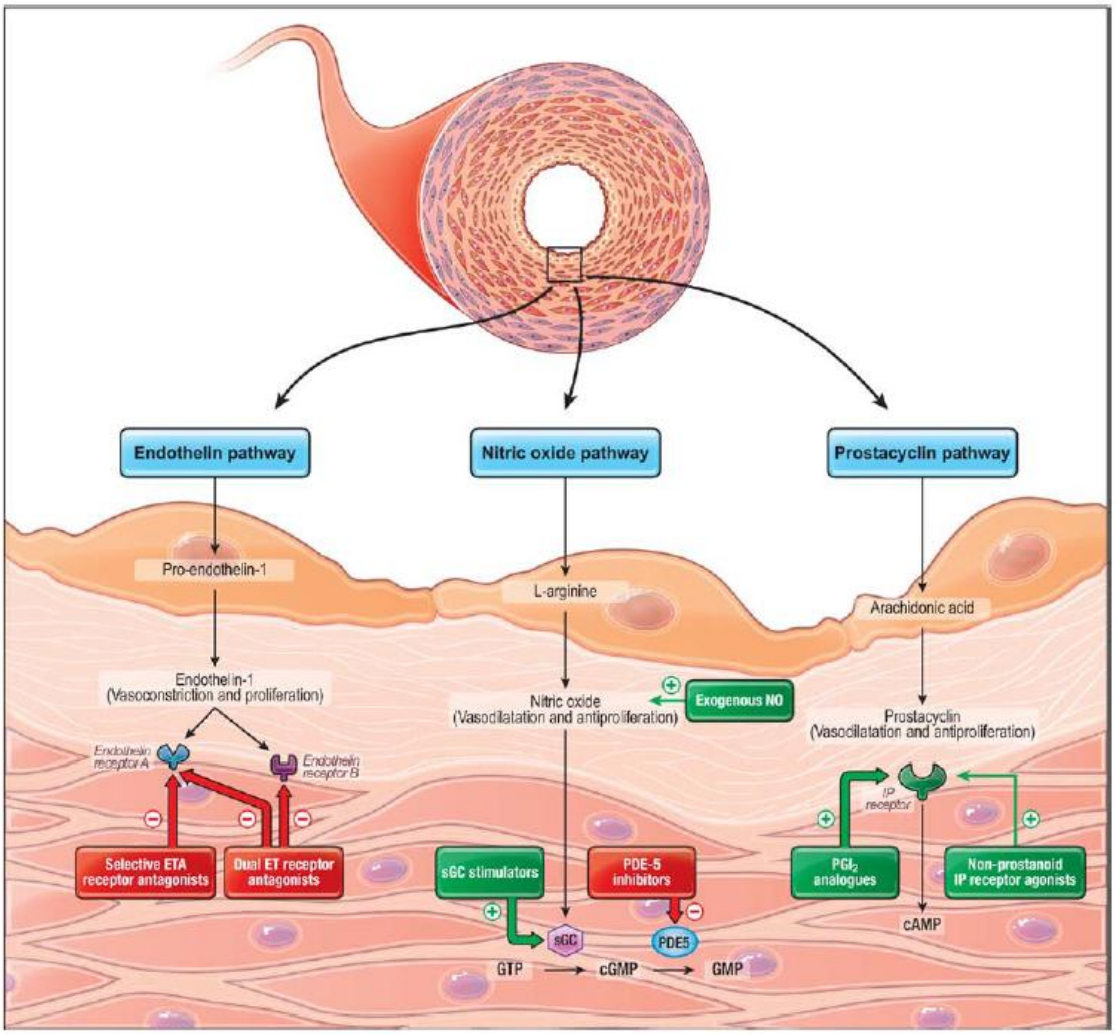

Figure 1.11 Vasodilating therapies in PAH

Drugs targeting the endothelin, nitric oxide and prostacyclin pathways are the only treatments shown to improve survival in human PAH. Figure from Humbert *et al.* (2014)

occur with epoprostenol due to internalization of the prostacyclin receptor, requiring up-titration of dose, however this may also reflect clinical worsening of PAH. Prostacyclins have a short half-life of 3-5 min and therefore require continual intravenous infusion via an indwelling cannula which carries the risk of catheter-related sepsis. For these reasons long-term intravenous prostacyclin therapy is usually not possible. The most recently available drug for PAH is selexipag, approved by the FDA in 2015, and is the first effective oral prostacyclin analogue. In a Phase III clinical trial selexipag reduced mortality in PAH patients receiving either ET antagonist or PDE-5 inhibitors by 40% (McLaughlin *et al.*, 2015).

1.7.3 Endothelin antagonists

The ET receptor anatagonist bosentan (non-selective ET_A and ET_B) was approved for use in PAH in 2001 and later ambrisentan (selective ET_A) in 2007. Treatment with bosentan for up to 12 weeks prevented clinical worsening and improved exercise capacity in patients with PAH (Rubin *et al.*, 2002). Bosentan is metabolized by CYP3A4 and is also an inducer of this enzyme, therefore certain other drugs may become ineffective if given in combination.

1.7.4 Nitric oxide pathway

PDE5 is highly expressed in the pulmonary vasculature of PAH patients and degrades cGMP thus reducing the vasodilating effect of NO. There are two PDE5 inhibitors currently approved for use in PAH: tadalafil (approved in 2003) and sildenafil (approved in 2007). PDE5 inhibitors prevent the degradation of cGMP thus increasing PKG activity and vasodilation. Sildenafil and tadalafil produce a similar reduction in mortality, although some patients do not respond to treatment due to a lack of endogeneous NO production (Giaid & Saleh, 1995; Galiè *et al.*, 2009). Certain beneficial effects of sildenafil have been attributed to a direct effect on the RV myocardium, however chronic sildenafil exacerbated hypertrophy in a rat model of PAH with a fixed afterload, suggesting the survival benefits are primarily due to the afterload lowering effect (Andersen *et al.*, 2008). The major route for both sildenafil and tadalafil metabolism is oxidation via CYP3A4. A new class of sGC activators has recently been developed as an alternative to PDE5 inhibitors which bypasses the need for NO synthesis and promotes cGMP production rather than preventing its degradation. Riociguat was granted FDA approval in 2013 and a randomized controlled trial of over

400 PAH patients found improvements in haemodynamics, exercise capacity and time to clinical worsening (Ghofrani *et al.*, 2013).

1.7.5 β-adrenoceptor blockers?

There is substantial clinical evidence of over-activation of the sympathetic axis in patients with PAH, including: increased circulating levels of noradrenaline, decreased heart rate variability, decreased RV β_1AR expression (see Kurzyna and Torbicki (2007), Maron and Leopold (2015) and references therein). In addition the degree of sympathetic activation in patients correlates with the severity of haemodynamic compromise (Nootens *et al.*, 1995). Similar findings have been reported in preclinical models of PAH which have further shown increased GRK2 expression (Piao *et al.*, 2012), decreased basal levels of cAMP (Seyfarth *et al.*, 2000) and decreased inotropic response to β_1-AR agonists (Vescovo *et al.*, 1989). Given the obvious parallels with chronic adrenergic activity in LV failure it is surprising β-blockers have not been the subject of large clinical trials in PAH patients. The most recent European Society of Cardiology guidelines for the treatment of PAH go as far as to state β-blockers are not recommended in PAH unless required to treat comorbidities (Galiè *et al.*, 2015b).

This hesitance to use β-blockers in PAH is often justified on the basis of a highly cited study by Provencher *et al.* (2006b) showing improved exercise capacity 2 months after withdrawal of propranolol from 10 PAH patients with portopulmonary hypertension. However this finding was likely influenced by an acute inotropic effect of withdrawal of β-blockers and the use of a non-selective β_1/β_2 blocker which may have aggravated pulmonary vasoconstriction. A case study by Peacock and Ross (2010) describing a patient with portopulmonary hypertension who developed severe systemic hypotension when administered metoprolol is also a source of anxiety, however this extreme response was most likely due to inhibition of metoprolol breakdown by other medications. The most compelling argument against β-blockers in PAH is the relatively high load-dependence of RV SV, meaning cardiac output in PAH patients is highly dependent on heart rate (Abel & Waldhaus, 1967; Groepenhoff *et al.*, 2010), and therefore negative chronotropic effects could lead to ventriculo-arterial uncoupling as was reported in an animal study (Brimioulle *et al.*, 2003). It is worth noting this same argument was first made against using β-blockers to treat LV failure, as contemporary thinking was that inotropic support was needed to treat heart failure, however ultimately this proved to increase mortality (Packer *et al.*, 1984; Packer, 1993). It took 25 years from the development of propranolol by Sir James Black in 1964 to the first

demonstrated long-term survival benefit from chronic metoprolol in LV failure (Black *et al.*, 1964; Waagstein *et al.*, 1989); what is currently unknown is the long term effect of chronic β-blocker treatment in PAH as no clinical trials have tested this.

Despite the two aforementioned reports there is growing interest in the therapeutic potential of β-blockers in PAH. Recent retrospective analyses of PAH patients receiving β-blockers for co-morbidities have revealed no clinical worsening compared to patients without β-blockers (So *et al.*, 2012; Thenappan *et al.*, 2014; Bandyopadhyay *et al.*, 2015), however these matched but non-randomised cohort studies were not designed to answer the question of whether β-blockers are *beneficial* in PAH. Evidence of beneficial effects comes from a small number of preclinical investigations showing improvements in RV function and survival in rats with PAH (Bogaard *et al.*, 2010; de Man *et al.*, 2011; Perros *et al.*, 2015). On this basis further study into the mechanisms underlying the putative benefits of β-blockers in PAH is warranted.

Metoprolol (1-[4-(2-methoxyethyl)phenoxy]-3-(propan-2-ylamino)propan-2-ol) is a competitive β_1-selective adrenergic receptor blocker which lacks sympathomimetic properties and is an inverse agonist (Maack *et al.*, 2000) (Figure 1.12). It was first synthesized by the *para*-substitution of phenoxy-hydroxypropylamines (Brandstrom *et al.*, 1976). In cats it was shown to be cardioselective as it caused a negative chronotropic response to isoprenaline infusion but did not inhibit isoprenaline-induced systemic vasodilation or bronchial smooth muscle relaxation (Åblad *et al.*, 1973). In humans metoprolol exhibits β_1AR selectivity at low doses but spills over into β_2AR block at higher doses (Zebrack *et al.*, 2009). Non-specific block of β_2AR may be ameliorated by the use of controlled-release metoprolol succinate rather than the rapidly available metoprolol tartrate (Kendall *et al.*, 1990). A target dose of 200 mg per day, as used by the Metoprolol CR/XL Randomised Intervention Trial in Congestive Heart Failure (MERIT-HF) study, is currently recommended in left heart failure, although the actual dose achieved in that study was only 159 mg per day (Hjalmarson *et al.*, 2000; López-Sendó *et al.*, 2004). A subgroup analysis of MERIT-HF revealed some patients were more sensitive and achieved an equivalent heart rate reduction and survival benefit from a lower mean dose of 76 mg per day, compared to patients who tolerated a high dose (mean 192 mg per day); this may be due to genetic polymorphisms encoding the CYP2D6 enzyme affecting the rate of drug clearance from blood plasma (Wikstrand *et al.*, 2002; Wojtczak *et al.*, 2014).

Isoprenaline

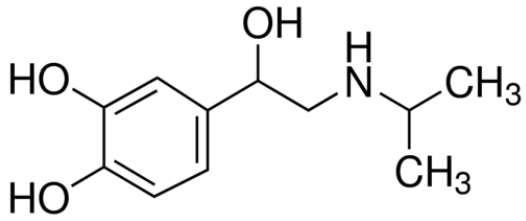

Metoprolol

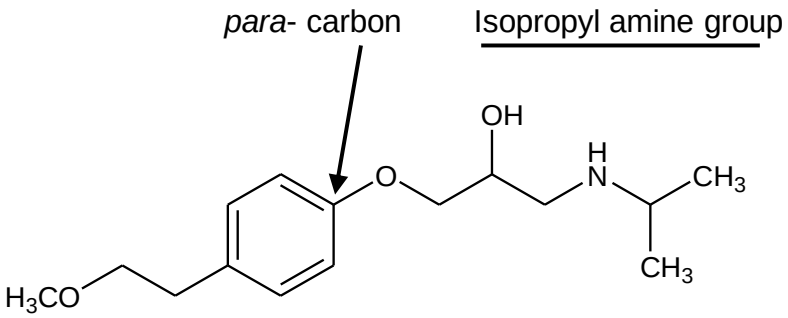

Figure 1.12 Structure of β-receptor agonist, isoprenaline, and antagonist, metoprolol

The isopropyl amine group of isoprenaline and metoprolol confers specificity to β-receptors. Isoprenaline structure from Sigma-Aldrich (http://www.sigmaaldrich.com/catalog/product/sigma/i5627) and metoprolol structure from DrugBank (http://www.drugbank.ca/drugs/DB00264) Accessed 09/12/2015.

The ability of metoprolol to significantly improve survival and function in left heart failure (Hjalmarson *et al.*, 2000), increase expression of β_1AR (Gilbert *et al.*, 1996), improve Ca^{2+} handling irregularities (Chen *et al.*, 2012) and avoid broncho- and vasoconstriction in the pulmonary vasculature which could occur with non-selective β-blockers (Åblad *et al.*, 1973) makes it an ideal β-blocker for trial in PAH. Metoprolol is unlikely to affect vascular resistance therefore any functional gains should occur by directly increasing RV contractility. Furthermore, metoprolol is the most widely prescribed β-blocker therefore if found beneficial in PAH these results will have the immediacy of translation into clinical trials.

1.8 Preclinical models of pulmonary arterial hypertension

Animal models of cardiovascular disease can never fully replicate all aspects of the human condition, however different models may lend themselves more to particular aspects of a disease and all have provided invaluable insight into the processes and pathways underpinning pathological remodelling.

1.8.1 Pulmonary artery banding

Pulmonary artery banding (PAB) involves the surgical placement of a ligature or metal clip around the pulmonary trunk which increases the afterload experienced by the RV but which leaves the pulmonary vasculature distal to the clip unaffected. As the afterload is fixed this is an ideal model for studying direct effects of drugs on the RV in numerous species including mice, rats, cats, dogs and bovines. With the exception of immediate mortality following surgery, PAB generally results in a compensated RV hypertrophy without significant mortality (Faber *et al.*, 2006b; Borgdorff *et al.*, 2013). This may occur due to the sudden, proximal occlusion of the pulmonary artery which also tends to be better tolerated in humans, for instance in the case of pulmonary thromboembolism. Alternatively PAB can be performed on young animals such that as the animal grows there is progressive constriction of the pulmonary artery (Bogaard *et al.*, 2009). This also results in a compensated hypertrophy which might reflect the adaptive capacity of the RV to overload early in life, such as in the case of congenital heart defects which are generally less detrimental than acquired PAH. Downsides to this model include the highly invasive procedure and microsurgical expertise required.

1.8.2 Chronic hypoxia

Hypoxic or hypobaric chambers have been used to simulate high altitude hypoxic vasoconstriction in rats and calves which results in mild PAH (Meyrick & Reid, 1980; Walker *et al.*, 2011b). A more severe phenotype can be induced by injecting the VEGF inhibitor Su-5416 prior to the start of hypoxia (SuHx). VEGF promotes survival in endothelial cells during hypoxia, however blocking VEGF selects for a population of apoptosis-resistant proliferating endothelial cells. This results in obstructive vascular remodelling and is one of the few models of PAH which produces plexiform lesions. Severe PAH results which progresses to RV failure and death in some but not all animals after 8 weeks or longer (Taraseviciene-Stewart *et al.*, 2001). The similarities between vascular remodelling in SuHx and human PAH make it an ideal model to study the role of the pulmonary vasculature in PAH.

1.8.3 Monocrotaline

Monocrotaline (MCT) is a pyrrolizidine alkaloid isolated from the seeds of the *Crotalaria spectabilis* plant and is commonly used as a model of progressive PAH in rats. MCT is typically injected in its inactive form intraperitoneally into 200-250 g rats at a dose corresponding to 60-80 mg/kg which is sufficient to induce PAH, RV hypertrophy and overt right heart failure within 3-4 weeks (Lamberts *et al.*, 2007a; de Man *et al.*, 2011). Lower doses of 30-40 mg/kg result in a compensated hypertrophy without overt heart failure and have been used to study the long term effects of PAH on the RV and LV (Benoist *et al.*, 2012; Ruiter *et al.*, 2013). Higher doses of 80-300 mg/kg have also been used but may cause acute lung injury, interstitial pulmonary fibrosis and hepatic veno-oclusive disease (Copple *et al.*, 2003). In the liver MCT is oxidized by mixed function cytochromes P450 CYP3A4 to the short-lived reactive MCT pyrrole compound (Mattocks *et al.*, 1990; Kasahara *et al.*, 1997); induction of these enzymes increases the production of MCT pyrrole (Reid *et al.*, 1998). The active MCT pyrrole enters the venous circulation then is pumped by the RV into the pulmonary vasculature. MCT damages the endothelial cells of pulmonary arterioles in its first pass through the pulmonary vascular bed resulting in apoptosis, although the exact mechanism through which this occurs is not yet clear. This damage to the endothelium impairs barrier function allowing infiltration of macrophages and initiates a cascade of proliferation and remodelling of the underlying smooth muscle cells eventually resulting in lung fibrosis (Pleština & Stoner, 1972; Pan *et al.*, 1993; Sahara *et al.*, 2007). Loss of endothelial NO synthase, release of proliferative growth factors and inhibition of BMPRII through

loss of caveolae have been observed in endothelial cells exposed to MCT which initiates a process of smooth muscle cell proliferation, constriction and hypertrophy (Ramos *et al.*, 2007; Huang *et al.*, 2010). Due to its short half-life the systemic circulation is not directly affected by MCT and total peripheral resistance is unchanged (Correia-Pinto *et al.*, 2009). It has been suggested that MCT also damages the hepatic veins causing fibrotic occlusion and hepatic congestion, however this appears to occur at very late stages of the disease (Roth *et al.*, 1981; Gomez-Arroyo *et al.*, 2012); furthermore the reduction in liver weight of rats treated with a low dose of 40 mg/kg MCT is reversible beyond 4 weeks, arguing against hepatic veno-occlusion as the cause of death in rats (Ruiter *et al.*, 2013). MCT causes more severe PAH in male rats compared to female rats, therefore male rats are typically used to study RV failure. Ovariectomised female rats injected with MCT develop similar pulmonary artery pressures and RV hypertrophy as male rats, whereas infusion of metabolites of estrogen is protective against vascular remodelling in male MCT rats (Tofovic *et al.*, 2005; Yuan *et al.*, 2013). The protective effect of estrogen against PAH may be through elevating levels of antioxidant enzymes in the pulmonary vasculature (Bal *et al.*, 2013).

1.9 Study aims

This study aims to test the hypothesis that β_1-AR blockade is beneficial to survival and RV function in the rat MCT model of PAH. The MCT model was chosen as it is a well-characterised model of RV failure which consistently recapitulates many of the pathological changes reported in human RV failure and does so within a relatively short period of time, while reducing animal suffering due to its minimally invasive nature. The β_1 AR blocker metoprolol was chosen because the detrimental effects of noradrenaline are primarily mediated through the β_1 signalling pathway; it has been proven to significantly reduce mortality in LV failure (Waagstein *et al.*, 1993; Hjalmarson *et al.*, 2000) as effectively as more expensive non-selective β-blockers (Tang *et al.*, 2003; Fröhlich *et al.*, 2015) and its effects show greater selectivity for the myocardium than the pulmonary vasculature. The specific aims and hypotheses to be tested were:

I. To establish a chronic metoprolol treatment regime which improves survival in established rat MCT PAH.

II. Using *in vivo* techniques, characterise the function and remodelling of the RV in PAH compared to healthy rats, and test whether these were improved by metoprolol treatment.

III. To test whether altered energy metabolism was a source of contractile dysfunction in the failing RV and if so, whether this was improved by metoprolol.

IV. To test whether metoprolol restores dysfunctional excitation-contraction coupling in failing RV cardiomyocytes.

V. To test whether a shorter sarcomere length increase the likelihood of Ca^{2+} waves occurring.

There has been little investigation into the mechanisms underlying the salutary effect of β-blockers in PAH; the work contained in this thesis aims to address this gap in knowledge and comes during a resurgence of interest in β-blockers as a potential therapy (Andersen *et al.*, 2015; Bandyopadhyay *et al.*, 2015; Bristow & Quaife, 2015; Perros *et al.*, 2015).

Chapter 2 Methods

2.1 Monocrotaline model of pulmonary artery hypertension

Monocrotaline (MCT; Sigma, UK) was prepared fresh on the day of injection by dissolving 68 mg MCT in a small volume of 1 M HCl with 140 mM NaCl, pH was adjusted to 7.4 with 5 N NaOH, the final concentration of MCT was 20 $mg.mL^{-1}$.
Male Wistar rats bred at the University of Leeds weighing 200 ± 20 g were given an intraperitoneal injection of 60 mg/kg MCT to induce PAH, or an equivalent volume of 140 mM saline for control (CON) rats. Milli-Q grade water was used for all experiments. Rats were housed three per cage at 20-22°C in 50% humidity on a 12 h light/dark cycle with *ad libitum* access to food and drinking water. Rats were weighed and checked for signs of heart failure twice per week from the day of MCT injection (day 0) then daily from day 21 onwards. FAIL rats were killed upon showing symptoms of heart failure such as cachexia (10 g in one day or 20 g over several days), lethargy, dyspnoea, cold extremities or piloerection. Experiments in CON rats were performed on temporally equivalent days. Experiments were conducted in accordance with the Animals (Scientific Procedures) Act (1986) and local ethical approval.

2.2 Chronic treatment with metoprolol

The goal of this work was to establish a β-blocker treatment regime therefore we first attempted to replicate the treatment regime of Bogaard *et al.* (2010) but for reasons described in Appendix A a *de novo* regime had to be devised; the results from this first attempt are presented in Appendix A. Rats were trained to drink a placebo solution containing 20% (v/v) Ribena and 10% (w/v) sucrose (placebo) voluntarily from a 1 mL syringe starting several days after MCT or saline injection. Chronic treatment with metoprolol tartrate (10 mg/kg/day; Santa Cruz Biotechnology, TX) was initiated 15 days after MCT injection (MCT+BB and FAIL+BB groups), when PAH and hypertrophy are already established (Lee *et al.*, 1997; Jones *et al.*, 2002). Metoprolol was dissolved in placebo at a concentration of 1.25 mg/mL, which was found to be the highest concentration rats would willingly consume without displaying an aversion to taste (Figure 2.1). Dosing was administered within 2 h prior to the start of the dark cycle. Daily dose volume was around 2.5 mL and adherence was calculated from any remaining unconsumed solution in the syringe. The target dose was well adhered to by all rats, however 3/9 FAIL+BB rats reduced their consumption in the days leading up

Figure 2.1 Drug treatment by voluntary syringe feeding

Rats were trained to voluntarily drink from a 1 mL syringe containing placebo solution, or placebo plus metoprolol (1.25 mg/mL). The volume was adjusted daily to achieve a target dose of 10 mg metoprolol/kg body weight/day. Rats were fed within the 2 h preceding the start of the dark (active) cycle.

to failure. Metoprolol and placebo solutions were prepared fresh every 2 days and covered in aluminium foil to prevent photoinactivation of metoprolol.

2.3 In vivo characterisation of right ventricle function

2.3.1 Anaesthesia

Rats were anaesthetised in a Perspex chamber ventilated with 5% isoflurane (IsoFlo, Abbott Laboratories, IL) mixed with medical O_2. Anaesthesia was confirmed by the lack of pedal-withdrawal reflex in response to a toe-pinch. Rats were transferred to a heated platform and secured in a supine position with pieces of autoclave tape over the paws. Anaesthesia was maintained under ~1.5% isoflurane and adjusted according to breathing frequency. The chest was shaved with electric clippers and depilatory cream applied to remove remaining hair. For recovery experiments, rats were allowed to awaken on the heating pad while breathing medical O_2.

2.3.2 Echocardiography

Serial non-invasive transthoracic echocardiography was performed on anaesthetised rats using a Vivid7 ultrasound (GE Healthcare, WI) with a curvilinear 11.5 MHz 10s probe (GE Healthcare, WI). Ultrasound gel (Cardiacare, Essex, UK) was generously applied to the shaved chest, taking care to avoid air bubbles. The probe was lightly pressed against the chest and oriented to view the heart in transverse cross-section. Geometry of the RV and LV were measured using brightness (B-) and motion (M-) modes taken from the parasternal short axis (PSAX) view at the level of the LV papillary muscles. Imaging depth was set to 2 cm with a data recording rate of 100 Hz. Care was taken to avoid reflections and shadows in the viewing window due to the lungs and ribs.

Two-dimensional B-mode and one-dimensional M-mode measurements were taken when chamber area or diameter was greatest in diastole and smallest during systole. RV and LV areas were measured in B-mode by tracing the endocardium of the ventricles. The LV endocardial perimeter was measured to calculate the LV circularity index (LVSCI), which is an indicator of the mechanical interaction between the RV and LV across the septum and reflects the trans-septal pressure gradient (Portman *et al.*, 1987). The LVSCI quantifies how circular the LV is during systole as a percentage, 100% being a perfect circle, and is calculated by:

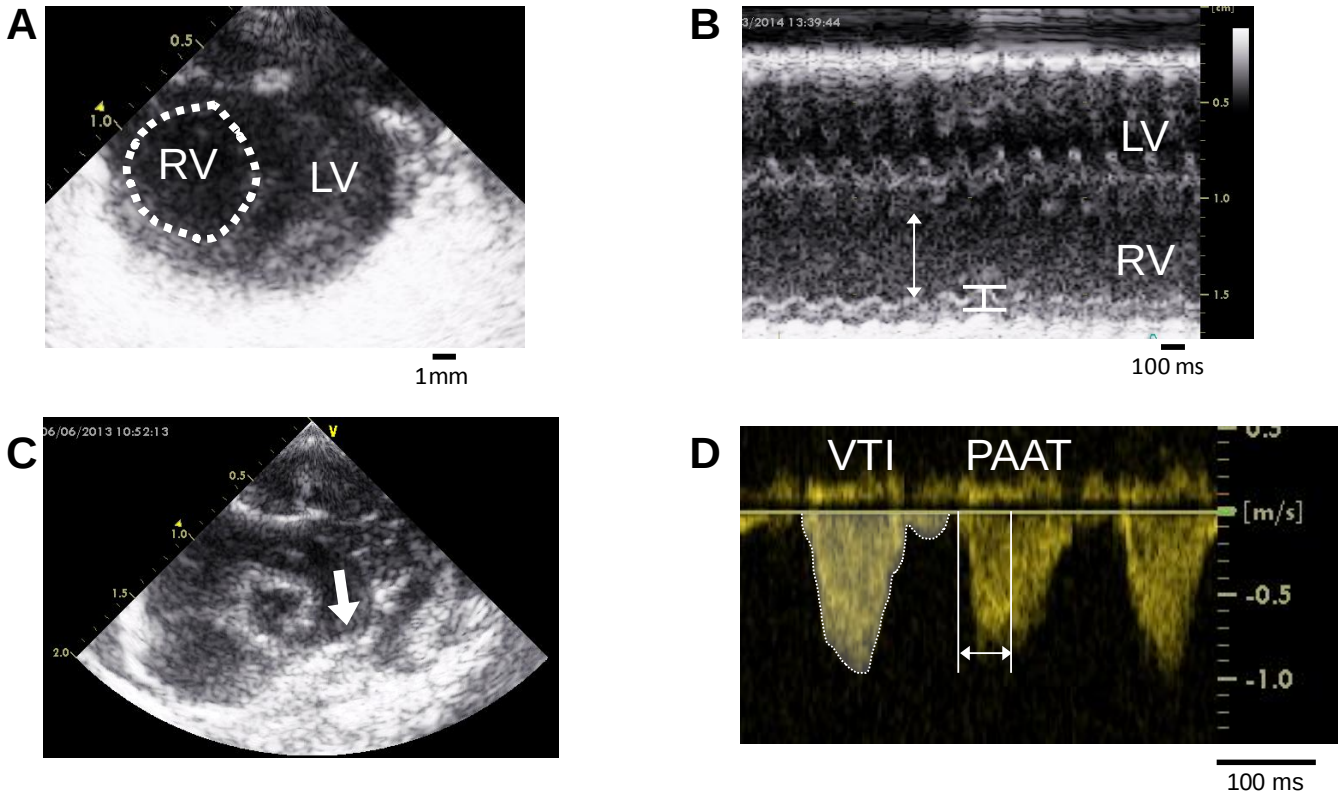

Figure 2.2 Echocardiography measurement modes

A 2D B-mode images were used to calculate chamber areas (*white dashed line*). **B** Wall thickness (*white line, flat caps*) and chamber diameter (*white line, arrow caps*) were measured in M-mode. **C** The PA blood flow was measured 1-2 mm from the pulmonary valve leaflets, parallel to the direction of blood flow (*white arrow*). **D** Blood flow through the PA was measured using Doppler ultrasound. PA acceleration time (PAAT) was measured from the onset of flow to peak forward velocity. Velocity-time integral was measured from the start to the end of systolic blood flow.

$$LVSCI = \frac{4 \times \pi \times LVA_s}{C^2} \times 100$$

Where LVA_s = LV end-systolic area and C = LV chamber perimeter at end-systole. M-mode images were constructed by stacking the pixel values along a line bisecting the heart through the RV, septum and LV as a function of time. Wall thickness, chamber diameter and pulmonary artery diameter (PAD) were measured in M-mode.

Pulmonary artery (PA) blood flow was measured using Doppler ultrasound taken from the PSAX view near the base of the heart at the level of the pulmonary arch (Figure 2.2). The Doppler effect is a shift in wave frequency occurring when a wave passes through a medium moving relative to the observer. This property of sound is utilised in pulsed-mode Doppler echocardiography to measure blood flow through arteries and across the heart valves by alternating the transducer crystal between transmitting and recording signals. The shift in frequency of the returning wave is processed online using a fast Fourier transform and converted to flow velocity by solving the Doppler equation (Lewis *et al.*, 1984):

$$V = \frac{\Delta F \times V_m}{2F_o \times Cos\theta}$$

Where V = blood velocity (m/s), ΔF = frequency shift, V_m = the speed of sound in the medium (approximately 1540 m/s in tissue and blood), F_0 = emitting frequency of the transducer (11.5 MHz), θ = angle of incidence between sound waves and direction of blood flow. When θ<20° it has minimal influence on the calculated velocity (Feigenbaum, 2004); images were acquired from a region of the PA with maximal laminar flow, therefore no angle correction was applied and θ was assumed to be 0° (Cos (0) = 1). The B-mode image screen rate is reduced to 6 Hz during Doppler ultrasound to allow correct positioning of the transducer. Data were recorded from a 1 mm sample volume placed 1-2 mm from the PA valve leaflets.

Pulmonary artery acceleration time (PAAT) was measured from the onset to the peak of systolic flow. The PA velocity-time integral (VTI) was measured from the start to the end of systolic flow. Cardiac output was calculated by multiplying stroke volume (SV) by heart rate. RV SV was calculated from the VTI and PAD, assuming a circular PA cross-sectional area:

$$SV\ (\mu L) = VTI\ \times \left(\frac{PAD}{4}\right)^2 \times 1000$$

The cardiac index was calculated as the ratio of cardiac output to body surface area (BSA). BSA was predicted according to Meeh's formula, where *k* is an empirically derived constant (9.83) and *W* is body weight in grams (Gouma *et al.*, 2012):

$$BSA\ (cm^2) = kW^{2/3}$$

Each echocardiography examination was assigned a unique identifier consisting of a computer-generated 5-digit random number, allowing image analysis to be performed blinded to the group and time point of the rat. Each parameter was measured offline from a total of 9 cardiac cycles from 3 separate video files and the mean value calculated and used for subsequent statistical analyses.

2.3.3 Right heart catheterisation

In some cases following the ultrasound scan an experienced investigator (Dr Mark J Drinkhill) performed terminal right heart catheterisation to measure *in vivo* RV haemodynamics in anaesthetised and mechanically ventilated rats. Body temperature was maintained using a heating lamp positioned above the rat. Pressure was calibrated before the start of the experiment using a mercury manometer. The chest was opened with a medial sternotomy and the heart exposed. The RV free wall was pierced with a needle close to the apex and a Millar pressure-volume catheter (SPR-869, Millar Instruments, TX) inserted transmurally into the RV chamber and secured in place with suture thread. Load-independent parameters of contractile function were obtained by transient occlusion of the ascending vena cava. The end-diastolic and end-systolic pressure-volume relationships were fitted with a linear regression to calculate the slope. Pulmonary vascular resistance (PVR) was calculated according to the following equation, assuming a constant LV diastolic pressure of 8 mmHg (as found by Correia-Pinto *et al.* (2009) in up to 6 weeks post injection of 60 mg/kg MCT in rats). PVR was expressed in Wood units (mmHg.min.mL^{-1}):

$$PVR = \frac{mean\ RV\ pressure - LV\ diastolic\ pressure}{cardiac\ output}$$

Time-varying volume, V(t), was calculated from the time-varying conductance, G(t), measured between two outer and two inner ring electrodes separated by a fixed distance, L, and the resistance of blood, ρ, measured after the experiment in a cuvette (P/N 910-1048, Millar Instruments, TX) filled with a known volume of fresh heparinized blood. Uncorrected volume was thus given by:

$$V(t) = L^2 \, \rho G(t)$$

The myocardium and lungs also conduct electricity, therefore volumes were corrected by subtracting non-blood sources of conduction, termed parallel conductance (G_P) (Baan *et al.*, 1984). G_P was calculated by infusing a 20 µL bolus of hypertonic saline into the left jugular vein to increase the conductivity of the blood without altering ventricle volume or the properties of the surrounding tissue. During the period of saline infusion the apparent end-diastolic volume (V_{ED}) is plotted against end-systolic volume (V_{Es}) and fitted with a linear regression. G_P is found by solving the equation of this line to find the point of intersection with the line of equivalence ($V_{ED} = V_{ES}$). The point of intersection represents conductance due to non-blood sources. Thus, blood volume corrected for parallel conductance becomes:

$$V(t) = L^2 \, \rho(G(t) - G_P)$$

An additional factor, α, may be incorporated to account for the fact volumes measured by conductance catheter generally underestimate true volumes due to the apical and basal volumes not being measured and inhomogeneity of the electrical field due to the use of point-source electrodes (Cardozo *et al.*, 2003). α can be calculated from the ratio of stroke volume measured by an independent method such as thermodilution, to stroke volume measured by conductance catheter. The resulting absolute corrected ventricle volume would therefore be:

$$V(t) = L^2 \, \rho(G(t) - G_P)\alpha$$

Correcting for α is of greater importance in animals with larger hearts due to the greater distance between catheter electrodes, whereas in small hearts such as those of rats and mice, α is thought to be less problematic and therefore was assumed to be equal to 1 (Pacher *et al.*, 2008).

2.4 Histology

Rats were killed by the approved UK Home Office Schedule 1 method of cranial stunning and cervical dislocation. The diaphragm was cut along the ribcage and a bilateral incision made towards the head to expose the heart. The sternum was retracted and the heart removed by cutting the main blood vessels above the base of the heart. The heart was immediately placed in 4 °C isolation solution (I.S.), containing, in mM: 130 NaCl, 5.4 KCl, 0.4 NaH_2PO_4, 5 HEPES, 10 glucose, 10 creatine, 20 taurine, 1.4 $MgCl_2$, pH 7.4 with 5N NaOH. Fat was trimmed from around the atrium, the heart weighed then cannulated via the aorta on a Langendorff apparatus. The time from opening the ribcage to cannulating the aorta was usually less than 1 min. The heart was perfused retrograde at a constant flow of 7 mL/min with I.S. containing 100 μM EGTA to arrest the heart in diastole and clear the coronary circulation of blood.

The heart was cut down from the cannula and dissected into a base, mid and apex portion in ice-cold EGTA I.S. using a safety razor blade. The mid RV free wall was dissected free and divided into two equal pieces following the long axis of the heart. One of these pieces, along with the RV free wall from the base and apex, was frozen for subsequent biochemical analysis, the remaining piece of RV mid free wall was frozen for histology. The RV was pinned to a 20 mm diameter cork specimen disk and maintained in a vertical orientation against a piece of liver also pinned to the cork (Figure 2.3). The sample was covered in a layer of OCT (optimal cutting temperature; VWR, Lutterworth, UK) then the whole sample inverted and frozen in isopentane, precooled by liquid N_2. The LV was processed in a similar manner, however only the mid LV free wall was used, due to there being no clear boundary between LV and septum at the apex. Samples were tightly wrapped in PVC film and stored in airtight plastic bags at -80 °C.

Samples were warmed to -20°C in a cryostat (CM1900, Leica, Milton Keynes, UK) and 10 μm thick sections were cut orthogonal to the long axis of the tissue using a microtome. Sections were transferred to poly-L-lysine coated microscope slides (Polysine Microscope Adhesion Slides, VWR, Lutterworth, UK) marked with a 5-digit computer-generated random number unique to each heart, which allowed image acquisition and analysis to be performed blinded to the origin of the sample.

2.4.1 Measurement of fibrosis

Sirius Red is a large, linear (length ~46 Å), anionic dye with six sulphonic acid groups which preferentially bind basic side group amino acids in collagen (Figure 2.4) (Junqueira *et al.*, 1979). The parallel alignment of the dye to the collagen fibres causes strong birefringence under polarized light, making polarised light microscopy an ideal detection method (Whittaker *et al.*, 1994). Alternatively, co-staining the myocardium yellow with picric acid provides contrast against the red-stained collagen, allowing the area of fibrosis to be quantified using standard light microscopy and colour thresholding image analysis.

Slides were immersed for 1 h in 4% formaldehyde in phosphate-buffered saline (PBS) containing, in mM: 137 NaCl, 2.7 KCl, 9.6 Na_2PO_4, 1.5 KH_2PO_4, pH 7.4 with HCl, then rinsed twice in PBS for 5 min and air dried and stored at 4°C until use. Slides were permeabilised in 0.1% Triton X-100 in water for 25 min. A saturated picric acid solution was made by dissolving 6.5 g picric acid crystals in 500 mL water; saturation was confirmed by the presence of picric acid crystals after 24 h. A 0.1% picrosirius solution was made by dissolving 0.5 g Direct Red 80 (Sigma-Aldrich, Poole, UK) in 500 mL saturated picric acid, pH 2.15 with HCl. Slides were stained in picrosirius dye for 90 min then excess stain was removed by immersion in 0.01 M HCl for 10 min. Slides were dehydrated by washes in 50, 70, 90 and 100% EtOH for 2 min each. Slides were cleared in Histoclear (National Diagnostics, Atlanta, GA) to prevent air bubbles forming within the tissue when non-aqueous mounting media was applied. A drop of DPX (distyrene, plasticiser (butyl, pfthalate, styrene), xylene; Sigma, UK) mounting media was applied to each section and a glass coverslip carefully applied, avoiding air bubbles. Slides were left to cure at 22±1°C and stored at 4°C in the dark until imaging.

Slides were imaged on a Nikon Eclipse E600 light microscope with a Nikon Plan Fluor 20X objective. Three separate 0.15 mm^2 areas of the sample were imaged at a resolution of 2560x1920 pixels using a camera (MicroPublisher 5.0, QImaging, Surrey, Canada) attached to the side port of the microscope. Only areas cut in good cross-section were used. Distances were calibrated using a micrometer graticule (Graticules Ltd, Kent, UK). Red collagen staining was identified using a colour thresholding algorithm in ImageJ (National Institute of Health, Bethesda, MA). The threshold was

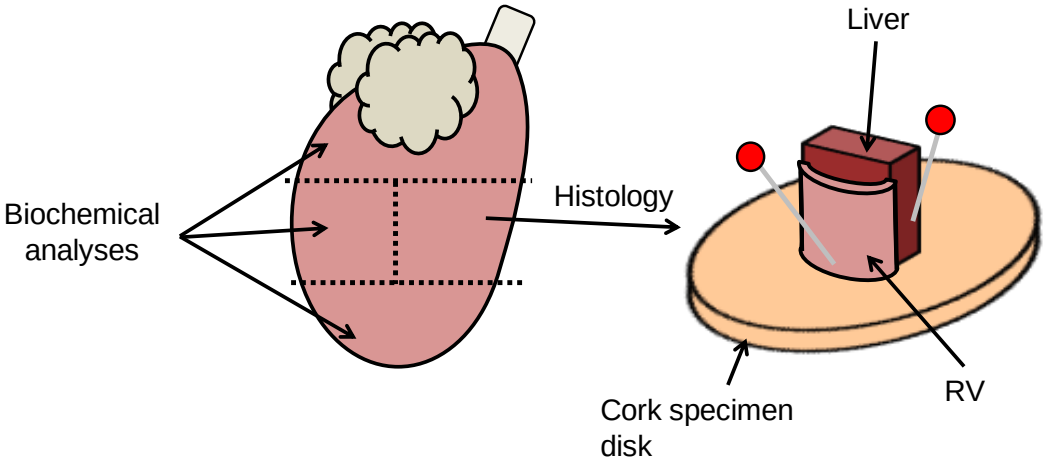

Figure 2.3 Preparation of tissue for biochemical and histological analyses

Hearts were dissected into a base, mid and apical portion. The basal, apical and half of the RV mid free wall was frozen for biochemical analysis. The remaining half was frozen for histology. The RV was pinned against a piece of liver to maintain the correct orientation during freezing in liquid N_2-precooled isopentane.

A

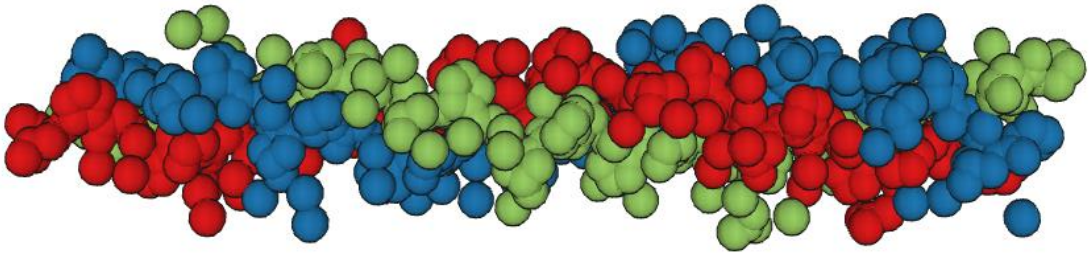

B

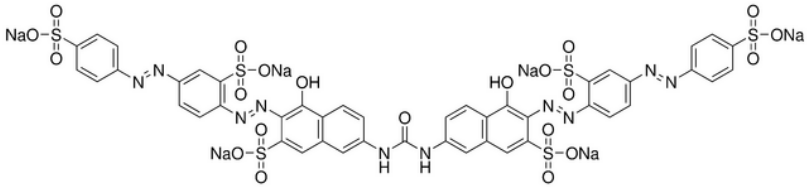

Figure 2.4 Structure of collagen triple helix and Sirius Red dye

A Collagen fibrils form linear strands of triple helices consisting of repeating units of proline, hydroxyproline and glycine amino acids. Separate strands of collagen are coloured in red, green and blue. Structure from Protein Data Bank entry: 1CAG (Bella *et al.* (1994)) **B** The linear structure of Sirius Red dye binds to basic amino acids in collagen and enhances its birefringence. Chemical structure of Direct Red 80 from http://www.sigmaaldrich.com

optimised for each section to account for possible variation in staining intensity but was kept constant for both ventricles of a particular heart. For each ventricle, the mean % area fibrosis of the 3 areas was calculated and used for statistical analysis.

2.4.2 Capillary density

Plant lectins are proteins which bind sugar residues including N-acetylglucosamine found in the glycocalyx of capillaries and cardiomyocytes. Sections were fixed in acetone on ice for 5 min then allowed to air dry and stored at -80°C until use. Slides were incubated in the dark for 1 h with fluorescein-conjugated lectin from *Griffonia simplicifolia* (Vector Laboratories, CA), at a final concentration of 10 µg/mL in PBS. Slides were rinsed in 3 washes of PBS then mounted in an anti-fade mounting medium (Vectashield, Vector Laboratories, CA) diluted 1:8 in PBS, sealed with a coverslip and stored in the dark until imaging (within 24 h). Slides were imaged using epifluorescence on a Nikon Eclipse E600 microscope with a Nikon Plan Fluor 20X objective. A 0.15 mm^2 area (~200-400 capillaries per field) was imaged at a resolution of 2560x1920 pixels using a camera (MicroPublisher 5.0, QImaging, Surrey, Canada) attached to the side port of the microscope. An LED lightsource provided excitation light which was filtered through a 487±10 nm bandpass filter and fluorescence collected through a 533±20 nm longpass filter. Only areas cut in good transverse cross-section were imaged.

2.4.2.1 Modelling myocardial PO_2

Capillaries were identified by eye by an observer blinded to the sample origin. Muscle fibres were counted following Gundersen's unbiased counting rule. Capillary distribution was converted to a binary image and processed using a finite element model implemented in the MatLab computing environment (The MathWorks Inc., Natick, MA) (described in detail in Al-Shammari *et al.* (2012) and (2014)). Capillary supply area was calculated using Voronoi polygons, in which points within the polygon lie closer to a central capillary than any other capillary. This avoids the complication of the inability to tesselate circles which would occur if Krogh and Erlang's cylindrical model was used (Krogh, 1919). Tissue O_2 flux (MVO_2) can be assumed to be proportional to tissue O_2 according to Fick's principal, so long as tissue PO_2 is above a critical value (generally approximated as 0.5-1 mmHg (Goldman, 2008)). All biophysical parameters (except MVO_2max) were obtained from published literature following the recommendation of Beard *et al.* (2003) and are presented in Table 2.1.

Table 2.1 Tissue PO_2 model parameters

Capillary radius	2 μm
Capillary PO_2	40 mmHg
Tissue PO_2 (half max Mb saturation)	2.39 mmHg
Tissue PO_2 at half max MVO_2	0.5 mmHg
Tissue O_2 solubility	4.42×10^{-5} mL O_2 / mL • mmHg
Free O_2 diffusivity in tissue	1.45×10^{-5} cm^2/s
Free Mb diffusivity in tissue	2.2×10^{-7} cm^2/s
Michaelis-Menten tissue VO_2max	3.81 μL O_2 / mL • s
Mb concentration in tissue	2.878 Mb μL / mL
Capillary mass transfer coefficient	0.00086

Mb, myoglobin; MVO_2, myocardial oxygen uptake

2.5 Isolated myocyte studies

Single cardiomyocytes were first successfully isolated nearly 40 years ago and since then have enabled properties of the heart to be studied without the confounding influence of electrical connections, complex geometry, non-cardiomyocyte cells and proteins and circulating hormonal factors (of course, all of these could equally be described as limitations) (Powell & Twist, 1976).

2.5.1 Ventricular myocyte isolation

Rats were killed by the approved UK Home Office Schedule 1 method and hearts removed and cannulated on a Langendorff perfusion system as described above. The heart was perfused retrograde at a constant flow of 7 mL/min/g with I.S. containing 750 μM Ca^{2+} until the coronary circulation cleared of blood and spontaneous sinus rhythm was re-established. Perfusion was switched to I.S. containing 100 μM EGTA for 4 min to arrest the heart in diastole. The heart was then perfused with 40 mL I.S. containing 50 μM Ca^{2+}, 1 mg/mL collagenase Type II (activity 270 U/mg, Worthington Biochemical, New Jersey, USA) and 0.1 mg/mL protease (Type XIV, Sigma, UK). Enzyme solution was collected and recirculated for a total digestion time of 7 min (Figure 2.5).

The heart was cut down from the cannula, reweighed and the enzyme solution collected for subsequent steps of the protocol. The RV, LV and septum were carefully dissected and weighed. The RV and LV were coarsely minced with scissors then placed in separate conical flasks with 4 mL enzyme solution. The tissue was gently agitated in a water bath at 37 °C for 4 min using a rotary shaker to liberate isolated cardiomyocytes. The tissue and enzyme solution was strained through 200 μm^2 nylon mesh and the enzyme solution centrifuged at 50 x g for 40 seconds. The supernatant was removed and the cell pellet resuspended in 750 μM Ca^{2+} I.S. The tissue was returned to the conical flasks with fresh enzyme solution and the shaking/centrifuge process repeated 3-4 times. If the heart was not properly perfused or went hypoxic (indicated by no increase in heart weight following perfusion) cells were not used. Cells were stored for up to 8 h at room temperature in experimental Tyrode solution containing, in mM: 137 NaCl, 5.4 KCl, 0.33 NaH_2PO_4, 0.5 $MgCl_2$, 5 HEPES, 5.6 glucose, 1 $CaCl_2$, pH 7.4 with 5N NaOH. In some experiments [Ca^{2+}] was raised to 1.8 mM or lowered to 0.75 mM depending on the nature of the experiment.

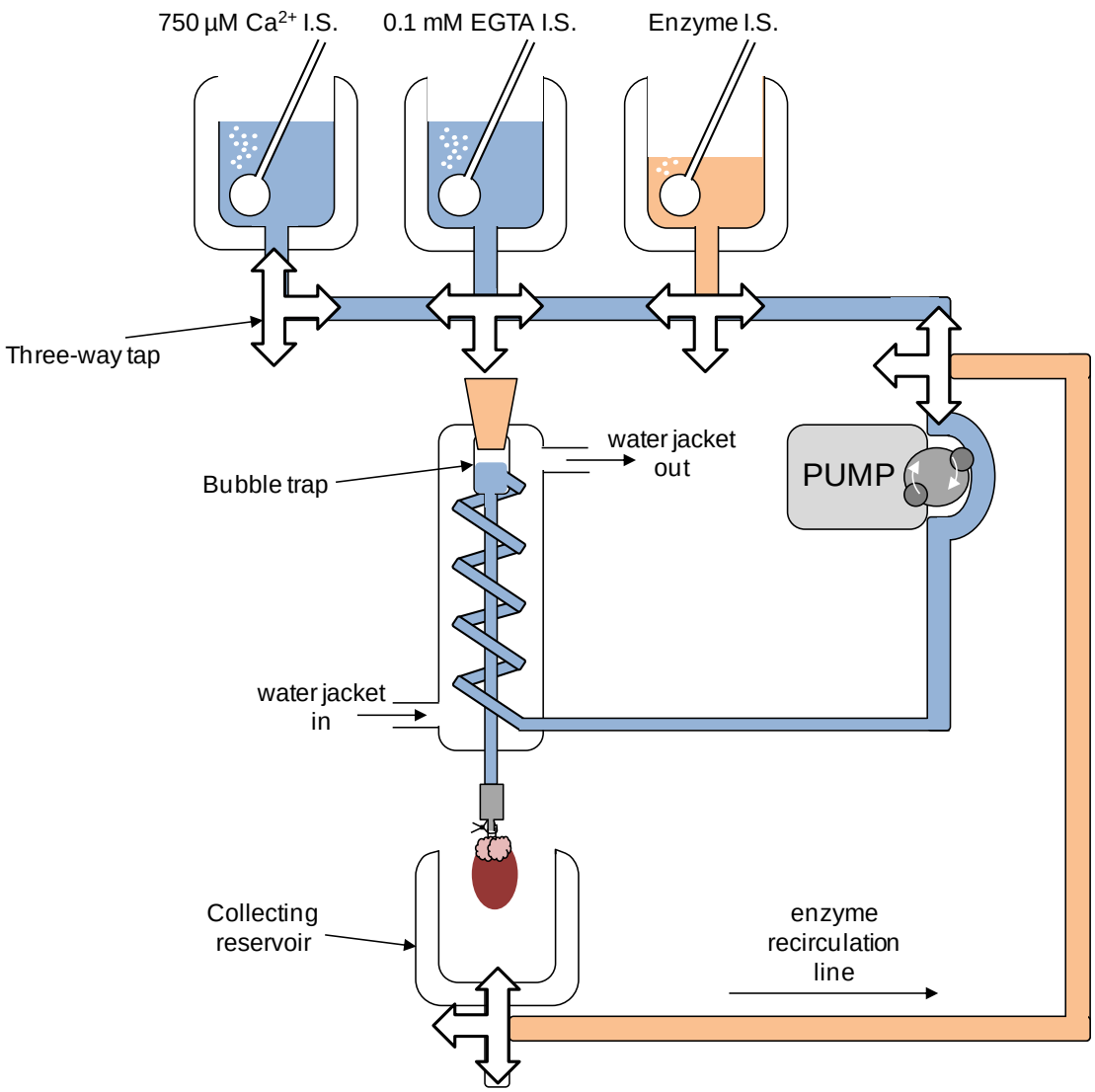

Figure 2.5 Langendorff perfusion apparatus

Hearts were secured via the aorta to a metal cannula with suture thread and perfused at 7 mL/min/g initially in 750 µM Ca^{2+} Isolation Solution (I.S.) to clear remaining blood from the coronary circulation. The solution was then switched to 0.1 mM EGTA I.S. for 4 min to arrest the heart. The heart was then digested for 7 min in enzyme I.S. Solutions were continuously bubbled with 100% O_2 and warmed to 37°C using glass water-jacketed reservoirs and a heating coil. A bubble trap prevented air entering the coronary circulation.

2.6 Simultaneous recording of contraction and cytosolic Ca^{2+} in myocytes

2.6.1 Unloaded shortening

A drop of cells was placed in the perfusion chamber on the stage of an inverted microscope (Eclipse TE300, Nikon, Japan) and viewed under a 40x objective (Nikon, Japan). Bulk flow through the bath was by gravity-fed reservoirs. Local perfusion of a single cell was achieved using an 8-channel pipette (MPRE8, Cell MicroControls, Norfolk, VA). Bulk and local perfusion temperature were controlled independently using a TC^2_{bip} bipolar temperature controller (Cell MicroControls, Norfolk, VA). To minimise the effect of a temperature gradient between the chamber inflow and outflow, bulk flow rate was adjusted to maintain a central region of the bath at 37±0.5°C. Contractions were recorded during electrical field stimulation delivered by two platinum electrodes placed at the sides of the bath. Pacing frequency was controlled between 1-7 Hz with a pulse duration of 5 ms using an analogue stimulator (SD9, Grass Instruments, Warwick, RI).

Rod-shaped, quiescent cells with clear striations were used for experiments. A video image of cells was acquired using a video camera (MyoCam-S, IonOptix, Milton, MA) mounted to the side port of the microscope and displayed on a computer monitor. Data were recorded at 250 Hz. Cell length and width were measured using a ruler overlaid on the computer monitor and calibrated with a micrometer graticule (Graticules Ltd, Kent, UK). Cell volume (pL) was estimated from cell length and width, assuming an elliptical geometry with 54% of the volume of a rectangular parallelepiped defined by length x width x depth, as found by (Satoh *et al.*, 1996). According to Natali *et al.* (2002), cell width is proportional to cell depth (W:D) in a ratio of 1.44±0.03. Therefore:

$$Cell\ volume\ (pL) = \ length\ (\mu m) \times width\ (\mu m) \times \frac{width}{W:D}(\mu m) \times 5.4 \times 10^{-4}(pL.\mu m^{-3})$$

Which can be solved to:

$$Cell\ volume\ (pL) = \frac{length\ (\mu m) \times width^{\,2}(\mu m^2)}{2667\ pL^{-1}.\mu m^{-3}}$$

The mean sarcomere length was calculated online using the SarcLen algorithm in IonWizard software (IonOptix, Milton, MA). The algorithm is based on a Fast Fourier transform of a region of the cell with alternating light and dark striations resulting from

the I- and A-bands. The inverse of the dominant spatial frequency was automatically calculated and displayed as the mean sarcomere length in μm.

2.6.2 Ca^{2+} fluorescence imaging with Fura-4F

The development of intracellular indicators sensitive to Ca^{2+} and other ions was pioneered by Roger Tsien and collaborators (Tsien, 1981). Ratiometric Ca^{2+} indicators such as Fura, developed from the Ca^{2+} buffer BAPTA (1,2-bis(o-aminophenoxy)ethane-N,N,N',N'-tetraacetic acid), avoid problems of variable dye loading. Attachment of an acetoxymethyl (AM) ester to the dye moiety allows it to pass through the cell membrane without the need to microinject the dye salt. Once inside the cell, intracellular esterases cleave the –AM group, trapping the dye within the cell.

Changes in cytosolic Ca^{2+} were followed using the cell permeant, –AM form of the ratiometric Ca^{2+} indicator Fura-4F (Fura-4F-AM, Invitrogen, UK). Fura-4F is derived by a single fluorine substituent on the BAPTA moiety of Fura-2, which reduces its Ca^{2+} binding affinity (K_d of Fura-4F 0.77 μM versus Fura-2 0.14 μM). Fura-4F was chosen over the more commonly used Fura-2 to reduce the Ca^{2+} buffering effect on contraction.

Fura-4F-AM was dissolved in DMSO to produce a 1 mM stock solution and stored frozen at -20°C. Cells were incubated with 2 μM Fura-4F-AM for 20 min at room temperature on a rocker and protected from light to prevent photobleaching. Cells were resuspended in fresh Tyrode and allowed to de-esterify for 30 min before being used for experiments.

A red filter was placed in the path of the microscope light source and experiments were conducted in the dark allowing the cell to be visualised while minimising photobleaching and fluorescence interference. This allowed simultaneous shortening and Ca^{2+} fluorescence measurements. A cell was centred in the field of view and a rectangular light excluding diaphragm adjusted to fit around the cell boundary. A monochromator (Optoscan, Cairn Research, Kent, UK) alternately illuminated cells with 10 ms pulses of 340±10 and 380±10 nm light. The excitation light source was a 150 W Xenon arc lamp [Cairn Research, Kent, UK). Returning light was directed through a dichroic mirror which separated light >600 nm towards the video camera for cell viewing and light <600 nm was passed through a 510 ± 20 nm bandpass filter into a photomultiplier tube and measured by a spectrophotometer integrated into the

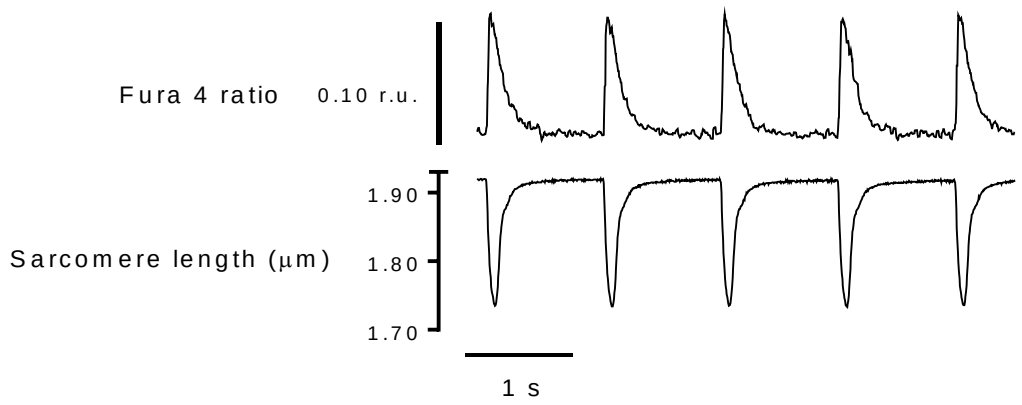

Figure 2.6 Simultaneous sarcomere length and Ca^{2+} monitoring

Sarcomere length in isolated cardiomyocytes was calculated online using IonWizard software (*bottom*). Intracellular Ca^{2+} was monitored using the cell permeant Ca^{2+} indicator Fura-4F-AM (*top*). The ratio of fluorescence collected at 510 nm during alternate excitation at 340 and 380 nm was used to follow changes in intracellular Ca^{2+}. A red filter placed in front of the light source minimized photobleaching while allowing simultaneous monitoring of sarcomere length and Fura-4 fluorescence.

monochromator unit. The resulting fluorescence collected at 510 nm in response to 340/380 nm excitation light was converted to a digital signal and output to IonWizard to automatically calculate and record the ratio at 200 Hz.

2.6.3 Sarcoplasmic reticulum Ca^{2+} content estimation

Caffeine opens the RyR2 in cardiac myocytes and as such, sarcoplasmic reticulum (SR) Ca^{2+} content can be estimated by the amplitude of the caffeine-evoked Ca^{2+} transient (Varro *et al.*, 1993). Cells loaded with Fura-4F were locally perfused with 1 mM Ca^{2+} Tyrode solution heated to 37°C using an 8-channel MPRE8 (Cell MicroControls, Norfolk, VA). Cells were paced at 5 Hz for 1 min then stimulation was stopped and the solution quickly switched to 1 mM Ca^{2+} Tyrode containing caffeine (20 mM).

The relative contribution of different Ca^{2+} removal pathways can be determined by the rate of Ca^{2+} decay during the systolic or caffeine-evoked Ca^{2+} transient (Negretti *et al.*, 1993). Single exponential functions were fitted to the systolic and caffeine-evoked Ca^{2+} decay (Figure 2.7). The rate of the caffeine-evoked Ca^{2+} decay ($K_{CAFFEINE}$) is a measure of SERCA-independent Ca^{2+} removal pathways (primarily NCX and the sarcolemmal Ca^{2+} ATPase). The rate of Ca^{2+} removal through SERCA (K_{SERCA}) is calculated as the difference in rate of decay between the systolic ($K_{SYSTOLIC}$) and caffeine-evoked Ca^{2+} transient.

2.6.4 Myofilament Ca^{2+} sensitivity in intact cells

During recovery from contraction cytosolic Ca^{2+} and relengthening are thought to reach a ‘dynamic equilibrium’ (Spurgeon *et al.*, 1992). This is apparent in phase-plane loops of cytosolic Ca^{2+} versus sarcomere length, as a linear change in Ca^{2+} and length near end diastole. The slope of this relationship is therefore an index of myofilament Ca^{2+} sensitivity in intact cells. Cells loaded with Fura-4F-AM (2 µM) were electrically paced at 1 Hz at 37°C and Fura-4 ratio and sarcomere shortening recorded. The Fura-4 record was interpolated to account for the different data acquisition rates of Fura-4 ratio and sarcomere length (200 vs 250 Hz). Instantaneous Fura-4 ratio was plotted against sarcomere length and the slope of the relationship near end diastole was calculated by linear regression.

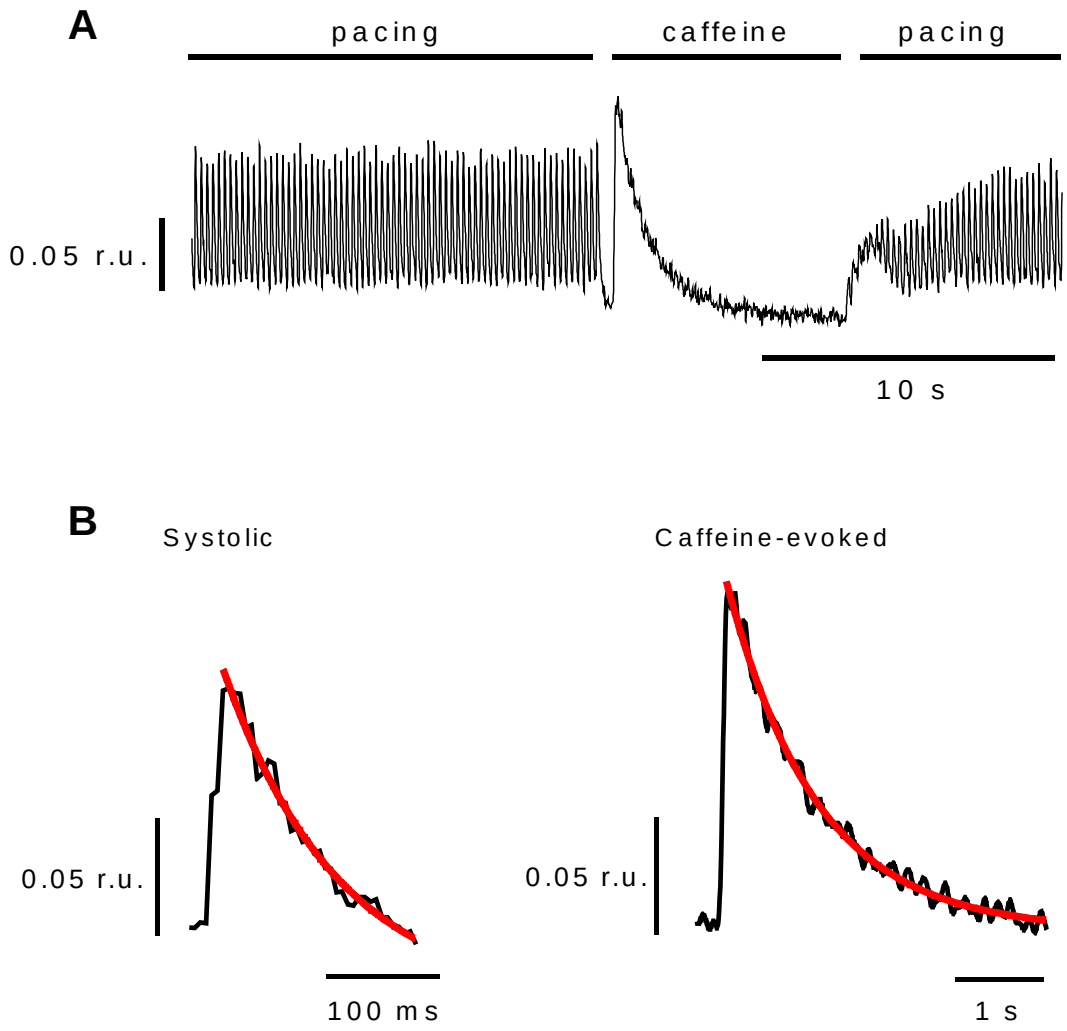

Figure 2.7 SR Ca^{2+} content analysis

A Example of Fura-4 recording for estimation of SR Ca^{2+} content. Cells were electrically paced to elicit systolic Ca^{2+} transients, then pacing was stopped and caffeine (20 mM) rapidly applied. **B** Expanded time view of a systolic and caffeine transient. SR Ca^{2+} content was estimated as the amplitude of the caffeine-evoked Ca^{2+} transient. Contributions from SERCA and non-SERCA Ca^{2+} removal pathways were calculated from the rate of systolic (*left*) and caffeine-evoked (*right*) Ca^{2+} transient decay. SERCA activity was calculated as the difference in the rate of decay of the systolic minus caffeine-evoked Ca^{2+} transient ($K_{SERCA} = K_{SYSTOLIC} – K_{CAFFEINE}$) (*red lines).*

2.7 Force measurement in intact myocytes

Force measurements in single cardiomyocytes were performed at the Vrijie Universiteit, Amsterdam. The force of electrically paced contractions was measured in isolated myocytes subjected to stretch in 1.8 mM Ca^{2+} Tyrode. A cell bath was made from a milled block of aluminium encircled by a 30 MΩ resistance wire connected to an mTCII-HT100 digital temperature controller (Cell MicroControls, Norfolk, VA) which maintained the solution temperature at 37±0.1°C. The bath coverglass was coated in poly-HEMA (2-hydroxyethyl methacrylate; Sigma, Poole, UK) to prevent firm cell attachment to the chamber. A piezo motor and force transducer were mounted on an optical-grade railing system allowing coarse positioning. Fine positioning was performed using motorized micromanipulators (MX7500, Siskiyou, OR) with push-button controllers (MC1000e, Siskiyou, OR). Cell length was adjusted using a command signal generated by IonWizard which was output to a Nano-Drive 1 controller (Mad City Labs, Madison, WI) driving a piezoelectric motor (Mad City Labs, Madison, WI). Video acquisition and online measurement of cell and sarcomere length were performed using the same equipment described in Section 2.6.1. Cells were electrically paced between 1-7 Hz with a MyoPacer (IonOptix, Milton, MA) controlled using IonWizard software.

2.7.1 MyoTak coating

Stiff glass fibres 30 µm in diameter were attached to the piezo motor and force probe with a small drop of beeswax and angled slightly downwards to prevent the force transducer or piezo contacting the bottom of the cell bath. The glass fibre tips were precoated in a suspension of 1 µm in diameter alumina silica aggregate in water (Buehler, Lake Bluff, IL). The precoat suspension was vortexed for 10 s then a 10 µL drop was pipetted onto a spare coverslip. Tips of the glass fibres were viewed under a 20x objective and dipped in the droplet for several seconds then withdrawn, leaving a thin coating. The process was repeated until the tips were covered in an even layer of precoat, then the coating was allowed to harden in air for 20 min.

MyoTak is a biological glue primarily consisting of cell membrane and extracellular matrix proteins in Dulbecco's Modified Eagle Medium (Sigma-Aldrich). It consists of soluble collagen IV (BD Biosciences, Franklin Lakes, NJ), laminin, entactin, heparin sulfate proteoglycan, gentamicin, and Alexa Fluor-647 conjugated to bovine serum albumin (Invitrogen, Carlsbad, CA) (Prosser *et al.*, 2011). 20 µL aliquots of MyoTak

were stored at -80°C. Soluble collagen IV rapidly polymerises at room temperature, therefore on the day of experiments an aliquot of MyoTak was thawed and kept on ice at all times. Pipette tips were also cooled on ice prior to use. Unused MyoTak was refrozen and used on subsequent days.

The tips of the glass fibres were viewed under a 40x objective and repeatedly moved in and out of a 1 µL drop of MyoTak pipetted onto a coverslip until a visible bead of glue could be seen covering the tip. The fibres were then quickly submerged in the cell bath to prevent drying. MyoTak was carefully removed from the glass fibres at the end of each experiment using a fine tipped Number 2 paintbrush (van Gogh Museum, Amsterdam, The Netherlands) dipped in 6 M glacial acetic acid.

2.7.2 Force measurements

A drop of cells was placed in the bath of an inverted microscope. MyoTak coated glass fibres were lowered onto the ends of a cell one at a time, pressing down until the membrane bulged slightly. Cells were then paced for 1 min at 4 Hz which is thought to improve the strength of attachment by increasing the cell surface attachment area (Iribe *et al.*, 2007). The cell was lifted off the coverslip when recording force or unloaded shortening. In some experiments the unloaded shortening-frequency relationship was first measured in cells attached to a single glass fibre, then the second fibre was attached and the isometric force-frequency relationship was measured in the same cell.

2.7.3 Interferometer force transducer

A high sensitivity (<10 nN resolution) optical force transducer (OptiForce, IonOptix, Milton, MA) (frequency response >3.3 kHz) was used to measure the force of contracting myocytes. Force is calculated from the change in path length of laser light guided along a single-mode optical fibre and directed against a gold-plated cantilever on the force probe. Some light is reflected at the interface between the tip of the optical fibre and the Tyrode solution, while the rest reflects off the cantilever and re-enters the optical fibre where a sensor measures the intensity of the returning light. If the two returning beams are in phase the intensity increases, whereas if they are out of phase the intensity decreases. Hence light intensity can be used to calculate the path length between the fibre and cantilever. Contracting myocytes cause a small deflection in the cantilever (<1 µm) which is of a known compliance (24.1 N/m), meaning the force

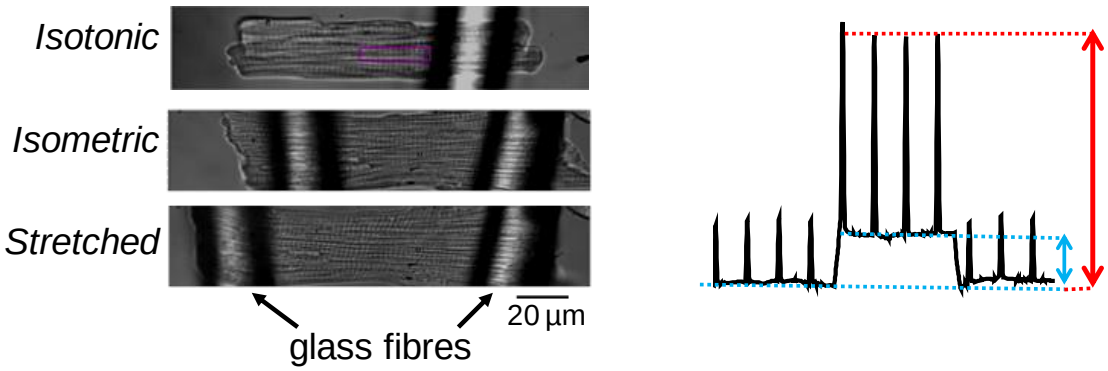

Figure 2.8 Intact cell stretch

Cells were attached to stiff glass fibres coated in MyoTak. Loaded and unloaded contractions were measured from the same cells by first attaching a single fibre and measuring cell shortening, then attaching a second fibre and measuring isometric force. Stretching the cell lead to an increase in end systolic force (*red arrow*) and end diastolic force (*blue arrow*).

applied to the cantilever can be calculated from the spring constant multiplied by the cantilever deflection.

2.8 Laser scanning confocal microscopy

Confocal microscopy comprises three fundamental components: 1) a laser providing excitation light which can be scanned across the X and Y axes 2) a confocal pinhole aperture which restricts light passage to a narrow focal plane 3) a photomultiplier to detect the emitted fluorescence. Adjustment of the focal plane allows an additional Z axis to be recorded.

2.8.1 di-8-ANEPPS staining of cell membrane

T-tubules are invaginations of the sarcolemma occurring at the Z-disk of muscle cells and are prominent in mammalian ventricular myocytes. The lipophilic potentiometric dye di-8-ANEPPS binds to the polarized sarcolemma allowing visualisation of the T-tubule network. A 1 mM stock solution of di-8-ANEPPS was prepared in DMSO and stored at -20°C. Cells were incubated with 5 μM di-8-ANEPPS for 10 min at room temperature and protected from light, then resuspended in fresh Tyrode and used immediately. Cells were scanned at 188 lines per second in XY imaging mode using a 488 nm sapphire laser. Emitted fluorescence was directed through a 560 nm long pass filter and collected with a PMT.

2.8.1.1 T-tubule analysis

Images were rotated until t-tubules aligned with a grid displayed onscreen. A thin rectangular area approximately the length of the cell was selected close to the level of the nuclei avoiding the surface membrane and a pixel intensity profile was generated using ImageJ. The mean pixel intensity values were imported into Origin and a Fast-Fourier Transform performed. A Gaussian best fit curve was fitted to the power spectrum in the frequency domain and used to calculate the amplitude of the first harmonic frequency (Figure 2.9) (Wei *et al.*, 2010). Orientation of tubules was assessed by first subtracting background to enhance contrast, applying median filtering to smooth the images, using automated thresholding to produce a binary image, then skeletonizing images and using the Directionality plugin in ImageJ (Figure 2.10) (Wagner *et al.*, 2012). Tubules oriented 90±5° to the long axis of the cell were considered transverse, while those at 0±5° to the long axis of the cell were considered longitudinal tubules.

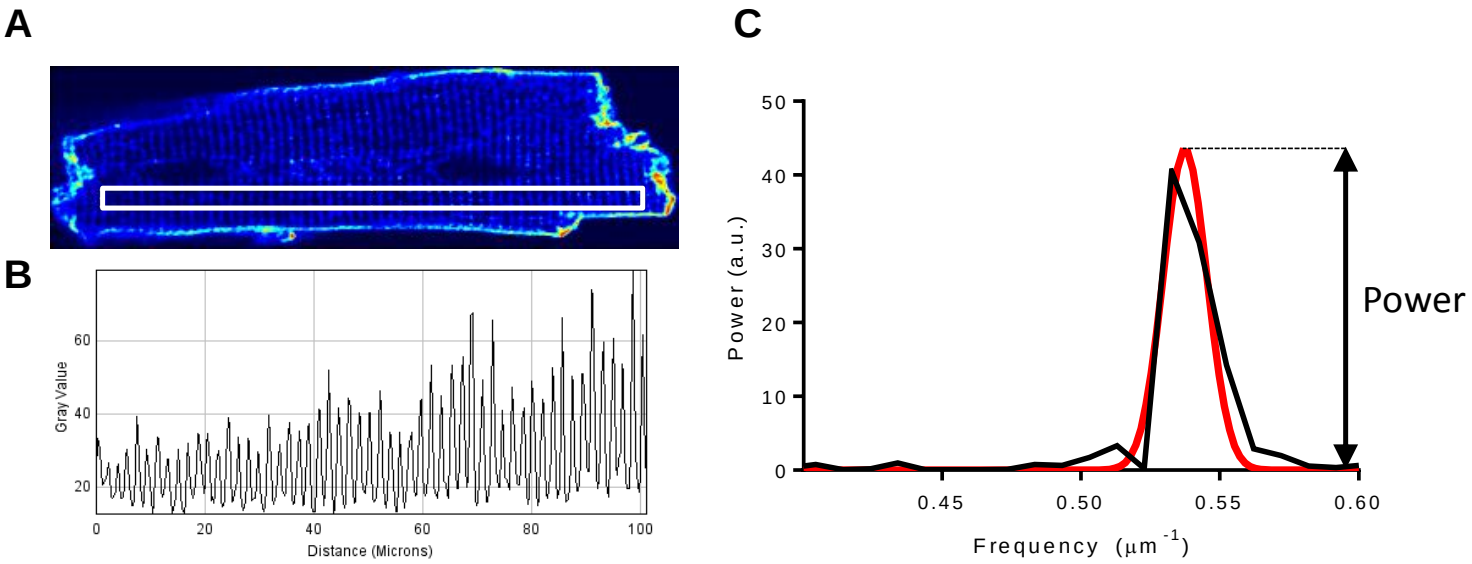

Figure 2.9 T-tubule regularity

The regularity of T-tubule spacing was analysed using a Fast-Fourier transform of the pixel intensity profile of a region across the long axis of the cell. **A** The image was rotated to maximise the orientation of T-tubules perpendicular to a rectangular region of interest across the length of a cell (*white box*). A fast-Fourier transform was applied to the pixel intensity profile (**B**) of the region of interest to find the power of the dominant spatial frequency. **C** A Gaussian curve (*red line*) was fitted to the first harmonic of the fast-Fourier transformed data in the Frequency domain. The amplitude of the curve (*black arrow*) indicates the regularity (or Power, in arbitrary units) of T-tubule spacing.

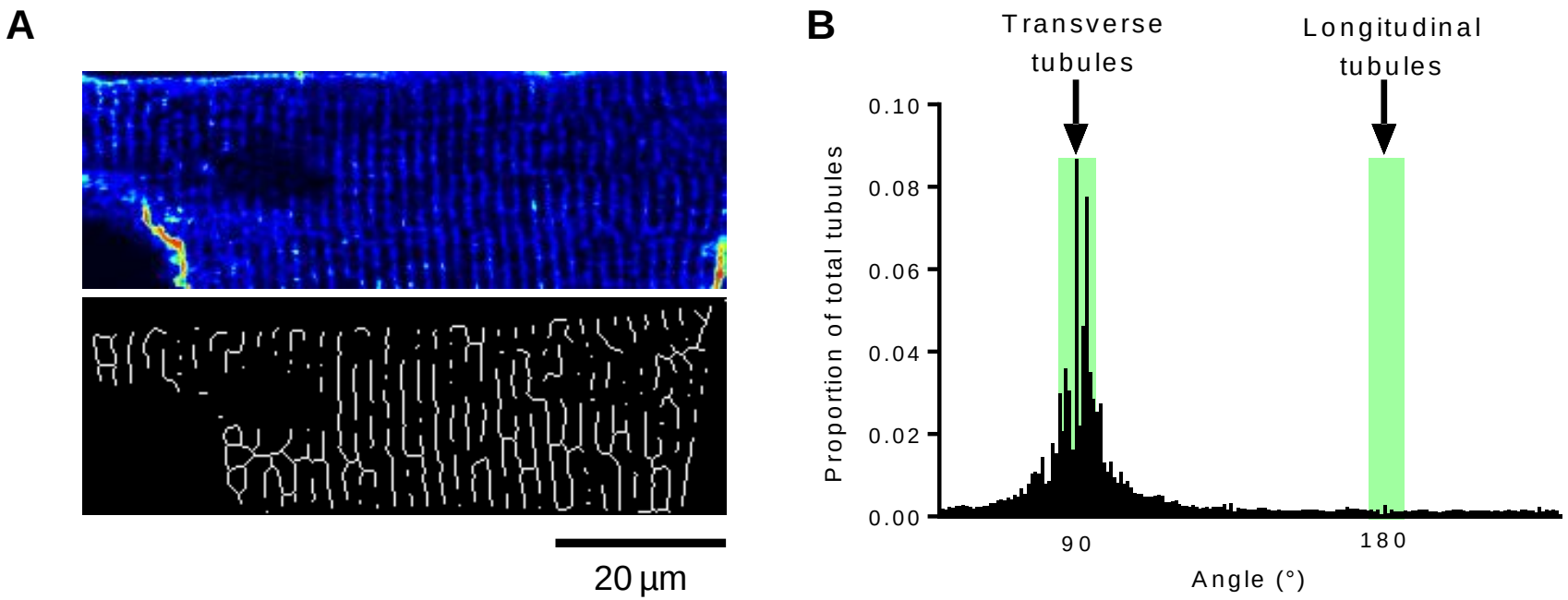

Figure 2.10 Analysis of tubule directionality

The proportion of tubules in the transverse and longitudinal orientation was determined in skeletonized images of di-8-ANEPPS stained cells imaged on a confocal microscope. **A** An area inside the cell was selected (excluding the surface sarcolemma) (*upper panel*) and converted to a binary image (*lower panel*) by pixel value thresholding. **B** A histogram of tubule angles was plotted and the proportion of tubules from 85-95° (transverse) and 175-185° (longitudinal) was counted.

2.8.2 Linescan Ca^{2+} imaging with Fluo-4

The spatiotemporal characteristics of Ca^{2+} release were measured in cells loaded with the non-ratiometric Ca^{2+} indicator Fluo-4-AM, using line scanning confocal microscopy. In line scan mode a mirror repeatedly scans the laser across the same line in a cell and the pixel values are stacked as a function of time. This allows discrete events such as Ca^{2+} sparks and regional variation in the timecourse of Ca^{2+} release to be visualised, which is not possible using epifluorescence.

A 1 mM stock solution of Fluo-4-AM (Invitrogen, UK) was made in DMSO and stored at -20°C. Cells were incubated with 6 µM Fluo-4-AM for 20 min at 22±1°C on a rocker and protected from light to prevent photobleaching. Cells were re-suspended in fresh Tyrode and allowed to de-esterify for 45 min at 4°C before being used for experiments. A drop of cells was placed in the bath of an inverted confocal microscope and continually perfused with 750 µM Ca^{2+} Tyrode at 22±1°C. Cells were electrically paced at 0.5 Hz with a 5 ms pulse duration (S48, Grass Instruments, Warwick, RI) using a pair of platinum electrodes. A 488 nm sapphire laser repeatedly scanned across a line in the focal plane of the long axis of a cell at 188 lines per second. Fluorescence was passed through a 520±20 bandpass filter and recorded using a PMT.

2.8.2.1 Ca^{2+} release dyssynchrony

The uniformity of Ca^{2+} release was quantified using the coefficient of variation of fluorescence at the beginning of a Ca^{2+} transient, termed the Dyssynchrony Index. A pixel intensity profile was measured across the length of a cell using confocal line scan images of Fluo-4-AM (6 µM) loaded cells electrically paced at 0.5 Hz. Regions of delayed Ca^{2+} release increased the variability (standard deviation) of pixel intensities. Dyssynchrony Index was calculated by dividing the standard deviation by the mean fluorescence multiplied by 100 to express as a percentage (Figure 2.11). The standard deviation of the time to half maximum Ca^{2+} (measured line-by-line across the length of the cell using pClamp 10 (Molecular Devices, CA)) was used as an additional measure of heterogeneity in Ca^{2+} release (Caldwell *et al.*, 2014).

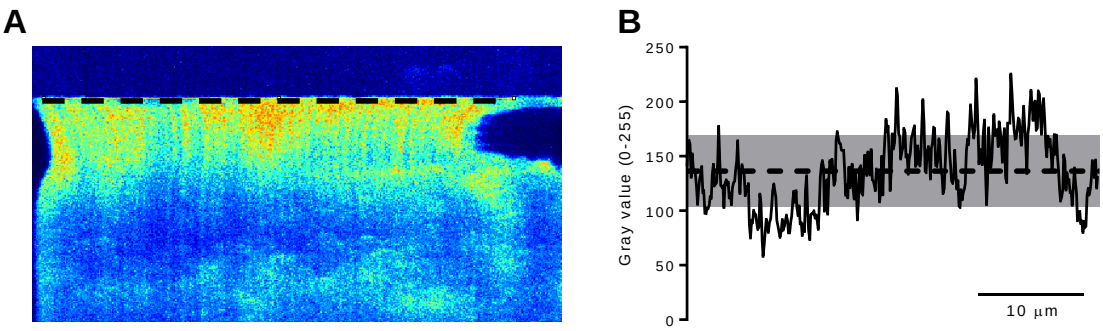

Figure 2.11 Quantification of Ca^{2+} release spatial and temporal synchrony

The spatial synchrony of Ca^{2+} release was measured in confocal linescan images during electrical pacing at 0.5 Hz. **A** A pixel intensity profile was measured at the onset of a systolic Ca^{2+} transient (black dashed line). **B** The standard deviation (*gray shaded area*) was divided by the mean (*black dashed line*) and multiplied by 100 to give the coefficient of variation (%). The coefficient of variation value ("dyssynchrony index") increases with greater variation in the time to Ca^{2+} release across the cell.

2.9 High-resolution respirometry

2.9.1 Equipment

Mitochondrial respiration experiments were performed in an Oxygraph-2k (Oroboros Instruments, Innsbruck, Austria). Two 2 mL glass chambers housed a Clark-type polarographic O_2 sensor and PVDF-coated stirrer bar set to 700 rpm. Both chambers were heated by a single Peltier heating block to 37±0.002°C. PVDF stoppers fitted with Viton O-rings were lowered to seal the chamber from the atmosphere; care was taken to ensure no bubbles were present when the stoppers were fully lowered. An injection port through the centre of the stopper allowed serial addition of substances to the chamber using a 5 or 25 µL Hamilton syringe (Figure 2.12). O_2 concentration was maintained between 200 and 400 µM by raising the stopper and injecting a few millilitres of 100% O_2 with a 25 mL syringe (Pesta & Gnaiger, 2012); preliminary experiments showed respiration was not inhibited until the chamber O_2 concentration fell below 50 µM.

Clark-type electrodes were first developed by Leland Clark in 1954 (Severinghaus & Astrup, 1986) and consist of a gold or platinum cathode and Ag-AgCl anode in a KCl reservoir separated from the sample solution by a thin (~25 µm) fluorinated ethylene-propylene copolymer membrane which is highly permeable to O_2. A constant potential (0.8 V) is applied which reduces O_2 at the cathode by the following reaction:

$$O_2 + 4\,e^- + 2\,H_2O \longrightarrow 4\,OH^-$$

The resulting current is directly proportional to the O_2 partial pressure in the experimental medium. Oxygen flux was corrected to account for this net consumption of O_2 by the O_2 sensor. The O_2 sensor was calibrated between two points: 1) a daily calibration was carried out in room air equilibrated respiration medium 2) a reference zero PO_2 calibration point was obtained by titrating 100 µL of sodium dithionite (10 mM) to fully deplete dissolved O_2 concentration to zero. The same reference zero PO_2 calibration value was used for all experiments. O_2 concentration and O_2 flux (the first derivative of the O_2 concentration slope) were recorded every 2 s and analysed using DatLab 5.2 software (Oroboros Instruments, Innsbruck, Austria). O_2 flux was allowed to stabilise after substrate or inhibitor addition before subsequent additions.

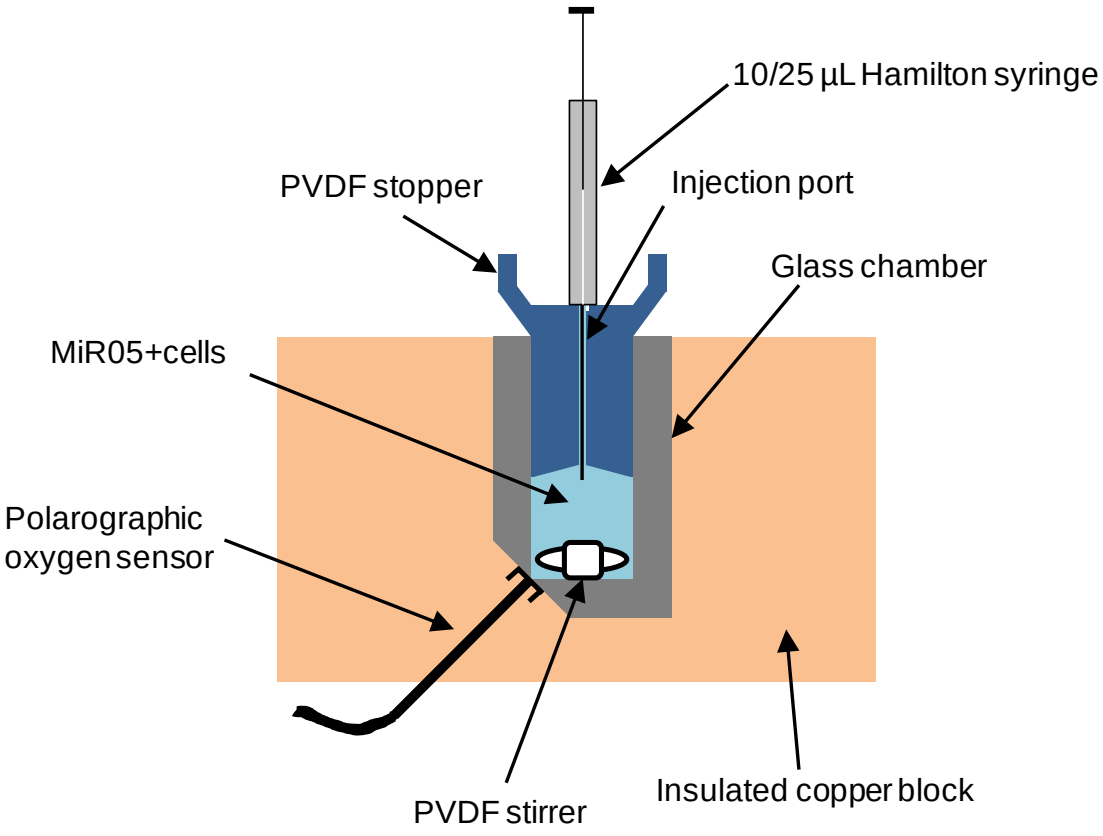

Figure 2.12 Measurement of mitochondrial respiration in an oxygraph chamber
Mitochodrial respiration was measured at 37°C in saponin permeabilised cells in the glass chamber of an Oxygraph 2K respirometer. Cells were suspended in a mitochondrial respiration medium (MiR05) and were continually stirred by a PVDF stirrer. A PVDF stopper sealed the chamber from atmospheric O_2, while an injection port allowed the addition of substances during an experiment. A polarographic O_2 sensor recorded O_2 concentration in the chamber every 2 s.

2.9.2 Myocyte permeabilization

Some aspects of mitochondrial function can be measured in intact tissue and cells, however certain substrates can only access the mitochondrial outer membrane if the sarcolemma is first selectively permeabilised with digitonin or saponin. Saponins have a steroid hydrophobic core which binds cholesterol and forms pores in the sarcolemma but leaves the mitochondrial and sarcoplasmic reticulum membranes relatively intact. This selectivity is due to the molar ratio of cholesterol to phospholipid being about 0.5 in the sarcolemma but only 0.1 in the sarcoplasmic reticulum and 0.07 in the mitochondrial outer membrane (Korn, 1969).

The density of isolated myocytes in solution was measured by pipetting 2 µL of cell suspension onto a microscope slide and counting cells under a microscope using a 20x objective. Five replicate counts were made, the highest and lowest values were excluded and the remaining 3 counts were averaged to give the mean cell density. The volume of cell suspension added to each chamber was calculated according to cell density to use a constant number of cells (5000 cells/mL for SUIT protocol, 10000 cells/mL for ADP titration protocol [see Section 2.9.3 and 2.9.4 for details]). Cells in Tyrode solution were centrifuged and re-suspended in two changes of Mitochondrial Respiration Medium 05 (MiR05), containing (in mM): 110 D-sucrose, 60 K-lactobionate, 20 HEPES, 20 taurine, 10 KH_2PO_4, 3 $MgCl_2$.6 H_2O, 0.5 EGTA, 1 mg/mL BSA, pH 7.1 with 5N KOH. The appropriate volume of cells was added to each oxygraph chamber to give a final volume of 2.1 mL in MiR05, then the chamber was sealed. Saponin from *Quillaja* bark (Sigma, UK) was injected into the chamber at a final concentration of 25 µg/mL, from a 25 mg/mL stock in water.

2.9.3 Substrate-uncoupler-inhibitor titration (SUIT) protocol

Serial addition of substrates feeding into complex I or II followed by selective inhibition of respiratory complexes allows individual complex activities to be determined in a functionally relevant manner. Each substrate or inhibitor was added sequentially after respiration has stabilized. FCCP, rotenone and Antimycin A were dissolved in EtOH, all other substances were dissolved in Milli-Q water. The following were added to the oxygraphy chamber in this order at these final concentrations (Lemieux *et al.*, 2011b):

- Saponin (25 µg/mL) selectively permeabilizes the cell membrane making the mitochondria accessible to exogenous substrates.

- Glutamate (10 mM), malate (0.5 mM), and pyruvate (5 mM) were added to stimulate dehydrogenases yielding NADH as a source of electrons feeding into complex I in the absence of oxidative phosphorylation due to lack of adenylates (respiratory State 2).
- ADP (2.5 mM) was added to maximally activate complex I supported oxidative phosphorylation (respiratory State 3).
- Cytochrome c (10 µM) does not cross the mitochondrial outer membrane and was added to test mitochondrial integrity. An increase in respiration <15% following cytochrome c addition indicated viable mitochondria (Wüst *et al.*, 2012).
- Succinate (10 mM) was added to maximally activate succinate dehydrogenase production of $FADH_2$ and thereby convergent complex I+II electron flow into complex III.
- Carbonyl cyanide p-trifluoro-methoxyphenyl hydrazone (FCCP) was titrated in 0.5 µM steps; FCCP is a protonophore which increases O_2 flux if the phosphorylation system limits oxidative phosphorylation capacity. In rat cardiac muscle the phosphorylation system is not limiting therefore the ratio of uncoupled:maximal respiration is ≤ 1, therefore only a single FCCP titration was added.
- The complex I inhibitor rotenone (0.5 µM) was added to measure complex II activity in the absence of convergent complex I+II respiration.
- The complex III inhibitor Antimycin A (2.5 µM) was added to inhibit cytochrome c reductase in complex III measure residual oxygen consumption in the absence of electron transport.
- N,N,N',N'-Tetramethyl-p-phenylenediamine dihydrochloride (TMPD) (0.5 mM) was added as an artificial substrate for cytochrome c oxidase which has been shown to correlate well with mitochondrial mass (Larsen *et al.*, 2012). Ascorbate (2 mM) was added to maintain TMPD in a reduced state and prevent uncontrolled autooxidation. A chemical background correction for TMPD autooxidation was applied.

2.9.4 ADP titration

ADP and ATP diffuses across the mitochondrial outer membrane through the voltage-dependent anion channel (VDAC). Coupling of mitochondrial CK (CK-mt) in the mitochondrial intermembrane space with the ATP/ADP translocase increases the sensitivity of mitochondrial respiration to cytosolic ADP by catalysing the transfer of

phosphate from ATP to Cr, producing PCr and ADP which can re-enter the mitochondrial matrix. Sequential titrations of ADP allow MOM permeability to be functionally assessed; addition of Cr to the medium further tests the ability of CK-mt to stimulate respiration.

Cells were added to both oxygraph chambers according to the methods described in Section 2.9.3; in one of the chambers MiR05 was supplemented with 25 mM creatine monohydrate (Sigma, UK). Glutamate (10 mM) and malate (0.5 mM) were added as reducing equivalents. ADP was titrated to give the cumulative concentrations (in mM): 0.05, 0.1, 0.2, 0.3, 0.4, 0.6, 0.8 and 1.0.

The ADP-stimulated respiration was normalised between 0% (glutamate+malate in the absence of ADP) and 100% (respiration in 1 mM ADP) (Kaasik *et al.*, 1999). The Michaelis-Menten equation was fitted to the data to determine the apparent K_m of mitochondria for ADP in the presence or absence of Cr.

2.10 Biochemical analyses

2.10.1 Tissue preparation and protein determination

Frozen ventricle samples were thawed on ice, weighed and coarsely minced in a volume of homogenization buffer (HZ buffer) corresponding to 100 mg tissue/mL HZ buffer. HZ buffer contained, in mM: 5 HEPES, 1 EDTA, 5 $MgCl_2$, 0.1% Triton-X100 (Brown *et al.*, 1989). Protease inhibitors (cOmplete™ Protease Inhibitor Cocktail, Roche, Bazel, Switzerland) and phosphatase inhibitors (Halt™ Phosphatase Inhibitor Cocktail, Thermo Scientific, Waltham, MA) were added to HZ buffer immediately prior to use. Tissue was homogenized on ice at 30,000 rpm for 4x20 s pulses using a handheld homogenizer (T10, Ika-Werke, Germany). Enzyme assays and CK isoform separation were performed on the crude homogenate (i.e. without centrifugation) and activity expressed as international units (IU) per mg protein. An aliquot was centrifuged at 12000 *g* and the supernatant used for determination of protein concentration.

2.10.2 Bicinchoninic acid (BCA) assay

Protein concentration was determined according to the method of Smith *et al.* (1985) using the Pierce™ BCA Protein Assay Kit (Thermo Scientific, Waltham, MA). In an alkaline environment divalent Cu^{2+} is reduced to monovalent Cu^{+} in the presence of peptide bonds, which occur equally with amino acids, turning purple in colour absorbing

maximally at 540 nm. Bicinchoninic acid (BCA) reacts with Cu^{+} forming a deeper purple which makes the shift in absorbance greater (maximally absorbs at 562 nm) and hence improves the sensitivity of the reaction. The reaction was performed in 96 well plates (Nunc™, Thermo Scientific, Waltham, MA). Bovine serum albumin (BSA) was used as a protein standard and pipetted into wells in duplicate to give a final protein concentration between 0-50 µg/mL. 3 or 4 dilutions of each sample was made ranging from 1:2 to 1:20 and pipetted into wells in triplicate. The reaction was started by adding BCA and copper(II) sulfate in a 50:1 ratio to each well to a final volume of 200 µL. The plate was incubated at 37°C for 30 min then the optical density of each well was recorded at 562 nm in a spectrophotometer (Varioscan Flash, Thermo Scientific, Waltham, MA).

2.10.3 Creatine kinase activity

CK activity was determined spectrophotometrically from the production of NADPH according to the Rosalki assay (Rosalki, 1967):

$$phosphocreatine + ADP \underset{CK}{\overset{Mg^{2+}}{\rightleftharpoons}} creatine + ATP \quad [1]$$

$$ATP + glucose \underset{hexokinase}{\overset{Mg^{2+}}{\rightarrow}} G\text{-}6\text{-}P + ADP \quad [2]$$

$$G\text{-}6\text{-}P + NADP \xrightarrow[dehydrogenase]{G\text{-}6\text{-}P} 6\text{-}phosphogluconate + NADPH \quad [3]$$

NADPH absorbs UV light maximally at 340 nm whereas NADP does not. β-mercaptoethanol (1 mM) was added to each sample prior to CK assay. CK activity assays were performed by medical technicians at Leeds General Infirmary, Leeds, UK.

2.10.4 Citrate synthase assay

Samples were prepared according to the methods described in Section 2.10.3. Citrate synthase catalyses the reaction of acetyl-CoA with oxaloacetate in the tricarboxylic acid cycle, forming citrate and regenerating coenzyme A [Equation 1]. It is only found in mitochondria and therefore has been used as a marker of mitochondrial mass (Larsen *et al.*, 2012). Citrate synthase activity was measured using a colorimetric assay, according to the method of Srere (1969):

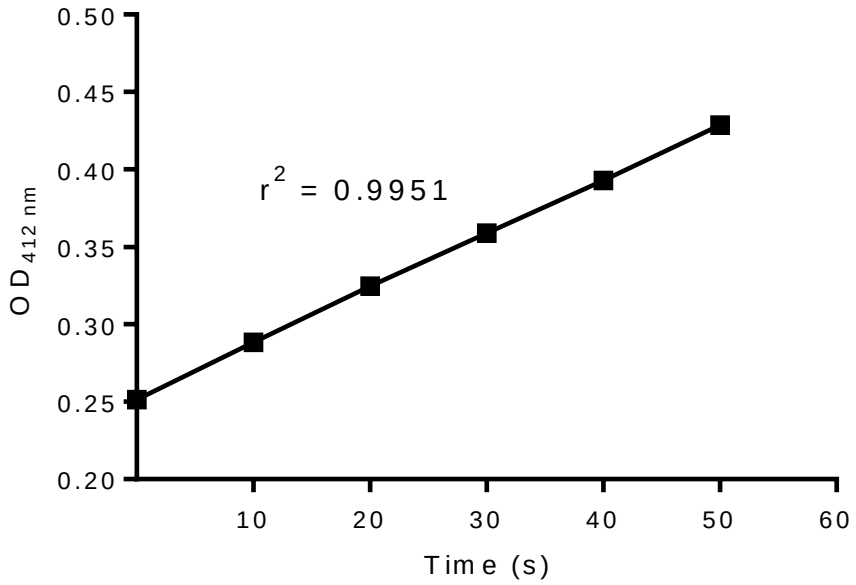

Figure 2.13 Citrate synthase assay

Example of a citrate synthase activity assay. The formation of TNB from CoA-SH and DTNB causes an increase in absorbance at 412 nm (OD_{412}). Reaction velocity was calculated between 0-30 s during which time the change in absorbance was linear.

$$Acetyl\text{-}CoA + oxaloacetate + H_2O \xrightarrow{\substack{citrate \\ synthase}} citrate + CoA\text{-SH} \quad [1]$$

$$CoA\text{-}SH + DTNB \longrightarrow TNB + CoA\text{-}S\text{-}S\text{-}TNB \quad [2]$$

CoA-SH chemically reacts irreversibly with 5,5'-dithiobis-(2-nitrobenzoate) (DTNB) forming 5-thio-2-nitrobenzoate (TNB) which strongly absorbs light at 412 nm. Thus the change in absorbance at 412 nm is proportional to citrate synthase activity.

The assay was performed in triplicate in clear round-bottom 96-well plates in a spectrophotometer. Homogenized samples were added to the reaction buffer containing, in mM: 150 Tris, 10 acetyl-CoA, 1 DTNB, pH 7.0 with HCl. The assay was followed at 30°C for 60 s to measure baseline levels of thiol and acetylase activity, then oxaloacetate (0.5 mM) was dispensed into each well via an automated injection pipette to start the citrate synthase reaction. The change in absorbance was followed for 60 s and enzyme activity calculated during a 30 s period when reaction velocity was linear (Figure 2.13). The saturation of DTNB and oxaloacetate was confirmed by the lack of change in reaction rate when further DTNB or oxaloacetate was added.

2.11 Statistics

Statistical analyses were performed in SigmaStat 3.5 (Systat Software, San Jose, CA) and Prism 6 (Graphpad, La Jolla, CA). Tests for normal distribution were performed in Prism 6. Parametric statistical tests were performed where data followed a normal distribution, otherwise depending on the skewedness it was transformed (by $\log_{10}$ or squared), and normality was re-tested. Parametric statistical tests were used on transformed data which passed tests for normality. In cases where data still did not pass tests for normality, equivalent non-parametric statistical tests were used on the original data. For reasons of clarity and consistency, all data are presented as mean±SEM, even when tests were performed on non-parametric or transformed data.

When two unrelated groups were compared (e.g. CON vs FAIL), an unpaired t-test was used. When three or more unrelated groups were compared (e.g. CON vs MCT+BB vs FAIL) a one-way ANOVA was used. When more than one measurement was taken from the same subject a paired t-test or one-way repeated measures ANOVA was

used. When multiple measurements were made from different groups (e.g. contraction at different pacing frequencies in CON vs MCT+BB vs FAIL) a two-way repeated measures ANOVA was used. $P_{INTERACTION}$ values are given in some cases where there was a significant main effect of a variable (e.g. pacing frequency). Categorical events (e.g. number of cells with and without Ca^{2+} waves in CON vs MCT+BB vs FAIL) were compared using Fisher's Exact test. Survival curves were compared using a Mantel-Cox (log rank) test. A *post hoc* Bonferroni correction was used where multiple comparisons were made.

$P<0.05$ was considered significant. The following conventions are used to illustrate significant differences on figures: *$P<0.05$, **$P<0.01$, ***$<P<0.001$ vs CON, $^{\dagger}P<0.05$, $^{\dagger\dagger}P<0.01$, $^{\dagger\dagger\dagger}P<0.001$ vs FAIL. Required sample sizes were calculated *a priori* using preliminary data or published results from the scientific literature. Number of rats, hearts or cells used in each experiment are provided in the figure legends.

Chapter 3 Therapeutic potential of β-blockers in pulmonary arterial hypertension

3.1 Introduction

The therapeutic goal of currently approved PAH drug therapies is to increase pulmonary vasodilation thereby reducing afterload and the mechanical load on the heart which slows remodelling and delays, but does not prevent, RV failure (Delcroix & Naeije, 2010). Despite RV failure being the leading cause of death in PAH patients it is not currently a target for drug treatment, which has led to calls for novel RV-specific therapies for this disease (Handoko *et al.*, 2010).

β-blockers are a mainstay of therapy in left heart failure due to their positive effects on morbidity and mortality following long-term treatment (Waagstein *et al.*, 1989), however they are contraindicated in PAH due to concern that acute cardiodepressive effects may lead to catastrophic RV pump failure (Provencher *et al.*, 2006a; Peacock & Ross, 2010). Indeed, the most recent European Society of Cardiology and European Respiratory Society guidelines for the treatment of PAH state: "No convincing data are available on the usefulness and safety of angiotensin-converting enzyme inhibitors, angiotensin II receptor antagonists, beta-blockers or ivabradine in patients with PAH (Galiè *et al.*, 2015b)". However, recent retrospective analyses have shown no increased risk of morbidity or mortality in PAH patients receiving β-blockers to control co-morbidities such as high blood pressure, left heart failure and coronary artery disease (So *et al.*, 2012; Thenappan *et al.*, 2014; Bandyopadhyay *et al.*, 2015). Furthermore, recent preclinical studies have demonstrated improvements in survival and RV function in rats with PAH treated with β-blockers (Bogaard *et al.*, 2010; de Man *et al.*, 2011), raising questions as to whether β-blockers are in fact detrimental to PAH, or might the long-term benefits of chronic treatment outweigh the short term negative inotropic effect.

This chapter describes the effect of chronic treatment with a β_1-specific AR blocker in rats with PAH. Metoprolol significantly improved the survival of MCT rats compared to placebo treatment. *In vivo* assessment of RV function using echocardiography and pressure-volume analysis showed metoprolol slowed the rate of RV functional deterioration without preventing PAH or regressing elevated pulmonary vascular resistance. This suggests β-blockers are a potential cardiac-specific therapy for the treatment of PAH.

3.2 Methods

Rats were injected with saline (CON) as control or 60 mg/kg monocrotaline (MCT) to induce PAH. A sugar placebo solution (CON and FAIL) or 10 mg/kg/day metoprolol (MCT+BB and FAIL+BB) was administered daily by voluntary syringe feeding from day 15 onwards. All rats underwent a transthoracic echocardiography examination on day 15 prior to their first dose of placebo or metoprolol. Echocardiography and terminal pressure-volume analyses were performed according to the methods described in Chapter 2. MCT+BB and FAIL+BB rats received identical treatment except that MCT+BB rats were taken on the median survival day of FAIL rats, whereas FAIL+BB rats were taken on the day heart failure symptoms developed (as described in Section 2.1).

A second echo examination and terminal cardiac catheterisation was performed: 1) on CON rats on the median survival day of FAIL rats (±1 day); 2) on MCT+BB rats on the median survival day of FAIL rats (±1 day); 3) on FAIL rats on the day heart failure symptoms developed; or 4) on FAIL+BB rats on the day heart failure symptoms developed.

Appendix A details a further group of rats given a higher dose of 150 mg/kg/day metoprolol by inclusion in the drinking water in an attempt to replicate the study by Bogaard *et al.* (2010). Despite extensive time and effort devoted to reproducing this study, no survival or functional benefit was found using this higher dose compared to placebo. A comprehensive echocardiographic and pressure-volume characterisation of these rats and possible reasons for the discrepancy between our study and that of Bogaard *et al.* (2010) is provided.

3.2.1 Validation of echocardiography

Echocardiography had not previously been performed within the Cardiac Research Group at the University of Leeds in rats. Therefore during the establishment of this technique the validity and reproducibility of measurements was characterised. Pulmonary artery acceleration time (PAAT) and stroke volume estimated using echocardiography were compared against their equivalents measured invasively by conductance catheter, and RV diastolic wall thickness was compared to the RV:LV+S ratio measured post-mortem (Figure 3.1).

There was a significant negative linear correlation between RV systolic pressure and PAAT, following the relationship: Pressure (mmHg) = 117.2-1.828[PAAT] (r^2 = 0.58, P<0.001). The slope of this relationship has been used as a non-invasive predictor of pulmonary artery systolic pressure in rats and humans (Jones *et al.*, 2002; Urboniene *et al.*, 2010). There was also a significant negative correlation between RV systolic pressure and PAAT/ET however the relationship was worse than PAAT alone (r^2 = 0.29) (P<0.05). There was a positive association between RV diastolic wall thickness and RV:LV+S ratio (r^2 = 0.43) (P<0.001). Stroke volume predicted by echo tended to increase with that measured by catheter (r^2=0.16, P=0.10), however this was highly significantly different to the line of equivalence (y=x) (P<0.001).

The reproducibility of blinded measurements was verified by repeating the analysis of a Doppler, M-mode and B-mode parameter following a gap of at least 8 months. There was a good correlation between the first and second measurement of PAAT (r^2 = 0.84), RV diastolic wall thickness (r^2 = 0.55), and RV diastolic area (r^2 = 0.82) (Figure 3.2). None of the slopes of these relationships significantly differed from the line of equivalence indicating that in our hands echocardiography is a reproducible method of monitoring the progression of PAH in rats.

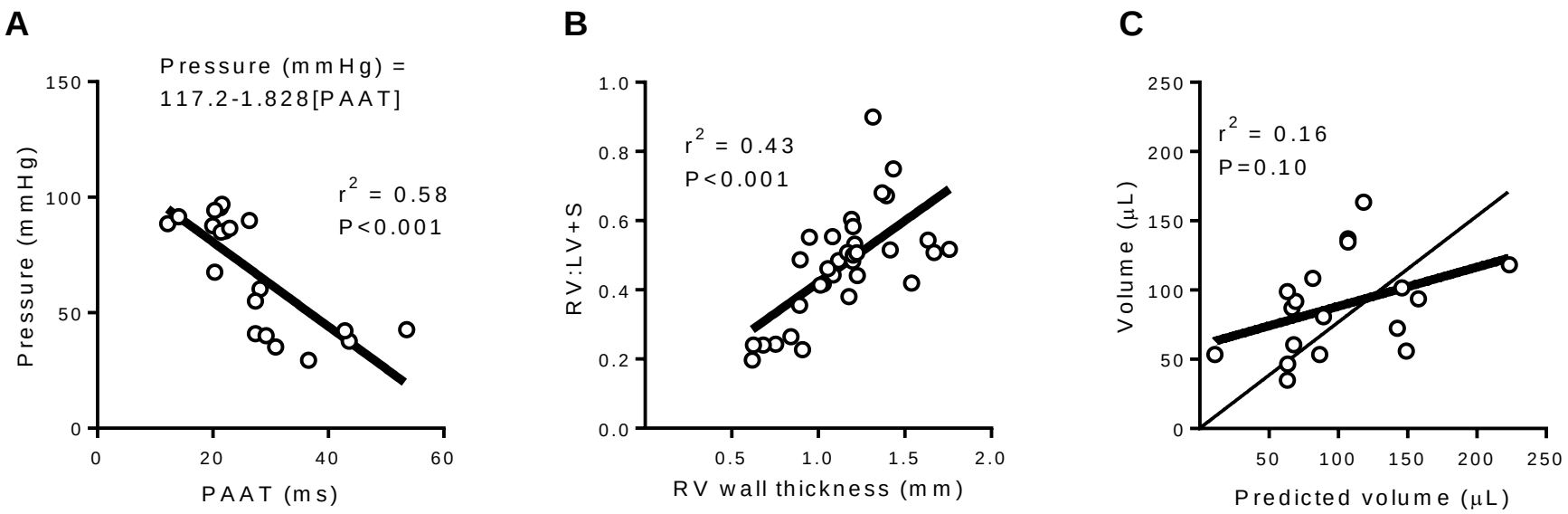

Figure 3.1 Correlation between echocardiography and independent biometric indices

A PAAT negatively correlated with RV systolic pressure measured during cardiac catheterisation. **B** RV wall thickness measured in M-mode increased with RV hypertrophy index **C** Stroke volume predicted from the Doppler flow tended to increase with conductance catheter measured stroke volume, however the relationship was significantly different from the line of equivalence (P<0.001).

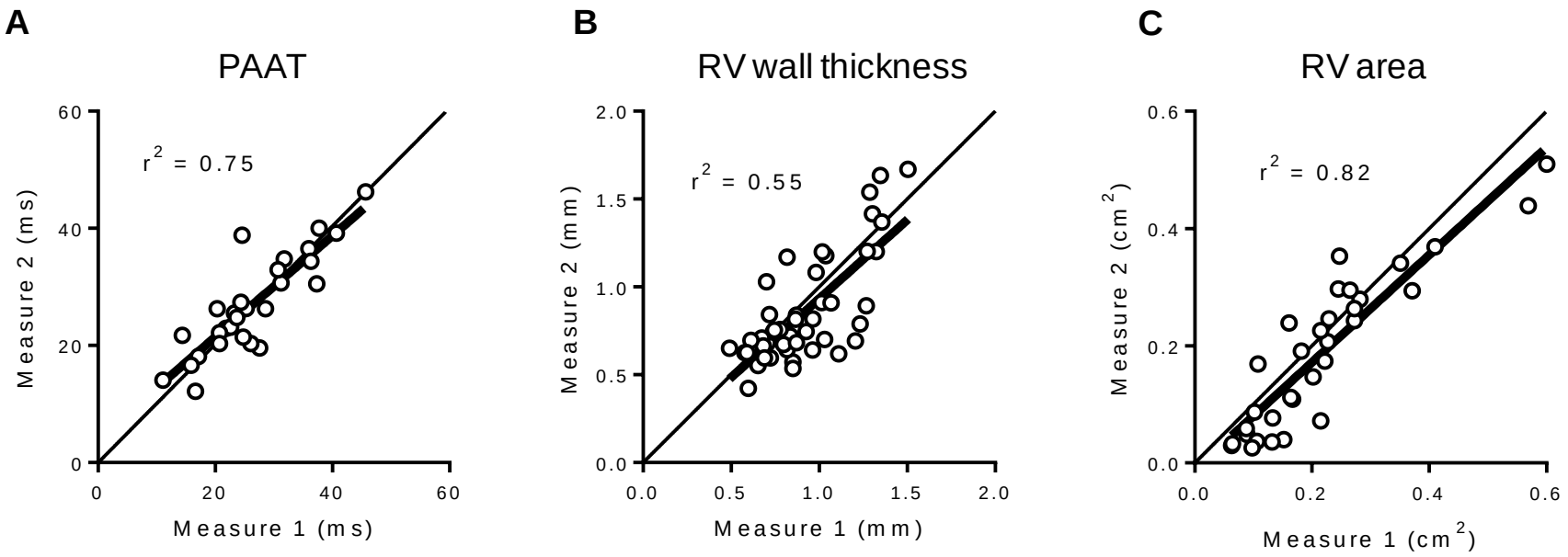

Figure 3.2 Reproducibility of echocardiographic measures

The reproducibility of Doppler, M-mode and B-mode measurements was verified by repeating the analysis under blinded conditions. (**A**) PAAT, (**B**) RV diastolic wall thickness and (**C**) RV diastolic area all showed a high degree of reproducibility as the slopes of Measure 1 vs Measure 2 (*thick line*) did not differ from the line of equivalence (y=x) (*thin line*) (PAAT P=0.17, RV wall thickness P=0.40 , RV area P=0.30).

3.3 Results

3.3.1 Survival and growth curve

Between days 0 and 15 (i.e. before the start of treatment or placebo) CON rats gained on average 5.6±0.3 g.day^{-1}, whereas MCT treated rats gained weight at a significantly slower rate (FAIL+BB 4.1±0.4 g.day^{-1}, P<0.01 vs CON; FAIL 4.1±0.2 g.day^{-1}, P<0.05 vs CON). Rats continued to gain weight during the treatment period (i.e. from day 15 onwards) however a loss of body weight occurred around day 21 in FAIL rats which indicated the onset of heart failure (see Section 2.1 for definitions). Weight gain in FAIL+BB rats tended to plateau around day 25 after which there was a loss of body weight over several days (Figure 3.3). On the day the humane endpoint was reached FAIL+BB rats lost on average 11.0±1.2 g and FAIL rats lost 8.7±1.1 g versus the previous day (not significantly different vs FAIL+BB). The final bodyweight of FAIL+BB (273±7 g) and FAIL rats (260±3 g) was significantly less than CON rats (CON 306±8g; P<0.001). The time taken to reach the humane endpoint was significantly increased from median day 23 in FAIL rats (N=12) to day 31 in FAIL+BB rats (N=15) (P=0.0019). This represents a 35% increase in longevity in metoprolol treated MCT rats compared to placebo.

3.3.2 Anatomical characteristics

The organs most affected by PAH were removed and weighed at the end of the pressure-volume experiment in CON, MCT+BB, FAIL+BB and FAIL rats. Data were expressed either as absolute values, normalized to bodyweight (BW) to account for the slower rate of growth and weight loss of MCT treated groups, or as the ratio of RV to LV+interventricular septum (LV+S). The hearts of MCT treated rats tended to be larger than those of CON rats. In absolute terms the hearts of MCT treated rats were between 7-26% heavier than CON, however there were no statistical differences between groups (Figure 3.4). However, when expressed relative to bodyweight the hearts of all MCT treated rats were significantly heavier than CON by between 28-33%. The RV of MCT treated rats was 81-120% heavier compared to CON rats, and expressed relative to bodyweight there was a greater than twofold increase in the RV:BW ratio. In contrast there were no significant differences in LV+S weight between MCT treated and CON rats, although the LV+S of MCT+BB rats was significantly heavier than FAIL rats. The increased LV+S weight in MCT+BB rats may have been due to the greater body weight, as there were no differences in LV+S:BW ratio

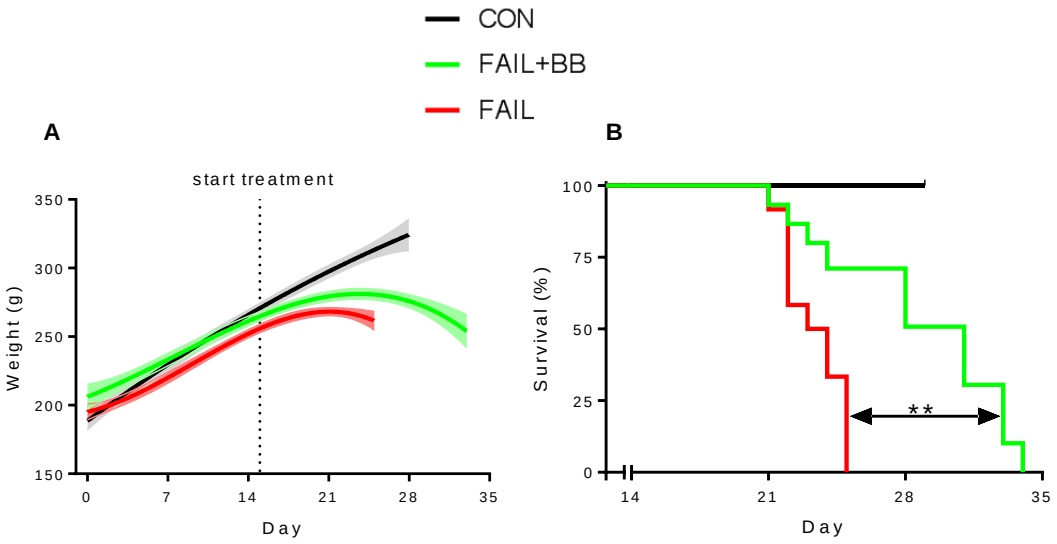

Figure 3.3 Growth and survival curve

Two groups of MCT rats treated with either 10 mg/kg/day metoprolol (FAIL+BB) or placebo (FAIL) starting on day 15 were allowed to progress to heart failure to establish survival curves **A** FAIL and FAIL+BB rats gained weight at a slower rate than CON rats then lost weight in the days preceeding the onset of heart failure. Data were fitted with a third-order polynomial curve; shaded areas represent 95% confidence intervals. **B** The median survival time of placebo treated FAIL rats was day 23, whereas in FAIL+BB rats the survival time was significantly increased to day 31. No CON rats died during this period. Mortality events were recorded as such if the symptom-limited humane endpoint was reached or the rat died unexpectedly. N= 11 CON, 15 FAIL+BB, 12 FAIL. **P=0.0019 FAIL vs FAIL+BB.

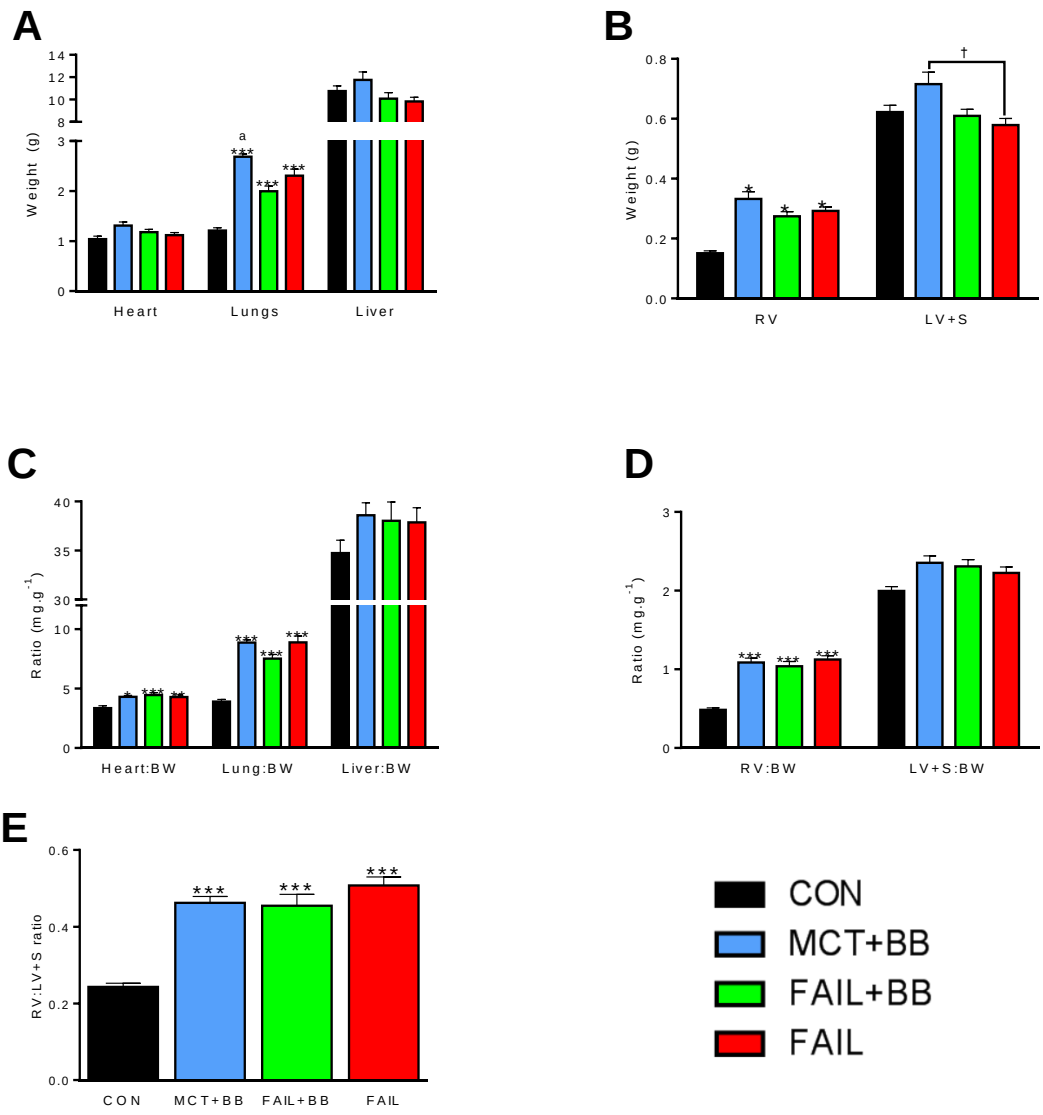

Figure 3.4 Post-mortem organ and ventricle weights

Rats were killed either on the day heart failure symptoms presented (for FAIL and FAIL+BB rats) or on the median survival day of FAIL rats (for CON and MCT+BB rats). Organs were removed and weighed and the heart dissected into RV and LV+interventricular septum (LV+S). Data are shown as absolute values (**A&B**), expressed relative to body weight (**C&D**), or normalized to LV+S weight. N=10 CON, 5 MCT+BB, 12 FAIL+BB, 12 FAIL rats. *P<0.05, **P<0.01, ***P<0.001 vs CON; †P<0.05 vs FAIL; [a]P<0.01 vs FAIL+BB.

between groups. Thus cardiac hypertrophy in MCT treated rats was mainly restricted to the RV, as shown by the RV:LV+S ratio (Figure 3.4). In CON rats the RV was 24% of the weight of the LV+S, whereas in FAIL rats the RV was 51% of the weight of the LV+S. The RV:LV+S ratio was 9-11% lower in metoprolol compared to placebo treated rats at the median and failing stage, but this was not statistically significant.

Lung congestion (reflective of elevated pulmonary artery pressure) was apparent in all MCT-treated groups, indicated by greater lung weight and lung:BW ratio (Figure 3.4). The liver weight and liver:BW ratio was not significantly different between groups, however owing to their lower bodyweight the liver:BW ratio tended to increase in MCT treated groups.

3.3.3 Serial monitoring of PAH progression using echocardiography

Echocardiography was performed on day 15 post-MCT injection and again on either the median survival day of FAIL rats or the day heart failure symptoms developed. Trends were emerging of early signs of hypertrophy and hypertension in MCT+BB and FAIL rats compared to CON although these were generally not statistically significant by day 15. There were no significant differences in Doppler measurements between groups on day 15, with the one exception of peak pulmonary artery ejection velocity which was reduced in MCT+BB compared to CON rats (Table 3.1). Systolic pressure was predicted from pulmonary artery acceleration time (PAAT) using an empirically derived formula (Section 3.2.1). Estimated systolic pressure was increased by 12% in the MCT+BB group and by 29% in the FAIL group, indicating pulmonary hypertension was established by day 15, however the difference between groups was not statistically significant. A trend towards chamber dilation was beginning in MCT treated rats, as the RV systolic chamber area measured in B-mode was significantly increased by 75% in FAIL compared to CON rats (Table 3.2). There were also no statistically significant differences in M-mode measurements between groups on day 15 (Table 3.3), however MCT treated rats tended to have a thicker RV by 7-10% and a more dilated RV chamber.

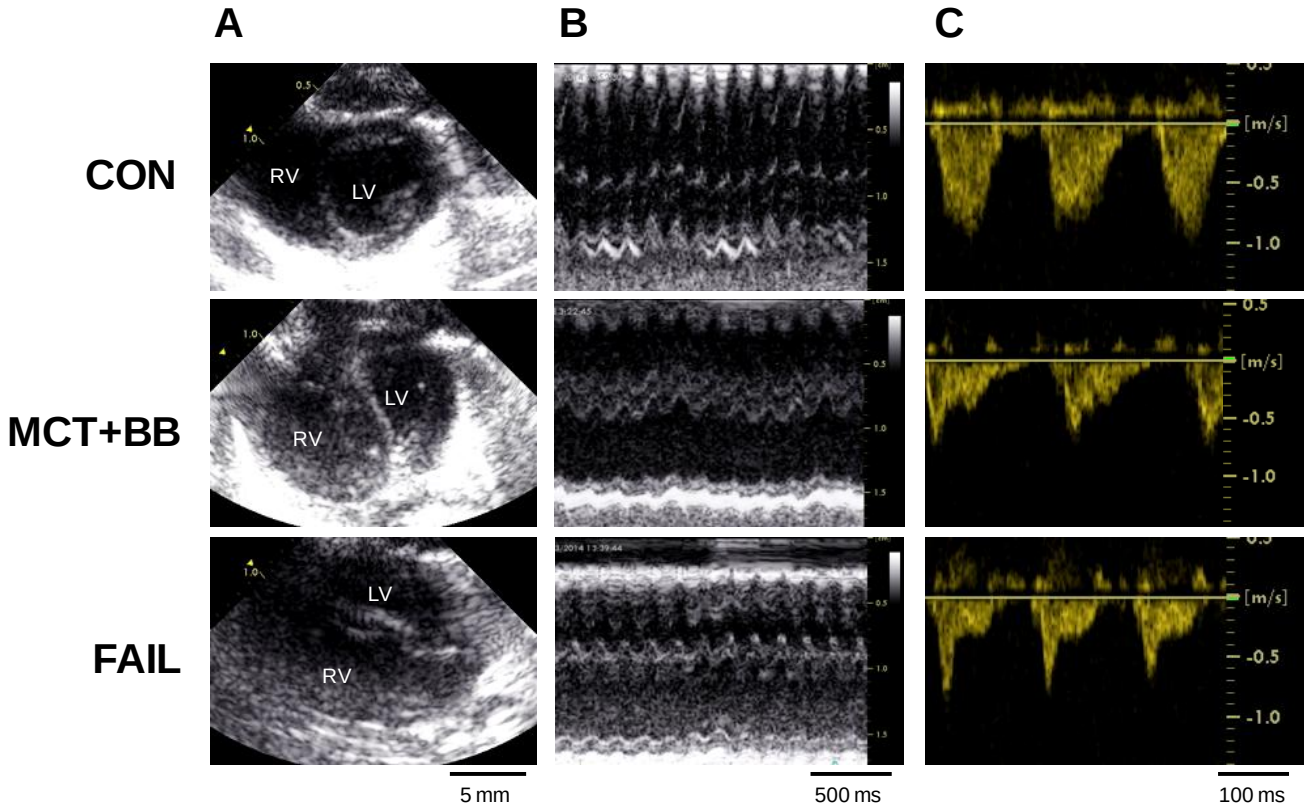

Figure 3.5 Representative echocardiographic images of a CON, MCT+BB and FAIL heart

A End-diastolic B-mode images in the PSAX view. The RV is visibly dilated in MCT+BB and FAIL rats. **B** The RV free wall is hypocontractile and thicker in MCT+BB and FAIL rats. The LV is at the top and the RV on the bottom of each image. **C** The parabolic or dome shaped Doppler blood flow profile in CON rats changes to triangular or peaked in MCT+BB and FAIL rats with a visible mid-systolic notch indicating early termination of flow.

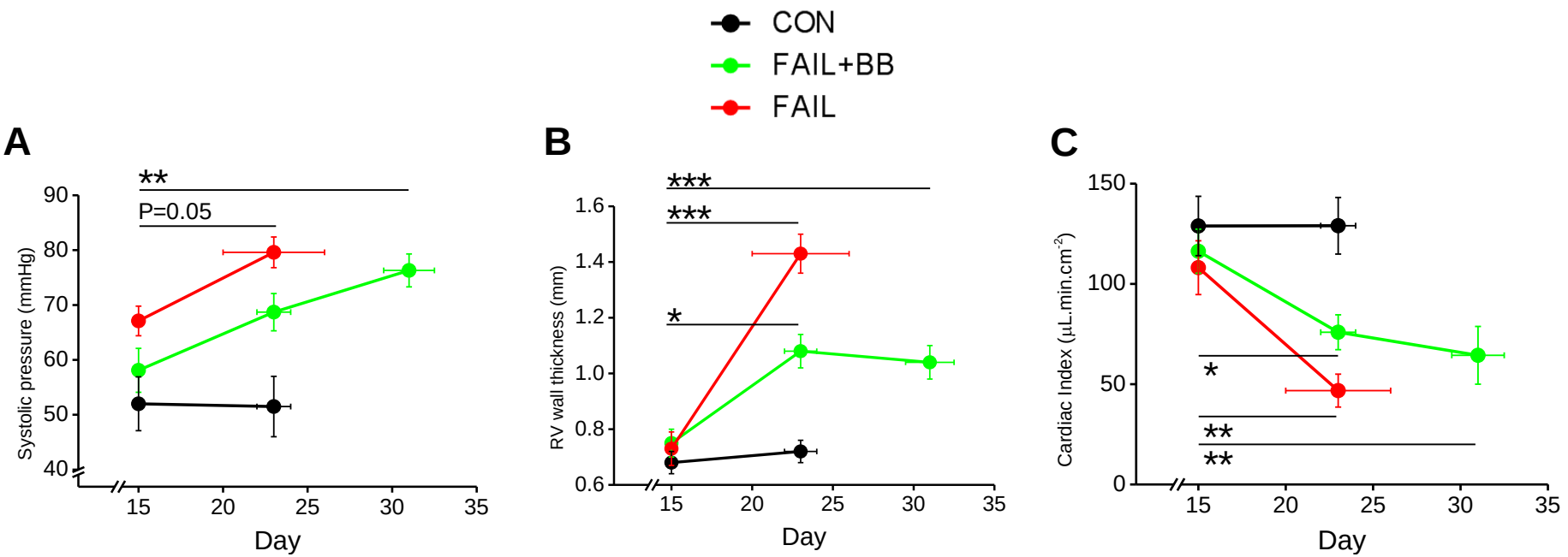

Figure 3.6 Progression of PAH measured by echocardiography

A Systolic PA pressure (predicted from PAAT) and (**B**) RV wall thickness increased, whereas (**C**) cardiac index (cardiac output normalized to body surface area) fell over time in FAIL and FAIL+BB rats. Note that measurements on day 23 and day ~31 were not taken from the same FAIL+BB rats, however as treatments were identical data are presented as a line graph. Pressure, wall thickness and cardiac index did not change over time in CON rats. Between-group differences are omitted for clarity but are detailed in Table 3.1 – 3.6. N=9 CON, 12 FAIL+BB, 7 FAIL rats. *P<0.05, **P<0.01, ***P<0.001 vs day 15.

The same rats were examined again on the day they went into heart failure (for FAIL+BB and FAIL groups) or on the median survival day of FAIL rats (for CON and MCT+BB rats). Representative echo images of a CON, MCT+BB and FAIL rat taken on the median or failing day are shown in Figure 3.5. Viewed in B-mode the RV chamber in CON rats appeared as a narrow crescent during diastole with a thin free wall, whereas the LV was nearly circular in cross-section and thicker walled. In contrast the geometry of the heart was dramatically altered in MCT+BB and FAIL rats, in so far as the RV was severely dilated and hypocontractile with a thicker RV free wall and a reduced LV cavity with a 'D' shape appearance due to compression by the interventricular septum. The heart of MCT treated rats appeared to be rotated slightly anti-clockwise in the chest when viewed in B-mode. M-mode analysis confirmed dilation and hypertrophy of the RV free wall. Flow velocity profiles of the pulmonary artery were used to predict systolic pressure and RV stroke volume. The parabolic Doppler flow velocity profile in CON rats changed towards a more asymmetric triangular shape with a mid-systolic notch in MCT+BB and FAIL rats.

Heart rate was reduced in all MCT treated rats at the failing stage compared to CON, but there were no differences in heart rate between metoprolol-treated and placebo treated MCT rats. PAAT was significantly reduced at the failing stage in MCT treated compared to CON rats and tended to be reduced in MCT+BB on the median day although to a lesser extent (P=0.06) (Table 3.4). Doppler estimated stroke volume was reduced by 44-63% in failing groups compared to CON, but was only reduced by 29% in MCT+BB rats on the median day which was not significantly different to CON. Cardiac output and cardiac index (cardiac output normalized to body surface area) progressively decreased with increasing severity of heart failure (Figure 3.6).

There was a three- to four-fold increase in systolic and diastolic RV chamber area in all MCT treated groups at the failing and median time points and fractional area change was reduced by about 50% compared to CON (Table 3.6). LV chamber area was reduced in MCT treated groups at the failing stage but not in MCT+BB rats on the median day. The LV chamber perimeter became less circular in cross-section in failing groups but was improved in MCT+BB rats and was not significantly different to CON.

Table 3.1 Doppler ultrasound measurements 15 days post-monocrotaline injection

	CON	MCT+BB	FAIL
Heart rate (bpm)	408 ± 7	396 ± 9	407 ± 11
PA acceleration time (ms)	35.7 ± 2.7	32.3 ± 2.2	27.4 ± 1.5
Velocity-time integral (cm)	6.04 ± 0.27	5.47 ± 0.20	5.17 ± 0.27
Peak velocity (m/s)	0.92 ± 0.03	0.79 ± 0.03*	0.86 ± 0.04
Ejection time (ms)	0.13 ± 0.01	0.14 ± 0.01	0.13 ± 0.01
Systolic Pressure (mmHg)	52.0 ± 4.9	58.1 ± 4.0	67.1 ± 2.7
Stroke Volume (µL)	129 ± 14	123 ± 10	106 ± 12
Cardiac Output (mL/min)	53.0 ± 6.1	48.0 ± 4.2	43.2 ± 4.9
Cardiac Index (µL/cm^2)	128.9 ± 14.8	116.3 ± 11.0	108.1 ± 13.4

Data are mean±SEM. Measurement were recorded 15 days after monocrotaline injection prior to the first dose of metoprolol or placebo. Calculated values are shown in italics. MCT+BB and FAIL+BB rats have been combined into a single group at this stage called MCT+BB. PA, pulmonary artery. N= 9 CON, 12 MCT+BB, 7 FAIL rats. *P<0.05 vs CON.

Table 3.2 B-mode ultrasound measurements 15 days post-monocrotaline injection

	CON	MCT+BB	FAIL
RV area diastole (cm^2)	0.08 ± 0.01	0.12 ± 0.01	0.13 ± 0.02
RV area systole (cm^2)	0.04 ± 0.01	0.06 ± 0.01	0.07 ± 0.01*
RV area change (%)	51.5 ± 6.0	51.3 ± 5.0	41.3 ± 4.8
LV area diastole (cm^2)	0.25 ± 0.01	0.25 ± 0.01	0.22 ± 0.02
LV area systole (cm^2)	0.10 ± 0.02	0.10 ± 0.01	0.07 ± 0.01
LV area change (%)	62.2 ± 4.1	61.3 ± 2.9	64.4 ± 3.3
LV circularity (%)	88.4 ± 1.2	86.4 ± 1.6	83.0 ± 2.9

Data are mean±SEM. Measurement were recorded 15 days after monocrotaline injection prior to the first dose of metoprolol or placebo. Calculated values are shown in italics. MCT+BB and FAIL+BB rats have been combined into a single group at this stage called MCT+BB. RV, right ventricle; LV, left ventricle. N= 9 CON, 12 MCT+BB, 7 FAIL rats. *P<0.05 vs CON.

Table 3.3 M-mode ultrasound measurements 15 days post-monocrotaline injection

	CON	MCT+BB	FAIL
RV thickness diastole (mm)	0.68 ± 0.04	0.75 ± 0.05	0.73 ± 0.06
RV thickness systole (mm)	0.81 ± 0.04	0.91 ± 0.06	0.81 ± 0.07
RVID diastole (mm)	2.13 ± 0.24	2.56 ± 0.38	2.74 ± 0.48
RVID systole (mm)	1.22 ± 0.22	1.35 ± 0.26	1.77 ± 0.32
RV wall shortening (%)	42.9 ± 6.9	50.0 ± 3.3	36.0 ± 5.5
IVS thickness diastole (mm)	1.73 ± 0.09	1.84 ± 0.11	1.82 ± 0.11
IVS thickness systole (mm)	2.21 ± 0.10	2.23 ± 0.13	2.30 ± 0.20
LV thickness diastole (mm)	1.83 ± 0.05	1.91 ± 0.10	1.93 ± 0.09
LV thickness systole (mm)	2.42 ± 0.12	2.75 ± 0.11	2.54 ± 0.18
LVID diastole (mm)	5.55 ± 0.21	5.53 ± 0.16	5.24 ± 0.36
LVID systole (mm)	3.66 ± 0.32	2.97 ± 0.26	2.81 ± 0.28
LV wall shortening (%)	34.9 ± 4.0	46.0 ± 4.5	46.9 ± 2.6

Data are mean±SEM. Measurement were recorded 15 days after monocrotaline injection prior to the first dose of metoprolol or placebo. Calculated values are shown in italics. MCT+BB and FAIL+BB rats have been combined into a single group at this stage called MCT+BB. RV, right ventricle; IVS, interventricular septum; LV, left ventricle; ID, internal diameter. N= 9 CON, 12 MCT+BB, 7 FAIL rats.

Table 3.4 Doppler ultrasound measurements at the development of heart failure or the median survival day

	Median		Failing	
	CON	MCT+BB	FAIL+BB	FAIL
Heart rate (bpm)	409 ± 9	340 ± 9**	330 ± 12***	364 ± 12*
PA acceleration time (ms)	35.9 ± 3.0	26.5 ± 1.8$^{\#}$	21.5 ± 1.4***	20.5 ± 1.5***
Velocity-time integral (cm)	5.96 ± 0.19	3.67 ± 0.44**	2.84 ± 0.55***	2.64 ± 0.41***
Peak velocity (m/s)	1.00 ± 0.03	0.76 ± 0.02*	0.63 ± 0.05***	0.67 ± 0.08***
Ejection time (ms)	0.12 ± 0.01	0.12 ± 0.01	0.10 ± 0.01	0.08 ± 0.01**
Systolic Pressure (mmHg)	51.5 ± 5.5	68.7 ± 3.4$^{\$}$	76.3 ± 3.0**	79.6 ± 2.8***
Stroke Volume (µL)	140 ± 13	100 ± 13	78 ± 15*	52 ± 9***
Cardiac Output (mL/min)	57.7 ± 6.4	34.0 ± 4.4*	26.1 ± 5.9**	18.9 ± 3.4***
Cardiac Index ($\mu L/cm^2$)	129.0 ± 14.1	75.9 ± 8.7*	64.4 ± 14.4**	46.8 ± 8.2***

Data are mean±SEM. Measurements were recorded on the day heart failure symptoms developed (Failing columns) or on the median survival day of FAIL rats (Median columns). Calculated values are shown in italics. PA, pulmonary artery. N= 9 CON, 5 MCT+BB, 7 FAIL+BB, 7 FAIL rats. $^{\#}$P=0.06, $^{\$}$P=0.07, *P<0.05, **P<0.01, ***P<0.001 vs CON.

Table 3.5 M-mode ultrasound measurements at the development of heart failure or the median survival day

	Median		Failing	
	CON	MCT+BB	FAIL+BB	FAIL
RV thickness diastole (mm)	0.72 ± 0.04	1.08 ± 0.06**††	1.04 ± 0.06**†††	1.43 ± 0.07***
RV thickness systole (mm)	0.87 ± 0.07	1.40 ± 0.08**	1.24 ± 0.08*†	1.59 ± 0.10***
RVID diastole (mm)	2.47 ± 0.26	4.68 ± 0.19	4.73 ± 0.46*	5.00 ± 0.26*
RVID systole (mm)	1.43 ± 0.17	4.10 ± 0.22***	3.69 ± 0.58***	4.10 ± 0.24***
RV wall shortening (%)	39.5 ± 7.4	12.4 ± 3.5	26.0 ± 9.2	18.1 ± 1.4
IVS thickness diastole (mm)	1.88 ± 0.14	2.70 ± 0.15**	2.24 ± 0.19	2.16 ± 0.10
IVS thickness systole (mm)	2.35 ± 0.15	3.16 ± 0.18*^{a}	2.36 ± 0.22	2.46 ± 0.17
LV thickness diastole (mm)	1.98 ± 0.14	2.43 ± 0.18	2.04 ± 0.12	2.00 ± 0.15
LV thickness systole (mm)	2.90 ± 0.20	3.34 ± 0.15	2.52 ± 0.23	2.45 ± 0.19
LVID diastole (mm)	5.55 ± 0.30	5.13 ± 0.27	5.45 ± 0.20	4.93 ± 0.34
LVID systole (mm)	3.02 ± 0.26	3.10 ± 0.40	3.32 ± 0.55	2.98 ± 0.45
LV wall shortening (%)	46.2 ± 2.3	40.0 ± 6.8	40.9 ± 6.9	39.4 ± 9.2

Data are mean±SEM. Measurements were recorded on the day heart failure symptoms developed (Failing columns) or on the median survival day of FAIL rats (Median columns). Calculated values are shown in italics. RV, right ventricle; IVS, interventricular septum; LV, left ventricle; ID, internal diameter. N= 9 CON, 5 MCT+BB, 7 FAIL+BB, 7 FAIL rats. *P<0.05, **P<0.01, ***P<0.001 vs CON; ††P<0.01, †††P<0.001 vs FAIL; ^{a}P<0.05 vs [failing] MCT+BB.

Table 3.6 B-mode ultrasound measurements at the development of heart failure or the median survival day

	Median		Failing	
	CON	MCT+BB	FAIL+BB	FAIL
RV area diastole (cm^2)	0.11 ± 0.01	0.30 ± 0.04**	0.31 ± 0.03***	0.34 ± 0.04***
RV area systole (cm^2)	0.05 ± 0.01	0.22 ± 0.02***	0.23 ± 0.03***	0.25 ± 0.03***
RV area change (%)	52.0 ± 3.7	23.9 ± 4.9**	29.8 ± 6.4**	27.4 ± 3.1**
LV area diastole (cm^2)	0.25 ± 0.02	0.18 ± 0.01	0.13 ± 0.02*	0.16 ± 0.02
LV area systole (cm^2)	0.09 ± 0.01	0.07 ± 0.01	0.04 ± 0.01**	0.06 ± 0.01$^{\#}$
LV area change (%)	61.8 ± 2.6	64.0 ± 2.9	69.9 ± 2.5	61.2 ± 7.4
LV circularity (%)	87.0 ± 0.9	76.2 ± 4.0^{a}	61.3 ± 5.3***	65.0 ± 2.2***

Data are mean±SEM. Measurements were recorded on the day heart failure symptoms developed (Failing columns) or on the median survival day of FAIL rats (Median columns). Calculated values are shown in italics. RV, right ventricle; LV, left ventricle. N= 9 CON, 5 MCT+BB, 7 FAIL+BB, 7 FAIL rats. $^{\#}$P=0.05, *P<0.05, **P<0.01, ***P<0.001 vs CON; ^{a}P<0.05 vs [failing] MCT+BB.

RV wall thickening and chamber dilation were apparent using M-mode analysis of MCT treated rats. This was specific to the RV as there were no changes in LV wall thickness, internal diameter or fractional shortening (Table 3.5). Diastolic RV wall thickness was significantly reduced at the median and end stage in MCT+BB rats compared to FAIL rats. The change in RV wall thickness from diastole to systole tended to be lower in FAIL (+11%) and FAIL+BB (+19%) compared to CON (+20%) and MCT+BB (+30%) although these differences were not statistically significant. RV fractional wall shortening tended to be reduced in MCT treated rats, however due to high variability there were no significant differences between groups.

3.3.4 *In vivo* haemodynamics at the onset of heart failure

PV analyses were performed in CON, MCT+BB, FAIL+BB and FAIL rats; FAIL+BB rats appeared to be particularly vulnerable to dying during the PV procedure from either pump failure or heart block. Increased sensitivity to inhaled anaesthesia and ventilation-perfusion mismatch has been reported in rats with heart failure which may have been exacerbated by β-blockers (Plante *et al.*, 2006; Balestra *et al.*, 2015). Consequently a dataset from only three rats was obtained at the failing stage and therefore has not been included in the statistical analysis but is presented in Appendix A. Invasive cardiac pressure-volume measurements were performed and analysed by Dr Mark Drinkhill.

The shape of cardiac PV loops in CON rats was fairly triangular with no obvious isovolumic contraction and persistent ejection during early relaxation (Figure 3.7). In contrast the shape of FAIL and MCT+BB PV loops was more rectangular with clear isovolumic contraction and relaxation phases which tended to result in faster maximal rates of pressure development and decay in these rats. The area enclosed by the workloop describes the work performed by the ventricle (stroke work) and tended to be greater in MCT+BB compared to CON and be less in FAIL rats compared to CON, but was significantly greater in MCT+BB compared to FAIL.

End-systolic pressure in FAIL and MCT+BB rats was more than double that of CON (Figure 3.8). Ejection fraction and stroke volume were significantly reduced in FAIL rats compared to CON, and there was a slight but not statistically significant increase in both of these measures in MCT+BB rats. Pulmonary vascular resistance was calculated assuming a left atrial pressure of 8 mmHg (Lourenço *et al.*, 2006). Vascular

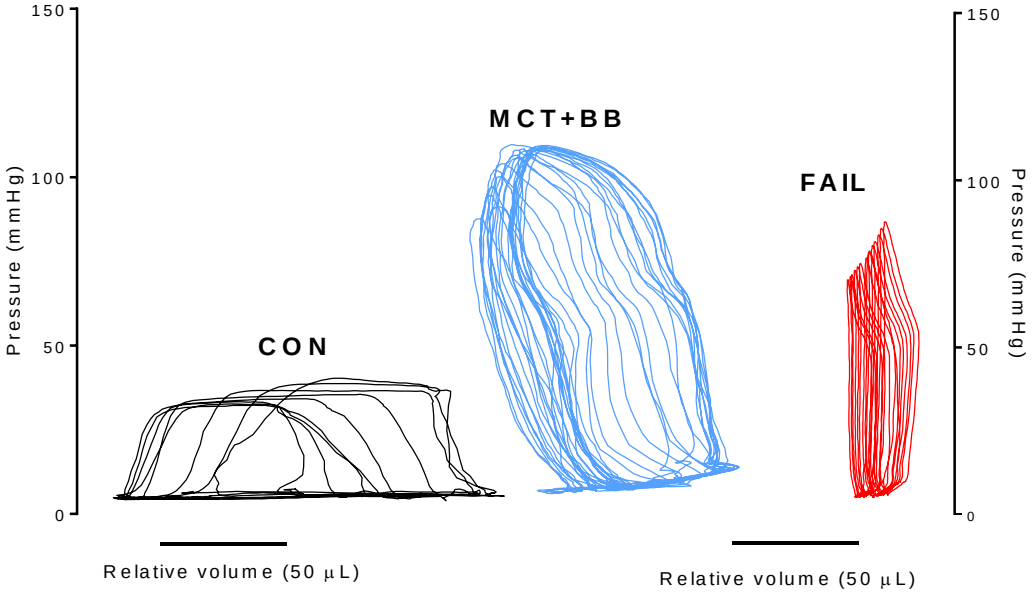

Figure 3.7 Right ventricle pressure-volume loops

RV pressure and volume were measured under terminal anaesthesia and cardiac work loops constructed. Traces rotate counter-clockwise during the contraction cycle starting from the lower right corner of each loop. Transient occlusion of the inferior vena cava allowed the measurement of load independent parameters at decreasing end-diastolic volumes. The CON recording shows a large stroke volume is achieved at low systolic pressure. Systolic pressure is greatly increased but stroke volume is reduced in MCT+BB and FAIL rats.

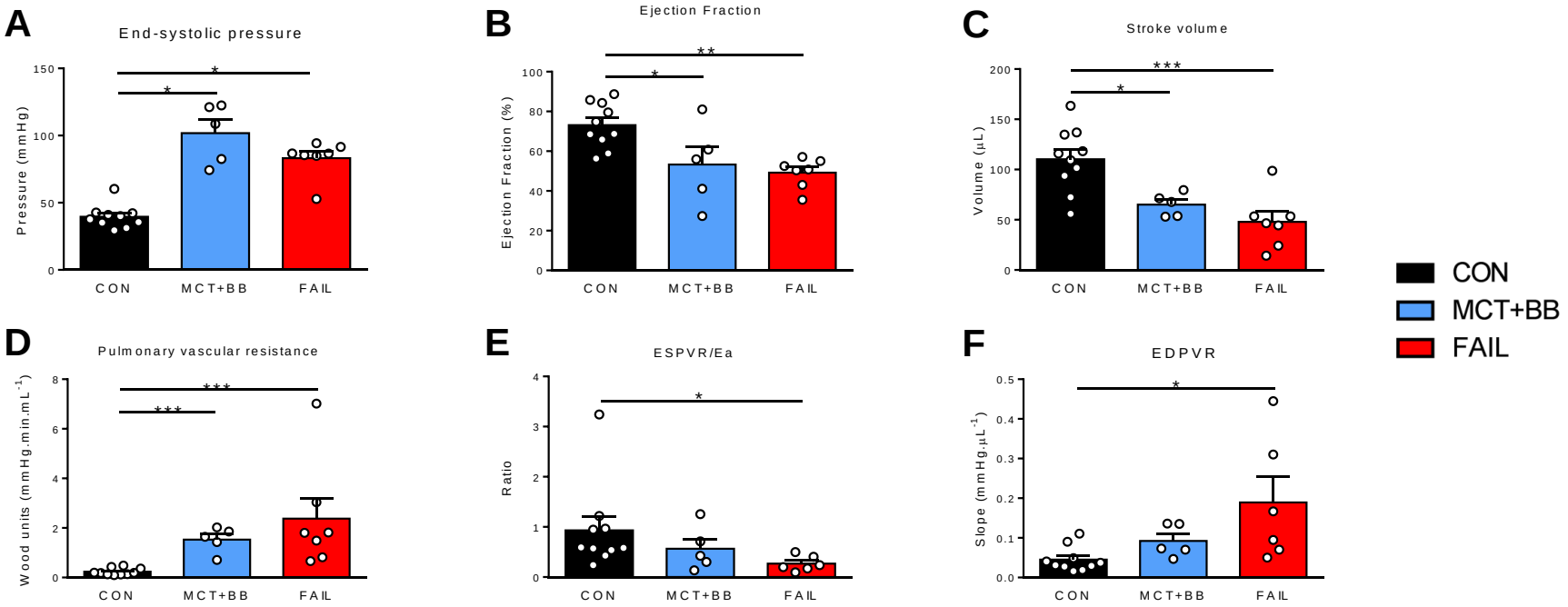

Figure 3.8 *In vivo* RV pressure-volume measurements

Pulmonary hypertension and RV dysfunction were evident in MCT+BB and FAIL rats as (**A**) elevated systolic pressure, (**B**) reduced ejection fraction and (**C**) depressed stroke volume. **D** Pulmonary vascular resistance was elevated and not significantly different between MCT+BB and FAIL rats. **E** Ventriculo-arterial coupling was assessed using the ratio of ESPVR to Ea, and was significantly depressed in FAIL compared to CON, while MCT+BB was intermediate between both groups. **F** The EDPVR was significantly increased in FAIL rats compared to CON, and was slightly reduced in MCT+BB. Values for individual rats are shown by white circles while the group mean and SEM are shown by the coloured bars. N=10 CON, 5 MCT+BB, 7 FAIL rats. *P<0.05, **P<0.01, ***P<0.001 vs CON.

Table 3.7 *In vivo* RV haemodynamic parameters recorded using a transmural conductance catheter

	CON	MCT+BB	FAIL
Heart rate (bpm)	366 ± 11	340 ± 12	349 ± 16
End-systolic pressure (mmHg)	39.5 ± 2.7	101.8 ± 9.9*	83.2 ± 5.2*
End-diastolic pressure (mmHg)	4.6 ± 0.7	9.9 ± 2.3*	9.6 ± 0.7*
dP/dt max (mmHg/s)	3165 ± 188	5723 ± 744***	4360 ± 371
dP/dt min (mmHg/s)	-2971 ± 198	-3330 ± 292	-2854 ± 214
Tau (ms)	11.2 ± 0.5	14.7 ± 1.1**	14.0 ± 0.3**
End-systolic volume (µL)	49 ± 6	78 ± 30	52 ± 10
End-diastolic volume (µL)	127 ± 10	133 ± 29	91 ± 19
Stroke volume (µL)	110 ± 10	65 ± 5*	48 ± 10***
Cardiac output ($mL.min^{-1}$)	40.4 ± 3.8	22.2 ± 2.3*	17.1 ± 4.1***
Stroke work (mmHg.µL)	3133 ± 343	4570 ± 467††	2111 ± 469
Ejection fraction (%)	73.1 ± 3.6	53.3 ± 9.1*	49.2 ± 2.8**
Arterial elastance (Ea) (mmHg/µL)	0.41 ± 0.06	1.62 ± 0.22***	2.49 ± 0.76***
ESPVR (mmHg/µL)	0.36 ± 0.10	0.75 ± 0.16	0.66 ± 0.21
EDPVR (mmHg/µL)	0.05 ± 0.01	0.09 ± 0.02	0.19 ± 0.06*
ESPVR/Ea	0.93 ± 0.27	0.57 ± 0.20	0.27 ± 0.06*
PVR ($mmHg.min.mL^{-1}$)	0.23 ± 0.04	1.53 ± 0.23***	2.38 ± 0.83***

Data are mean±SEM. Measurements in CON and MCT+BB rats were recorded on the median survival day of FAIL rats, or in FAIL rats on the day heart failure symptoms developed. dP/dt max, maximal rate of pressure development; dP/dt min, maximal rate of pressure decay; Tau, isovolumic relaxation time; Ea, arterial elastance; ESPVR, end-systolic pressure-volume relationship; EDPVR, end-diastolic pressure-volume relationship; PVR, pulmonary vascular resistance. N= 10 CON, 5 MCT+BB, 7 FAIL rats. *P<0.05, **P<0.01, ***P<0.001 vs CON; ††P<0.01 vs FAIL.

resistance was significantly elevated in both MCT+BB and FAIL rats, however there was no difference between MCT+BB and FAIL rats.

The ESPVR tended to increase in MCT+BB and FAIL rats compared to CON, however there was also a large increase in arterial elastance (Ea) in both groups of rats. This resulted in a fall in the ventriculo-arterial coupling (ESPVR/Ea) in FAIL rats which was improved in MCT+BB rats. The load-independent EDPVR was significantly elevated in FAIL rats compared to CON indicating reduced ventricle compliance to diastolic filling. EDPVR was intermediate in MCT+BB indicating a partial improvement of diastolic function. Other evidence of diastolic dysfunction in FAIL rats was significantly elevated end-diastolic pressures and prolonged isovolumic relaxation times (Tau) which were elevated to a similar extent in MCT+BB rats (Table 3.7).

3.4 Discussion

3.4.1 Monocrotaline-induced pulmonary arterial hypertension

Rats were injected with 60 mg/kg MCT as a minimally-invasive means to induce PAH which develops into right-sided heart failure within 4 weeks. We used a clinically relevant humane endpoint which defined the onset of heart failure based on its outward functional effects such as lethargy, dyspnoea, sustained weight loss and cold extremities. In the days preceding the onset of heart failure the activity level of rats monitored using running wheels is reduced and tachypnoea is apparent (Natali *et al.*, 2015). This is consistent with both the New York Heart Association classification of heart failure (1994) and the International Classification of Diseases, Ninth Revision (ICD-9) Code 428, which define heart failure according to the inability of the heart to maintain a sufficient blood supply to meet the metabolic demands of the body resulting in an exercise limitation.

FAIL rats all lost weight either suddenly (>10 g lost overnight) or over several days before the onset of heart failure indicating the presence of cardiac cachexia. Cachexia is an incompletely understood complication of chronic heart failure associated with worse prognosis which may arise due to reduced appetite, altered metabolic state and reduced nutrient absorption brought about by neurohormonal imbalance, altered blood flow and inflammation (Anker & Sharma, 2002; von Haehling *et al.*, 2007). The slower weight gain in FAIL rats is partly due to lower food intake, however this is not the sole cause as CON rats gain weight faster even when their food intake is restricted to that of

FAIL counterparts (Lourenço *et al.*, 2006). Reduced activity and limited cardiac output means blood is diverted away from the periphery and towards the vital organs, resulting in a cold tail to the touch. Congestion in the lungs due to accumulation of alveolar oedema may also occur and exacerbate dyspnoea. The arterial O_2 saturation of MCT rats is lower which suggests oedema or possibly acute lung injury becomes a barrier to gas exchange (Ishikawa *et al.*, 1991; Schermuly *et al.*, 2004).

An advantage of the MCT model is the relatively rapid onset of PAH which has been shown using echocardiography and continuous telemetry monitoring of PA pressure to occur within 2 weeks (Hess *et al.*, 1996; Jones *et al.*, 2002), and it is for this reason we chose to start treatment with metoprolol on day 15 as our aim was to treat existing PAH rather than prevent the onset of PAH, the former having more clinical relevance. We used non-invasive echocardiography to monitor the change in RV function and systolic pressure over time and consistent with previous reports found a tendency for MCT rats to have early signs of PAH by day 15 post-MCT injection as shown by decreased PAAT and slightly thicker RV free walls. This is in good agreement with the echocardiographic study of Jones *et al.* (2002) who found significantly reduced PAAT by day 15 and a tendency for increased RV wall thickness by day 17.

Functional changes in the hearts of MCT rats were largely confined to the RV, consistent with a lack of effects of MCT on the systemic circulation (Schermuly *et al.*, 2004). RV weight was significantly increased both in absolute terms and normalized to body weight. There was no direct effect of MCT on LV weight or wall thickness, although due to the lower bodyweight and weight loss in MCT rats the LV+S:BW ratio tended to increase. This is consistent with pressure overload being necessary to stimulate hypertrophic gene expression in MCT rats (Kögler *et al.*, 2003). In situations where adult body weight fluctuates, such as aging or in this case heart failure, normalizing heart weights to tibial length may correlate more closely with myocyte hypertrophy (Yin *et al.*, 1982), or alternatively Fulton's Index (the RV:LV+S ratio) may be used in the case of specifically RV hypertrophy.

Further evidence of RV specific dysfunction was reduced ejection fraction only in the RV and not the LV of MCT treated rats. The function of LV cardiomyocytes and trabeculae is generally found to be preserved or sometimes augmented in MCT rats (Kögler *et al.*, 2003), however eventually LV systolic pressure falls possibly as a result of interventricular interactions and reduced preload (Correia-Pinto *et al.*, 2009). A fall

in systemic pressure can be catastrophic as this reduces the coronary perfusion pressure and hence risks myocardial ischaemia. The flattening of the septum and reduced LV circularity results from the decreased interventricular pressure gradient which impairs LV filling due to pericardial constraint and thus reduces its force generating capacity (Figure 3.5) (Portman *et al.*, 1987). We did not find evidence of *in vivo* LV dysfunction at any stage of disease, however there was compression and reduced LV cavity area in failing rats. The orientation of the heart of MCT-treated rats was rotated anti-clockwise in the chest due to RV hypertrophy and dilatation. This would be detectable as right-axis deviation in the electrical axis of the heart recorded on an electrocardiogram.

The cause of death in rats which died suddenly could not be established due to the need to intervene at the humane endpoint when animals showed signs of distress. However there are reports that AV block is the most prevalent cause of death in conscious freely moving MCT rats monitored with telemetry (Liguo *et al.*, 2013), although spontaneous ventricular fibrillation leading to death has also been reported (Liles *et al.*, 2012; Rey *et al.*, 2012). This is consistent with sudden death occurring in around 20% of PAH patients, whereas RV pump failure is the most common cause, accounting for around 30% of deaths (Delcroix & Naeije, 2010). Some FAIL rats died when undergoing the PV procedure which was usually preceded by a progressive fall in RV force development suggesting the contractility of the failing RV is an important determinant of survival in MCT treated rats.

3.4.2 β-blockers improve survival in pulmonary arterial hypertension

The key finding of this chapter is that the β_1-specific AR blocker metoprolol significantly improved survival in rats with pre-exisiting PAH. The time to onset of heart failure was delayed by 35% when daily treatment with 10 mg/kg metoprolol was started on day 15. Concomitant with this was an improved functional status of the RV compared to time-matched FAIL rats. Using echocardiography it was possible to monitor the progression of PAH and RV dysfunction and it was found that while metoprolol slowed the deterioration in RV function, at the onset of heart failure RV function was similar in FAIL and FAIL+BB rats. This highlights the importance of the RV as a determinant of survival in PAH and justifies further investigation into the causes of contractile dysfunction and its subsequent rescue following chronic β-blocker therapy (van de Veerdonk *et al.*, 2011).

There have been limited investigations of β-blockers in rodent models of PAH which have used selective or non-selective blockers in different models of PAH, including MCT, PAB and chronic hypoxia. The most direct comparison to our study is that of Perros *et al.* (2015) who independently have also treated MCT rats with both 10 and 100 mg/kg/day metoprolol administered by daily subcutaneous injection starting on day 14 and performing PV analyses on all rats 7 days later on day 21. As such their MCT rats were at a compensated rather than failing stage, however no survival curve was established in this study. Their data is much in agreement with ours as 10 mg/kg metoprolol did not affect RV systolic pressure or RV hypertrophy but increased cardiac output, whereas in contrast to our study slightly reduced pulmonary vascular resistance. Interestingly none of these changes occurred with a higher dose of metoprolol which is in agreement with our findings using 150 mg/kg/day (Appendix A). Their main finding was that the third generation β-blocker and vasodilator, nebivolol, a highly selective (10x greater than metoprolol) β_1 antagonist and $\beta_{2/3}$ agonist exerted a greater benefit in compensated MCT rats by reducing pulmonary arteriole remodelling and vascular resistance through improved endothelial cell function. However in rats studied at 28 days post MCT, when rats are more likely to be in a failing stage, cardiac output was not different in nebivolol compared to untreated rats.

Bogaard *et al.* (2010) found a small improvement in survival in MCT rats treated with a higher dose of 150 mg/kg/day metoprolol dissolved in drinking water whereas 15 mg/kg/day carvedilol (non-selective $\alpha_1/\beta_1/\beta_2$ blocker) delivered by gavage produced a greater survival benefit when administered 2 weeks after MCT injection. The greater survival benefit using carvedilol was attributed to reduced muscularization of pulmonary arterioles which lowered PA pressure and reduced hypertrophy, in contrast to metoprolol which partially improved *in vivo* RV function but did not affect vascular remodelling or systolic pressure. In humans the recommended equivalent dose of metoprolol tartrate is 50 mg per 25 mg carvedilol (Poole-Wilson *et al.*, 2003; Di Lenarda *et al.*, 2005), therefore the 10-fold higher dose of metoprolol compared to carvedilol reported by Bogaard *et al.* (2009) may result from inaccuracies in the monitoring of drug intake.

de Man *et al.* (2011) treated MCT rats with 10 mg/kg bisoprolol (selective β_1 blocker) from day 10 until signs of heart failure were manifest or, in their absence, day 31 and found a significant improvement in survival without a regression of RV hypertrophy. Similar to our study, RV contractility was improved, as shown by a partial restoration of

ventriculo-arterial coupling (ESPVR/Ea), stroke volume and cardiac output, as well as improved diastolic function (decreased EDPVR). Increased phosphorylation of myofilament proteins downstream of PKA was reported suggesting resensitization of βAR signalling.

Cheng *et al.* (2012) found improved RV cardiomyocyte contraction and relaxation and reduced microtubule proliferation in a cat PAB model treated with propanolol (non-selective β_1/β_2 AR blocker), despite no change in RV systolic pressure or RV hypertrophy. However, the effectiveness of β-blockers in other models of RV failure has been equivocal, with some studies showing improvement whereas others have not. Andersen *et al.* (2014) found no beneficial *in vivo* haemodynamic effects of bisoprolol in rats with either moderate or severe PAB, although there were also no negative consequences. This discrepancy with our findings may be due to differences between models, as PAB causes a sudden and proximal occlusion of the PA whereas MCT causes a distal progressive increase in vascular resistance. Despite similar increases in RV systolic pressure MCT rats eventually progress to heart failure whereas PAB rats do not (Borgdorff *et al.*, 2013). Furthermore the stages of disease could be quite different, as even severe banding may only reduce cardiac output by 36% without significantly reducing the ESVPR/Ea ratio (Andersen *et al.*, 2014), whereas we found MCT reduced cardiac output by 58-66% and caused ventriculo-arterial uncoupling indicating a more severe heart-failure phenotype.

3.4.2.1 β-blocker dose equivalence

The US Food and Drug Administration (2002) warns against direct extrapolation of doses between animal and human studies according to body weight, and that normalizing by body surface area gives a better translation. Accordingly the human equivalent dose (HED) can be calculated by multiplying the animal dose by the ratio of animal to human mass per body surface area (K_m), where K_m is the empirically derived mean body weight (kg) divided by body surface area (m^2):

$$HED\ (mg/kg) = Animal\ dose\ (mg/kg) \times \frac{Animal\ K_m}{Human\ K_m}$$

We treated rats with a dose of 10 mg/kg/day metoprolol and the K_m for rats and adult humans is 6 and 37 kg/m^2, respectively (Reagan-Shaw *et al.*, 2008). Thus according to FDA recommendations the human equivalent dose we used was 1.62 mg/kg/day which

is very similar to the typical clinical dose of metoprolol prescribed in left heart failure: 150 mg per day, or ~2 mg/kg/day for a 75 kg human.

Comparisons between doses in animals and humans may further be affected by differences in the kinetics of uptake and metabolism which influence bioavailability. Extensive hepatic and intestinal first-pass metabolism of metoprolol by cytochrome CYP2D6 means its bioavailability in rat is around 20% of the oral dose compared to 40% in humans, and plasma concentrations peak within 30 min in rat compared to 1-2 h in humans (Darmansjah *et al.*, 1990; Johnson & Burlew, 1996). Therefore the bioavailability of the dose we used is expected to be on the lower end of a clinical dose. Administration routes may also affect the outcome, for instance gavage versus continuous infusion by osmotic minipump, or immediate versus slow release formulations will result in different circulating levels of metoprolol (Darmansjah *et al.*, 1990). The pharmacokinetics of metoprolol metabolism are saturable and dose-independent above oral doses of 2 mg/kg in rat (Yoon *et al.*, 2010), therefore a single bolus (as we used) will result in a greater area under curve than an equivalent total dose consumed in drinking water over several hours.

Interactions between potential therapies must also be considered as drugs can inhibit or compete for breakdown by the same enzymes and therefore remain in circulation for longer. For instance, accumulation of metoprolol due to inhibition of CYP2D6 by the anti-arrhythmic drug amiodarone was believed to cause severe systemic hypotension in a single case study of a patient with PAH (Fukumoto *et al.*, 2006; Peacock & Ross, 2010). The major breakdown pathways of sildenafil are through CYP3A4 and CYP2C9 whereas metoprolol is extensively metabolised by CYP2D6 (Johnson & Burlew, 1996; Wojtczak *et al.*, 2014), making dual therapy with these drugs a possibility in PAH so long as care is taken to avoid systemic hypotension. In contrast, carvedilol is also metabolized by CYP3A4 and CYP2C9 suggesting interactions between carvedilol and sildenafil could occur if administered simultaneously (Oldham & Clarke, 1997).

Heart rate reduction is a commonly used metric to compare the functional effects of different β-blockers which may differ in their pharmacological potency. The doses of β-blockers used by Bogaard *et al.* (2010) were titrated to lower heart rate by 20%, whereas a heart rate reduction of 10% was used by de Man *et al.* (2011). We found no significant difference in resting heart rate under anaesthesia in MCT+BB compared to FAIL rats, however heart rate tended to be reduced in both groups anyway possibly

due to increased sensitivity to anaesthetic (Benoist *et al.*, 2012). Heart rate reduction is an important but not the sole mechanism through which β-blockers are thought to work, for instance Sabbah *et al.* (2000) found 2 mg/kg/day metoprolol reduced apoptosis in a canine model of coronary microembolism without significantly affecting heart rate. Also, Nagatsu *et al.* (2000) found some improvement in cardiomyocyte contractility in a canine model of mitral regurgitation treated with atenolol (specific β_1 blocker) despite bradycardia being prevented using an implanted pacemaker.

3.4.3 Possible mechanisms of improved survival

Our data indicates the survival benefit conferred by chronic β-blocker treatment is independent of afterload reduction as there was no change in systolic pressure or pulmonary vascular resistance (Figure 3.8). This is consistent with the high β_1 selectivity of metoprolol acting on AR found predominantly on the myocardium. Consistent with our findings, Perros *et al.* (2015) and de Man *et al.* (2011) also found β_1 blockers had no effect on systolic pressure, little effect on pulmonary vascular remodelling and no difference in the RV:LV+S ratio in drug treated MCT rats. However in spite of the persisting mechanical load cardiac output was increased in the aforementioned studies as well as in the current work. This suggests the mechanism through which β_1 blockers improve PAH may be through directly enhancing or preserving the contractility of the RV.

The ESPVR is considered an index of contractility as it changes in response to inotropic agents which increase the contractility of cardiomyocytes. ESPVR is considered load-independent as it is not influenced by arterial resistance or preload, unlike SV and ejection fraction which are highly rate and afterload-dependent. However it is sensitive to diastolic stiffening and chamber geometry and therefore does not always give an accurate reflection of the contractile state of the heart. An important consideration is whether RV contractility is matched to vascular resistance, as stroke work and SV are highly dependent on arterial elastance (Ea). Burkhoff and Sagawa (1986) predicted that maximal stroke work was achieved when the ESPVR/Ea ratio was 2.0, but in healthy humans and rats the heart normally operates at a ratio closer to 1.6 where work efficiency is greater (Starling, 1993; Ruiter *et al.*, 2013). In FAIL rats Ea was significantly increased due to the high vascular resistance and although ESPVR also tended to increase this was not sufficient to prevent significant ventriculo-arterial uncoupling in these rats. This indicates the contractile capability of the RV is severely impaired in FAIL rats. Interestingly, the ESPVR/Ea ratio was partially restored

in MCT+BB rats, indicating enhanced RV contractility may be critical to the improvement in cardiac output in these rats. This was also found by de Man *et al.* (2011) in bisoprolol treated MCT rats, and although they did not study the mechanisms in detail, they suggest reduced fibrosis and increased phosphorylation of myofilament proteins targeted by PKA may improve the contractile capability of the RV.

Diastolic stiffness was significantly increased in FAIL rats compared to CON but was reduced in MCT+BB rats, however the end-diastolic pressure and Tau were still significantly elevated in MCT+BB compared to FAIL rats. Both of these factors are highly load dependent and therefore are likely to have been influenced by the larger EDV and systolic pressures which were not affected by β-blocker treatment. The steeper EDPVR in FAIL rats may include a slowly cycling crossbridge component brought about due to the inability to control cytosolic levels of ADP due to loss of CK (see Chapter 6 and Fowler *et al.* (2015a)), therefore the partial improvement in RV compliance may arise due to restoration of the CK system in MCT+BB rats. Increased CK expression was also reported in a rat model of MI treated with bisoprolol either early or late after induction of MI (Laser *et al.*, 1996). The extent to which the CK system was affected depended on the delay between MI and the initiation of treatment, suggesting early intervention is critical to preventing remodelling.

3.4.4 Echocardiography in pulmonary arterial hypertension

Echocardiography was a newly available technique at the University of Leeds at the start of this study therefore the validity and reproducibility of measurements was established. We found a good linear correlation between PAAT and RV systolic pressure which is in agreement with the findings of Dabestani *et al.* (1987) in humans and Jones *et al.* (2002) in MCT rats. This relationship occurs due to interference between the pulse wave and a reflected wavefront arising due to resistance from pulmonary arterioles (Naeije & Torbicki, 1995). Decreased arterial compliance in PAH causes an early collision of wavefronts which briefly increases pressure and decreases flow, resulting in a shortening of PAAT and the characteristic mid-systolic notch in the Doppler flow-velocity profile in severe PAH (Figure 3.5). This characteristic feature can also be used to discriminate the etiology of disease as PAH has a mid-systolic notch whereas thromboembolic pulmonary hypertension does not as the distal arterioles have normal compliance in these patients (Nakayama *et al.*, 1997). The relationship between PAAT and systolic pressure in the current study (117.2-1.828[PAAT]) was similar to that reported by Kosanovic *et al.* (2011) (~ 95-1.818[PAAT]) in MCT rats.

Our y-intercept was higher, possibly due to the relatively few values with a long PAAT and low systolic pressure. Kitabatake *et al.* (1983) found the relationship between PAAT and pressure was curvilinear and that the logarithm of PAAT vs pressure improved the correlation, however using the logarithm ($r^2 = 0.61$) or not ($r^2 = 0.58$) had little effect on the goodness of fit as our dataset had minimal skew.

There was a significant correlation between RV wall thickness measured by echo and RV:LV+S ratio. Interestingly there was a significant reduction in diastolic RV wall thickness in MCT+BB and FAIL+BB rats compared to FAIL but no significant difference in RV:LV+S ratio. It is possible the improved diastolic compliance in MCT+BB rats resulted in a tendency towards increased RV end diastolic volumes (Table 3.5) which would tend to stretch and therefore reduce the thickness of the RV measured using echo. In contrast, the reduced compliance in FAIL rats is likely to be due at least in part to the RV cardiomyocytes not fully relaxing (see Fowler *et al.* (2015a) and CHAPTER 4 and 6). Thus the increased wall thickness in FAIL rats may be partly due to hypertrophy and also partly due to impaired cardiomyocyte relaxation.

Stroke volume predicted from PA flow measured by echo tended to increase with volume measured by invasive cardiac catheterisation, however there was not a 1:1 relationship. This does not necessarily mean the Doppler measurement is unreliable, as Urboniene *et al.* (2010) found a good correlation in MCT rats between stroke volume measured by MRI and high resolution Doppler echocardiography. Our Doppler and catheter measurements were not taken simultaneously therefore there may have been some deterioration in cardiac function between the non-invasive echo examination and invasive catheterisation. Another possible source of error is in the volumes calculated using a conductance catheter in the RV which has a more complex geometry and anatomy than the LV. In humans this can be corrected by using multiple ring electrodes on the catheter to segment the RV, however the small size of rodent hearts precludes this strategy (Champion *et al.*, 2009). Alternatively volumes can be corrected against an independent volume measurement, termed α, such as Doppler predicted flow or thermodilution (Pacher *et al.*, 2008; Borgdorff *et al.*, 2013), however there are also errors associated with these methods, therefore correcting for α may simply compound the errors.

Due to the asymmetric nature of RV contraction neither fractional area change nor wall shortening measured in the parasternal short axis are ideal indicators of RV function

(Rudski *et al.*, 2010). This may explain the high variability and lack of significant differences between CON and MCT+BB groups, despite fractional RV shortening being around half that of CON rats. Fractional area change in the apical 4 chamber (A4C) view or tricuspid annular plane excursion (TAPSE) also measured in A4C, are better measures of RV function however accurate assessment of these imaging windows was not possible due to the limited resolution of our ultrasound system.

Using echocardiography we were further able to characterise the function of FAIL+BB rats at the onset of heart failure (echo data was usable from 7/7 rats) whereas due to a lower tolerance to the PV procedure invasive data could only be obtained from 3/7 FAIL+BB rats. Thus echocardiography could reduce animal usage. Our echo findings reveal the RV function of FAIL+BB rats at the onset of heart failure is similar to FAIL as cardiac index and fractional area change are reduced and systolic pressure is increased equally. This is in agreement with RV function being a key determinant of survival in PAH (van Wolferen *et al.*, 2007; Grünig *et al.*, 2013; Courand *et al.*, 2015).

A possible limitation of our findings is that we may have been measuring an acute functional improvement in the RV of MCT+BB and FAIL+BB rats due to the time between their last dose of metoprolol and the *in vivo* measurements (>14 h). Metoprolol tartrate has a short biological half-life and the majority of a single dose will be metabolized during this time (Yoon *et al.*, 2010; Lee *et al.*, 2013). However a measureable reduction in exercise heart rate, which is considered a better indicator of β-block than resting heart rate, persists in humans up to 12 h after a single dose of metoprolol tartrate despite minimal levels of the drug in the plasma, suggesting even low doses exert β-blocking activity (Darmansjah *et al.*, 1990).

Intraobserver reliability was best when measuring PAAT as the correlation coefficient was lowest (17%) compared to RV wall thickness (24%) and RV area (56%). A large part of the variability will be due to the level of experience in image analysis, for instance experienced clinical echocardiographers may have intraobserver variability as low as 7% for PAAT (Dabestani *et al.*, 1987). A further source of error lies in the resolution of our system since at maximum resolution (0.08 $mm.pixel^{-1}$) variation by 1 pixel could over or underestimate RV wall thickness by around 10%. For this reason all analyses were performed blinded to the treatment of the rat and the timepoint being measured. Evidence of successful blinding is clearly shown in Figure 3.6, in which there is negligible variability in CON parameters between days 15 and 23, but clear

early indications of PAH with progressive RV dysfunction over time in FAIL and MCT+BB rats.

3.4.5 Conclusions

The main finding of this work is that the β_1-specific AR blocker metoprolol significantly improved survival in MCT rats and partially restored RV function *in vivo* as shown by echocardiography and PV analyses. This is likely to have arisen due to an improved functional status of the RV, as when metoprolol-treated rats were allowed to progress to heart failure the RV function was similar to placebo treated FAIL rats. Importantly, these functional improvements arose independent of a reduction in pulmonary vascular resistance and systolic pressure. Metoprolol did not appear to have a preventative effect on RV hypertrophy indexed by RV:LV+S, perhaps because of the sustained mechanical load on the ventricle.

In light of the current findings and previously published preclinical literature, β-blockers appear to be safe and may confer benefits in PAH which includes increased survival and RV function (Bogaard *et al.*, 2010; de Man *et al.*, 2011). Non-selective β-blockers appear to work primarily through promoting vasodilation through PKG and nitric oxide pathways and preventing vascular remodelling thus unloading the RV (de Man *et al.*, 2011), whether this vasodilating effect would still occur if given in combination with traditional therapies in PAH patients in which nitric oxide synthesis is already impaired has yet to be investigated (Giaid & Saleh, 1995). In contrast, selective β_1-AR blockers appear to preserve RV contractility independent of afterload reduction, possibly by reducing apoptosis and increasing angiogenesis and signalling through PKA pathways (Bogaard *et al.*, 2010; de Man *et al.*, 2011).

In the past 15 years 9 drugs have been approved by the US Food and Drug Administration for use in PAH, all of which target either the endothelin, nitric oxide or prostacyclin signalling pathways, however survival is still poor and the efficacy of combination therapy with multiple vasodilators on survival has produced mixed results suggesting a ceiling has been reached using these treatments (McLaughlin *et al.*, 2014; Galiè *et al.*, 2015a). New treatment pathways are therefore needed and on the basis of our findings we propose β-blockers could be used as an adjunctive therapy alongside conventional afterload reducing treatments, thus targeting two independent causes of RV failure: progressive vascular remodelling and RV contractile dysfunction. Naturally there are important provisos to this suggestion: 1) interactions between β-

blockers and conventional therapies would first need to be established in preclinical investigations and 2) the efficacy of β-blockers would need to be shown in properly monitored clinical trials using a “start low, go slow” approach before wider uptake could be considered. Thus while we were not able to prevent heart failure, which is probably only possible by normalizing the mechanical afterload experienced by the RV, by using a β_1-specific AR blocker whose actions are primarily on the myocardium, we were able to significantly increase survival in rats with pre-existing PAH.

Chapter 4 Altered energy metabolism in pulmonary artery hypertension and rescue by β-blockers

4.1 Introduction

The heart is the most energy-consuming organ in the body, cycling through 30 kg of ATP per day, equivalent to around 300 mg ATP per heart beat, most of which is used to generate the mechanical forces required to pump blood through the vasculature (Weiss *et al.*, 2005; Ferrari *et al.*, 2006). The energy demand of the myocardium is proportional to cardiac work, therefore an increase in afterload must be met with an increase in energy supply (Khalafbeigui *et al.*, 1979). In human heart failure myocardial levels of high energy phosphates and flux through the CK system are reduced and are associated with worsening prognosis (Nascimben *et al.*, 1996; Brioschi *et al.*, 2012; Bottomley *et al.*, 2013), leading to the suggestion the failing heart is "energy starved" (Ingwall & Weiss, 2004). Altered mitochondrial energy metabolism is thought to play a major role in the pathogenesis of PAH by inducing vascular remodelling and impairing energy production in the RV (Paulin & Michelakis, 2014; Ryan & Archer, 2014). Conversely, overexpression of CK-M in mice with LV pressure overload improves ejection fraction and SV with increased energy flux through the CK system (Gupta *et al.*, 2012). In this chapter RV O_2 supply, energy metabolism and energy shuttling from the mitochondria to the cytosol via the mitochondrial CK system are investigated in MCT rats.

4.2 Methods

For detailed methods see Chapter 2.

4.2.1 Animal model

Rats were injected with MCT or saline as described previously in Chapter 2. Daily treatment with 10 mg/kg/day metoprolol (MCT+BB) was initiated 15 days after MCT injection. Experiments were performed on CON and MCT+BB rats on the median survival (±1 day) of FAIL rats, or on FAIL rats on the day heart failure symptoms developed.

4.2.2 Histology

Hearts were arrested in diastole using cold (4°C) 0.1 mM EGTA I.S. and dissected in EGTA I.S. on ice using a safety razor blade to prevent cutting injury producing contracted regions and morphological artefacts in the samples (Gerdes, 2015). A portion of the mid-RV free wall was frozen in OCT and 10 µm thick sections were cut using a cryostat. Sections were stained with picrosirius dye or fluorescein-conjugated lectin to identify collagen and capillaries, respectively. Tissue PO_2 was predicted from capillary distribution using the model of Al-Shammari *et al.* (2012) (see Section 2.4.2.1).

4.2.3 Mitochondrial function

Electron transport system

Mitochondrial respiration was measured in saponin permeabilized RV cardiomyocytes (isolated according to the methods described in Chapter 2) in the sealed chamber of an oxygraph recorder. Activities of different components of the electron transport system were interrogated by the sequential addition of substrates or inhibitors of different respiratory complexes (Kuznetsov *et al.*, 2008). The sequence of additions and a typical oxygraph recording are shown in Figure 4.1. TMPD (0.5 mM)+ascorbate (2 mM) feed electrons directly into complex IV and the resulting O_2 flux corresponds to mitochondrial mass, therefore data were normalized to TMPD O_2 flux measured at the end of the experiment (Larsen *et al.*, 2012). Flux control ratios (FCR) which are independent of cell density and mitochondrial mass were also calculated as the ratio of O_2 flux to a theoretical maximum uncoupled flux with convergent Complex I+II electron flow.

CK-mt coupling to respiration

The ability of CK-mt to stimulate respiration was investigated by the sequential titration of submaximal concentrations of ADP to the oxygraph chambers with or without creatine (25 mM). Data were normalized to basal respiration without ADP and maximum respiration in 1 mM ADP and fitted with the Michaelis-Menten equation to calculate the apparent K_m for ADP and maximum respiration (V_{max}).

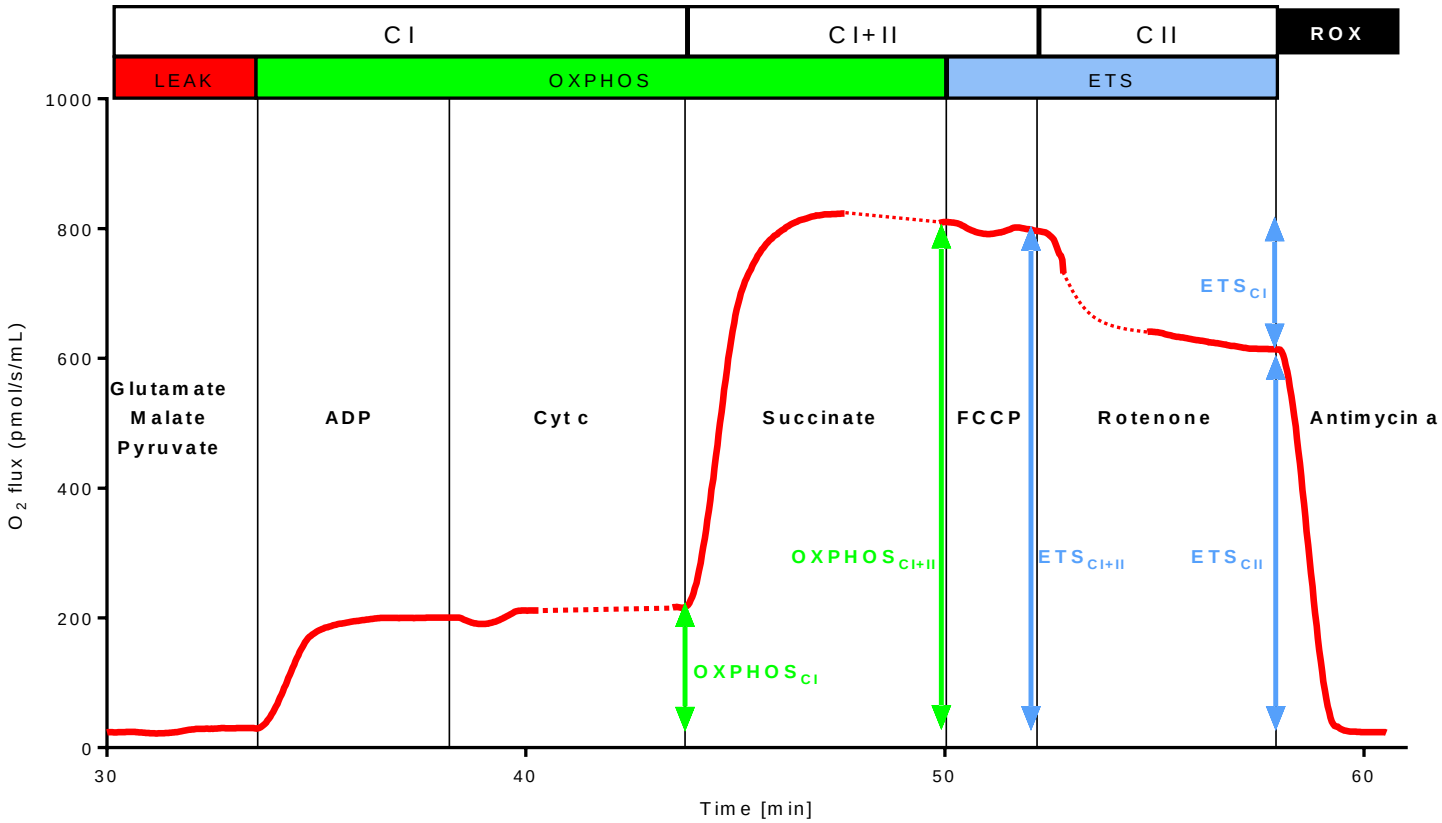

Figure 4.1 Substrate uncoupler inhibitor titration protocol

Oxygen flux (*red line*) was measured in saponin permeabilized cells. LEAK respiration was measured in the presence of CI substrates. Addition of ADP initited oxidative phosphorylation (OXPHOS). Succinate addition initiated maximal convergent CI+II OXPHOS. CII activity was measured in the presence of rotenone. Residual oxygen consumption (ROX) was measured using Antimycin a. Flux control ratios were calculated normalized to the theoretical maximal uncoupled CI+II activity (ETS_{CI+II}). Dashed lines in the trace indicate reoxygenation events.

4.3 Results

4.3.1 Coronary microcirculation

RV cryosections were stained with fluorescein-conjugated lectin and viewed under an epifluorescent microscope to visualise and quantify myocardial capillary supply. Brightly stained capillaries were apparent with clear boundaries and a circular lumen. Lectin also faintly stained the glycocalyx surrounding myocytes allowing the identification of muscle fibre boundaries.

Capillary density (CD) progressively decreased from 2400 capillaries per mm^2 in CON hearts to 1700 per mm^2 in MCT+BB and 1200 per mm^2 FAIL. CD was significantly reduced by 49% in FAIL compared to CON, and there was a trend for CD to be lower (by 28%) in MCT+BB compared to CON (P=0.06) (Figure 4.2). Consequently the mean area of myocardium supplied by each capillary increased from 427 μm^2 in CON to 648 μm^2 in MCT+BB and 869 μm^2 in FAIL. Myocyte hypertrophy alone could account for the reduced capillary density in FAIL rats, therefore the capillary to muscle fibre ratio (C:F) was calculated. The average C:F in CON and MCT+BB rats was 1.21 and 1.25 respectively, whereas it was around 25% lower in FAIL (0.90), although differences between groups were not statistically significant.

Tissue PO_2 was predicted from the spatial distribution of capillaries and diffusivity of O_2 in tissue. The dense and fairly homogeneous distribution of capillaries in CON hearts resulted in high levels of tissue oxygenation with relatively few areas of hypoxia (Figure 4.3). In contrast the majority of tissue in MCT+BB and FAIL rats was hypoxic due to the sparse population of capillaries, although MCT+BB tended to be intermediate in oxygenation between CON and FAIL. The mean tissue PO_2 in CON hearts was 13.7 mmHg, whereas it was 65% lower in MCT+BB (6.2 mmHg) and 82% lower in FAIL (2.5 mmHg).

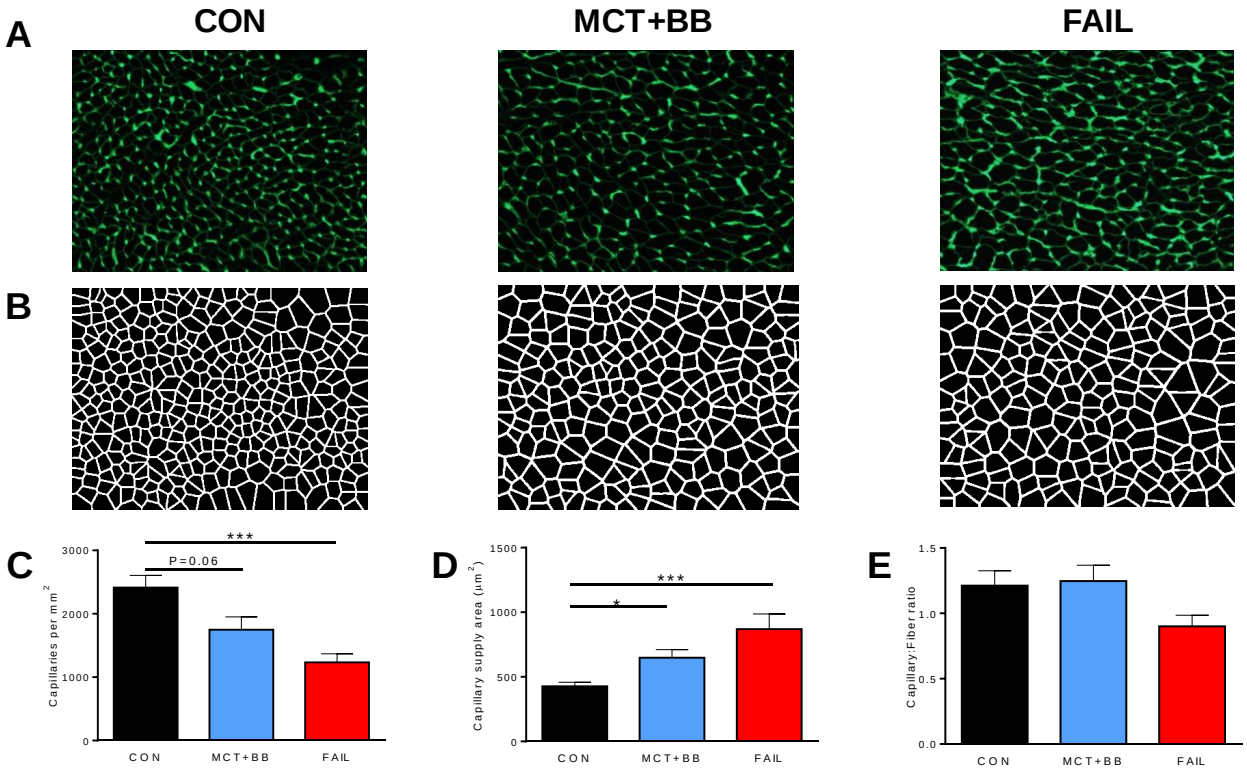

Figure 4.2 Myocardial capillary supply

A Representative images of RV sections stained with fluorescein-labelled lectin showing capillaries as bright green spots and muscle fibre boundaries. **B** Voronoi cells showing supply area of capillaries in (**A**)**. C** Capillary density was lower in MCT+BB rats (P=0.06) and FAIL compared to CON. **D** The area of myocardium supplied by each capillary increased in MCT+BB and FAIL compared to CON. **E** The capillary to muscle fibre ratio tended to stay the same in MCT+BB compared to CON but decrease in FAIL, although not significantly so. N=6 rats in each group. *P<0.05, ***P<0.001

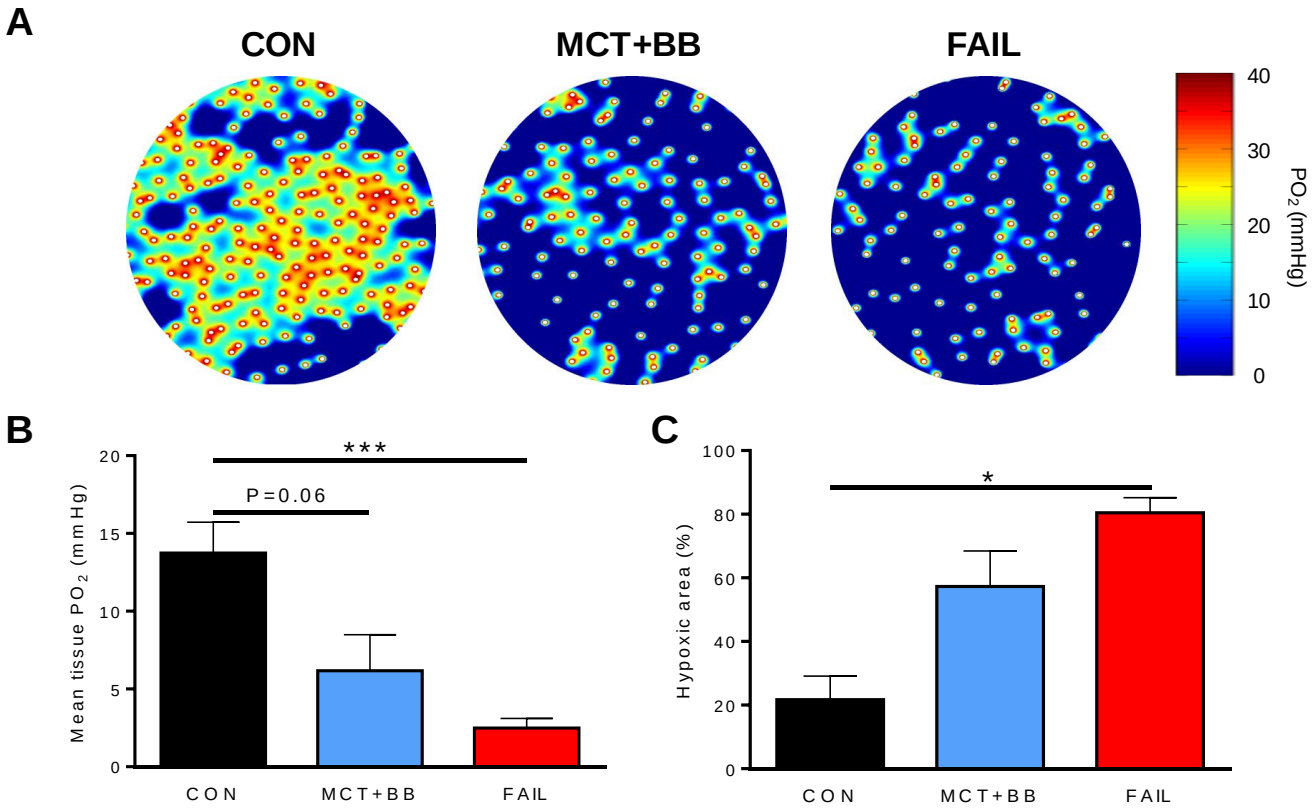

Figure 4.3 Prediction of myocardial tissue oxygenation

A Heat map showing capillary distribution (*white circles*) and predicted tissue PO_2. Capillary distribution in RV sections was digitised and finite element calculations applied to model the spatial profile of tissue PO_2. **B** Mean tissue PO_2 was greatly reduced in MCT+BB and FAIL rats. **C** The fractional area of myocardium which was hypoxic (PO_2 < 0.5 mmHg) was greater in MCT+BB and FAIL rats. N= 6 rats in each group. *P<0.05, ***P<0.001

4.3.2 Myocardial fibrosis

Myocardial fibrosis was estimated histologically in transverse RV and LV cryosections using picrosirius red staining. Collagen fibres which contain a high proportion of basic amino acid residues stain red whereas the cytosol of myocytes is stained yellow by picric acid. Collagen staining was clearly identifiable as punctate points of deep red colour in contrast to light yellow muscle fibres (Figure 4.4). The faintly stained perimysial collagen demarcating the muscle fibre boundaries was not included in the analysis, also regions containing arterioles (which are strongly stained due to perivascular collagen) were avoided during image capture. The fractional area of collagen was not different between CON, FAIL or MCT+BB rats in either the RV or LV. Collagen fractional area ranged from a minimum of 1.6% to a maximum of 4.7% in all samples.

4.3.3 Mitochondrial mass

Citrate synthase (CS) is the first enzyme of the TCA cycle and is located exclusively in the matrix of mitochondria allowing it to be used as a biomarker of mitochondrial mass (Larsen *et al.*, 2012). CS activity was measured in RV homogenates using a colorimetric assay and normalized to protein concentration. CS activity tended to be lower in FAIL and MCT+BB RV compared to CON, by 19% and 20% respectively, however the difference between groups was not statistically significant (Figure 4.5). CS activity was plotted as a function of HW:BW ratio to see if CS activity was associated with the extent of hypertrophy. The average HW:BW ratio was increased in both FAIL and MCT+BB compared to CON (CON 4.02±0.10 $mg.g^{-1}$, MCT+BB 5.15±0.27 $mg.g^{-1}$, FAIL 5.01±12 $mg.g^{-1}$; $P<0.01$ vs CON), however there was no significant correlation between CS activity and HW:BW ratio ($P=0.31$).

4.3.4 High-resolution mitochondrial respiration *in situ*

Mitochondrial respiration was measured in isolated RV cardiomyocytes *in situ* by selectively permeabilizing the sarcolemma with saponin and supplying exogeneous substrates for respiration following a SUIT protocol (Kuznetsov *et al.*, 2008). Data were expressed normalized either to TMPD (as a marker of mitochondrial mass (Larsen *et al.*, 2012)) or to an internal reference of maximum and minimum oxygen flux. Viable results were only obtained from 13/26 rats (subsequently found to be due to retention of rotenone within the oxygraph chambers) meaning a partial data set from

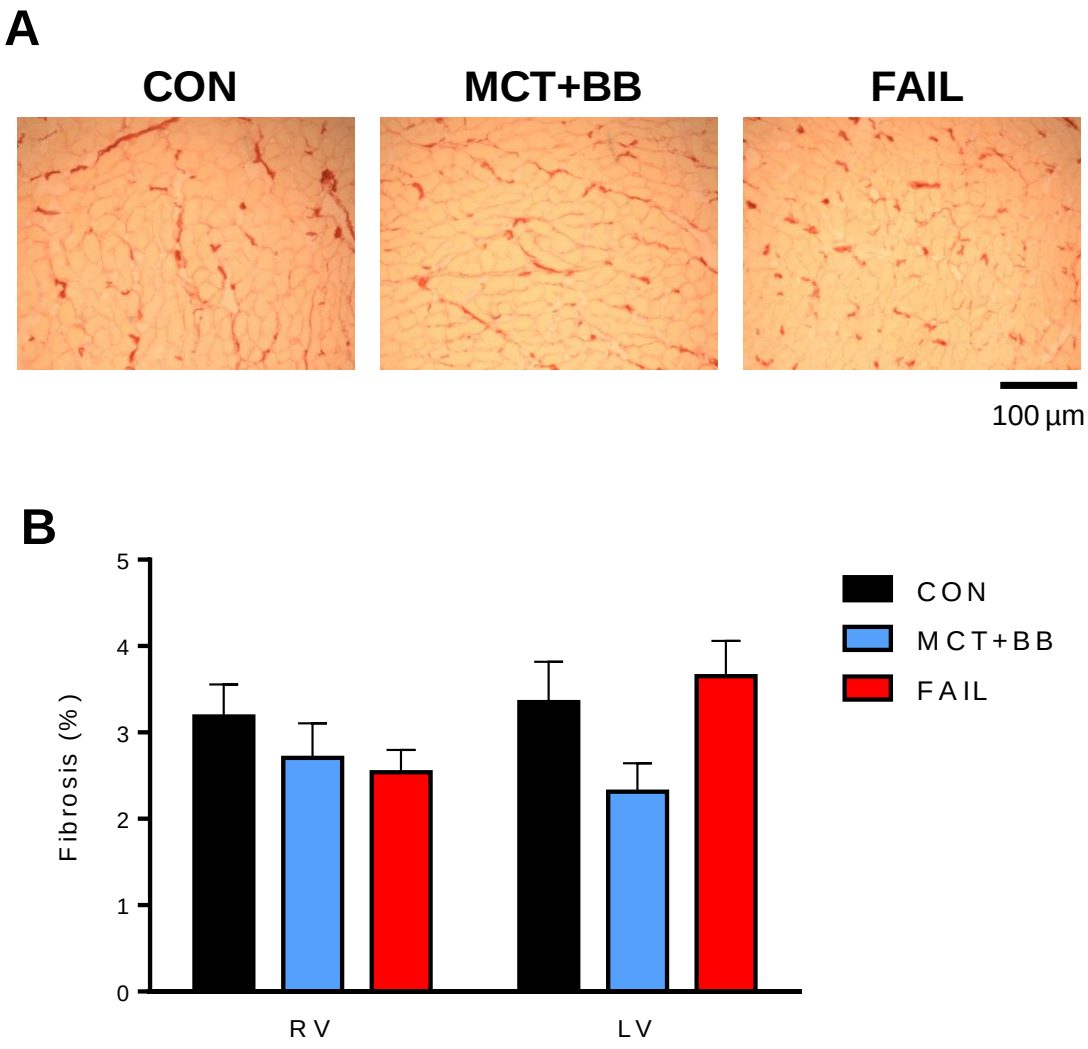

Figure 4.4 Myocardial fibrosis

A Representative images of RV sections stained with picrosirius dye. Collagen areas are stained red whereas myocardium stains yellow. The fractional area occupied by red staining was used as an index of fibrosis. **B** There were no statistical differences in collagen fractional area between groups of rats in either the RV or LV. N=5 CON, 6 MCT+BB, 6 FAIL RV samples, N=6 CON, 5 MCT+BB, 6 FAIL LV samples.

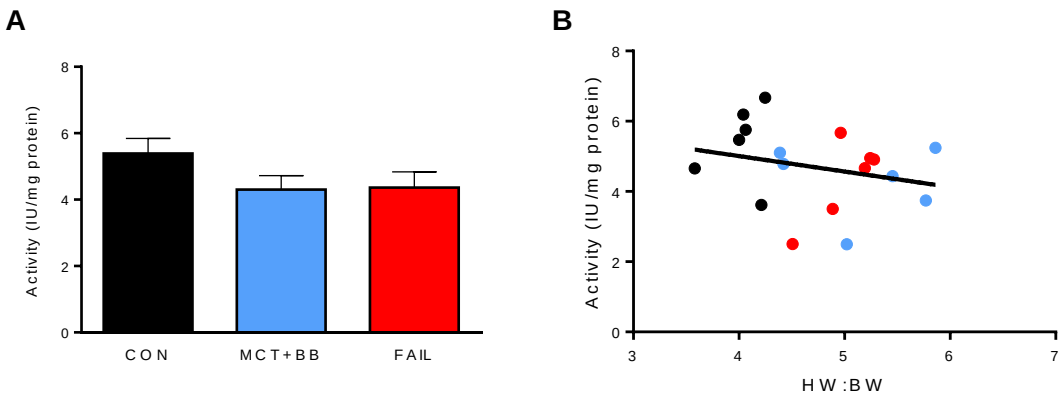

Figure 4.5 Citrate synthase activity

A Activity of the mitochondrial marker enzyme citrate synthase was not different in RV homogenates from different groups of rats. **B** There was no correlation between citrate synthase activity and HW:BW (P=0.31). N= 6 rats per group.

only two MCT+BB rats was obtained in the time available. Therefore only CON and FAIL groups were analysed statistically and any P values reported are for comparisons between these two groups (t-test); however there were no significant differences between CON and FAIL for any parameter measured therefore MCT+BB data has also been presented in the figures purely for reference. Cells from one CON rat produced a greater than 15% increase in respiration following addition of Cyt c indicating damage to the mitochondrial inner membrane and was therefore excluded from analysis; all other cells had <15% increase in respiration indicating viable mitochondria (Kuznetsov *et al.*, 2004; Wüst *et al.*, 2012).

Oxidative phosphorylation (OXPHOS) driven by complex I substrates in the presence of saturating ADP ($OXPHOS_{CI}$) tended to be lower in FAIL compared to CON, but elevated in MCT+BB compared to CON and FAIL (Figure 4.6A). The addition of the complex II substrate succinate caused a large increase in respiration driven by maximal convergent electron flow into the Q-junction ($OXPHOS_{CI+II}$). $OXPHOS_{CI+II}$ also tended to be lower in FAIL compared to CON, but increased in MCT+BB cells (Figure 4.6B). Respiration in the absence of ATP production due to lack of adenylates and therefore mainly due to leak of protons back across the inner membrane due to the proton pumping action of CI (LEAK) also tended to be decreased in FAIL but increased in MCT+BB compared to CON cells (Figure 4.6C). The coupling of respiration to the phosphorylation system was tested by measuring the increase in CI respiration following the addition of ADP (acceptor control ratio, ACR). There was an increase in ACR in FAIL, which was nearly double that of CON (P=0.065, t-test); ACR in MCT+BB cells was similar to CON (Table 4.1). Residual O_2 consumption (ROX) in the absence of electron transport and therefore primarily due to cellular oxidase enzymes was similar between all groups. ROX as a proportion of $OXPHOS_{CI+II}$ was also similar between groups.

The protonophore FCCP was added to test for possible limitation of respiration by the F_1F_0-ATP synthase and measure maximal uncoupled capacity of the electron transport system with convergent CI+II substrates. There was no significant difference in maximal respiration before ($OXPHOS_{CI+II}$) and after (ETS_{CI+II}) uncoupling in either CON, MCT+BB or FAIL cells (Table 4.1). Maximal uncoupled respiration tended to be slightly lower in FAIL compared to CON, but increased in MCT+BB in relation to both (Figure 4.7A). Uncoupled respiration driven by CII (ETS_{CII}) was measured by addition of rotenone to inhibit CI; ETS_{CII} was maintained between CON and FAIL and slightly

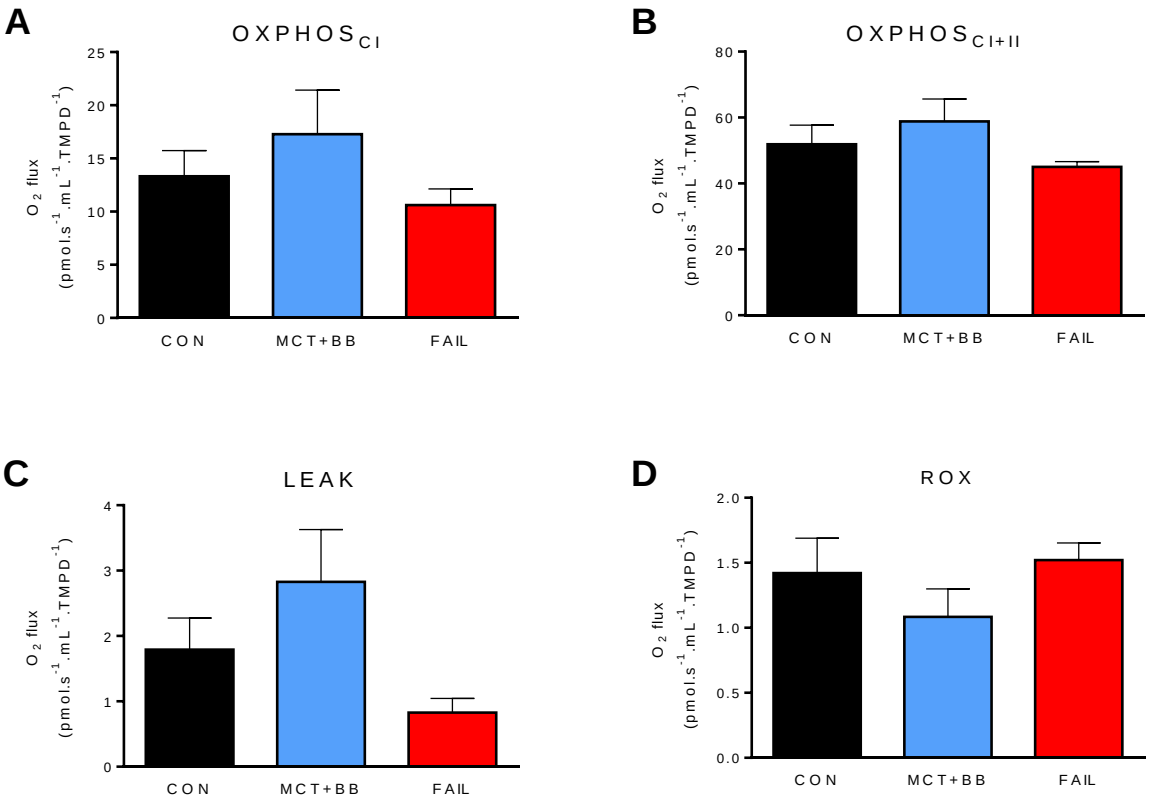

Figure 4.6 Phosphorylating and non-respiratory O_2 flux in RV cells

There were no significant differences between (**A**) CI driven OXPHOS or (**B**) maximal OXPHOS through convergent CI+II electron flow. **C** Non-phosphorylating respiration (in the absence of adenylates) tended to be lower in FAIL than CON and MCT+BB cells. **D** Residual O_2 consumption (ROX) was not different between groups. O_2 flux in each condition was normalized to flux with the artificial electron donor TMPD. RV cells from N= 5 CON, 2 MCT+BB (excluded from statistical analysis), 6 FAIL rats.

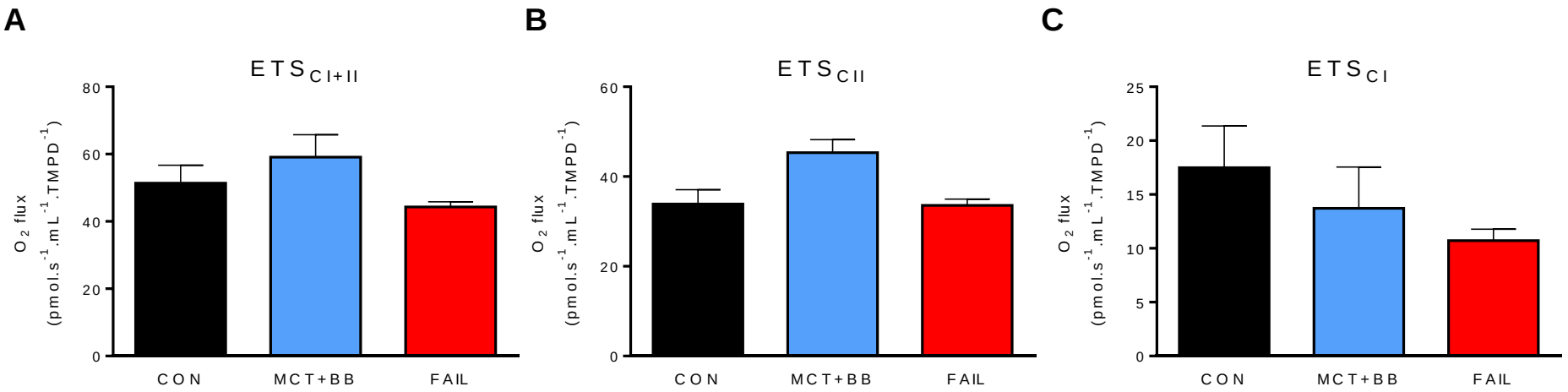

Figure 4.7 Uncoupled capacity of the electron transport system

Uncoupled respiration was measured in RV cells in the presence of FCCP. **A** Maximal uncoupled respiration with convergent CI and CII substrates (ETS_{CI+II}). **B** Uncoupled respiration driven by CII substrates (ETS_{CII}) was measured in the presence of rotenone. **C** Uncoupled respiration driven by CI was calculated by subtracting ETS_{CII} from ETS_{CI+II}. O_2 flux in each condition was normalized to flux with the artificial electron donor TMPD. RV cells from N= 5 CON, 2 MCT+BB (excluded from statistical analysis), 6 FAIL rats.

Table 4.1 Flux control ratios in RV cells

	CON	MCT+BB	FAIL
$OXPHOS_{CI}/ETS_{CI+II}$	0.27 ± 0.04	0.29 ± 0.04	0.24 ± 0.03
$OXPHOS_{CI+II}/ETS_{CI+II}$	1.00 ± 0.07	1.00 ± 0.03	0.98 ± 0.06
ETS_{CI}/ETS_{CI+II}	0.33 ± 0.05	0.23 ± 0.04	0.24 ± 0.02
ETS_{CII}/ETS_{CI+II}	0.67 ± 0.05	0.77 ± 0.04	0.76 ± 0.02
ETS_{CI}/ETS_{CII}	0.53 ± 0.13	0.32 ± 0.04	0.30 ± 0.07
$LEAK/ETS_{CI+II}$	0.04 ± 0.01	0.05 ± 0.01	0.02 ± 0.01
$ROX/OXPHOS_{CI+II}$	0.03 ± 0.01	0.02 ± 0.01	0.03 ± 0.01
ACR	8.7 ± 1.7	6.3 ± 0.4	18.5 ± 4.0$^{\#}$

Data are mean±SEM. For definitions of respiratory states and substrates please see Methods. ROX, residual oxygen consumption; ACR, acceptor control ratio. N= 5 CON, 2 MCT+BB (excluded from statistical analysis), 6 FAIL rats. $^{\#}$P=0.065 vs CON

increased in MCT+BB. Uncoupled CI respiration (ETS_{CI}) was calculated by subtracting ETS_{CII} from ETS_{CI+II}; ETS_{CI} tended to decrease from CON > MCT+BB > FAIL (Figure 4.7C).

Internal normalization was achieved by dividing O_2 flux under different substrates by maximal uncoupled respiration (ETS_{CI+II}) to obtain flux control ratios (FCR). There were no significant differences in any of the FCR between groups (Table 4.1). The ETS_{CI} FCR tended to decrease whereas the ETS_{CII} FCR tended to increase in FAIL compared to CON (P=0.105, t-test); similar results were seen in MCT+BB cells. Thus the proportional reliance on CI *versus* CII respiration tended to shift from 53% in CON to 32% in FAIL (P=0.14, t-test); a similar change was seen in MCT+BB cells. LEAK FCR was low in all groups of cells accounting for between 2-5% of maximal respiration. The ROX FCR was also low in all groups and contributed 2-3% of O_2 flux under maximal uncoupled conditions.

4.3.5 CK system

Total creatine kinase (CK) activity was measured spectrophotometrically in RV tissue homogenates. CK activity decreased by 33% in FAIL and similarly was reduced by 30% in MCT+BB compared to CON (Figure 4.8). CK activity in each sample was plotted against its corresponding HW:BW ratio to test whether CK activity changed in relation to hypertrophy. There was a significant linear negative correlation between HW:BW ratio and CK activity. We have previously reported decreased expression of the mitochondrial CK isoform (CK-mt) in Fowler *et al.* (2015a) and wanted to test whether reduced CK-mt expression was linked to reduced coupling to respiration.

Mitochondrial sensitivity to exogeneous ADP and the functional coupling of CK-mt to respiration were assessed in permeabilized cardiomyocytes supplied with NADH-linked substrates by the sequential titration of submaximal concentrations of ADP in the presence and absence of creatine. In the absence of creatine there was a progressive increase in respiration with each titration of ADP which appeared to plateau close to 1 mM ADP (Figure 4.9B). Cells from the same heart were tested simultaneously in a second oxygraph chamber with 25 mM creatine. A greater increase in O_2 flux occurred in the presence of creatine at lower concentrations of ADP and flux tended to plateau between 0.6 and 0.8 mM ADP in CON cells, whereas a smaller leftward shift in the curve was seen in MCT+BB and FAIL cells (Figure 4.9A). Maximum O_2 flux (V_{max}) was

calculated by fitting data with the Michaelis-Menten equation. V_{max} was not significantly different between groups, or in the presence or absence of creatine (Table 4.2).

The data was well described by the Michaelis-Menten equation, allowing the apparent K_mADP to be calculated. In CON cells in the absence of creatine the high K_mADP indicated low sensitivity of respiration to exogeneous ADP. The K_mADP without creatine was 29% and 57% lower in FAIL and MCT+BB than CON respectively, although these differences were not significant. Creatine significantly reduced the K_mADP in CON cells whereas there was a non-significant reduction in MCT+BB and FAIL (Table 4.2). The functional coupling or efficiency of CK-mt to stimulate respiration was measured as the percentage difference in K_mADP in the presence or absence of creatine (De Sousa *et al.*, 1999). The change in K_mADP with creatine was greatest in CON cells and progressively fell in MCT+BB and FAIL cells, indicating reduced coupling of CK-mt to respiration in MCT treated rats (Figure 4.9C). There was a significant negative correlation between percentage change in K_mADP and HW:BW ratio, indicating that CK-mt coupling decreased when hypertrophy increased (Figure 4.9D).

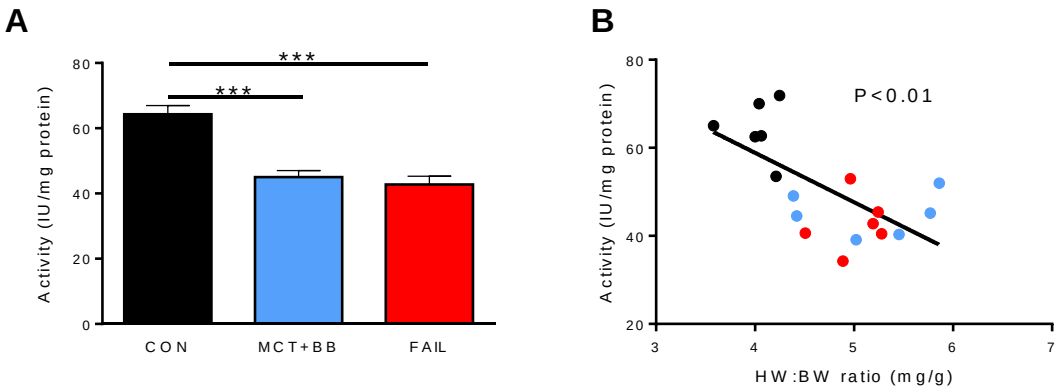

Figure 4.8 Total creatine kinase activity

A Total CK activity in RV homogenates was significantly reduced in MCT+BB and FAIL rats. **B** There was a significant negative correlation between CK activity and the corresponding HW:BW. N=6 rats per group. ***P<0.001 vs CON.

Table 4.2 Creatine stimulated respiration in mitochondria *in situ*

	CON		MCT+BB		FAIL	
		+Creatine		+Creatine		+Creatine
V_{max} (pmol.s^{-1}.mL^{-1})	120 ± 15	145 ± 14	74 ± 3	93 ± 8	305 ± 122	421 ± 165
K_mADP (mM)	0.35 ± 0.05	0.14 ± 0.02*	0.20 ± 0.04	0.11 ± 0.02	0.25 ± 0.03	0.18 ± 0.03

Data are mean±SEM. Oxygen consumption was measured in RV cells from the same heart simultaneously in the presence or absence of creatine, during titrations of submaximal concentrations of ADP. Data were fitted with the Michaelis-Menten equation to calculate maximal flux (V_{max}) and the apparent Km for exogeneous ADP (K_m[ADP]). RV cells from N= 8 CON, 3 MCT+BB, 5 FAIL rats. *P<0.05 vs CON without creatine.

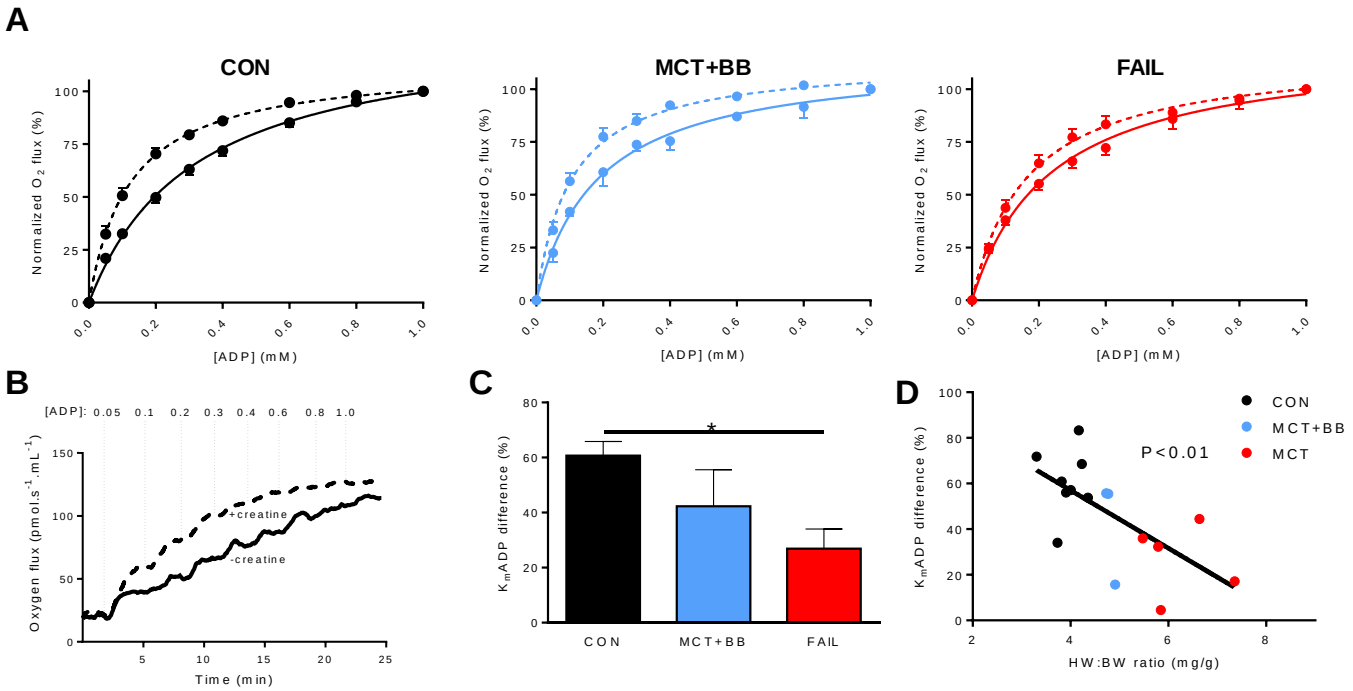

Figure 4.9 Mitochondrial creatine kinase coupling

A Average O_2 flux of RV cells in the presence (*broken lines*) and absence (*solid lines*) of creatine. Data was normalized to maximum (in 1 mM ADP) and minimum (0 mM ADP) OXPHOS respiration. Creatine caused a leftward shift in the curve indicating increased sensitivity of respiration to exogenous ADP. **B** Typical oxygraph recording of CON RV cells in the presence (*broken lines*) and absence (*solid line*) of creatine. **C** There was a greater change in the apparent K_m for exogeneous ADP in the presence of creatine in CON cells compared to MCT+BB and FAIL cells. **D** There was a significant negative correlation between change in K_m[ADP] and HW:BW ratio. Some error bars are smaller than symbols. RV cells from N=8 CON, 3 MCT+BB, 5 FAIL rats. *P<0.05

4.4 Discussion

4.4.1 Microvascular alterations in heart failure

Myocardial O_2 uptake is closely related to cardiac work and systolic wall stress. Using echocardiography we calculated a 140% increase in RV wall stress in FAIL rats due to elevated systolic pressures and more dilated ventricles, indicating RV O_2 demand will also be increased (Benoist *et al.*, 2014). Wong *et al.* (2011b) also showed that heart rate and systolic pressure are the main determinants of myocardial O_2 uptake in patients with PAH. Accordingly, van Wolferen *et al.* (2008) showed RV coronary perfusion is higher in PAH patients on average as a group compared to healthy control patients, however within the PAH group mean RV coronary perfusion negatively correlated with RV mass, suggesting myocardial perfusion and oxygenation may limit function in severe PAH. β-blockers may be beneficial to an ischaemic RV by reducing heart rate and prolonging the diastolic interval as well as promoting angiogenesis which will increase perfusion and improve myocardial oxygenation (Ferrari *et al.*, 2006; Bogaard *et al.*, 2010).

Hauton *et al.* (2015) replicated the effect of capillary rarefaction by infusing polystyrene microspheres into Langendorff perfused rat hearts which lead to heterogeneous regional hypoxia and a fall in the force of contraction. Using the same model we now show similar heterogeneity occurring in the RV of FAIL rats which may impair pump function, whereas it was partially improved in MCT+BB rats. Improved RV oxygenation could account for the enhance stroke work in MCT+BB rats compared to FAIL, identified in Chapter 3 (Khalafbeigui *et al.*, 1979). Ischaemia may be a stimulus for altered substrate utilisation as carbohydrate oxidation yields a greater energy output per litre O_2 (21.14 kJ) than fatty acid oxidation (20.04 kJ) suggesting a switch from primarily fatty acid oxidation in health to carbohydrate oxidation and glycolysis in failing hearts could compensate for reduced oxygenation (Piao *et al.*, 2010). A further consequence of reduced oxygenation could be non-contractile cells which would increase the load of the ventricle and reduce mechanical efficiency; a decrease in mechanical efficiency has been reported in RV trabeculae from MCT rats which correlated with the extent of cardiomyocyte hypertrophy (Wong *et al.*, 2010). Stretch of non-contracting cells may cause another undesirable effect through stretch activated ion channels triggering arrhythmias (Kohl *et al.*, 2001); MCT rats have previously been shown to exhibit a pro-arrhythmic phenotype (Benoist *et al.*, 2012).

Figure 4.2 shows capillary density (CD) decreases in both MCT+BB and FAIL rats thereby increasing the area supplied by each capillary. The partial restoration of capillary density in MCT+BB rats could be due in part to a reduction in muscle fibre hypertrophy, but also a normalization of the capillary to fibre ratio (CF). These data are in agreement with well conducted studies on CD in healthy versus hypertrophic human (3300 vs 2500 mm^{-2} (Roberts & Wearn, 1941)) and rat ventricle (3400 vs 2900 mm^{-2} (Gerdes *et al.*, 1979)). Reduced CD has previously been reported in the rat MCT and PAB models, however in both these cases treatment with bisoprolol did not restore CD (de Man *et al.*, 2011; Andersen *et al.*, 2014), whereas in the SuHx rat model metoprolol restored CD (Bogaard *et al.*, 2010). These differences may be due to differential effects on the regression of hypertrophy following treatment which profoundly influences CD; CF is therefore a better indicator of capillary angiogenesis or rarefaction. CF showed a tendency for a reduction in FAIL rats, whereas it was preserved in MCT+BB and CON, suggesting capillary rarefaction may be prevented by β-blockers. Capillary rarefaction may occur due to decreased HIF-1α and VEGF expression as well as increased expression of VEGF inhibitors such as p53 (Sano *et al.*, 2007), as was found in MCT rats during the transition to decompensated heart failure (Redout *et al.*, 2007; Sutendra *et al.*, 2013).

The oxygen diffusion model assumes all parameters remain constant in all samples except capillary location, however certain factors could change between CON and FAIL which could affect diffusion, for instance mitochondrial density, diffusion through the interstitial space and myoglobin concentration. It is reasonable to assume the first two are unchanged as there was no change in mitochondrial mass (citrate synthase activity) or fibrosis in FAIL rats which would be expected to promote hypoxic regions by increasing O_2 extraction proximal to the capillaries and reducing O_2 diffusion through the interstitial space. Myoglobin concentration has also been found not to change in MCT heart failure (Des Tombe *et al.*, 2002; Mouchaers *et al.*, 2009). A reduction in systemic arterial O_2 saturation has been reported in MCT rats which would exaggerate myocardial hypoxia (Schermuly *et al.*, 2004).

However, a recently developed technique of estimating mitochondrial PO_2 *in vivo* argues against an O_2 limitation in MCT heart failure (Mik *et al.*, 2009). In this method, rats are injected with 5-aminolevulinic acid which is a precursor to protoporphyrin IX and accumulates in mitochondria. Protoporphyrin IX is the final precursor to haeme and has an oxygen-dependent triplet state which can be populated by blue light and

emits red light upon return to the ground state, therefore its lifetime of delayed fluorescence depends on O_2 concentration (Mik *et al.*, 2008). Using this method Balestra *et al.* (2015) found no difference in the proportion of mitochondria with low PO_2 (<20 mmHg) in open chest anaesthetised MCT rats (42%) ventilated with room air compared to CON (53%), and concluded energy production rather than O_2 delivery was at fault in MCT rats. Using a cut-off PO_2 of 0.5 mmHg for hypoxic tissue we found the area of CON tissue which was hypoxic was 22%, which is the same value reported by Hauton *et al.* (2015) using the same model in healthy rat LV, and similar to the value reported by Beard *et al.* (2003) (~20%) who used a different three-dimensional volume simulation. The data of Balestra *et al.* (2015) are not necessarily at odds with ours: firstly ischaemic regions may not have been adequately perfused with the precursor and therefore the results will be skewed towards regions with better flow and higher PO_2. Furthermore, as this was measured *in vivo*, only the subepicardium was measured, however Kobayashi *et al.* (1994) found significant transmural variation in the CF in the RV of MCT rats. Finally, according to their description measurements were likely taken from the RV close to the apex where wall stress is lower, whereas our measurements were taken from the mid RV free wall where stress is likely to be greater and therefore hypertrophy may be greater (Quaife *et al.*, 2006).

Myocardial oxygenation was measured in patients with non-ischaemic dilated cardiomyopathy using O_2 sensitive MRI by Dass *et al.* (2015) who found no difference in oxygenation despite having lower coronary flow. However, the same group also found oxygenation and coronary perfusion in response to vasodilator stress was reduced in patients with hypertrophic cardiomyopathy suggesting the role of myocardial oxygenation may differ depending on the disease etiology (Karamitsos *et al.*, 2013).

4.4.2 No evidence of myocardial fibrosis in RV failure

Given the tendency for reduced myocardial oxygenation, severe pressure overload and steeper EDPVR *in vivo* (Chapter 3), chronic β-adrenergic activation (Seyfarth *et al.*, 2000; Leineweber *et al.*, 2003), and increased apoptosis and pro-apoptotic enzymes reported in this model (Umar *et al.*, 2012), we had reason to expect increased fibrosis in the RV of FAIL rats. However, as this was not the case it suggests proliferation of the extracellular matrix is not a leading cause of the steeper EDPVR in FAIL rats.

There is likely to be a temporal discontinuity between cell death and proliferation of the extracellular matrix, as was found by Campian *et al.* (2009) by serially monitoring

apoptosis and fibrosis in MCT rats. Apoptosis increased to a peak around day 22 post-MCT and then declined, whereas significant fibrosis occurred after day 27. Increased fibrosis and expression of MMP-2 and MMP-9 has also been reported by groups which have allowed MCT rats to progress to a point with higher mortality events (Umar *et al.*, 2012; Kaur *et al.*, 2015; Okumura *et al.*, 2015). This does not preclude a role for collagen in diastolic myocardial stiffness, for instance a higher proportion of collagen crosslinking may be more important than total collagen in reducing myocardial compliance (Badenhorst *et al.*, 2003; Cingolani *et al.*, 2004). Also, Ishikawa *et al.* (1992a) found that while total collagen measured by hydroxyproline assay was not increased at 4 weeks in MCT rats, there was a shift in collagen isoform from the stiffer and more predominant Type I collagen towards the more compliant foetal Type III collagen (Medugorac, 1982).

The range of collagen fractional area we found (3-4%) is within a typical range for normal myocardium without scarring (e.g. due to myocardial infarction) measured using electron microscopy (Page *et al.*, 1971), however many studies report much higher collagen content in healthy myocardium. It is likely this difference is due to the inclusion or exclusion of perimysial collagen in the analysis, instead of only the thicker punctate or 'seams' of fibrosis (as used in this study). Inclusion of perivascular fibrosis would also dramatically increase the fractional collagen area (c.f. representative images in Fig 2C of Umar *et al.* (2012)). Conversely, alternative stains such as Masson's trichrome may produce lower values of fibrosis due to lower sensitivity to thin collagen fibres (Whittaker *et al.*, 1994). It is for these reasons we analysed fibrosis blinded to the origin of the samples.

Protein expression of full length caspase-3 was increased in the RV of FAIL and MCT+BB rats suggesting they are currently in the midst of apoptosis (R. Norman, personal communication). In the SuHx model in rats both carvedilol and metoprolol reduced the number of terminal deoxynucleotidyl transferase dUTP nick end labeling (TUNEL) positive cells, indicating fewer cells were undergoing apoptosis, which coincided with reduced fibrosis. In a canine model of coronary microembolism in which small coronary vessels are blocked by polystyrene beads resulting in ischaemic heart failure, chronic low dose metoprolol (~2 mg/kg/day) significantly reduced apoptosis and decreased caspase-3 expression without altering resting heart rate (Sabbah *et al.*, 2000). These data suggest a possible mechanism through which β-blockers increase survival is by favouring cell survival thus enhancing the contractility of the heart.

4.4.3 Preserved mitochondrial mass in RV failure

At rest the healthy RV extracts about 50% of O_2 supplied by the coronary circulation but increases extraction during exercise, whereas the LV extracts around 75% O_2 at rest and relies on increased coronary flow to increase MVO_2 (Zong *et al.*, 2005). Reduced myocardial perfusion in PAH could be compensated for by an increase in RV O_2 extraction, as was demonstrated by Wong *et al.* (2011a) who found it increased to 75% at rest in NYHA class III PAH patients, suggesting patients may have decreased coronary flow reserve and a possible O_2 limitation during activity. Increased mitochondrial mass could increase the arterio-venous O_2 difference and compensate for reduced RV perfusion in PAH, conversely loss of mitochondria could exacerbate RV failure by reducing the energy producing capacity of the heart.

There was no difference in CS activity between any of the groups of rats. CS activity, cardiolipin protein expression and Complex IV activity measured respirometrically with TMPD+ascorbate, are commonly used as a markers of mitochondrial mass which closely correlate with mitochondrial fractional area measured using electron microscopy (Larsen *et al.*, 2012). Mitochondrial mass is usually found not to change (Rosca *et al.*, 2008; Lemieux *et al.*, 2011a) or decrease (De Sousa *et al.*, 1999; Stride *et al.*, 2013) in human and animal models of heart failure which may reflect the duration or severity of disease, but also possibly the method of normalization (Kilbaugh *et al.*, 2015). CS enzyme activity can also be depressed independent of a change in mitochondrial mass, for instance by oxidative modification, resulting in underestimation of mitochondrial mass or respiratory capacity if data are normalized to CS activity (Chepelev *et al.*, 2009). While we did not find a decrease in mitochondrial mass at this stage of disease, others have reported decreased PGC-1α mRNA expression in MCT rats which could eventually cause a loss of mitochondria and activity of ETS complexes (Enache *et al.*, 2013).

4.4.4 Preserved electron-transport system in heart failure

Gross measures of mitochondrial function such as the acceptor control ratio (ACR) are sensitive indicators of coupling between substrate oxidation and ATP synthesis as any defect along the electron transport system can reduce the ACR. We found the ACR actually tended to increase in FAIL cells, largely due to decreased LEAK respiration, indicating coupling of oxidative phosphorylation was preserved in failing cells.

Mitochondrial dysfunction has been found in other models of PAH such as SuHx rats, in which the ADP/O_2 ratio was reduced in isolated RV mitochondria. Interestingly this was restored by chronic treatment with carvedilol which also promoted the expression of genes responsible for mitochondrial biogenesis and maintenance (Drake *et al.*, 2013). However, gross measures such as the ACR or ADP/O_2 are insensitive to opposing changes (e.g. a reduction in LEAK respiration could increase ACR even with reduced maximal respiration) furthermore they do not allow identification of the source of mitochondrial dysfunction, therefore we employed a substrate uncoupler inhibitor titration protocol to interrogate individual components of the electron transport system for defects which could impair energy production (Kuznetsov *et al.*, 2008).

Maximal respiration in the presence of both CI+II substrates was slightly but not significantly lower in RV cells from FAIL rats compared to CON. This occurred due to a tendency for CI respiration to be lower, whereas CII activity was unchanged in MCT rats, resulting in a shift in the relative contribution of CI to respiration from 50% in CON rats to 30% in FAIL and MCT+BB rats. Our results are in accord with those of Daicho *et al.* (2009) who found CI respiration was preserved in MCT rats up to 4 weeks post-injection, but decreased beyond 4 weeks, whereas CII respiration did not change throughout (Daicho *et al.*, 2009). Leaving our rats beyond the current endpoint may have made these changes statistically significant but would also incur an unacceptably high mortality rate (c.f. 90% mortality in MCT rats by week 6 (Sutendra *et al.*, 2013)). Thus stage-dependent reduction in CI respiration seems to occur in MCT rats due to decreased expression of NADH dehydrogenase (Schott *et al.*, 2005).

In healthy human myocardium the phosphorylation system exerts a strong limitation on maximal respiration resulting in an OXPHOS/ETS ratio close to 0.5, however in heart failure the ratio decreases indicating reduced capacity of the phosphorylation system (Lemieux *et al.*, 2011a). In healthy rat myocardium the phosphorylation system is not limiting meaning OXPHOS/ETS is equal to 1.0, as show in Table 4.1, however we tested whether this could change in MCT rats by titrating the uncoupler FCCP. There was no increase in respiration with FCCP in any group of rats indicating the phosphorylation system does not limit respiration in healthy or failing myocardium in rats. This concords with unchanged protein expression of the F_1F_0-ATPase in the MCT RV found by Redout *et al.* (2007).

A high mitochondrial membrane potential creates a driving force for leak of H^+ back across the inner membrane resulting in a basal, LEAK, respiration which is non-phosphorylating and therefore decreases the efficiency of ATP production. However, there was no difference in LEAK respiration in FAIL compared to CON rats in line with preserved intactness of the MIM tested by the addition of cytochrome c. ROS production was also not different between groups suggesting mitochondria are not a primary source of oxidative stress at this stage in our rats. Decreased mitochondrial ROS production has been reported in MCT rats with compensated hypertrophy, which reverses upon the transition to decompensated heart failure (Sutendra *et al.*, 2013). Cytosolic oxidase enzymes such as NADPH oxidase and xanthine oxidase are increased in heart failure and may contribute substantial amounts of ROS in PAH (Redout *et al.*, 2007; Hirsch *et al.*, 2012).

4.4.5 CK energy shuttle in heart failure

There was a large reduction in total CK activity in FAIL and MCT+BB RV homogenates, which is in line with our previous observation that expression of the two predominant CK isoforms, CK-M and CK-mt, is reduced in the RV of FAIL rats (Fowler *et al.*, 2015a). However CK activity was not restored or partially increased with β-blocker treatment which was unexpected considering sarcomere length was partially restored in MCT+BB rats. CK-M and CK-mt protein expression was intermediate in MCT+BB compared to FAIL rats (R. Stones, personal communication) suggesting post-translational inactivation of CK may have occurred.

Changes in expression do not necessarily directly correlate with changes in activity, for instance Shen *et al.* (2005) found in a canine tachypacing model of heart failure, that CK-M and CK-mt activity returned to normal after pacing was switched off despite protein expression remaining depressed. The CK catalytic site contains cysteine residues sensitive to oxidation which may reversibly (e.g. in the case of S-nitrosation (Konorev *et al.*, 1998)) or irreversibly (e.g. in the case of peroxynitrite (Stachowiak *et al.*, 1998; Mihm & Bauer, 2002)) inhibit enzyme activity. The location of CK-mt within mitochondria makes it particularly vulnerable to respiratory ROS (Schlattner *et al.*, 2006).

β-adrenergic stimulation appears to acutely regulate CK isoform expression, as decreased CK-M and increased CK-B mRNA expression occurred in Langendorff perfused rat hearts following 3h infusion with 10 nM isoproterenol (Hammerschmidt *et*

al., 2000). Changes in CK activity and isoenzyme distribution in heart failure can revert back to a normal phenotype if the noxious stimulus is removed or attenuated by drug therapy. For instance, reducing the mechanical load on the heart with a ventricle assist device restored expression of CK-M and CK-mt in patients with LV failure (Park *et al.*, 2002), while in a rat model of MI pharmacological treatment with bisoprolol attenuated changes in CK-mt and CK-B mRNA expression (Laser *et al.*, 1996).

4.4.6 CK-mt functional coupling in heart failure

There may not be a direct relationship between the specific activity of an enzyme (a product of its abundance and enzymatic activity) and its biological functional activity (which arises due to its proximity and interactions with other enzymes or substrates). For instance, hypoosmotic treatment of mitochondria releases CK-mt from the MIM and abolishes the creatine stimulated increase in respiration, yet as the enzyme remains trapped in the intermembrane space its specific activity is unaffected (Kuznetsov *et al.*, 1989). Results from the SUIT protocol revealed the machinery of the ETS was largely preserved in FAIL cells, however mitochondria are not normally working at maximum capacity, therefore the functional consequences of loss of CK-mt protein were investigated as this is likely to have a larger impact on mitochondrial submaximal respiration at physiological ADP concentrations (~50-100 µM).

There was a smaller change in the apparent K_m for ADP with creatine in FAIL compared to CON cells and it was intermediate in MCT+BB and interestingly, the stimulatory effect of creatine was inversely correlated with RV hypertrophy (Figure 4.9D). Reduced CK-mt function has also been reported using a similar protocol in human dilated and ischaemic cardiomyopathy (Popovich *et al.*, 1995; Stride *et al.*, 2013), rat LV pressure overload (De Sousa *et al.*, 1999) and in Syrian cardiomyopathic hamsters (Veksler *et al.*, 1988). Reduced CK-mt activity could make failing hearts less responsive to a sudden increase in cardiac work.

The *in vivo* consequences of reduced CK-mt functional coupling are illustrated by a highly significant positive correlation between creatine-stimulated respiration and ejection fraction in human systolic heart failure, whereas it negatively correlates with end-diastolic pressure (Popovich *et al.*, 1995). This indicates subcellular changes in the CK energy shuttle may affect contraction by limiting energy supply to cytosolic ATPases. Interestingly, in several of these studies the ACR, which is considered a sensitive indicator of mitochondrial dysfunction, was not significantly different between

healthy and failing conditions (Veksler *et al.*, 1988; De Sousa *et al.*, 1999; Stride *et al.*, 2013). This was also a finding of the current work and implies that even if the TCA cycle and ETS are preserved in heart failure, reduced phosphocreatine energy shuttling may impair energy delivery to the myofilaments and reduce the contractility of the heart.

In the absence of creatine there was a tendency for K_mADP to be lower in RV cells from MCT treated rats indicating increased permeability of the MOM, although this was not statistically significant. Interestingly, increased MOM permeability was also found in other circumstances where the CK system is impaired such as LV muscle fibres of CK-M$^{-/-}$ (Veksler *et al.*, 1995) and CK-M/mt$^{-/-}$ double knockout mice (Kaasik *et al.*, 2001), and rats depleted of creatine by β-guanidinopropionic acid feeding (Clark *et al.*, 1994). Similarly, during the early development of mice from day 1 up to 3 months old, a fall in MOM permeability is inversely correlated with an increase in CK-mt expression (Anmann *et al.*, 2014). Conversely, Roosimaa *et al.* (2013) found the MOM diffusion barrier to ADP was greater in dilated human atrial tissue, however total and CK-mt functional activity were unchanged in these samples. Also, ter Veld *et al.* (2005) found the K_mADP of isolated cardiac mitochondria was higher in CK-M/mt$^{-/-}$ double knockout mice but not single knockout mice, which they suggest is an adaptation to higher resting levels of ADP; however isolated mitochondria lack the influence of tubulin on the VDAC pore and therefore the implications of this *in situ* where K_mADP is much higher is unclear. Therefore increased MOM permeability may be a compensatory adaptation to maintain energy production despite the lack of a functioning CK system.

Adenylates cross the MOM through the VDAC whose permeability is determined by the open state of the pore which, despite its name, is primary modified by free tubulin (Rostovtseva *et al.*, 2008). Experimentally modifying free and polymerized tubulin using colchicine to destabilize, or paclitaxel to polymerize, microtubules leads to a decrease or increase, respectively, of MOM permeability (Maldonado *et al.*, 2010). Similarly, oxidative muscle fibre types have a low MOM permeability and a high proportion of free tubulin whereas glycolytic muscle fibres have a high MOM permeability and low proportion of free tubulin (Varikmaa *et al.*, 2014). The tendency for MOM permeability to be increased in MCT treated rats could be due to the decreased ratio of free:total β tubulin in FAIL RV cells identified by Stones *et al.* (2013).

The shift in K_mADP with creatine is a commonly used method of determining CK-mt function, however this protocol has been criticised on the grounds that cytosolic ATPases and cytosolic CK could regenerate ADP either through ATP hydrolysis or the reverse CK reaction, ATP+Cr→ADP+PCr, which could be sufficient to shift the Km to lower values (Callahan & Supinski, 2007; Guzun *et al.*, 2009). The magnitude of this effect has yet to be quantified, however since our solutions lack Ca^{2+} the activity of the main ATPases in cardiomyocytes (SERCA and myosin ATPase) is likely to be relatively small.

4.5 Conclusion

There was a large reduction in capillary density in the RV of FAIL rats leading to substantial areas of myocardium poorly supplied with O_2, suggesting O_2 delivery to the myocardium may be limiting in PAH. The RV of MCT+BB rats may be better oxygenated, in part due to less hypertrophy of muscle fibres and also prevention of capillary rarefaction. We found no evidence of a general trend towards mitochondrial damage or dysfunction in MCT treated rats, however there was a clear difference in the ability of CK-mt to stimulate respiration. The preserved maximal respiration and mitochondrial mass indicates neither reduced mitochondrial availability nor specific defects in the machinery of oxidative phosphorylation play a leading role in the pathogenesis of MCT heart failure. Re-instigating blood flow to ischaemic regions may awaken 'hibernating' myocardium and restore contractility to the failing RV. β-blockers appear to improve oxygenation through reduction of cardiomyocyte hypertrophy and prevention of capillary rarefaction which may contribute to the enhanced RV contractility of MCT+BB rats.

Chapter 5 Ventricular myocyte contractile function in β-blocker treated rats

5.1 Introduction

The causes of impaired RV contractility in PAH are likely to be multifactorial; electrical remodelling, Ca^{2+} homeostasis, neurohormonal desensitization, myofilament changes, fibrosis, and altered energy metabolism have all been identified as possible contributory elements. Ultimately, the ability of the myocardium to generate force is determined by the electrically synchronised cycling of Ca^{2+} in cardiomyocytes which effects actin-myosin crossbridge formation. Dysfunctional excitation-contraction coupling in LV failure is known to profoundly influence the pathophysiology of the disease, therefore its role in RV dysfunction in PAH warrants detailed investigation.

In the previous chapters chronic treatment with a low dose of metoprolol was shown to significantly improve survival and RV function *in vivo* in rats with existing PAH and was associated with partial restoration of oxygen delivery to the myocardium. In this chapter the intrinsic contractility and Ca^{2+} handling of RV cardiomyocytes were investigated as possible causes of improved RV function and survival in MCT+BB rats. In failing RV myocytes deranged Ca^{2+} handling is shown to coincide with structural abnormalities and an inability to cope when stressed. Ca^{2+} handling was partially or fully restored in RV cells from MCT+BB rats, which improved their ability to contract at faster pacing frequencies. These data provide insight into dysfunctional Ca^{2+} handling in RV myocytes as a cause of poor RV contractility and demonstrate β-blockers prevent or reverse these changes. This provides mechanistic evidence supporting the therapeutic potential of β-blockers as a novel treatment for PAH.

5.2 Methods

5.2.1 Animal model

Rats were injected with MCT or saline as described previously in Chapter 2. Daily treatment with 10 mg/kg/day metoprolol (MCT+BB) was initiated 15 days after MCT injection. Experiments were performed on CON and MCT+BB rats on the median survival (±1 day) of FAIL rats, or on FAIL rats on the day heart failure symptoms developed. RV and LV cardiomyocytes were isolated as described in Chapter 2.

5.2.2 Identification of Ca^{2+} wave initiated 'action potentials'

Cells loaded with Fura-4F-AM were electrically paced at 5 Hz for 1 min, then pacing was switched off for 1 min and the number of spontaneous Ca^{2+} waves counted by visually identifying deflections in the Fura-4 ratio recording. A method was developed to categorize waves as propagating (if it travelled through the cell without a global Ca^{2+} transient occurring) or as waves which triggered a global Ca^{2+} transient and therefore an action potential (wave-initiated 'APs'); this designation was chosen on the premise that a global Ca^{2+} transient indicated synchronized membrane depolarization and Ca^{2+} channel opening, whereas a propagating wave reflected Ca^{2+}-induced Ca^{2+}-release between neighbouring Ca^{2+} release units (Figure 5.1). The validity of this method was first established by comparing the morphology of Fura-4 recorded Ca^{2+} waves (which lack spatial definition) with Ca^{2+} waves recorded in Fluo-4 loaded cells. Spatially averaged x-t linescan images of propagating waves showed a slow monophasic upstroke and decay. In contrast, the spatially averaged profile of wave-initiated 'APs' produced a biphasic slow initial upstroke followed by a secondary rapid upstroke and decay. These waveforms were also observed in Fura-4 recordings suggesting a common cause. Wave-initiated 'APs' were considered as such if the upstroke velocity was ≥50% that of a systolic Ca^{2+} transient recorded in the same cell. The fluorescence derivative was filtered using a 10 Hz Zero-Phase Lowpass filter (IonWizard, IonOptix, Milton, MA) with a width of 21 points to assist identification of wave-initiated 'APs'.

5.2.3 Myofilament Ca^{2+} sensitivity in intact cells

During late relaxation of unloaded cell shortening there is a dynamic equilibrium between cytosolic Ca^{2+} and lengthening which can be visualised as a linear relationship in Ca^{2+}-length plots (Spurgeon *et al.*, 1992). Sarcomere shortening was recorded in Fura-4F-AM (2 µM) loaded cells while cytosolic Ca^{2+} was monitored according to the methods described in Chapter 2. The Fura-4 recording was interpolated to account for the different data recording rates of Fura and sarcomere length (200 vs 250 Hz). Fura-4 ratio was plotted against sarcomere length and the slope of the relationship during late diastole used as an index of myofilament Ca^{2+} sensitivity.

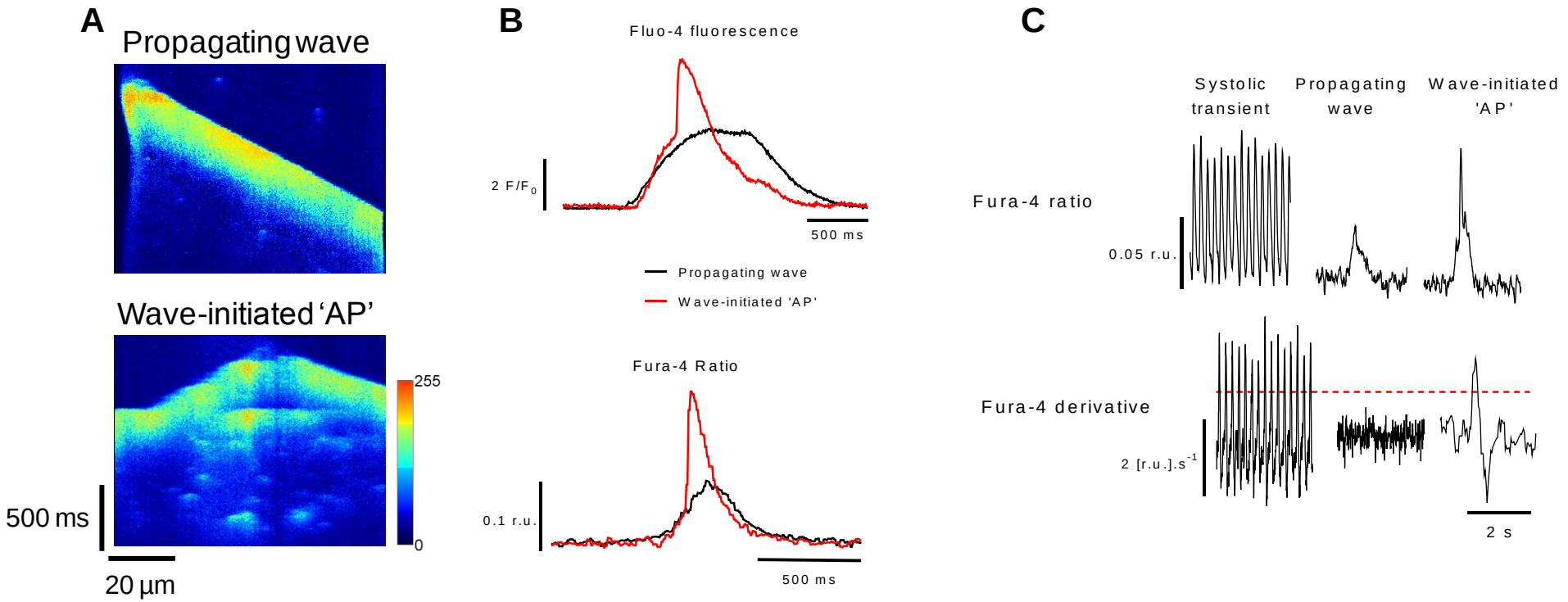

Figure 5.1 Identification of Ca^{2+} wave-initiated 'action potentials'

A Example confocal linescan recordings of a propagating Ca^{2+} wave (*upper panel*) and a Ca^{2+} wave triggering a global Ca^{2+} transient (*lower panel*). **B** *Upper panel* Averaged pixel intensity profiles of the waves in (**A**). Wave-initiated 'APs' displayed a distinctive biphasic slow then rapid Ca^{2+} upstroke and decay, in contrast to slow monotonic propagating waves. *Lower panel* Similar wave morphologies were identifiable using widefield fluoresence recordings of Fura-4 loaded cells . **C** The first derivative of the Fura-4 recording was used to categorise waves as wave-initiated 'APs' if the upstroke velocity was ≥50% the systolic upstroke velocity (*red dashed line*), otherwise they were designated as propagating.

5.3 Results

5.3.1 Cell geometry

Cellular hypertrophy was evident in RV cells from MCT-treated groups, as evidenced by increased cell width, width:length ratio and predicted cell volume, but was significantly greater in FAIL compared to MCT+BB cells (Figure 5.2). Cell width was 9% greater in MCT+BB and 22% greater in FAIL, compared to CON RV cells. Cell length tended to decrease from CON>MCT+BB>FAIL. Cell length was 2.6% shorter in MCT+BB and 7.3% shorter in FAIL, compared to CON RV cells. This resulted in an 11% increase in MCT+BB and a 32% increase in FAIL cell width:length ratio, compared to CON RV. Cell volume was predicted from cell length and width and was increased by 15% in MCT+BB and 37% in FAIL, compared to CON RV cells.

There were no significant differences between LV cells from CON, MCT+BB or FAIL rats in cell width, length, width:length ratio or cell volume. LV cell length tended to be slightly shorter in LV FAIL cells compared to LV MCT+BB by 2.6% but this was not significant.

5.3.2 Resting sarcomere length

SL was measured in quiescent isolated cardiomyocytes. Resting SL in RV and LV cells from CON rats was approximately 1.90 µm. SL in RV cells from MCT treated rats was shorter than in CON rats, though was intermediate between CON and FAIL in MCT+BB RV cells (Figure 5.3). Resting SL in MCT+BB myocytes was 2.5% shorter, and FAIL cells 7.5% shorter, compared to CON RV cells. In LV cells, SL was slightly reduced by 1.6% in FAIL and slightly increased by 0.7% in MCT+BB, compared to CON, however these differences were not statistically significant. There was however a significant 2.3% decrease in SL in LV FAIL cells compared to MCT+BB cells. The cause and implications of the shorter resting SL will be explored more in Chapter 6.

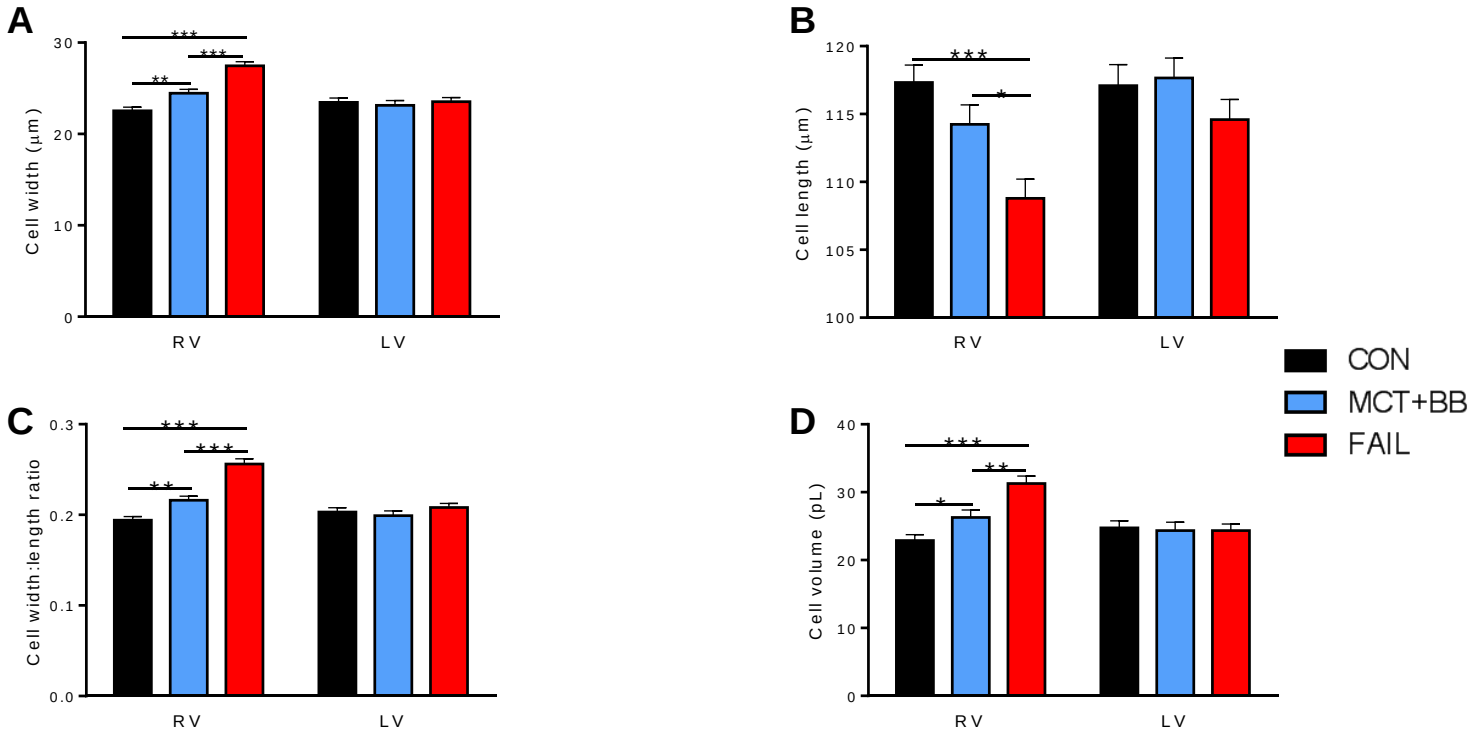

Figure 5.2 Geometry of isolated ventricular cardiomyocytes

A There was pronounced hypertrophy of RV FAIL cells, shown by increased width, which was attenuated in MCT+BB cells. **B** Cell length in RV FAIL cells decreased in a stepwise manner from CON>MCT+BB>FAIL. **C** Cell width:length ratio was increased in MCT+BB and FAIL RV cells compared to CON, but reduced in MCT+BB compared to FAIL. **D** Cell volume was predicted from cell length and width. Increased cell volume in RV FAIL cells was reduced in MCT+BB cells. There were no differences between groups of LV cells in any of these parameters. N=79 CON, 73 MCT+BB, 70 FAIL RV cells, N=64 CON, 64 MCT+BB, 66 FAIL LV cells. * P<0.05, ** P<0.01, *** P<0.001.

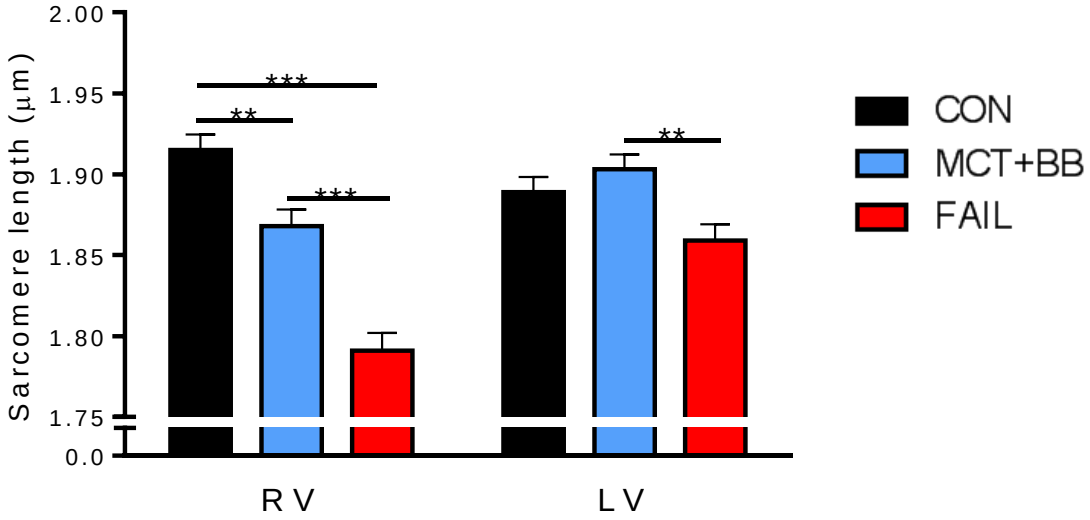

Figure 5.3 Resting sarcomere length in isolated RV and LV cells

There was a stepwise decrease in resting SL in RV cells from MCT+BB and FAIL rats compared to CON, but was increased in MCT+BB compared to FAIL. This did not occur in LV cells, where SL was not different between CON and MCT+BB cells, but was significantly shorter in LV FAIL compared to MCT+BB. N=30 cells in each group. **P<0.01, ***P<0.001.

5.3.3 Transverse tubule system

The T-tubule network was imaged in di-8-ANEPPS stained RV cells using a confocal microscope. Regular striated T-tubule structures were apparent in CON and MCT+BB cells, whereas in FAIL cells the transverse staining was less obvious and appeared more disorganised (Figure 5.4). Power spectrum analysis of fast-Fourier transformed intensity profiles across the length of cells revealed reduced regularity (decreased power of the first harmonic frequency) of T-tubules in RV FAIL cells, by 65% compared to CON and 60% compared to MCT+BB. T-tubule power was not significantly different in CON compared to MCT+BB. In RV CON and MCT+BB cells, tubules were primarily oriented transverse to the long axis of the cell with a much smaller proportion of tubules parallel to the long axis of the cell, whereas in RV FAIL cells there were fewer t-tubules and more longitudinal tubules compared to CON and MCT+BB. In RV FAIL cells there was a significant reduction in the proportion of T-tubules by 54% and an increase in longitudinal tubules by 87%, compared to RV CON. This decreased the ratio of transverse:longitudinal tubules in FAIL RV cells to 1.6, compared to a ratio of 6.4 in CON cells and 6.9 in MCT+BB.

5.3.4 Spatiotemporal characteristics of systolic Ca^{2+} release

Electrically-evoked Ca^{2+} transients were recorded in Fluo-4 loaded RV cells using confocal line scan. Time to peak Ca^{2+} release was measured in the spatially averaged fluorescence transient. The time to peak Ca^{2+} was significantly slower in FAIL cells compared to CON cells by 42% (Figure 5.5B). Time to peak Ca^{2+} was 18% slower in MCT+BB compared to CON but this was not statistically significant.

Electrical stimulation resulted in a rapid spatially and temporally homogeneous release of Ca^{2+} across the length of the cell in CON and MCT+BB RV cells, whereas FAIL cells often had regions of delayed Ca^{2+} release. Dyssynchrony was 17% greater in FAIL cells compared to CON and 28% greater compared to MCT+BB, but not different between CON and MCT+BB cells (Figure 5.5C). There was greater heterogeneity in the time to 50% Ca^{2+} release in FAIL compared to CON and MCT+BB cells (Figure 5.5D). There was a significant positive linear correlation between dyssynchrony index and time to peak Ca^{2+} ($P<0.001$, Spearman correlation).

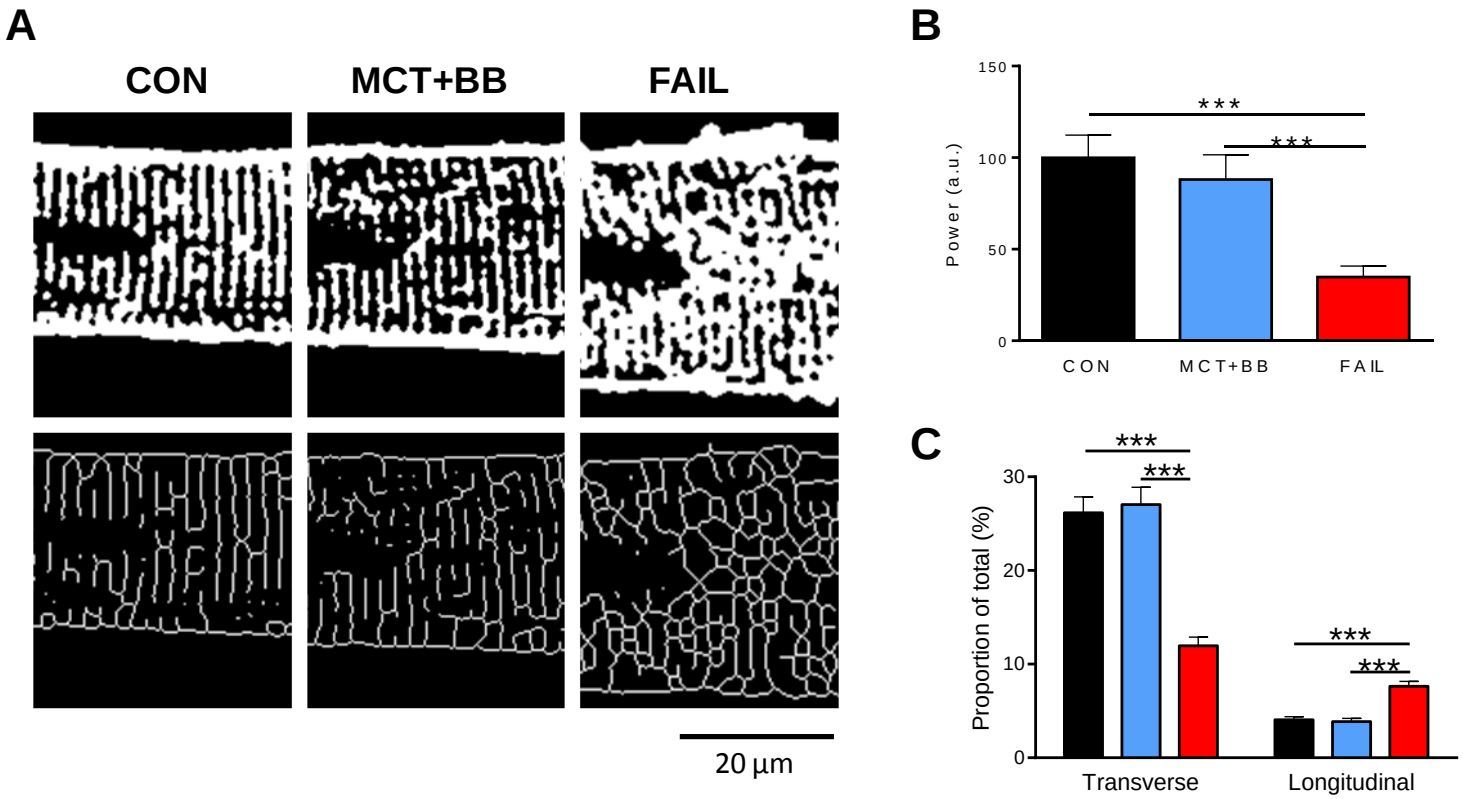

Figure 5.4 T-tubule organisation in RV cells

A *Upper panel* Representative images of RV cells showing the highly structured t-tubule system in CON and MCT+BB cells is lost in FAIL cells. *Lower panel* Skeletonized images of tubules. **B** FFT power decreased in RV FAIL cells compared to CON and MCT+BB. **C** The proportion of t-tubules was lower, and longitudinal tubules higher, in FAIL compared to CON and MCT+BB cells. N=30 cells in each group. *** P<0.001

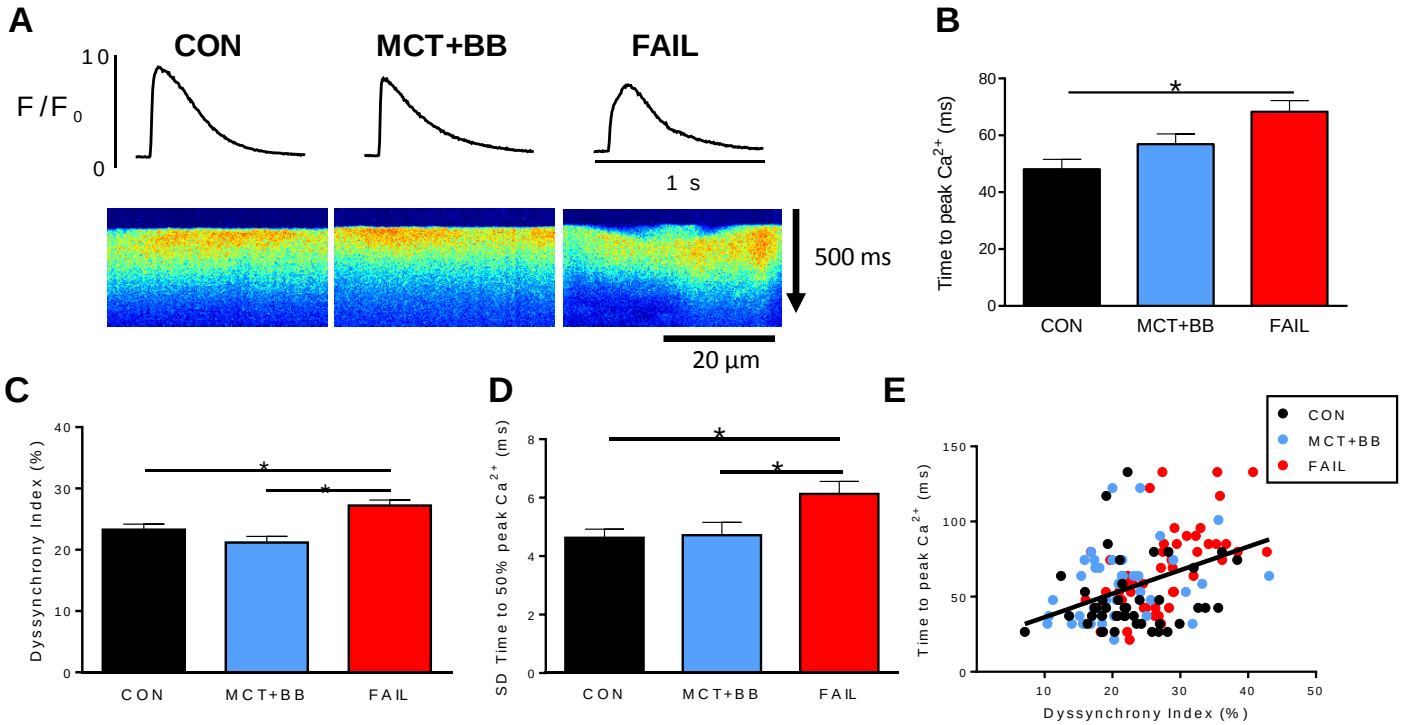

Figure 5.5 Spatiotemporal characteristics of systolic Ca^{2+} release

A *Lower panel* Confocal linescan recordings of systolic Ca^{2+} release in a CON, MCT+BB and FAIL cell. Regions of delayed Ca^{2+} release are apparent in the FAIL cell. *Upper panel* The resulting averaged Ca^{2+} transients show the time to peak Ca^{2+} is delayed in the FAIL cell. **B** Time to peak Ca^{2+} was significantly longer in RV FAIL cells than CON. **C** The variance in rise of Ca^{2+} at the start of the transient was greater in FAIL cells than CON and MCT+BB. **D** The standard deviation (SD) in the time to 50% peak Ca^{2+} was greater in FAIL cells. **E** There was a significant positive linear relationship between the Dyssynchrony Index and time to peak Ca^{2+} ($P<0.001$). N= 46 CON, 43 MCT+BB, 50 FAIL cells. * $P<0.05$, ** $P<0.01$, *** $P<0.001$. Data was collected by E. Steer and E. Fowler and analysed by E. Fowler.

5.3.5 Contraction-frequency relationship

The unloaded contraction-frequency relationship in RV CON cells displayed an overall positive relationship, with fractional shortening at 3-7 Hz being significantly greater than at 1 Hz (Figure 5.6A) ($P<0.001$). Fractional shortening was also significantly greater at 5 Hz compared to 3 Hz ($P<0.05$), but shortening plateaued at 5% of diastolic length between 5 and 7 Hz. In contrast, RV FAIL cell fractional shortening was greater at 1 Hz compared to CON, but displayed a pronounced negative relationship at faster pacing frequencies. Fractional shortening fell in response to an increase in frequency from 3-7 Hz ($P<0.05$). Fractional shortening in RV MCT+BB cells at 1 Hz was comparable to CON cells, but unlike CON and FAIL cells was stable across the range of frequencies and showed neither a positive nor negative response. Some FAIL (10 out of 28 cells) and MCT+BB cells (6 out of 28 cells) were unable to maintain stable contractions at 7 Hz; the difference in number of cells contracting at 7 Hz was not significantly different between FAIL and MCT+BB ($P=0.38$, Fischer's Exact test).

The contractile characteristics of LV CON cells were similar to RV CON; fractional shortening increased as pacing frequency increased from 1 to 5 Hz, then did not increase further beyond 5 Hz (Figure 5.6B). LV FAIL fractional shortening was greater at 1 and 3 Hz compared to LV CON, but did not change across the range of frequencies. LV MCT+BB cells displayed a slightly positive contraction-frequency relationship as shortening was greater at 5 and 7 Hz compared to 1 Hz.

Cytosolic Ca^{2+} was simultaneously monitored with SL and in general the systolic Ca^{2+} transient amplitude-frequency relationship was similar to the shortening-frequency relationship (Figure 5.7A). Ca^{2+} release was greater in FAIL cells at 1-5 Hz and in MCT+BB cells at 1-3 Hz, compared to CON. The Ca^{2+} transient amplitude in MCT+BB cells was intermediate between CON and FAIL at all frequencies measured. Ca^{2+} release in LV cells was greater in FAIL cells at 1-5 Hz compared to CON (Figure 5.7B). At most frequencies measured MCT+BB Ca^{2+} transient amplitude was intermediate between CON and FAIL. Diastolic Ca^{2+} significantly increased in RV and LV cells at faster pacing frequencies, however the main effect of frequency on diastolic Ca^{2+} was not different between groups of RV ($P=0.70$) or LV cells ($P=0.80$).

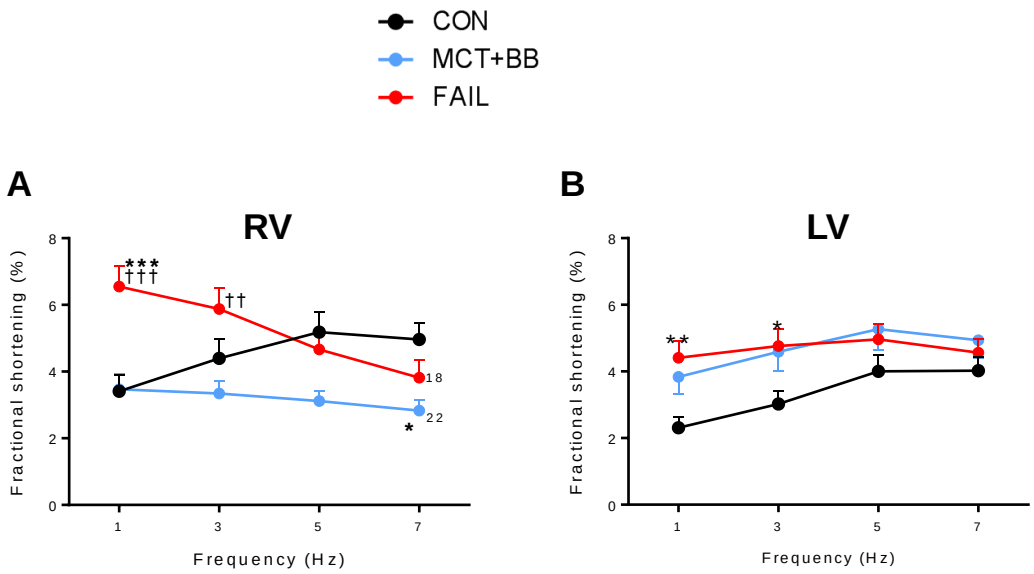

Figure 5.6 Shortening-frequency relationship in electrically paced cells

A Fractional shortening was greater in RV FAIL cells at low pacing frequencies but there was a steep monotonic decline when frequency was increased. Shortening in RV CON cells increased with frequency up to 5 Hz then plateaued. MCT+BB RV cell shortening was intermediate between CON and FAIL, and showed neither a positive nor negative response to frequency. Some FAIL and MCT+BB cells could not entrain to stimulation at 7 Hz, therefore the number of surviving cells is annotated on the figure. N=30 CON, 28 MCT+BB, 28 FAIL RV cells. **B** LV cells from CON and MCT+BB rats were similar in their positive response to pacing up to 5 Hz, above which there was no further increase in shortening. LV FAIL cell shortening was greater than CON at low pacing frequencies, but did not increase with faster pacing. N=24 CON, 22 MCT+BB, 22 FAIL LV cells. * P<0.05, ** P<0.01, *** P<0.001 vs CON, †† P<0.01, ††† P<0.001 vs MCT+BB.

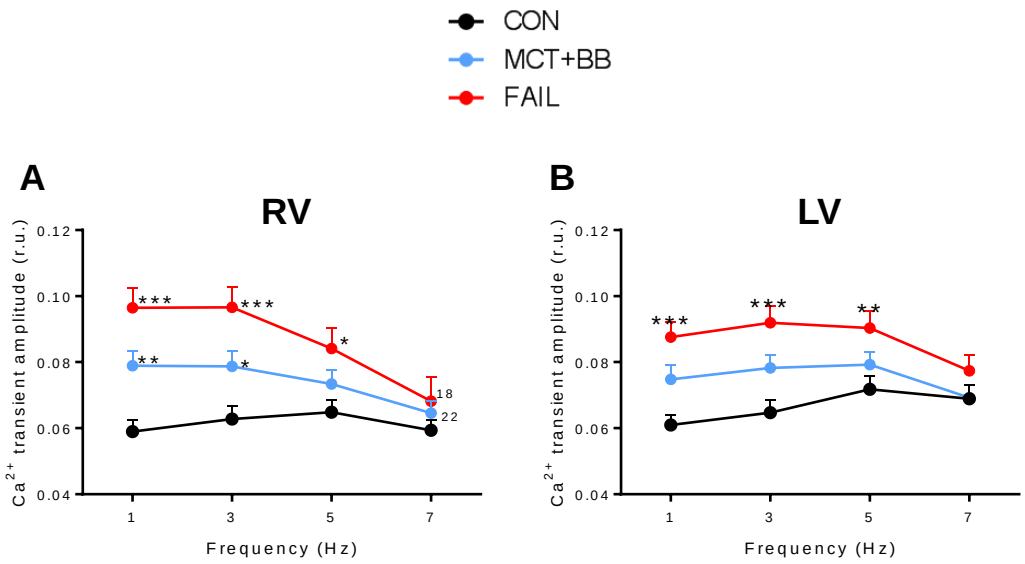

Figure 5.7 Ca^{2+} transient-frequency relationship in electrically paced cells

A Ca^{2+} transient amplitude was significantly greater in RV FAIL and MCT+BB cells compared to CON at low pacing frequencies. Ca^{2+} release increased up to 5 Hz in CON cells, whereas there was a decline in release in monocrotaline-treated groups which was steeper in RV FAIL cells. N=30 CON, 28 MCT+BB, 28 FAIL RV cells. **B** Between 1-5 Hz LV FAIL Ca^{2+} transient amplitude was greater than CON. Ca^{2+} release increased in LV CON cells up to 7 Hz, whereas it was stable in MCT+BB between 1-7 Hz, and in FAIL between 1-5 Hz. N=24 CON, 22 MCT+BB, 22 FAIL cells. * P<0.05, ** P<0.01, *** P<0.001 vs CON.

5.3.6 Myofilament Ca^{2+} sensitivity in intact cells

Phase-plane loops of Fura-4 fluorescence and corresponding sarcomere shortening were plotted to calculate the slope of the Ca^{2+}-length relationship during late relaxation as an index of myofilament Ca^{2+} sensitivity (Figure 5.8). The slope was not significantly different between CON and FAIL RV cells, but was shallower in MCT+BB RV cells indicating MCT+BB cells were less Ca^{2+} sensitive. A similar trend was observed in MCT+BB LV cells compared to CON and FAIL, however between-group differences were not significant.

5.3.7 Sarcoplasmic reticulum Ca^{2+} handling

SR Ca^{2+} content was estimated from the amplitude of a caffeine evoked Ca^{2+} transient in cells electrically paced at 5 Hz. Representative recordings of a caffeine-evoked Ca^{2+} transient in CON, MCT+BB and FAIL cells are shown in Figure 5.9. The amplitude of the Ca^{2+} transient was similar in the CON and MCT+BB cell, but higher in the FAIL cell. The rate at which the cytosolic Ca^{2+} returned to baseline was also slower in the MCT+BB and FAIL cell than the CON cell.

The SR Ca^{2+} content in RV FAIL cells was 32% greater than CON and 20% greater than MCT+BB. MCT+BB SR content was increased by 10% compared to CON but this was not statistically significant. The rate of decay of the systolic Ca^{2+} transient was not significantly different between any of the groups of RV cells but tended to be faster in MCT+BB compared to other groups. The rate of Ca^{2+} decay in the presence of caffeine ($K_{CAFFEINE}$) through primarily NCX Ca^{2+} efflux, was lower in MCT-treated groups of cells compared to CON. $K_{CAFFEINE}$ was reduced by 23% in MCT+BB and by 19% in FAIL, compared to CON cells. The rate of Ca^{2+} removal through SERCA (K_{SERCA}) is the difference between $K_{SYSTOLIC}$ and $K_{CAFFEINE}$. K_{SERCA} was not significantly different between any groups of cells but tended to be faster in MCT+BB RV cells.

Fractional SR Ca^{2+} release was calculated as the amplitude of the electrically stimulated Ca^{2+} transient as a percentage of the caffeine-evoked Ca^{2+} transient amplitude. In CON cells the systolic Ca^{2+} transient amplitude was 49% of total releasable SR Ca^{2+}. Fractional Ca^{2+} release was higher at 58% in MCT+BB cells. Fractional release was slightly higher in FAIL cells at 54% compared to CON, however this was not statistically significant.

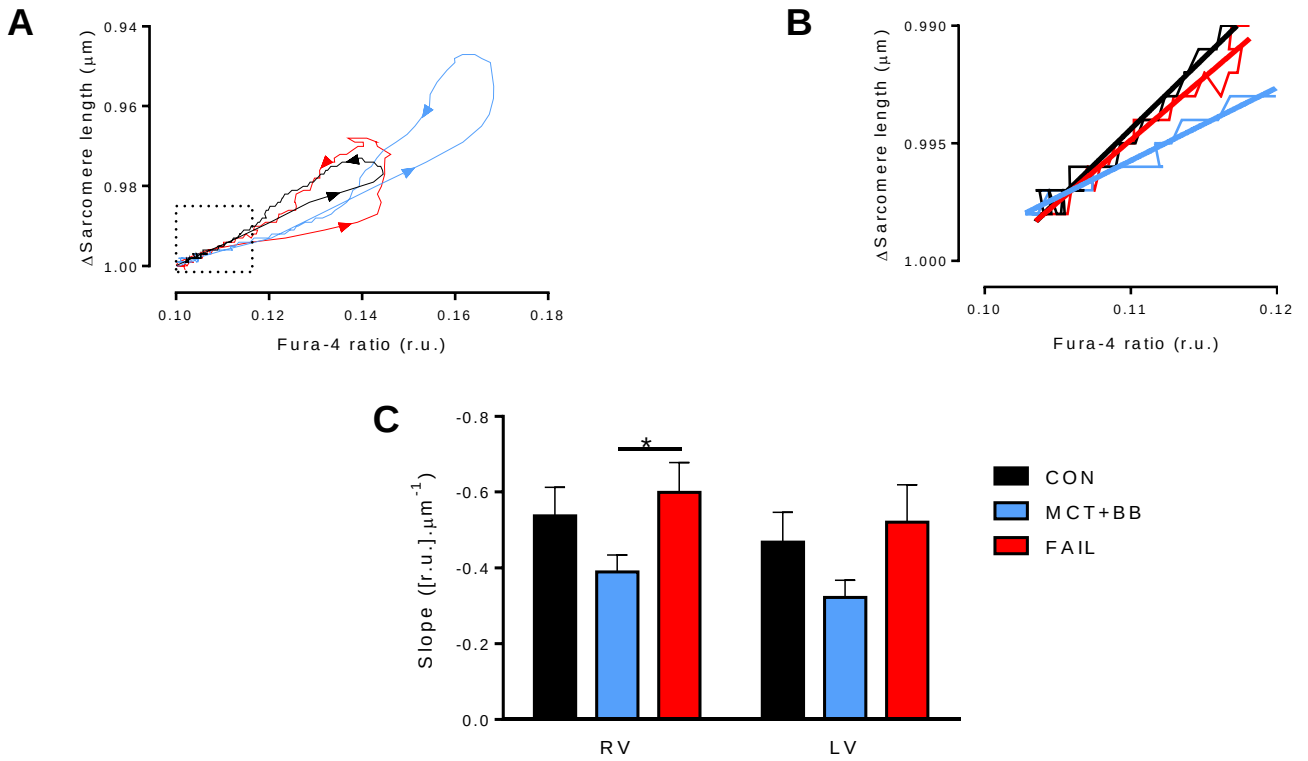

Figure 5.8 Intact cell myofilament Ca^{2+} sensitivity

A Fura-4 ratio-length trajectory plots of a CON, MCT+BB and FAIL RV cell paced at 1 Hz. Arrows indicate the anticlockwise direction of travel. **B** Expanded view of the highlighted region in (**A**) showing the 'dynamic equilibrium' reached between Ca^{2+} and length during late relaxation, the slope of which indicates myofilament Ca^{2+} sensitivity. **C** The average slope of RV CON and FAIL cells was not different, although in MCT+BB the slope was shallower than FAIL indicating reduced sensitivity. The average slopes did not significantly differ between LV groups, although they tended to follow the same general trend as RV cells. N=17 CON, 24 MCT+BB, 14 FAIL RV cells and N= 20 CON, 16 MCT+BB, 17 FAIL LV cells. * P<0.05.

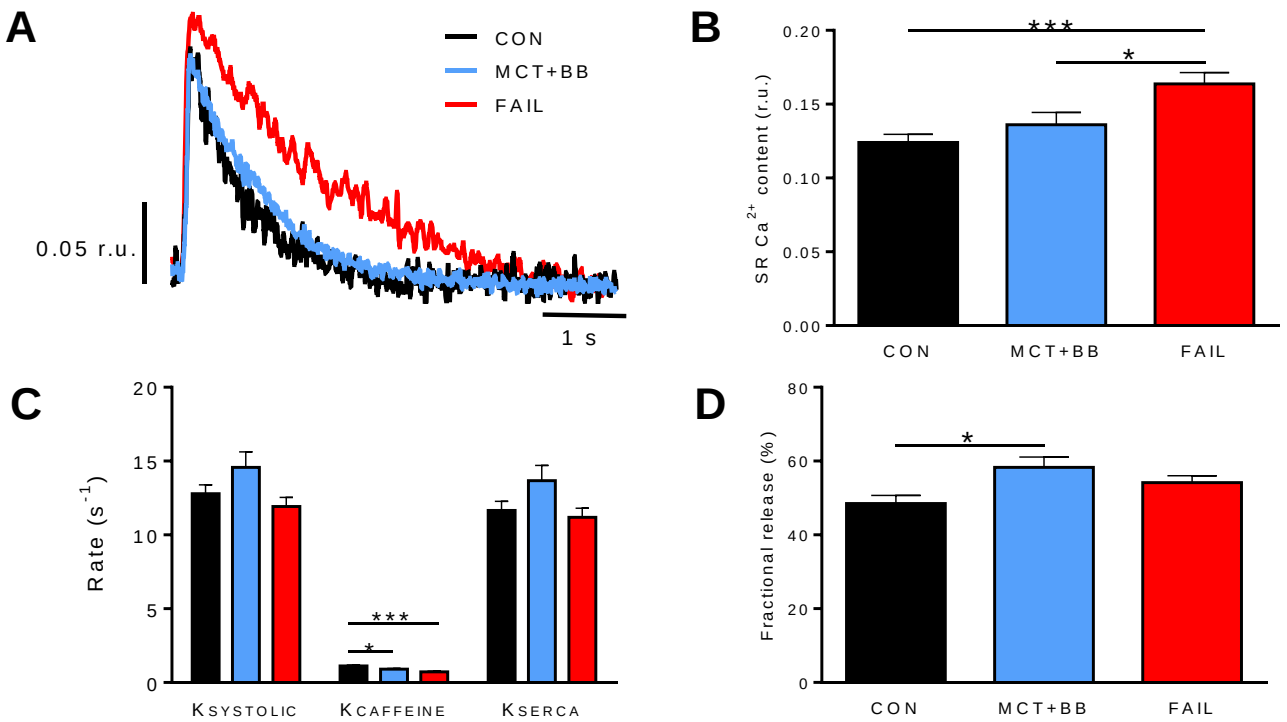

Figure 5.9 Sarcoplasmic reticulum Ca^{2+} handling in RV cells

A Representative recordings of SR Ca^{2+} release during brief caffeine application **B** SR Ca^{2+} content was significantly increased in FAIL cells compared to CON and MCT+BB. **C** The rate of Ca^{2+} decay during electrical stimulation ($K_{SYSTOLIC}$) was not different between groups. The rate of decay during caffeine ($K_{CAFFEINE}$) was significantly slower in MCT+BB and FAIL compared to CON. SERCA activity (K_{SERCA}) was not different between groups. **D** SR fractional Ca^{2+} release was significantly greater in MCT+BB cells compared to CON, and tended to be greater in FAIL though this was not statistically significant. N= 24 CON, 21 MCT+BB, 20 FAIL RV cells. *P<0.05, ***P<0.001.

5.3.8 Spontaneous Ca^{2+} waves

Spontaneous Ca^{2+} waves were counted during 1 min rest which was preceded by 1 min pacing at 5 Hz. In CON cells 15/24 cells exhibited ≥ 1 Ca^{2+} wave, and in both FAIL and MCT+BB groups 19/21 cells exhibited ≥ 1 Ca^{2+} wave. The proportion of cells exhibiting Ca^{2+} waves was not significantly different between groups. Of the cells which produced at least one wave, the mean number of waves was significantly greater in FAIL (9±2 waves.min^{-1}) and MCT+BB (6±1 waves.min^{-1}) compared to CON (2±1 waves.min^{-1}). Wave frequency was significantly lower in MCT+BB than FAIL RV cells. Resting Fura-4 ratio was not different between groups of cells (CON 0.19±0.01, MCT+BB 0.19±0.01, FAIL 0.19±0.01). There were more wave-initiated 'APs' as a proportion of total waves in FAIL and MCT+BB cells compared to CON, but the proportion was significantly smaller in MCT+BB compared to FAIL (Figure 5.10).

The velocity of Ca^{2+} wave propagation was calculated from confocal linescan images of Fluo-4 loaded RV cells at 22±1°C in 750 µM Ca^{2+} Tyrode without intentional SR loading and with a short 20 s observation period. Data for these confocal experiments was collected by Emma Steer; analysis was performed by Ewan Fowler. Wave velocity was 34% greater in FAIL compared to MCT+BB cells. There were fewer Ca^{2+} waves in this experiment (1/67 CON cells, 14/72 MCT+BB cells, 17/61 FAIL cells) compared to the previously described experiment in Fura-4 loaded cells, therefore the single CON cell (velocity 77.5 µm.s^{-1}) was not included in the statistical analysis.

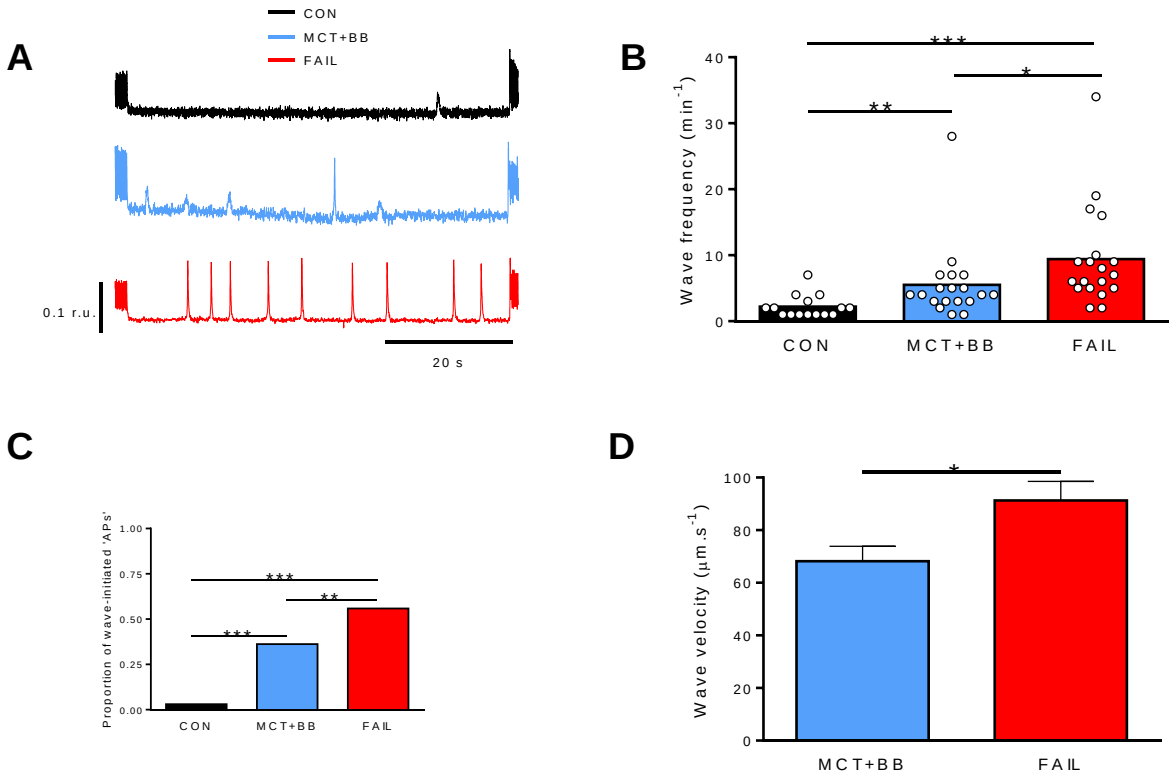

Figure 5.10 Spontaneous Ca^{2+} release in isolated cells

A Representative Fura-4 recordings of spontaneous Ca^{2+} waves during 1 min rest following pacing at 5 Hz. **B** Wave frequency was greater in MCT+BB and FAIL compared to CON, but was significantly reduced in MCT+BB compared to FAIL. **C** The proportion of wave-initiated 'APs' was greatest in FAIL, lowest in CON and intermediate in MCT+BB cells. **D** Wave velocity was faster in FAIL compared to MCT+BB cells. Data in (**D**) was collected by E. Steer and analysed by E. Fowler. N= 14 MCT+BB, 17 FAIL RV cells. *P<0.05, **P<0.01, ***P<0.001.

5.4 Discussion

5.4.1 Hypertrophy

RV myocytes from FAIL rats had pronounced hypertrophy driven by an increase in cell width, in accordance with the elevated systolic pressures in MCT treated rats, but was significantly reduced in MCT+BB rats towards CON levels. The increase in cross-sectional area likely reflects the increased afterload and wall stress experienced by the RV (Benoist *et al.*, 2014). Resting cell length was actually shorter in MCT treated rats and closely corresponded to a reduction in resting sarcomere length. Horan *et al.* (1981) found a close correlation between RV mass and RV free wall area using the postmortem findings of over 1500 patients, suggesting RV dilation, presumably through series addition of sarcomeres, is a major cause of RV enlargement in humans. Our rats may have succumbed to their symptoms before there had been sufficient time for the RV to dilate. Mechanotransduction is clearly an important factor in determining cell growth in the transverse or longitudinal direction, as cardiomyocytes cultured on transformable gel matrices grow longitudinally in response to axial stretch or increase cross-sectional area following transverse stretch (Gopalan *et al.*, 2003). The mechanisms through which the cell senses the direction of strain and responds accordingly are not fully understood, although myofilament protein interactions between titin, telethonin, and cytoskeletal connections with signalling complexes at the intercalated disk and sarcolemma are likely to be involved (Knöll *et al.*, 2002; Israeli-Rosenberg *et al.*, 2015). Kerckhoffs *et al.* (2012) have proposed a single law governs remodelling either to maintain an optimal sarcomere length or interfilament spacing in response to volume or pressure overload respectively.

Activation of adrenergic receptors by catecholamines is also a potent stimulus for hypertrophy through the activation of hypertrophic signalling cascades by PKA and PKC. Metoprolol may have reduced signalling through the β_1 pathway thus partially reducing hypertrophy (Fowler *et al.*, 2015b), but not affected the afterload meaning the mechanical stimulus for hypertrophy was still present. Alternatively, the αAR pathway or other circulating factors could be driving hypertrophy; if this were the case LV myocytes should also be hypertrophic, however as this did not happen it suggests mechanical stress and β_1AR activation are the main drivers of hypertrophy. Kögler *et al.* (2003) reported the mechanical stress of pressure overload resulted in differential gene transcription in the RV and LV of MCT rats. Further reductions in hypertrophy

may be possible if metoprolol were given in combination with an afterload lowering drug such as sildenafil.

5.4.2 Resting sarcomere length and creatine kinase

We have previously reported the shorter resting SL in RV FAIL cells occurs through a Ca^{2+}-independent mechanism (Fowler *et al.*, 2015a) and found strong evidence pointing towards reduced CK-M expression as the cause. Around 10-30% of CK-M is bound to the myofilaments and efficiently removes ADP and regenerates ATP using PCr (Ventura-Clapier *et al.*, 1987a; Hornemann *et al.*, 2003); loss of CK-M may impair control over cytosolic ADP resulting in slowly cycling rigor-like crossbridges which increase cell stiffness. We now show a partial recovery of resting SL in MCT+BB cells towards CON length, implying a partial recovery of the CK system. This is in accord with the partial improvement in the EDPVR found in Chapter 3.

As well as reduced total CK activity, there is reportedly a shift in isoenzyme distribution patterns in MCT and LV heart failure towards greater proportional expression of the foetal CK-B isoform (Ishikawa *et al.*, 1995). CK-B is loosely associated with the I-band of sarcomeres in complexes of glycolytic enzymes (Kraft *et al.*, 2000), however in isolation this is unlikely to account for the increased SL as CK-B in the I-band favours PCr and ADP formation, whereas myofilament bound CK-M favours ATP and Cr formation and the removal of ADP. On this basis it is proposed that the increased SL in MCT+BB RV cells is due to increased CK-M expression.

5.4.3 Restoration of t-tubule structure

T-tubule loss, disorganisation and dilation in failing rats is likely due to altered expression, localisation, and/or degradation of proteins integral to their formation and maintenance such as JP2 and BIN-1 (Wagner *et al.*, 2012). JP2 protein expression is progressively increased during postnatal development coinciding with t-tubule proliferation, and downregulated in the transition from compensated hypertrophy to decompensated heart failure coinciding with loss of t-tubules (Wei *et al.*, 2010; Xie *et al.*, 2012). This suggests loss of JP2 prevents the sarcolemma attaching to the junctional SR therefore resulting in early termination of t-tubule invaginations. Preserving JP2 protein levels by transgenic overexpression is protective against pressure overload induced hypertrophy (Guo *et al.*, 2014), whereas knockdown of JP2 results in a dilated cardiomyopathy in neonatal mice (Chen *et al.*, 2013). Treatment

with the afterload lowering drug sildenafil was also found to restore t-tubule structure and JP2 expression in MCT rats (Xie *et al.*, 2012). Microtubule densification in heart failure may also play a role in trafficking JP2 from t-tubules to the surface sarcolemma, as JP2 redistribution and t-tubule loss can be prevented by colchicine or enhanced by paclitaxel (Zhang *et al.*, 2014).

The membrane folding protein BIN-1 is recognised as an important regulator of t-tubule formation and also as a scaffolding domain for the localisation of L-type Ca^{2+} channel to t-tubules (Hong *et al.*, 2014). BIN-1 knockout in mice is perinatal lethal with mice developing a hypertrophic cardiomyopathy (Muller *et al.*, 2003), similarly in rat MI and pressure overload heart failure BIN-1 expression decreases (Lyon *et al.*, 2012; Caldwell *et al.*, 2014) and in human dilated cardiomyopathy (Hong *et al.*, 2012) which may account for the decreased density of transverse and longitudinal tubules in these diseases. We found the t-tubule system was increasingly disorganised in failing cells, but in general did not find large areas devoid of tubules as reported by others (e.g. Caldwell *et al.* (2014)). The proportional increase in longitudinal tubules in failing cells is reminiscent of neonatal murine cardiomyocytes which possess primarily longitudinal tubules which are not tethered to the junctional SR (Chen *et al.*, 2013). Interestingly, silencing RNA knockdown of JP2 in cultured rat ventricular myocytes also led to a reorientation of tubules from transverse to longitudinal, without an overall reduction in tubule density (Caldwell *et al.*, 2014), whereas knockdown of BIN-1 reduced density without changing orientation (Hong *et al.*, 2014). On this basis it is possible to speculate BIN-1 expression may be unaltered in FAIL rats, whereas JP2 is decreased.

The complete normalization of the transverse-axial tubule system and systolic Ca^{2+} release in MCT+BB rats may be due to increased expression of JP2. For instance, Chen *et al.* (2012) found chronic metoprolol treatment soon after MI in mice ameliorated t-tubule loss through preservation of JP2 expression. The JPH2 gene has a Myocyte enhancing factor-2 (Mef-2) promoter region and Mef-2 is upregulated in the RV of rat PAH at the compensated stage, but then sharply declines when the heart decompensates, suggesting MCT+BB rats may remain in a compensated disease stage for longer (Paulin *et al.*, 2015). Conversely, mechanically unloading the LV of rats with MI increased t-tubule regularity without significantly increasing JP2 expression (Ibrahim *et al.*, 2012). T-tubule signalling microdomains may also be restored as protein expression of caveolin-3 thought to be critical in localising β_2-AR to t-tubules is

fully normalized in MCT+BB rats compared to CON, whereas it is reduced in FAIL (R. Norman, personal communication).

5.4.4 Improved synchrony of Ca^{2+} release

Loss of t-tubules in failing cells coincided with increasing heterogeneity of Ca^{2+} release which in turn was associated with a slower Ca^{2+} transient upstroke. This phenomenon has also been identified in large animal models of chronic ischaemia and in failing human ventricular cardiomyocytes (Louch *et al.*, 2004; Heinzel *et al.*, 2008). A slowing of the time to peak Ca^{2+} was reported in intact murine hearts with t-tubule disruption due to short hairpin-RNA knockdown of JP2 (Chen *et al.*, 2013). The net effect of dyssynchronous Ca^{2+} release is a slowing of the velocity and force of muscle contraction which slows the rate of pressure development and ejection of blood from the ventricle (Louch *et al.*, 2006; Ferrantini *et al.*, 2014). Orphaning RYR2 on the SR from L-type Ca^{2+} channels on t-tubules is likely to delay Ca^{2+} release in regions lacking T-tubules as Ca^{2+} must diffuse from neighbouring RYR2 to initiate CICR. Evidence for this comes from detubulation of myocytes using osmotic shock which increases the heterogeneity of Ca^{2+} release and slows the upstroke velocity of the Ca^{2+} transient (Kawai *et al.*, 1999; Louch *et al.*, 2004).

Given that L-type Ca^{2+} channels and NCX are predominantly located on T-tubules the currents carried by these channels may be expected to be reduced in failing cells (Despa *et al.*, 2003). However I_{CaL} density is reportedly preserved in failing MCT rats and in LV cells from a rat model of chronic MI, suggesting there may be a redistribution of L-type Ca^{2+} channels from the T-tubule network to the surface sarcolemma (Lee *et al.*, 1997; Benoist *et al.*, 2011; Bryant *et al.*, 2015). A similar redistribution of NCX was suggested to occur in rat MI by Gadeberg *et al.* (2015), however we found Ca^{2+} removal through NCX was lower in failing and MCT+BB cells, possibly due to reduced NCX protein expression as found by Xie *et al.* (2012). This may contribute to the SR Ca^{2+} overload in FAIL cells, as detubulation with formamide shock also increases SR Ca^{2+} content by reducing Ca^{2+} removal from the cell (Bovo *et al.*, 2014).

5.4.5 β_1 blockers and response to increasing pacing frequency

Healthy RV myocytes showed a positive Ca^{2+} transient-frequency relationship which peaked at 5 Hz which is in agreement with other studies of rat myocytes under current clamp (Dibb *et al.*, 2007). The inability to cope when challenged by increased demand

is a defining characteristic of heart failure and was apparent in FAIL RV cells as a steep fall in contractility at faster pacing. This was closely paralleled by a precipitous fall in systolic Ca^{2+} release in these cells. In contrast the contractility and Ca^{2+} release of MCT+BB RV cells was better preserved even at the upper range of *in vivo* heart rates in rat. The preservation of contractile function seemed to occur due to a smaller fall in systolic Ca^{2+} release at higher pacing frequencies, which contrasted with a dramatic decline in Ca^{2+} release in failing cells. The improved contractility and Ca^{2+} handling in MCT+BB cells was not fully restored to healthy RV function, suggesting MCT+BB rats are in a compensated stage of heart failure rather than end-stage heart failure.

The Ca^{2+} transient amplitude was increased in FAIL compared to CON at low pacing frequencies which could be due to the prolonged AP in FAIL cells, long diastolic interval and reduced NCX efflux excessively loading the SR (Benoist *et al.*, 2012). Prolonging the AP duration in healthy rat cardiomyocytes under voltage clamp increases the amplitude of the Ca^{2+} transient by slowing I_{CaL} inactivation thus increasing Ca^{2+} influx to the cell (Bouchard *et al.*, 1995); conversely in SHR rats which develop compensated hypertrophy, AP prolongation, and increased Ca^{2+} transient amplitude, shortening the AP to the duration of a healthy cell reduces the Ca^{2+} transient (Brooksby *et al.*, 1993). The AP duration in FAIL rats shows steep restitution at shorter cycle lengths, suggesting reduced Ca^{2+} entry to the cell may impair Ca^{2+} release. The cause of the AP duration restitution is not known, although a rate dependent opening of ATP-sensitive I_{KATP} channels, possibly due to loss of coupled CK (Crawford *et al.*, 2002), could shorten the AP and effective refractory period which could promote arrhythmias (Uchida *et al.*, 1999). Reduced activity of SERCA would be an alternative explanation as the SR could become depleted and cause a rate dependent increase in diastolic Ca^{2+} (Hasenfuss *et al.*, 1994), however even at 5 Hz SR Ca^{2+} content was elevated in failing RV cells and there was no difference in the rate of rise in diastolic Ca^{2+} with frequency between groups, suggesting the fault lies with Ca^{2+} release rather than uptake. A possible mechanism for the greater resilience of Ca^{2+} release across pacing frequencies in MCT+BB rats could be a flatter AP duration restitution curve or altered phosphorylation status of RyR2 reducing its refractoriness (Poláková *et al.*, 2015).

In contrast to the profoundly dysfunctional Ca^{2+} handling in failing RV cells, LV cell contractility and Ca^{2+} release was preserved or augmented in MCT+BB and FAIL rats.

A similar finding was reported in the LV of Langendorff perfused MCT hearts (Lamberts *et al.*, 2007b) and in isolated LV muscle strips (Kögler *et al.*, 2003). The LV does not experience the elevated afterload encountered by the RV, therefore other factors such as circulating catecholamines are likely to affect LV remodelling. Changes in β_1-AR expression are more modest compared to the RV, indicating a mechanical stimulus is also required to initiate remodelling (Leineweber *et al.*, 2002). The LV is not free from the mechanical effects of PAH however, as interventricular interactions between the RV and LV can reduce LV end diastolic dimensions as a result of increased RV diastolic pressure and reduced left atrial filling. For instance in Langendorff perfused healthy rat heart, overextending the RV with an indwelling balloon does not impair LV developed pressure due to the higher compliance of the RV (Pett & Hauton, 2012), whereas in MCT treated rats RV compliance is reduced and an increase in RV volume causes a greater increase in LV diastolic pressure (Lamberts *et al.*, 2007b). Enhanced contractility in LV cells in PAH may represent a compensatory mechanism to overcome reduced LV preload.

5.4.6 Myofilament Ca^{2+} sensitivity

In the current investigation the slope of the Fura-4 ratio-SL relationship was used as an index of myofilament sensitivity where the sarcolemma is intact (thus retaining the intracellular milieu) and the cell is contracting at 37°C (Spurgeon *et al.*, 1992). Ca^{2+} sensitivity was unchanged in FAIL compared to CON RV cells, whereas it was decreased in MCT+BB cells. A consequence of this can be seen in the contraction- and Ca^{2+}-frequency relationship, in which shortening at 1 Hz is the same in CON and MCT+BB RV cells, despite a significantly higher Ca^{2+} transient in MCT+BB cells. This indicates the enhanced fractional shortening in FAIL and MCT+BB cells at low pacing frequencies occurs primarily due to the augmented systolic Ca^{2+} transient. Similar changes were seen in LV cells although these did not reach statistical significance. Neuroendocrine factors do not stimulate the same gene and protein expression patterns in the LV compared to the RV in MCT heart failure due to the lack of mechanical overload, suggesting the similarity between Ca^{2+} sensitivity in the RV and LV of different groups may be due to altered phosphorylation rather than changes in protein expression (Kögler *et al.*, 2003; Schott *et al.*, 2005).

Different methods of measuring Ca^{2+} sensitivity are available with different advantages and disadvantages. We have previously reported decreased Ca^{2+} sensitivity in failing RV and LV cells measured during tetanic contractions in intact cells at room

temperature (Fowler *et al.*, 2015a) which is in conflict with the current findings. A possible methodological reason for this could be elevation of cytosolic Ca^{2+} in the tetanic experiments by thapsigargin activating a Ca^{2+} dependent kinase, such as CaMKII or PKC, resulting in phosphorylation of the myofilaments. A similar mechanism could explain the frequency-dependent decrease in Ca^{2+} sensitivity reported by Lamberts *et al.* (2007a), who also found PKC-α expression was increased in the RV of MCT rats. The length-dependent increase in myofilament Ca^{2+} sensitivity is generally unaffected by heart failure indicating the Frank-Starling mechanism is preserved (Fan *et al.*, 1997; Walker *et al.*, 2011b; Benoist *et al.*, 2014).

5.4.7 Sarcoplasmic reticulum Ca^{2+} handling

Altered expression and phosphorylation of PLB is thought to have a key causal role in contractile abnormalities in heart failure through modifying SR content and therefore contractile force (Sande *et al.*, 2002). SR Ca^{2+} content was estimated by briefly applying a high concentration of caffeine which opens RyR2 causing rapid depletion of SR Ca^{2+} stores (Varro *et al.*, 1993). SR load was significantly elevated in FAIL RV cells, whereas it was not significantly different in MCT+BB compared to CON cells. The fraction of Ca^{2+} released during electrical stimulation in CON cells was 49% of available SR content, which is close to the value of 55% in healthy rat myocytes reported by Delbridge *et al.* (1997). Fractional release was not different between FAIL and CON, but was significantly elevated in MCT+BB. These data indicate the increased systolic Ca^{2+} transient in FAIL cells occurs due to increased SR load, whereas in MCT+BB cells increased fractional release is also a factor.

Our data suggest the increased fractional release in MCT+BB cells might be due to increased RyR2 open probability, as SR load was not different to CON and I_{CaL} density was previously shown to be unchanged in MCT RV cells (Lee *et al.*, 1997; Benoist *et al.*, 2012). Further support for this is given by the finding of increased Ca^{2+} spark amplitude and spark mediated leak in MCT+BB cells compared to FAIL cells (E. Steer, personal communication). Fractional Ca^{2+} release decreased from 54% to 37% in a ferret aortic banding model of hypertrophy, coinciding with a decrease in SR load by 20% (Díaz *et al.*, 2004), however an equivalent decrease in fractional release was also seen in a rat aortic banding model without a change in SR load or I_{CaL}, highlighting the importance of RyR2 open probability (Delbridge *et al.*, 1997).

The use of the caffeine-evoked Ca^{2+} transient amplitude as a surrogate for SR Ca^{2+} content may not be valid if the high cytosolic Ca^{2+} saturates the Ca^{2+} indicator. We used the low affinity Fura-4F Ca^{2+} indicator and saw a clear Ca^{2+} transient peak in all recordings arguing against indicator saturation. An alternative method would be to directly measure and integrate the inward NCX tail current generated during caffeine exposure (Varro *et al.*, 1993).

Steady state SR load was increased in FAIL cells without significant changes in SERCA activity. This was somewhat surprising as SERCA2a expression was shown to be significantly reduced in failing MCT rats (Reilly *et al.*, 2001; Benoist *et al.*, 2014), however in MCT rats with compensated PAH SERCA activity was not depressed compared to CON despite SERCA expression negatively correlating with HW:BW, suggesting factors other than expression influence its activity. Expression of PLB decreased in failing MCT rats preserving the PLB:SERCA ratio, whereas the ratio of phosphorylated Thr^{17}:total PLB actually increased thus relieving its inhibition of SERCA (Mattiazzi *et al.*, 2005; Benoist *et al.*, 2014). NCX activity was decreased in MCT treated rats suggesting reduced Ca^{2+} efflux may further cause accumulation of Ca^{2+} within the SR (Acsai *et al.*, 2007). These data suggest our rats were taken at the onset of heart failure rather than end-stage heart failure.

5.4.8 Diastolic Ca^{2+} leak

Ca^{2+} wave frequency and likelihood of wave-initiated 'APs' was increased in RV cells of MCT treated rats and corresponded to the severity of disease. The increased wave frequency in FAIL cells is likely due to increased SR Ca^{2+} which increases Ca^{2+} spark frequency. Wave frequency was also increased in MCT+BB cells despite no significant change in SR load, suggesting a different mechanism may be responsible in these cells. Elevated cytosolic Ca^{2+} can be excluded, as resting Fura-4 ratio did not differ between groups of cells. One possible explanation could be increased RYR2 sensitivity, as Ca^{2+} spark frequency and fractional Ca^{2+} release were both increased in these cells.

The probability of a wave-initiated 'AP' progressively increased from CON<MCT+BB<FAIL. In FAIL rats the increased SR Ca^{2+} content will increase the amplitude of the Ca^{2+} wave and therefore the total inward NCX current (Miura *et al.*, 2011). Furthermore, the Ca^{2+} wave velocity was greater in FAIL compared to MCT+BB, meaning this current will be discharged more quickly thus causing a larger

membrane depolarisation potentially sufficient for sodium channel opening. Too few Ca^{2+} waves occurred in CON cells at room temperature to analyse statistically, however a value of ~70 µm/s is typically reported which is comparable to the velocity of MCT+BB waves (Lukyanenko & Györke, 1999). Shorter distances between Ca^{2+} release units is predicted to highly increase the velocity of waves (Keizer *et al.*, 1998; Izu *et al.*, 2006), therefore the shorter SL in FAIL cells compared to MCT+BB cells may contribute to the increased wave velocity (this will be explored in more detail in Chapter 6). Increased wave velocity was also reported in RV trabeculae of MCT rats which correlated with the magnitude of membrane depolarization (Miura *et al.*, 2011). Reduced repolarizing currents in heart failure such as IK_1 will further increase the extent of depolarization during a wave and therefore the likelihood of a wave-initiated 'AP' (Berlin *et al.*, 1989; Benoist *et al.*, 2011). Our characterisation of propagating and wave-initiated 'APs' hinges upon the morphology of an epifluorescent Ca^{2+} transient, however validation of this method will require simultaneous monitoring of cell membrane potential; Fujiwara *et al.* (2008) showed this phenomenon occurred in Langendorff-perfused rat hearts dual loaded with voltage and Ca^{2+} sensitive dyes therefore the reduced likelihood of wave-initiated 'APs' occurring in MCT+BB cells may be protective against fatal ventricular arrhythmias. (Liles *et al.*, 2012) reported a case of spontaneous ventricular fibrillation leading to death in a freely moving MCT rat implanted with telemetry.

5.5 Conclusions

RV myocyte contractile function was partially rescued in MCT+BB rats through improved excitation-contraction coupling. A higher resilience when challenged by pacing frequency may translate into improved RV function during periods of elevated heart rate, such as during exercise, and thus improve the quality of life in PAH. Improved diastolic Ca^{2+} handling with β-blocker treatment may reduce the susceptibility of PAH rats and patients to spontaneous ventricular arrhythmias (Delcroix & Naeije, 2010; Umar *et al.*, 2012).

Importantly these improvements occurred independent of altered pulmonary vascular resistance identified in Chapter 3. Current afterload reducing therapies for PAH such as sildenafil do not prevent RV dysfunction when afterload is fixed (Schäfer *et al.*, 2009; Borgdorff *et al.*, 2012), and no additional morbidity or mortality benefit is accrued from combination therapy with different vasodilators suggesting a ceiling has been reached in targeting the vasculature alone (McLaughlin et al., 2014). Our work shows

β-blockers may improve survival by restoring EC coupling to failing RV cardiomyocytes and therefore represent a potential adjunctive therapy in PAH.

Chapter 6 Mechanical and geometric involvement in right ventricle function dysfunction

6.1 Introduction

The ability of the heart to eject blood is influenced by intrinsic properties of the cardiomyocytes (such as the ability to cycle Ca^{2+} or synthesise ATP) but also the loading state which varies depending on venous return and arterial resistance. The majority of data on systolic function in isolated cardiomyocytes is from mechanically unloaded cell shortening, however in the heart, myocytes experience a dynamic load which changes throughout the cardiac cycle. How isolated myocytes from failing hearts respond to a dynamic load during contraction is not currently known.

The passive properties of the myocardium are a key determinant of cardiac function through the Frank-Starling mechanism, which responds to acute changes in end diastolic volume on a beat-to-beat basis to preserve stroke volume by modifying the force of contraction. Much of the work on the passive properties of cardiomyocytes has been performed in chemically permeabilized cells lacking a working excitation-contraction coupling system and in which the cytosolic milieu equilibrates with the bulk solution. Consequently, little is known of the diastolic properties of electrically-excitable cells and their relation to cardiac function in heart failure. Defective Ca^{2+} handling may be detrimental to diastolic function, for instance through spontaneous Ca^{2+} waves which can trigger ventricular arrhythmias and sudden death (Heinzel *et al.*, 2011). Computer simulations indicate the geometric arrangement of RYR2 in cardiomyocytes also has a profound influence on spontaneous Ca^{2+} waves (Keizer & Smith, 1998; Izu *et al.*, 2006).

This chapter details studies that did not involve β-blocker treatment but instead sought to extend the work of the laboratory on the mechanisms associated with MCT induced RV failure. Systolic and diastolic function in healthy and failing cardiomyocytes was investigated under a variety of mechanical loading conditions. Under all loading conditions myocytes from failing hearts responded worse to increasing demand (pacing frequency) compared to healthy cells, which may be associated with impaired energy transfer within the cell. Failing cells are shown to be less compliant and relax more slowly, a characteristic of diastolic dysfunction. Ca^{2+} waves are shown to exhibit sarcomere length-dependence in failing cells. Studies further implicating CK in RV dysfunction are also included. These findings suggest ventricular myocytes are an

important cause of poor cardiac performance in MCT heart failure and therefore should be investigated as a potential target for therapy in PAH.

6.2 Methods

Experiments involving loaded contractions were performed at the Vrijie Universiteit, Amsterdam, in 1.8 mM Ca^{2+} Tyrode using a modified cell isolation procedure. All other experiments were performed in 1 mM Ca^{2+} Tyrode in cells isolated according to the method detailed in Chapter 2.

6.2.1 Modified ventricular myocyte isolation

We found the suitability of cells for stretch experiments was improved using a cell isolation protocol used by the Lederer laboratory (Prosser *et al.*, 2011). The primary difference compared to our standard isolation procedure is the omission of protease from the enzyme mix. Rats were anaesthetised with isoflurane which was confirmed by the lack of pedal-withdrawal reflex in response to a toe pinch. The heart was excised and perfused on a Langendorff apparatus with a modified isolation solution (digestion buffer, D.B.) containing, in mM: 130 NaCl, 5.4 KCl, 3 Pyruvate, 25 HEPES, 0.5 $MgCl_2$, 0.33 NaH_2PO_4, 22 glucose, 0.2 EGTA, pH 7.4 with NaOH. Perfusion was switched to a D.B. without EGTA containing 50 µM Ca^{2+} and 1.2 mg/mL collagenase Type II (activity 270 U/mg, Worthington Biochemical, New Jersey, USA) for 7 min. The RV was coarsely minced then mechanically triturated with a plastic Pasteur pipette for 3 min in D.B. containing 0.1 mM Ca^{2+} and 10 mg/mL BSA. Cells were centrifuged at 50 *g* for 1 min and resuspended in three changes of D.B. containing 0.25, 0.5, 1 mM Ca^{2+}.

6.2.2 Isometric contractions in intact myocytes

RV myocytes were attached to glass fibres connected to a force transducer and piezo motor using MyoTak glue. Isometric contractions were recorded between 1-7 Hz at resting cell length. The end-systolic (ESFLR) and end-diastolic force-length relationship (EDFLR) was calculated in cells paced at 1 Hz and stretched in steps of 2.5, 5, 7.5 and 10 µm, separated by a return to resting length. The points at end-diastole and end-systole were fitted with a least squares linear regression to calculate the slope of the force-length relationship. Slopes from different cells were compared using an unpaired t-test. Force was normalised to cell cross-sectional area according to the methods described in Section 2.6.1.

6.2.3 Physiological work loop style contractions

Work loops were synchronised to the electrical pacing marks. A “preload” (10-20% of isometric developed force) and “afterload” (70-80% of isometric developed force) was chosen for each cell which defined the force the cell was stretched to in diastole, or held at by shortening the cell during systole (Figure 6.1). Feedback from the force transducer was processed by an FPGA chip which ran the control algorithm driving the piezo motor to shorten the cell when force exceeded the afterload or stretch the cell when force dropped below the preload. A control signal generated by IonWizard software was automated such that every contraction had a different preload and afterload, allowing the ESFLR and EDFLR to be constructed in < 30 s. External work (µJ) was calculated as Force (µN) X Motor Displacement (µm), using Labchart 7 (AD Instruments, Oxford, UK) (Figure 6.2).

Time varying elastance, E(t), is the slope of the line connecting instantaneous points of force and length with the intercept of the ESFLR and EDFLR. E(t) was calculated at 1 Hz at the initial preload and afterload. The time to peak elastance and the time constant of isometric relaxation, Tau, was calculated from the normalised E(t) (Figure 6.3) (Suga & Sagawa, 1974).

6.2.4 Myocyte shortening and Ca^{2+} monitoring

Cytosolic Ca^{2+} transients were monitored in cells loaded with the Ca^{2+} indicator Fura-4F-AM (2 µM). Local perfusion of cells with 1 mM Ca^{2+} Tyrode, Tyrode+blebbistatin (10 µM), or Tyrode+caffeine (20 mM) was achieved using an 8-channel pipette with temperature control (37±0.5°C). Cells were paced between 1-7 Hz, or left unpaced for 1 min to record spontaneous Ca^{2+} waves.

Blebbistatin is a reversible inhibitor of actin-myosin crossbridge formation and is used as a mechanical uncoupler of muscle contractions (Farman *et al.*, 2008). Blebbistatin blocks P_i release from the M•ADP•P_i complex leaving it in a state with low actin affinity (Kovács *et al.*, 2004). Blebbistatin experimental solution (10 µM) was prepared fresh each day from an 85.5 mM stock in DMSO (final DMSO <0.1%). Blebbistatin solutions were kept in the dark to prevent photoinactivation (Kolega, 2004; Sakamoto *et al.*, 2004).

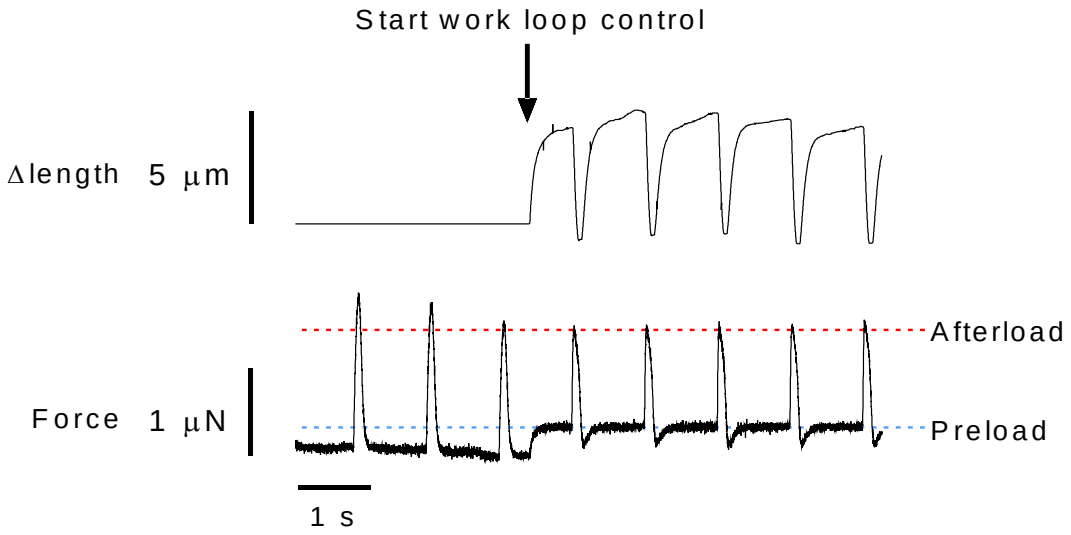

Figure 6.1 Isometric and force clamp contractions

Example recording of isometric force generated by a cell contracting at 1 Hz. At the time indicated, work loop control is initiated and the systolic and diastolic force clamped at a pre-determined level by dynamically stretching and shortening the cell with a piezo motor.

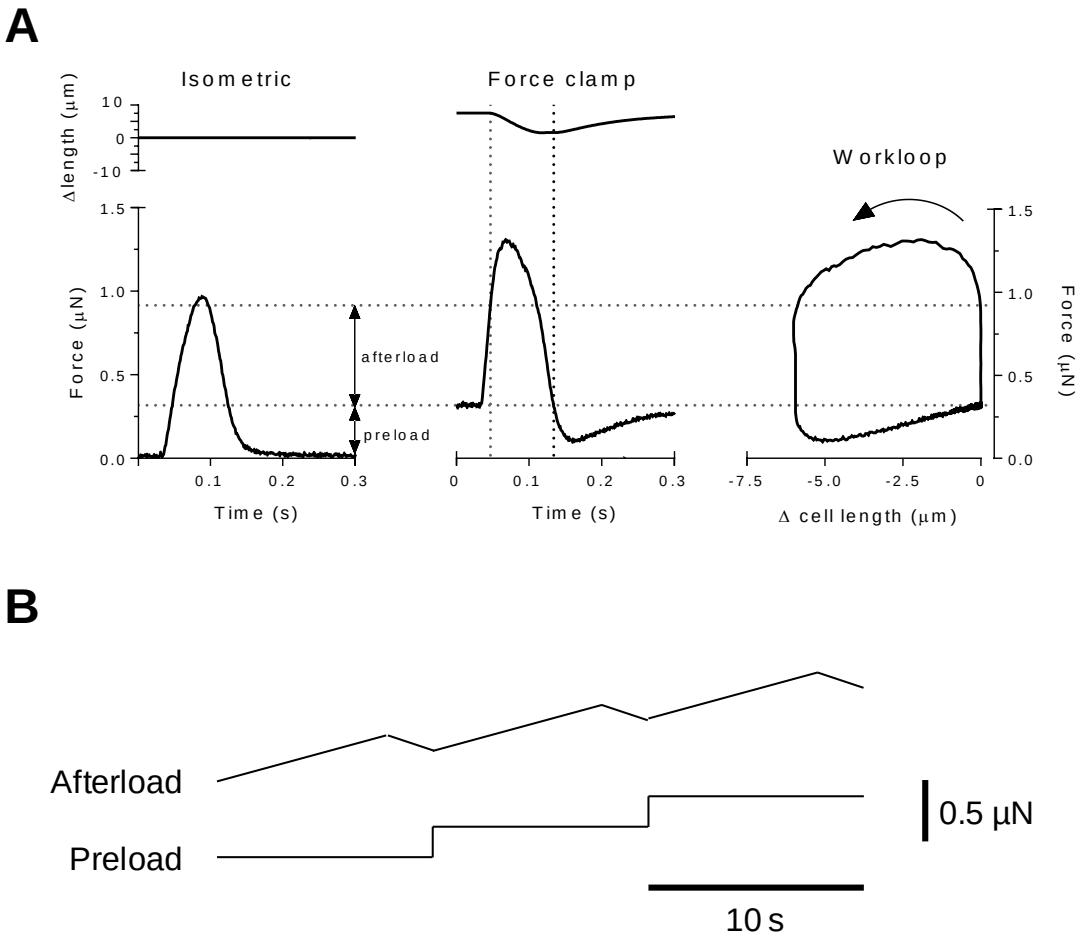

Figure 6.2 Reconstruction of work loops in single cells

A An initial "preload" and "afterload" force was chosen during isometric contractions (*left*). During workloop control a piezo motor shortened the cell when force exceeded the afterload or stretched the cell to return force to the preload value (*middle*). Plotting force against motor displacement allowed cellular work [Work (μJ) = Force (μN) X Displacement (μm)] to be calculated from the area inside the loop (*right*). Upper panels show motor displacement, lower panels show force, time and piezo position. **B** The command signal generated by the software to control the piezo was automated to progressively vary preload and afterload from the initial values.

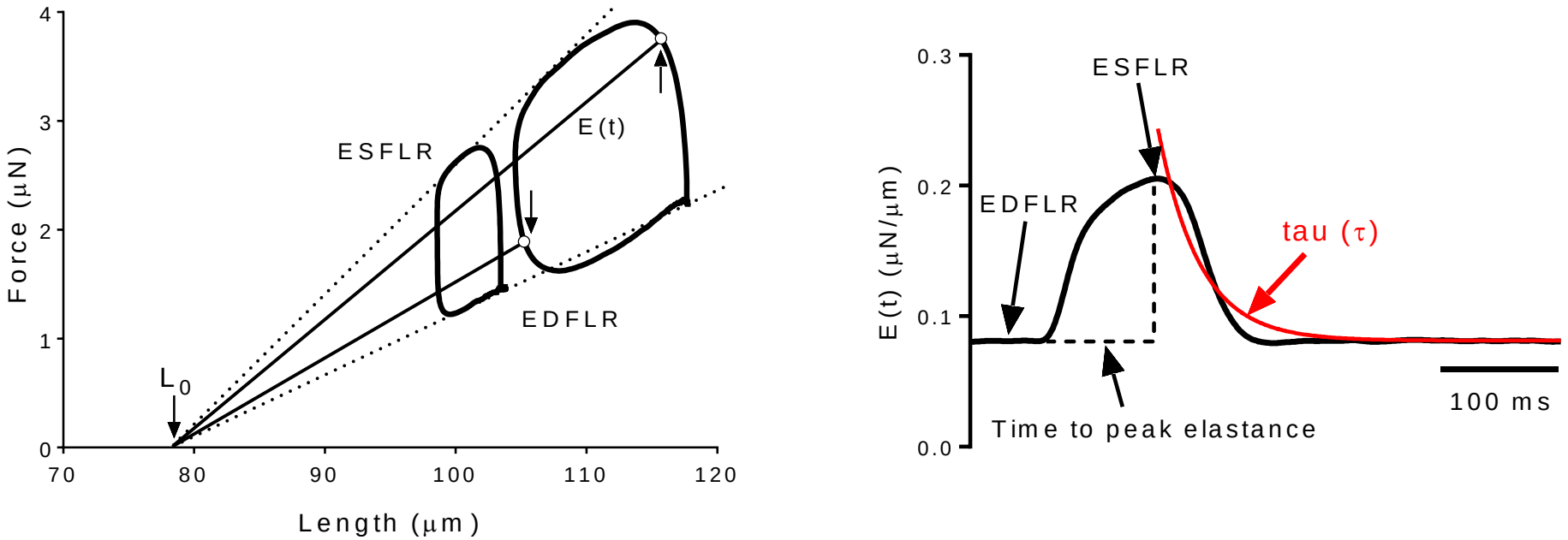

Figure 6.3 Time-varying elastance in single cells

A Time varying elastance, E(t), gives a time domain description of contractile function during workloop contractions. E(t) is the slope of the line (solid black lines) connecting points of instantaneous force and length with a length intercept, L_0, defined by the intersection of the ESFLR and EDFLR. The slopes of the ESFLR and EDFLR therefore represent the maximum and minimum elastance (broken lines). **B** E(t) over a contraction cycle plotted as a function of time. The time to peak elastance and time constant of relaxation (tau) were calculated using E(t).

1-Fluoro-2,4-dinitrobenzene (DNFB) is a sulfhydryl-modifying irreversible inhibitor of all creatine kinase isoforms (Gercken & Schlette, 1968). Cells were incubated with DNFB (20 μM) (from a 20 mM stock in ethanol, final EtOH <0.1%) for 10 min at room temperature then resuspended in fresh Tyrode and used immediately.

6.2.5 Exogeneous creatine kinase

Saponin (0.01 mg/ml) was used to permeabilize myocytes in an intracellular-like solution containing, in mM: 130 K^+, 30 Na^+, 135.7 Cl^-, 25 HEPES, 10 PCr, 5.7 Mg^{2+}, 5 ATP, 0.5 EGTA, 0.01% BSA, pH adjusted to 7.0 with 8N KOH, free Mg^{2+} was 1 mM (Steele & Smith, 1993). CK-M from bovine heart muscle (Sigma, UK) was included in the intracellular-like solution at a concentration of 4.4 mg/ml (total activity 250 U/ml). Cells were incubated in intracellular solution with or without exogenous CK for 30 min before SL was measured at 20-23°C. In some experiments the CK substrate PCr was omitted from the intracellular solution to test whether exogeneous CK was functionally active.

6.3 Results

6.3.1 Mechanical function in response to load and stretch

6.3.1.1 Physiologically-loaded contractions

Cellular work (generation of force while shortening) was calculated in CON and FAIL RV cells under physiological loading. There was a tendency for work performed at resting length at 1 Hz to be greater in FAIL cells (5.4±0.8 μJ, N=16 cells) compared to CON (3.4±0.8 μJ, N=8 cells), however this was not significant (P=0.126). Increasing preload by stretching cells up to 16% significantly increased cellular work by 140% in CON and 180% in FAIL cells (Figure 6.4B). The ESFLR tended to be steeper in FAIL than CON (by 21%) and the EDFLR also tended to be steeper (by 17%) however this was not statistically significant (Figure 6.4 C+D). The time course of contraction was measured during work loops at resting length according to the concept of time-varying elastance. The time to peak elastance was significantly longer in FAIL cells by 19%. The time constant of relaxation was not different in CON or FAIL cells (Figure 6.5).

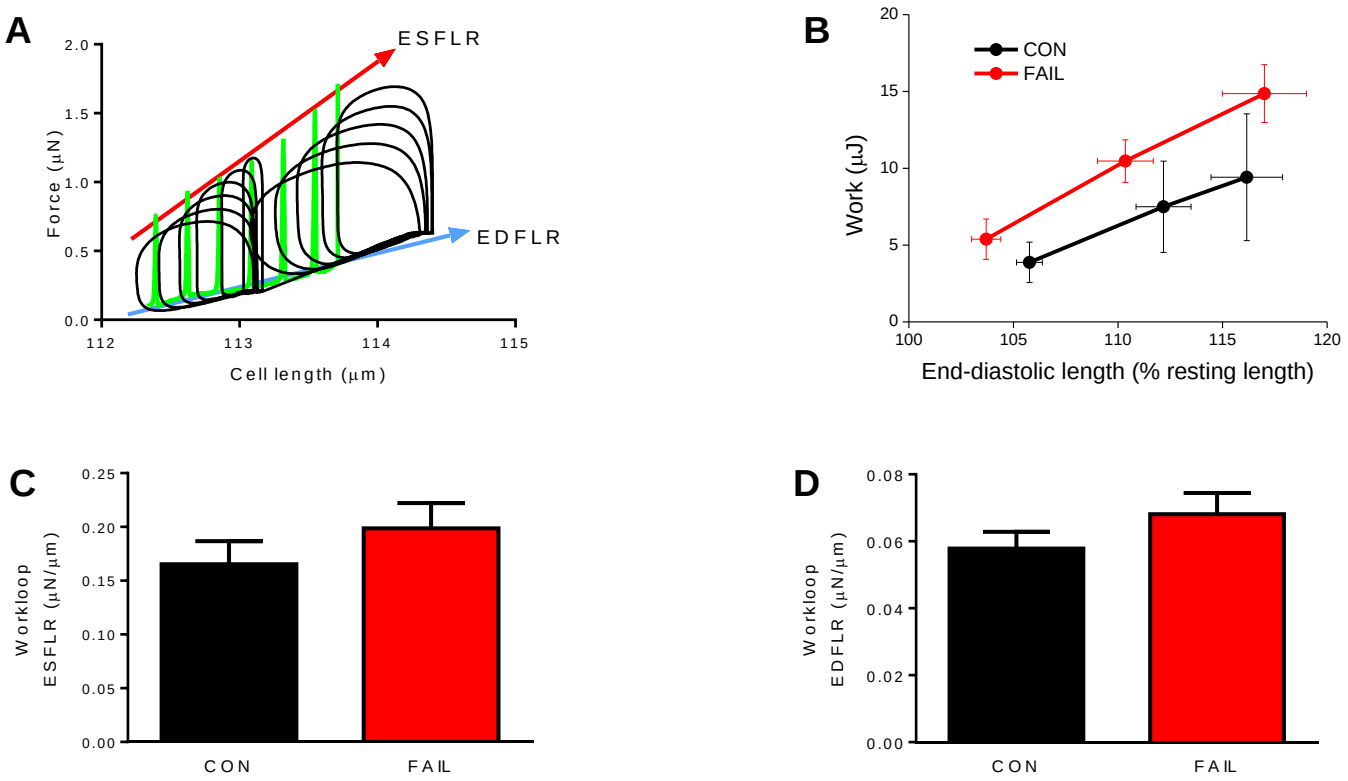

Figure 6.4 Workloop-style contractions in CON and FAIL RV cells

A The end-systolic (ESFLR) and end-diastolic (EDFLR) force length relationship found using workloop (*black loops*) and isometric contractions (*green spikes*) were qualitatively similar. **B** Increasing preload led to a significant increase in work in both CON and FAIL cells (N= 4 CON, 7 FAIL RV cells, P<0.001). **C** The ESFLR and (**D**) EDFLR measured using the work loop technique tended to be steeper in FAIL than CON but not significantly so. N=6 CON, 7 FAIL RV cells. Experiments were performed in 1.8 mM Ca^{2+} Tyrode.

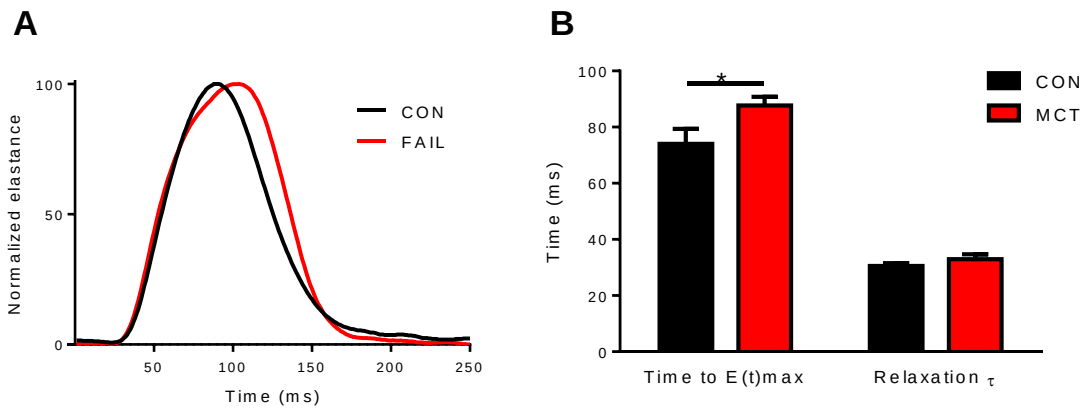

Figure 6.5 Time-varying elastance in CON and FAIL RV cells

A Normalized time-varying elastance (E(t)) of a CON and FAIL cell during a work loop contraction at 1 Hz. **B** The time to peak elastance (E(t)max) was significantly slower in FAIL cells. There was no difference in the time constant of relaxation (Tau) between groups. N=6 CON, 7 FAIL RV cells. * P<0.05. Experiments were performed in 1.8 mM Ca^{2+} Tyrode.

Feedback-controlled work loop contractions could not be performed as consistently as isometric contractions, consequently a full characterisation of cardiomyocyte function under dynamic load was not accomplished in the time available. Work loop failure was sometimes caused by an insufficient system response time which is necessary to clamp force during contractions at 37°C. This resulted in an overshoot of force during systole and an undershoot during diastole (Figure 6.2A middle panel) which induced a rebound overcompensation occasionally triggering resonance in the system. A LV cell dataset could not be collected in the time available during the visit to the Vrijie Universiteit, Amsterdam.

Several of the parameters we planned to measure using work loops are conceptually and empirically comparable to data obtained from isometric contractions subjected to stretch (Nishimura *et al.*, 2004; Iribe *et al.*, 2007). There was good agreement between the ESFLR and EDFLR measured using work loop or isometric contractions (Figure 6.4A). Therefore to increase the statistical power the ESFLR and EDFLR were also measured by step changes in length under isometric conditions and the results are presented below.

6.3.1.2 Systolic and diastolic properties during static stretch

Progressive stretch of RV cells contracting isometrically at 1 Hz led to an increase in end-systolic force. There was a positive linear ESFLR in both CON and FAIL cells. The ESFLR was 97% steeper in RV FAIL cells compared to CON (Figure 6.6 B+C). The ESFLR also comprises a diastolic component, therefore the ratio of the ESFLR to EDFLR (Frank-Starling Gain index, FSG (Bollensdorff *et al.*, 2011)) was calculated as a measure of preload recruitable active force. FSG was not different differ between CON (3.9 ± 0.7) and FAIL (3.7 ± 0.4, P=0.82).

Stretch raised the diastolic force progressively at greater levels of stretch. This relationship could also be described as positive and linear (Figure 6.6). The slope of the EDFLR was 99% greater in RV FAIL compared to CON cells (Figure 6.6 D+E). For consistency with previous reports in normal rats, data are presented as the EDFLR (in μN/μm), however RV FAIL cells tended to have a larger cross-sectional area (XSA) (FAIL 551±60 μm^2, CON 375±29 μm^2, P=0.06) consistent with myocyte hypertrophy. Additionally, although there was no significant difference in the distance between glass fibres at the start of the experiment (CON 95.0±4.9 μm, FAIL 95.6±2.5 μm, P=0.90), we tested whether differences in relative stretching could account for the steeper EDFLR

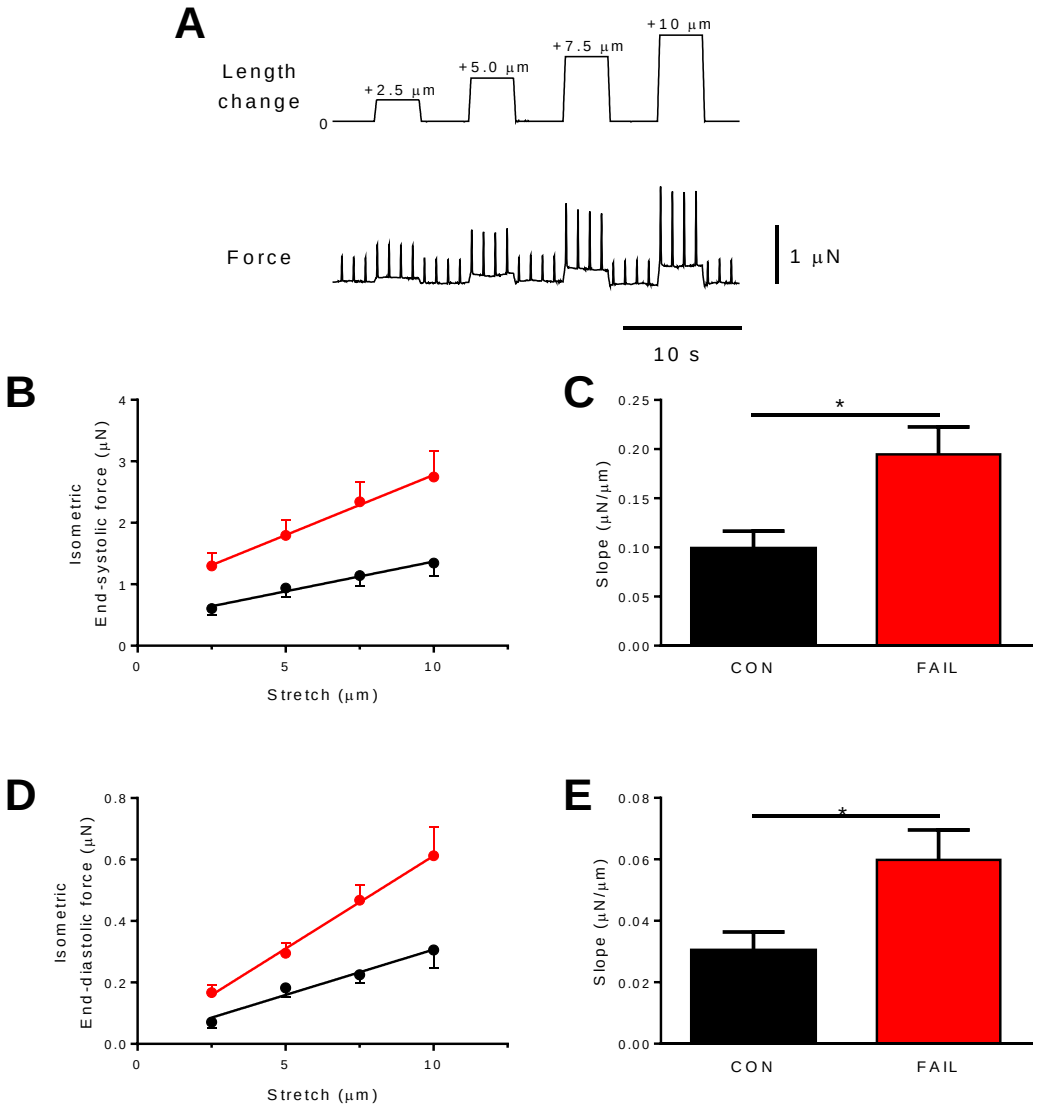

Figure 6.6 Systolic and diastolic properties of twitch contractions during stretch

A Isometric contractions were recorded in myocytes paced at 1 Hz and progressively stretched in steps of 2.5 µm. Cells were returned to resting length between stretches. **B** Mean isometric ESFLR in CON and FAIL cells. **C** The slope of the ESFLR was significantly steeper in RV FAIL cells compared to CON. **D** Mean isometric EDFLR in CON and FAIL cells. **E** The slope of the EDFLR was also significantly steeper in FAIL cells, indicating reduced FAIL cell compliance. N=8 CON, 13 FAIL cells. *P<0.05. Experiments were performed in 1.8 mM Ca^{2+} Tyrode.

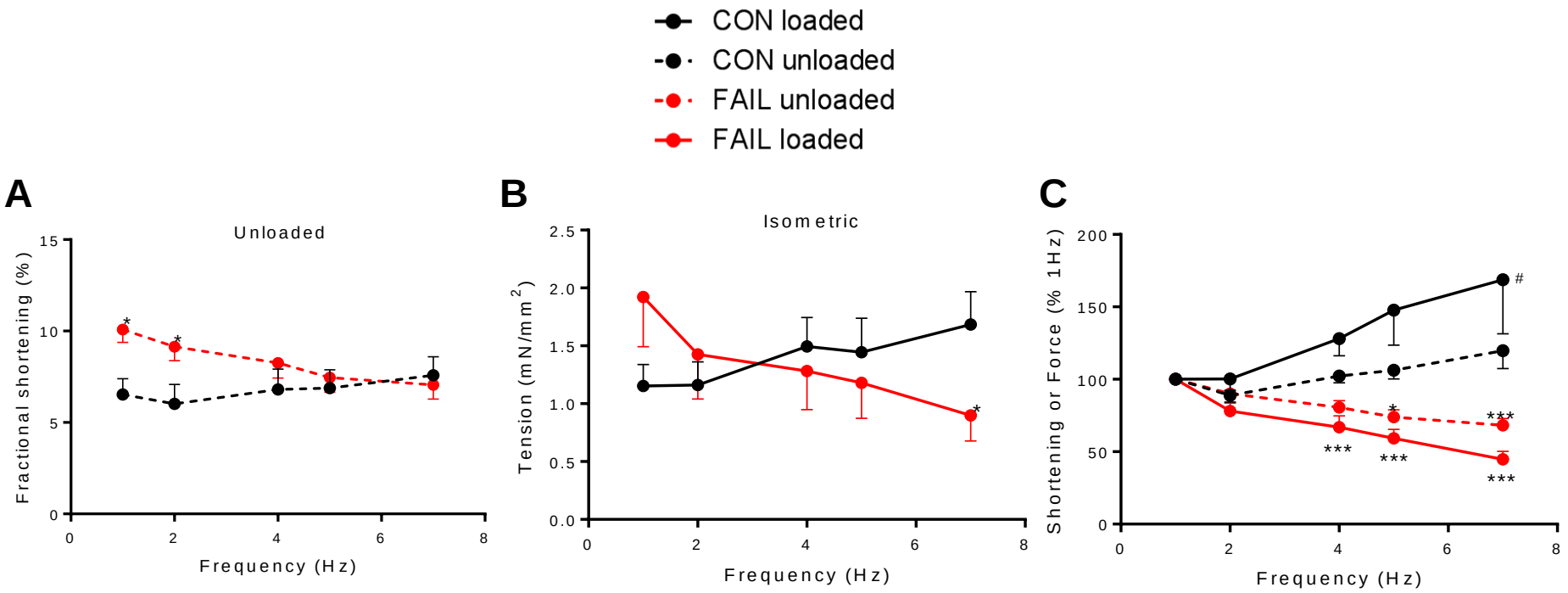

Figure 6.7 Paired comparison of loaded and unloaded contractions in single cells

A Unloaded shortening was greater in FAIL RV cells at low pacing frequencies but declined as frequency increased, whereas CON cell shortening increased. **B** The isometric tension-frequency relationship was similar but steeper than unloaded contractions measured in the same cells. **C** Data in (**A+B**) normalized to contraction at 1 Hz. N= 8 CON, 13 FAIL RV cells. *P<0.05, ***P<0.001 vs CON in the same loading condition, #P<0.05 vs CON unloaded. Experiments were performed in 1.8 mM Ca^{2+} Tyrode.

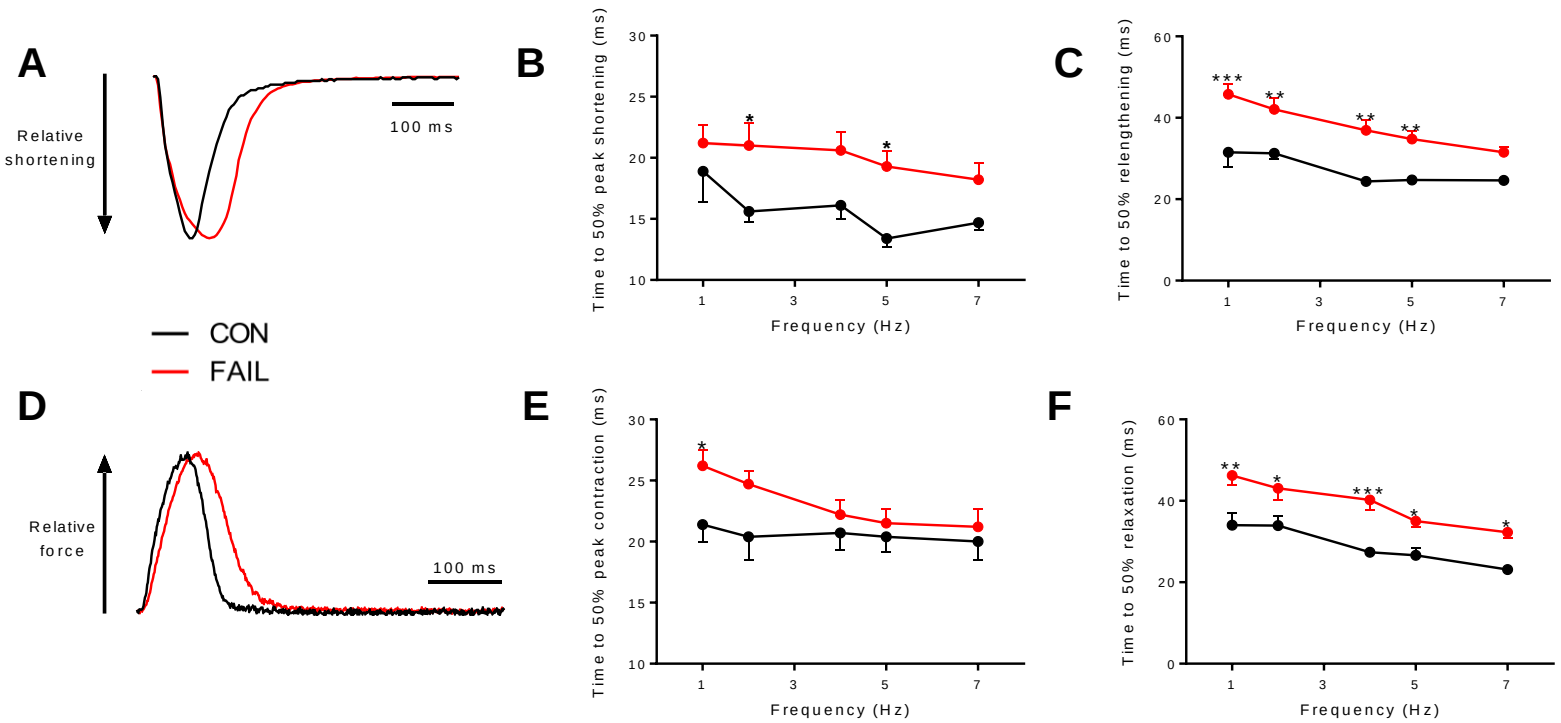

Figure 6.8 Time course of unloaded and isometric contractions

A+D Representative recordings of unloaded sarcomere shortening and force generation of a CON and FAIL cell. **B+E** RV FAIL cells had a slower time to 50% peak shortening and force than CON. **C+F** The time from peak to 50% relengthening was slower in RV FAIL than CON cells. N= 8 RV CON, 13 RV FAIL myocytes. *P<0.05, **P<0.01, ***P<0.001 vs CON. Experiments were performed in 1.8 mM Ca^{2+} Tyrode.

in FAIL cells. The EDFLR was still significantly steeper in FAIL cells after normalizing for XSA and percentage length change (CON 0.07±0.01, FAIL 0.13±0.03 $mN.mm^{-2}.\%^{-1}$ length change, $P<0.05$).

Developed force at resting length during the inter-stretch intervals was normalized to developed force prior to the stretching protocol. There was no difference in developed force during the inter-stretch intervals in either CON (100%, 99.9±2.0%, 100.6±3.3%, 96.3±3.8%, N=13 cells, P=0.29) or FAIL cells (100%, 101.0±3.6%, 104.1±4.0%, 95.1±4.3%, N=23 cells, P=0.15) indicating no loss of cell attachment during stretch.

6.3.1.3 Contraction-frequency relationship under load

The contractile function of RV CON and FAIL cells was measured at low (unloaded shortening) and high afterload (isometric contractions) at different pacing frequencies. Unloaded fractional shortening in RV CON cells initially decreased from 1 to 2 Hz, but as pacing frequency was progressively increased fractional shortening also increased (Figure 6.7A). As a result, in CON cells there was a relative increase in fractional shortening by 20% at 7 Hz compared to 1 Hz. In contrast, every increase in pacing frequency led to a decline in fractional shortening in RV FAIL cells. Fractional shortening in FAIL cells began significantly higher than CON cells at 1 and 2 Hz, however there was a relative fall in fractional shortening by 32% at 7 Hz compared to 1 Hz. As such, fractional shortening at 5 and 7 Hz in both groups was similar.

Isometric contractions were then measured from the same cells and the pacing protocol was repeated under load (Figure 6.7B). The overall shape of the tension-frequency relationship was very similar to the low afterload condition, however the positive and negative inotropic effect of increasing frequency in CON and FAIL cells appeared steeper. As such, the pacing frequency at which the relationships intersected occurred earlier, between 2-4 Hz.

The time course of contraction as a function of pacing frequency was investigated in both loading conditions. The time taken for FAIL cells to reach 50% of their maximal shortening or force tended to be longer than CON cells at all frequencies (Figure 6.8 B+E). In unloaded cells there was an inverse relationship between time to 50% peak contraction and pacing frequency, which did not differ between CON and FAIL ($P_{INTERACTION}$ = 0.45), whereas under isometric conditions time to 50% peak contraction only shortened in FAIL cells ($P_{INTERACTION}$ = 0.015). The time from peak to 50%

relaxation or relengthening was significantly slower in FAIL cells compared to CON at nearly all pacing frequencies. There was also an inverse relationship between frequency and time to 50% recovery from isometric or unloaded contraction in CON and FAIL cells. The main effect of loading on time course of contraction and relaxation was only significantly different in CON cells in the time to 50% relaxation, where it was significantly slower by 7% in isometric compared to unloaded conditions (P=0.019) (Figure 6.8 C+F).

6.3.2 Sarcomere length dependence of Ca^{2+} waves

Resting SL was significantly shorter by 5.1% in RV FAIL compared to CON cells, whereas there was no significant difference between LV FAIL and LV CON (Figure 6.9A). The diastolic Fura-4 ratio was measured during this time and was not different between CON and FAIL in either RV (RV CON 0.22±0.01 vs RV FAIL 0.22±0.01) or LV cells (LV CON 0.23±0.01 vs LV FAIL 0.22±0.01).

CON and FAIL RV cells were paced at 5 Hz followed by 1 min without pacing and the number of spontaneous Ca^{2+} waves recorded during this time (Figure 6.9B). The proportion of RV FAIL cells in which spontaneous Ca^{2+} waves occurred (0.94) was significantly greater than the proportion of RV CON cells (0.53) (P<0.001). There was no significant difference in the proportion of wave-producing LV CON cells (0.73) compared to LV FAIL cells (0.61) (P=0.71). The frequency of waves in cells which produced ≥1 wave during the 1 min observation was also significantly greater in RV FAIL (9±1 wave.min^{-1}) than RV CON (2±1 wave.min^{-1}), but not different between LV FAIL (3±1 wave.min^{-1}) and LV CON (2±1 wave.min^{-1}) (Figure 6.9C).

We investigated a possible SL-dependence of Ca^{2+} wave frequency in RV cells using two approaches to modify resting SL: 1) the actin-myosin crossbridge inhibitor blebbistatin, and 2) the irreversible creatine kinase inhibitor DNFB. We hypothesised blebbistatin would lengthen, and DNFB shorten, resting SL and hence decrease and increase wave frequency, respectively. This investigation focused on RV cells from CON and FAIL rats as there were no differences in wave frequency between LV CON and FAIL cells.

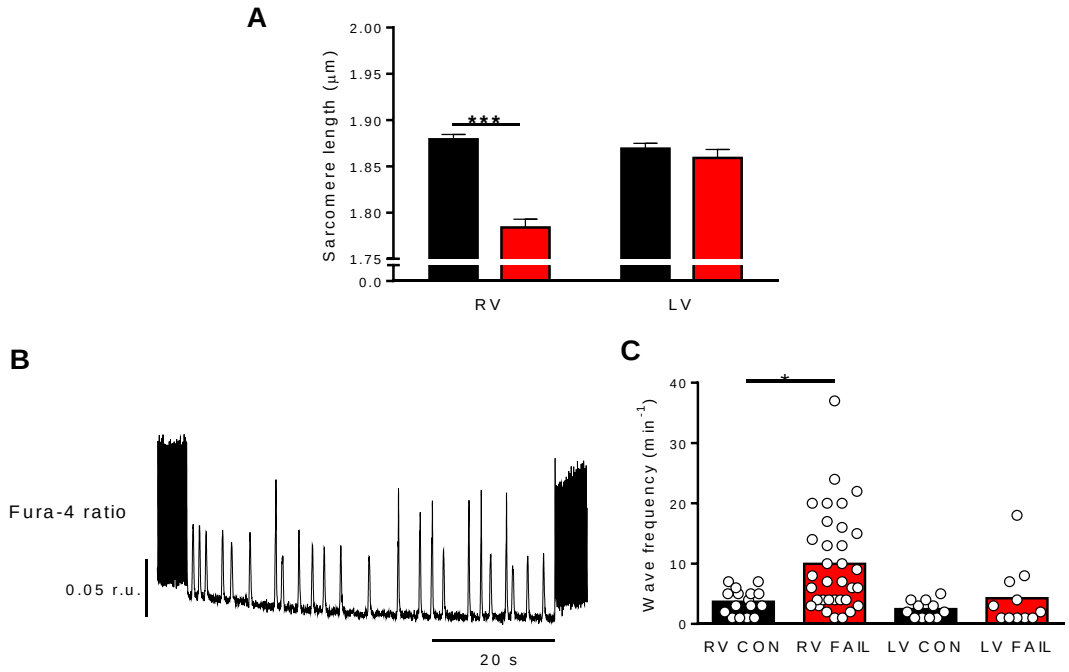

Figure 6.9 Sarcomere length and Ca^{2+} waves in quiescent cells

A Resting SL was shorter in RV FAIL than CON cells. SL was not different in LV CON and FAIL cells. **B** Spontaneous Ca^{2+} waves were recorded in Fura-4 loaded myocytes during 1 min rest following pacing at 5 Hz. **C** Wave frequency was greater in RV FAIL than CON in cells which produced ≥1 spontaneous wave. Wave frequency was not significantly different in LV FAIL and CON cells. N= 30 CON, 31 FAIL RV cells, 15 CON, 18 FAIL LV cells. *P<0.05, ***P<0.001

6.3.2.1 Increasing sarcomere length using blebbistatin

Within a few minutes of switching the local bathing solution from Tyrode (TYR) to blebbistatin (BLEB) shortening was effectively abolished in both CON and FAIL cells. Systolic Ca^{2+} transients still occurred, however the amplitude tended to be lower than before BLEB. Ca^{2+} wave frequency was not different in RV CON cells with or without BLEB, however in RV FAIL cells BLEB caused a significant reduction in wave frequency by an average of 2 waves.min^{-1} (Figure 6.11). Resting SL was significantly increased in the presence of BLEB in both CON and FAIL cells, and there was no significant difference in the magnitude of lengthening between the two groups. Diastolic Fura-4 ratio was not different in TYR or BLEB in CON (TYR 0.22±0.01 vs BLEB 0.22±0.01) or FAIL cells (TYR 0.22±0.01 vs BLEB 0.23±0.01).

We were concerned the reduced Ca^{2+} wave frequency in RV FAIL cells may have been due to off-target effects of BLEB on Ca^{2+} handling. The experiment was repeated in RV FAIL cells, with the additional estimation of SR Ca^{2+} content using caffeine. A group of RV FAIL cells underwent the same protocol but without BLEB to serve as time-matched controls (TYR-only) (Figure 6.12).

BLEB abolished contractions within several minutes and reduced Ca^{2+} transient amplitude to approximately 75% of the amplitude in TYR. In contrast, contractions and Ca^{2+} transient amplitude were stable throughout the entire experiment in TYR-only cells. In TYR-only cells the resting SL during the second rest period was significantly shorter than the first, and in BLEB cells there was no significant change in resting SL. There was no significant change in Ca^{2+} wave frequency in TYR-only cells, and unlike Figure 6.10 (without caffeine) there was also no change in wave frequency in BLEB cells (Figure 6.13). SR Ca^{2+} content was not different between the first and second measurement in TYR-only cells, but was significantly reduced by 19% in BLEB cells. There were no significant changes in the rates of Ca^{2+} efflux pathways in either group of cells, however there was a trend for Ca^{2+} removal during caffeine (primarily through NCX) to be faster in BLEB (TYR 0.63±0.08 [r.u.].s^{-1}, BLEB 0.86±0.14 [r.u.].s^{-1}, p=0.058).

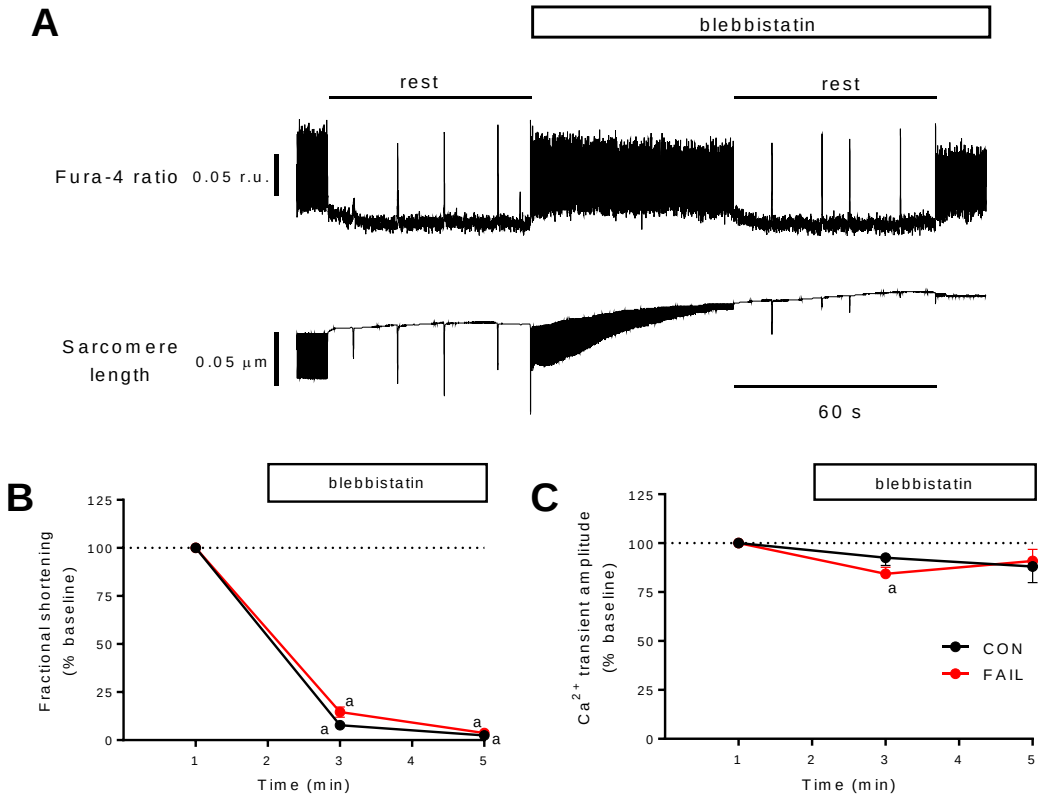

Figure 6.10 Blebbistatin abolishes contractions

A Shortening and Ca^{2+} transients were recorded in TYR then in BLEB. Resting SL and Ca^{2+} waves were recorded during 1 min unpaced. Shortening and Ca^{2+} transients were normalized to pacing in Tyrode. **B** BLEB reduced shortening within 2 min, and abolished contractions by 4 min. **C** Ca^{2+} transient amplitude was significantly reduced after 2 min in BLEB compared to TYR in FAIL cells and tended to decrease over time in CON cells. N=14 CON, 14 FAIL RV cells. $^{a}P<0.05$ vs Min 1

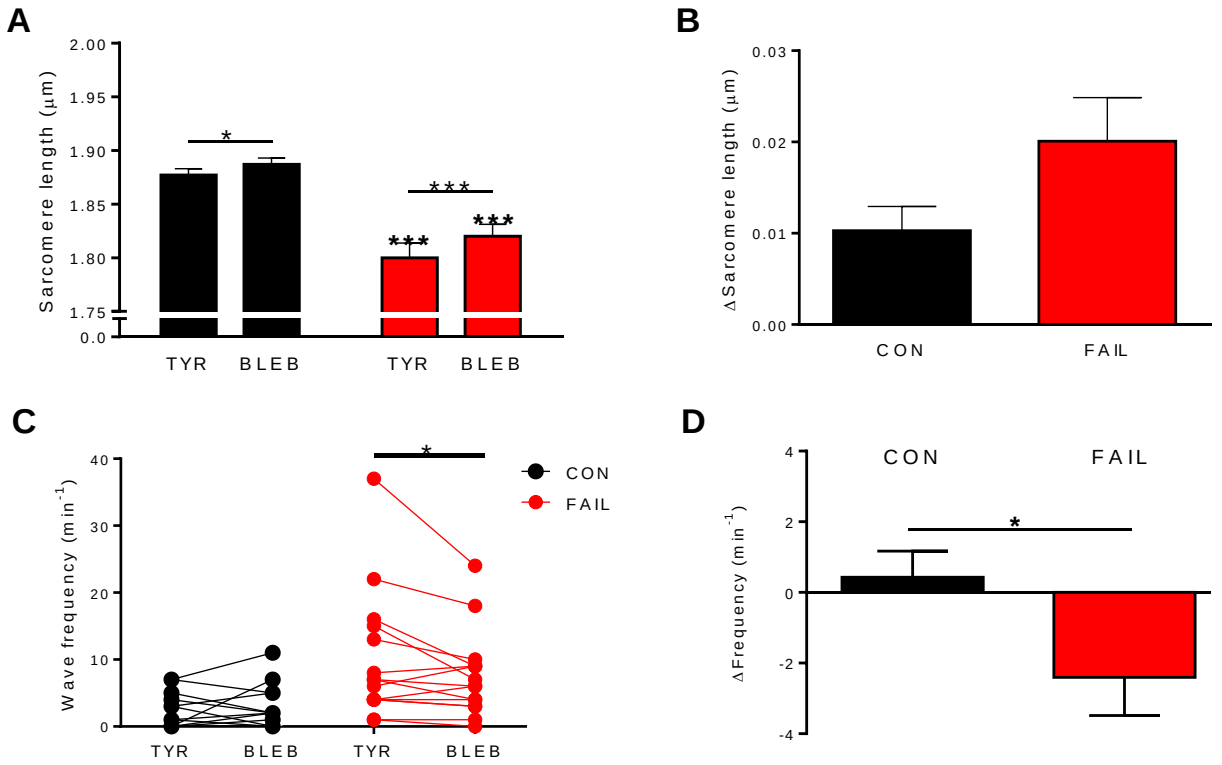

Figure 6.11 Longer sarcomere length and fewer Ca^{2+} waves in blebbistatin

A BLEB significantly increased resting SL in CON and FAIL cells, however SL remained shorter in FAIL compared to CON. **B** BLEB tended to have a greater lengthening effect in RV FAIL cells but this was not significantly different to CON (P=0.088). **C** Ca^{2+} wave frequency in RV CON cells was not different in BLEB compared to TYR, but was significantly reduced in BLEB compared to TYR in RV FAIL cells. **D** The mean change in wave frequency (BLEB-TYR) was thus greater in FAIL cells compared to CON cells. N= 14 CON, 15 FAIL RV cells. *P<0.05, ***P<0.001

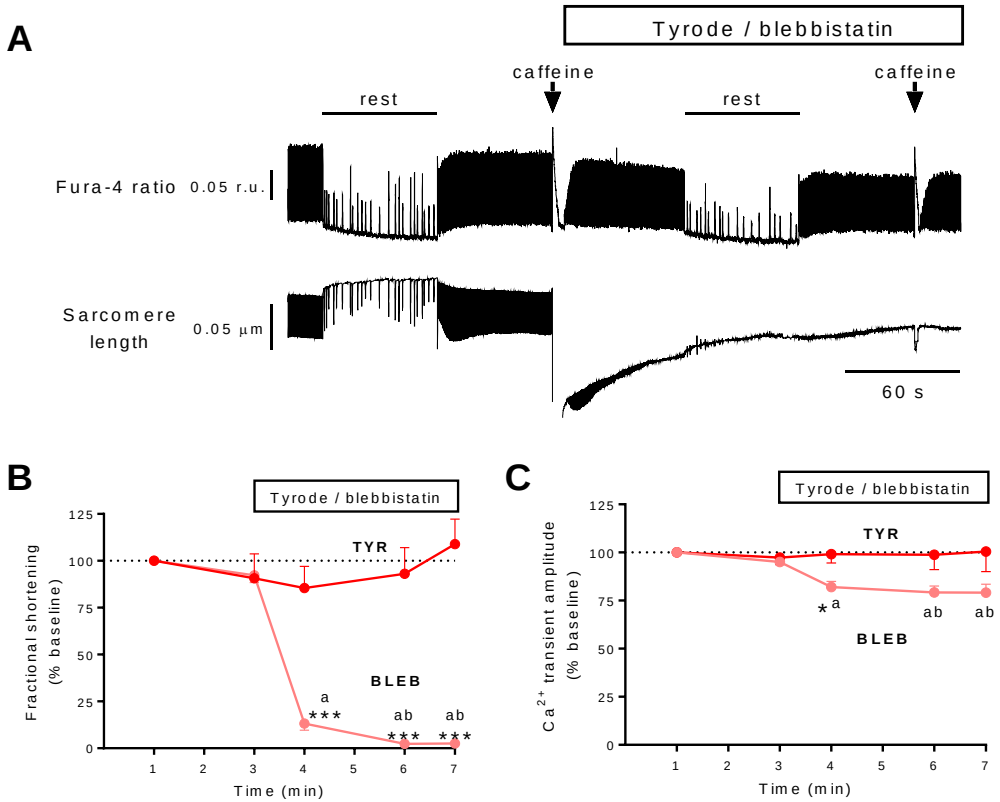

Figure 6.12 Blebbistatin depresses Ca^{2+} transient amplitude

A Effects of blebbistatin on SR Ca^{2+} handling was investigated in a group of RV FAIL cells using caffeine (20 mM) to estimate SR Ca^{2+} content in Tyrode (TYR) and blebbistatin (BLEB) solutions. **B** Contraction was stable throughout the 7 min in TYR, whereas in BLEB there was a sudden and complete cessation of contraction. **C** Ca^{2+} transient amplitude was stable over 7 min in TYR, but declined upon switching to BLEB. N=12 RV FAIL+BLEB, 9 RV FAIL+TYR cells. $^{a}P<0.05$ vs Min 1, $^{b}P<0.05$ vs Min 3, *P<0.05, ***P<0.001 vs TYR

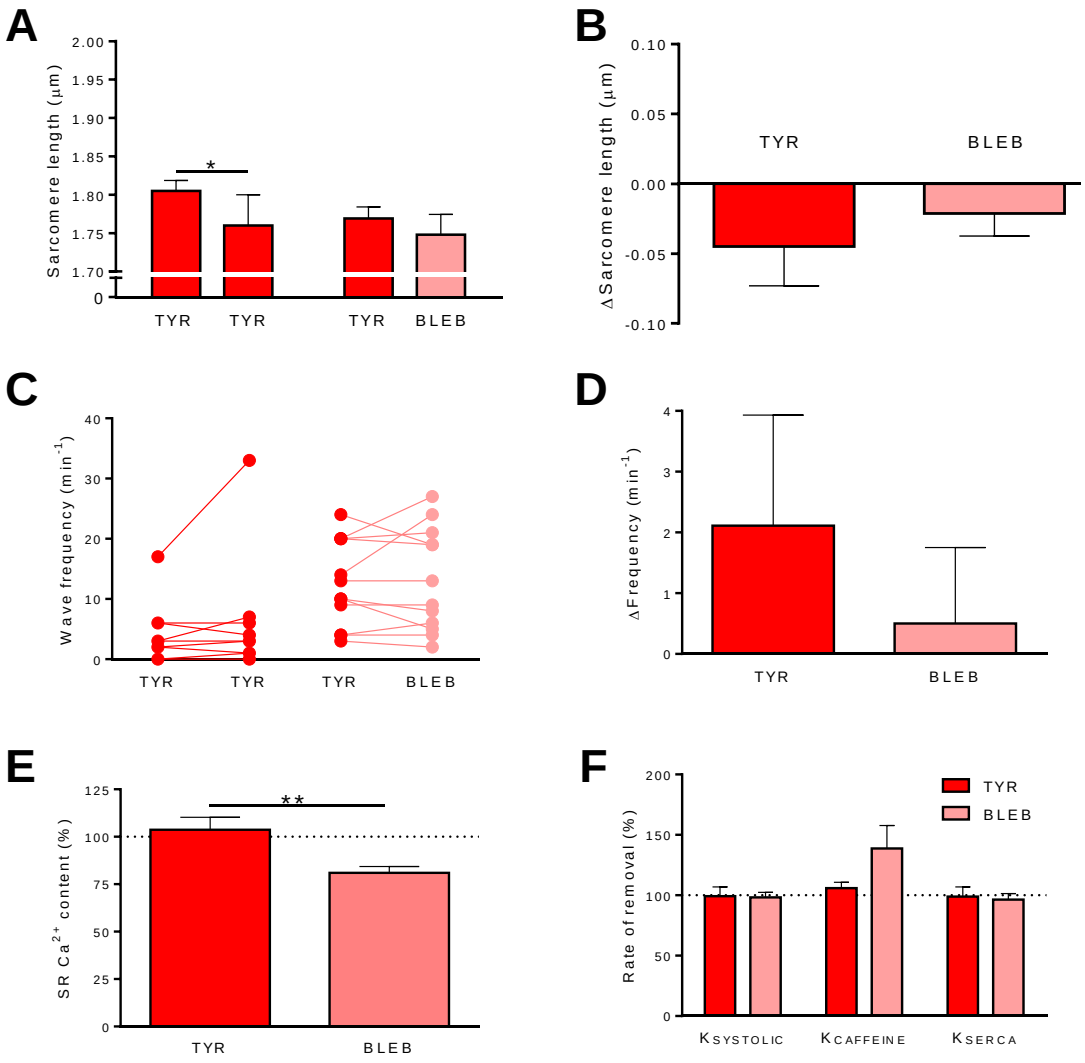

Figure 6.13 Decreased SR content in blebbistatin

A SL was shorter during the second rest period in TYR, and was not significantly different before and after BLEB. **B** There was a net reduction in SL during the second rest period in both groups of cells, which was not different between groups. **C** Wave frequency was not different in the second rest interval in TYR-only or BLEB cells. **D** The mean change in wave frequency was not different in TYR-only or BLEB cells. **E** SR Ca^{2+} content decreased in BLEB cells compared to TYR-only. **F** Ca^{2+} removal during caffeine (primarily though NCX) tended to increase in BLEB. N= 9 RV FAIL+TYR, 12 RV FAIL+BLEB cells. *P<0.05, **P<0.01.

6.3.3 Role of CK in Ca^{2+} handling and mechanical dysfunction in myocytes

The irreversible creatine kinase inhibitor DNFB was used to shorten resting SL in RV CON cells (Fowler *et al.*, 2015a; Sequeira *et al.*, 2015b). We first attempted to replicate the paired study design as in Figure 6.10-6.13 but found cells often became arrhythmic and died during DNFB perfusion. Instead, RV CON cells were pre-incubated with DNFB (DNFB cells) and compared to RV CON cells without DNFB in normal Tyrode (TYR cells) using unpaired statistics.

Resting SL was significantly shorter in DNFB by 14% compared to TYR cells (Figure 6.14). There was no significant difference in the proportion of DNFB cells which developed Ca^{2+} waves (0.64) compared to Tyrode cells (0.50) ($P=0.51$). In cells producing ≥1 Ca^{2+} wave, the frequency was significantly higher in DNFB compared to TYR (TYR 4±1 wave.min^{-1}, DNFB 11±2 wave.min^{-1}). Diastolic Fura-4 ratio was significantly elevated in DNFB (0.29±0.01 r.u.) compared to TYR cells (0.22±0.01 r.u.) ($P<0.001$). SR Ca^{2+} content was significantly elevated in DNFB by 63% compared to TYR cells. The rate of systolic Ca^{2+} decay and efflux due to SERCA removal were not different in DNFB or TYR cells, however the rate of Ca^{2+} removal during caffeine was significantly reduced by 39% in DNFB cells.

6.3.3.1 Contraction-frequency relationship with CK inhibition

The flat or positive contraction-frequency relationship in RV CON cells contrasted with the steep negative relationship in RV FAIL and DNFB cells which overlapped (Figure 6.15). At 7 Hz both DNFB cells and RV FAIL cell fractional shortening was significantly reduced to 44 and 61% respectively, of shortening at 1 Hz. The Ca^{2+} transient amplitude-frequency relationship measured in Fura-4 loaded cells was also steeply negative in DNFB and RV FAIL cells in contrast to an overall positive relationship in RV CON. At 7 Hz the Ca^{2+} transient amplitude was reduced by 27% and 30% compared to 1 Hz in DNFB cells and RV FAIL cells, whereas the amplitude in RV CON cells increased by 3% compared to 1 Hz.

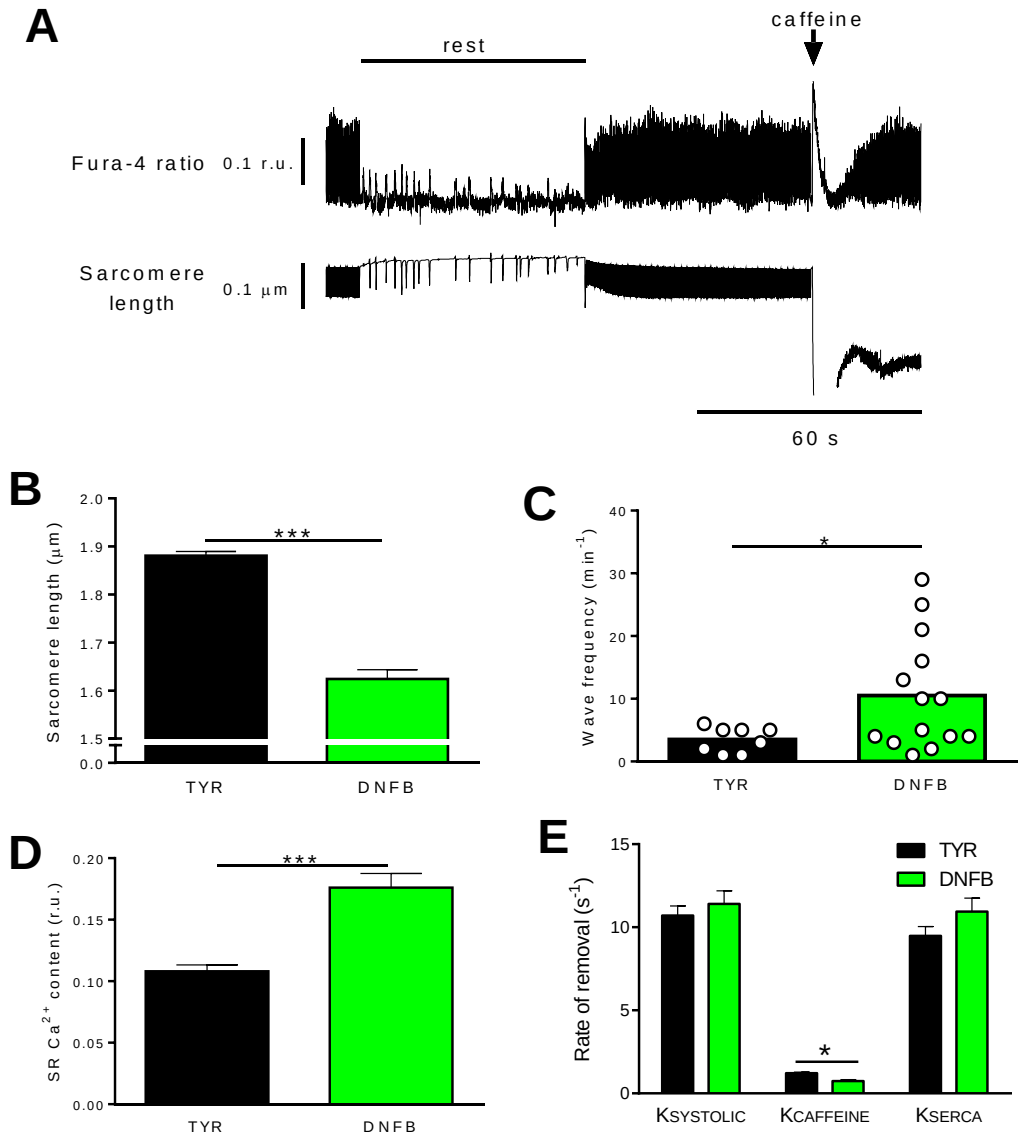

Figure 6.14 Creatine kinase inhibition shortens sarcomere length and increases Ca^{2+} waves

A RV CON cells were preincubated with TYR or DNFB (20µM) then SL, Ca^{2+} wave frequency and SR Ca^{2+} content were measured. **B** Resting SL was shorter in DNFB than TYR cells. **C** In cells producing ≥1 spontaneous Ca^{2+} wave, frequency was greater in DNFB compared to TYR cells. **D** SR Ca^{2+} content was significantly elevated in DNFB cells. **E** The rate of Ca^{2+} efflux during caffeine was significantly slower in DNFB-treated cells. N= 16 CON+TYR RV cells, 22 CON+DNFB RV cells. *P<0.05, ***P<0.001.

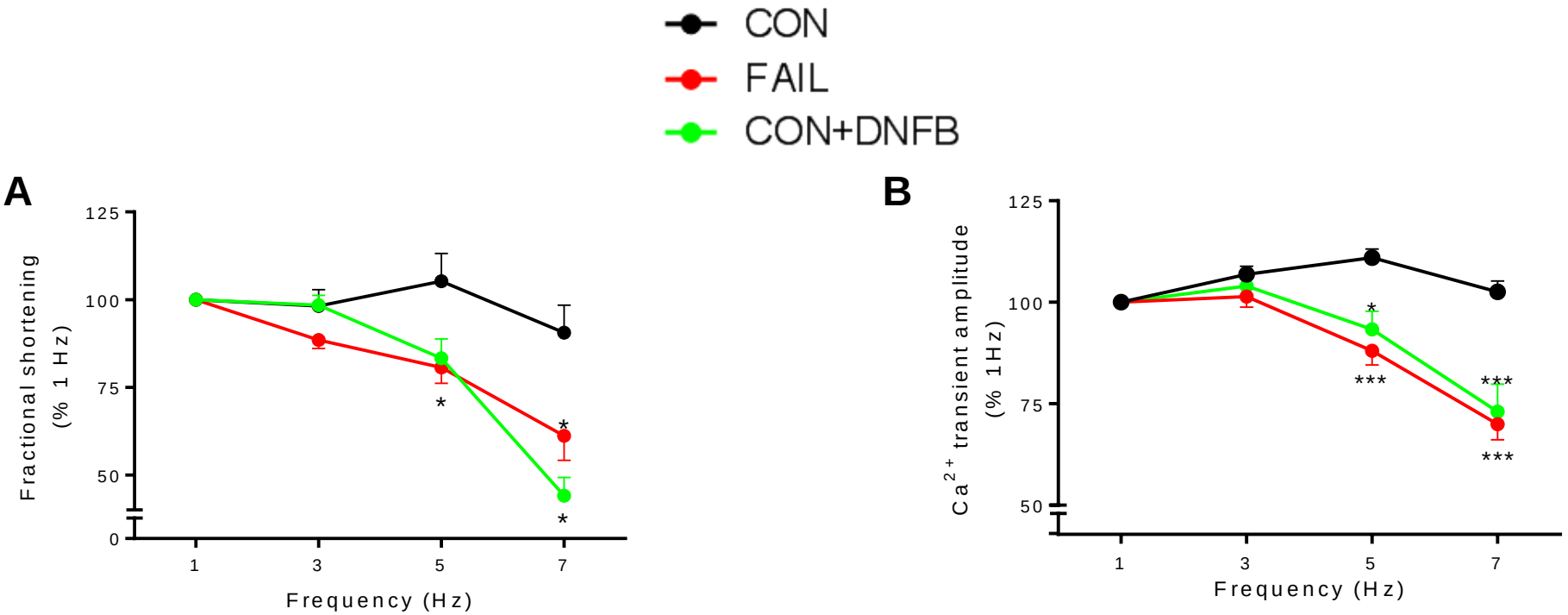

Figure 6.15 Creatine kinase inhibition reproduces the failing contractile phenotype in CON cells

A The unloaded contraction-frequency relationship was measured in RV CON, FAIL, and DNFB-treated CON cells. Contraction was fairly stable in CON cells between 1-7 Hz, whereas fractional shortening was significantly reduced in FAIL cells at 5 and 7 Hz compared to CON. Similar to FAIL cells, DNFB-treated CON cells also showed a negative contraction-frequency relationship. N=23 CON, 28 FAIL, 25 CON+DNFB cells. **B** There was a fall in systolic Ca^{2+} transient amplitude measured in Fura-4 loaded FAIL and DNFB-treated CON cells at 5 and 7 Hz. N=28 CON, 30 FAIL, 8 CON+DNFB. **P<0.05, ***P<0.001 vs CON.

6.3.3.2 Reintroducing CK-M to failing cells

Resting SL was measured in saponin permeabilized cells incubated in Ca^{2+}-free intracellular-like solutions in the presence or absence of exogeneous CK-M and/or PCr. Resting SL was significantly shorter in RV FAIL cells incubated with only ATP, PCr, or CK compared to RV CON cells incubated with the equivalent solution by 4.1-5.5% (Figure 6.16); however SL in RV FAIL cells incubated in CK+PCr solution was not significantly different to CON and was significantly longer than RV FAIL cells in the other solutions. There were no differences in resting SL between different solutions in CON RV and LV cells, or between any groups of CON and FAIL LV cells. To summarise, RV FAIL resting SL was significantly lengthened only when cells were incubated in a solution containing CK and its substrate PCr (Figure 6.16).

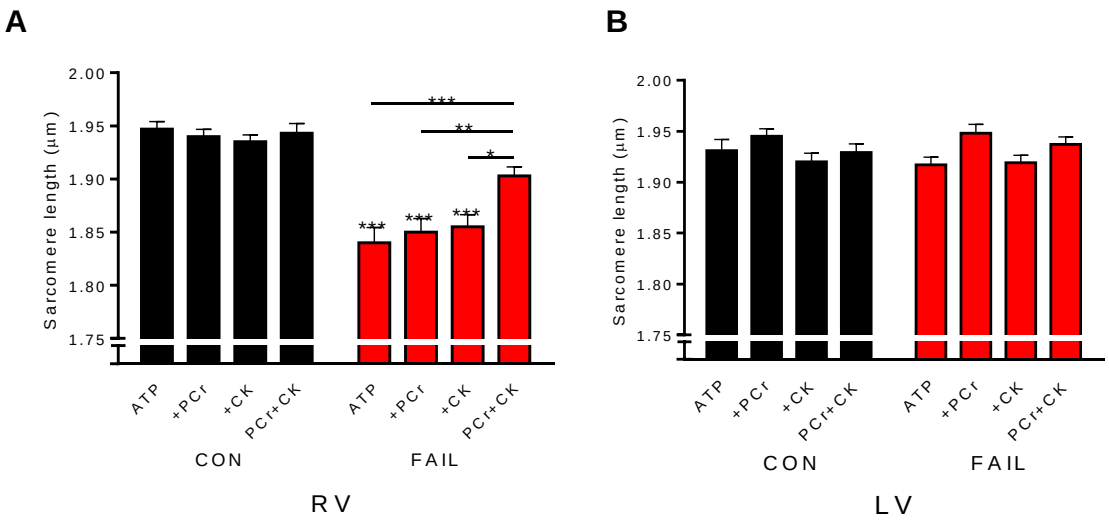

Figure 6.16 Exogenous creatine kinase lengthens failing sarcomere length

SL was measured in saponin permeabilized **(A)** RV or **(B)** LV cells in intracellular-like solution in the absence of both PCr and exogenous CK (ATP); the presence of either PCr or CK (+PCr, +CK) or the presence of both (PCr+CK). SL of RV FAIL cells was significantly shorter than equivalent CON groups with the exception of the (PCr+CK) groups. FAIL RV in the presence of PCr+CK had significantly longer SL than other FAIL RV groups (***P<0.001). There were no significant differences between LV groups. N = 36 cells in each group. *P<0.05, **P<0.01, ***P<0.001 vs CON in equivalent solution.

6.4 Discussion

RV contractile function prognosticates survival in human PAH, for instance RV ejection fraction below 25%, reduced stroke volume, and reduced contractile reserve during exercise are associated with a 20-40% higher mortality in PAH patients over 4-5 years (van Wolferen *et al.*, 2007; Grünig *et al.*, 2013; Courand *et al.*, 2015). In LV failure the incidence and mortality of patients with Heart Failure with reduced Ejection Fraction (HFrEF, or systolic heart failure) and Heart Failure with preserved Ejection Fraction (HFpEF, or diastolic heart failure) are approximately equal (Bhatia *et al.*, 2006; Owan *et al.*, 2006), however in PAH less is known regarding the impact of diastolic dysfunction in the pathophysiology of RV failure. Poor RV diastolic function measured using tissue Doppler echocardiography correlated with elevated serum levels of brain natriuretic peptide and worse survival in patients with chronic pulmonary thromboembolism or PAH (Shiina *et al.*, 2009a; Shiina *et al.*, 2009b), however these measurements are difficult to perform in the RV due to its complex geometry and anatomy and are not load-independent. Sudden cardiac death accounts for 20% of mortality in PAH patients and spontaneous ventricular fibrillation has also been reported in MCT rats (Delcroix & Naeije, 2010; Liles *et al.*, 2012; Umar *et al.*, 2012). We investigated the contractile function of isolated RV myocytes under a variety of loading conditions and the geometric influence of SL on spontaneous Ca^{2+} wave frequency.

6.4.1 Work loop contractions in isolated myocytes

Forces exerted by, and upon, ventricular myocytes vary throughout the cardiac cycle and influence the volume of blood ejected with each contraction. Shortening and force-generation are related but distinct indices of contraction, meaning ventricular contractility cannot be inferred solely from isometric, auxotonic or isotonic contractions of isolated myocytes. Cellular work is a composite parameter involving shortening against an external load, and as such may be more sensitive to changes in function and translatable to *in vivo* cardiac performance.

Cardiac work loops were first characterised by Suga *et al.* (1973) using open-chested dogs as a load-independent means to characterise the contractile state of the heart. Since then the concept has been employed to study a hierarchy of complexity, from isolated hearts (Suga & Sagawa, 1974), papillary muscles (Wong *et al.*, 2010), trabeculae (Han *et al.*, 2012) and most recently isolated cardiomyocytes. The first afterloaded contractions in cardiomyocytes were performed at room temperature in

cells from frog ventricle by Parikh *et al.* (1993) and later in rat ventricle cells at 37°C by Yasuda *et al.* (2001). The data presented in this thesis are the first recordings of cellular work performed by failing ventricular myocytes using feedback-controlled work loop contractions at 37°C.

Cellular work by failing RV cells was similar to control cells, which concurs with our finding of augmented unloaded and isometric contractions at low frequencies. This is also in agreement with our finding that stroke work *in vivo* is not different in control and failing rats (Chapter 3). Wong *et al.* (2010) found papillary muscles from hypertrophic MCT rats paced at 5 Hz performed similar amounts of work as those from healthy rats, however the O_2 cost was higher in MCT rats meaning the failing myocardium was less efficient at generating work. Reduced RV work efficiency was also reported by the same group in human PAH patients using positron emission tomography and ^{15}O imaging (Wong *et al.*, 2011b). Possible reasons for the reduced mechanical efficiency could be increased ATP turnover required to cycle Ca^{2+} or increased ROS production by intracellular oxidases.

Nishimura *et al.* (2004) and Iribe *et al.* (2007) found the ESFLR and EDFLR in isolated ventricular myocytes were similar over physiological ranges of stretch whether measured by work loop or isometric contractions. Recently however, Iribe *et al.* (2014) found the ESFLR to be steeper at low afterloads, which we also found. This may be due to shortening inactivation of the thin filament at short SL.

A possible limitation of the work loop method is the use of a rectangular shaped loop which is not the normal shape of a pressure-volume loop in a healthy RV which is more triangular due to a short isovolumic contraction period and sustained ejection during relaxation. However, in RV failure the PV loop becomes more rectangular and similar to LV PV loops (Redington *et al.*, 1988; Redington *et al.*, 1990). Future work could investigate whether intrinsic properties of RV and LV myocytes are better suited to these two modes of ejection by modifying the work loop control algorithm.

6.4.1.1 Preserved Frank-Starling mechanism in failing cells

Increasing the end-diastolic volume of the heart leads to an immediate increase in the force of contraction, known as the Frank-Starling mechanism. We found an increase in cellular work in both healthy and failing myocytes when preload was increased, and a steeper ESFLR during isometric stretch in failing cells. The ESFLR in our healthy rat

cells (0.1 µN/µm) was less steep than was reported for guineapig LV cells (0.2 µN/µm). The reason for this discrepancy may lie in species and regional differences in the force-length relationship, such as occur between rat and ferret, and from different regions of the heart (Cazorla *et al.*, 2000b; Bollensdorff *et al.*, 2011).

The usefulness of the ESFLR is limiting as by definition it is influenced by diastolic force. The 'Frank-Starling Gain index' (FSG), or ratio of ESFLR:EDFLR, has been proposed as a measure of preload recruitable active force which, due to being unitless, is not influenced by variable cell width or diastolic compliance (Bollensdorff *et al.*, 2011). The FSG values of 3.9 in CON and 3.7 in FAIL RV cells calculated by us are very similar to the value for rat RV cells (3.6) reported by the proponents of FSG (Bollensdorff *et al.*, 2011). There was no difference in FSG between healthy and failing cells suggesting the Frank-Starling mechanism is preserved in failing rats.

A preserved Frank-Starling mechanism was previously found using the carbon fibre technique in intact and permeabilized MCT rat myocytes (Benoist *et al.*, 2014). The Frank-Starling mechanism is also generally preserved in LV failure in humans (Holubarsch *et al.*, 1996; von Lewinski *et al.*, 2009), in RV trabeculae from failing human hearts (Milani-Nejad *et al.*, 2015), and in PAH (Rain *et al.*, 2013), although some studies have found it depressed, e.g. in dilated cardiomyopathy (Schwinger *et al.*, 1994). The impaired Frank-Starling mechanism in dilated cardiomyopathies may result from proteolytic degradation of titin reducing its ability to narrow myofilament lattice spacing (Hein *et al.*, 1994). This implies the limited ability to increase stroke volume in pressure overloaded hearts is most likely not due to intrinsic failure of the Frank-Starling mechanism. Cardiomyocytes are thought to only operate on the ascending limb of the force-length curve *in vivo* (Shiels & White, 2008), therefore the high wall stresses resulting from the law of Laplace means cardiomyocytes in a dilated ventricle are working towards the isometric end of the force-velocity relationship, and as a result the majority of the stress generated goes towards preventing further dilation with less going towards ejecting blood. For this reason preload-reduction with diuretics is a first line treatment to reduce volume overload in PAH (Matthews & McLaughlin, 2008).

6.4.1.2 Reduced compliance of failing cells

Rain *et al.* (2013) measured RV compliance *in vivo* and in chemically skinned muscle fibres from PAH patients and ascribed the increased stiffness of both to a combination

of reduced phosphorylation of the giant protein titin and increased fibrosis. They found no evidence of residual crossbridge activity as myofilament Ca^{2+} sensitivity was unchanged and 2,3-BDM did not affect the passive stiffness of chemically skinned fibres. In contrast, we have shown evidence that loss of CK from the myofilaments in rat PAH shortens SL likely due to accumulation of ADP causing rigor-like crossbridges (Figure 6.16 and Fowler *et al.* (2015a)). This same mechanism was proposed by Mulieri *et al.* (2002) to explain prolonged crossbridge attachment time in skinned fibres from human failing hearts, and by Yoshikawa *et al.* (2013) to explain increased transverse stiffness of cardiomyocytes in isoproterenol-induced heart failure in rats. Nishimura *et al.* (2005) showed the passive stiffness of normal cardiomyocytes to axial stretch (which contain a smaller proportion of Ca^{2+}-independent crossbridges) could be reduced by uncoupling with 2,3-BDM, therefore we believe the same mechanism may be responsible for the increased stiffness to stretch in isolated FAIL cells and therefore potentially the failing RV. A possible reason for the differences between our study and Rain *et al.* (2013) may be their use of chemically skinned myocytes, whereas we used membrane-intact cells which may better retain their cytosolic constituents.

Future work could investigate the contribution of crossbridges and passive elements to stiffness in MCT cells using 2,3-BDM, as no reports have been published on the role of titin in MCT diastolic dysfunction. Changes in titin were not investigated in this thesis, however as rats primarily express the shorter N2B isoform, whereas humans also express the longer, more compliant N2BA isoform, any changes would likely be though altered phosphorylation or oxidative crosslinking of sulfhydryl groups in the Ig domain (Cazorla *et al.*, 2000a; Grutzner *et al.*, 2009; Zile *et al.*, 2015).

We did not find a change in collagen volume fraction in our MCT rats (Chapter 4). At physiologically-relevant degrees of stretch, titin and actin-myosin crossbridges are thought to be the main determinants of stiffness, whereas collagen becomes increasingly important when end-diastolic volumes are very large, such as when the heart decompensates (Chung & Granzier, 2011). This suggests RV myocytes themselves may be an important source of passive stiffness in the failing heart, and therefore treatments which improve cellular energetics may improve diastolic function.

The EDFLR we measured in healthy rat RV cells (0.03 µN/µm) was similar to the compliance of guinea pig LV cells (0.02 µN/µm) reported by Iribe *et al.* (2007). The present finding contrasts with recent work from this laboratory which found no

difference in passive tension in intact RV FAIL myocytes stretched using the carbon fibre technique (Benoist *et al.*, 2014). Korstjens *et al.* (2002) found a tendency for passive stiffness in RV trabeculae to be greater in rats injected with 44 mg/kg MCT, however this difference was not significant. The greater magnitude of stretch achievable using MyoTak combined with a high sensitivity force transducer may have helped identify sub-microNewton differences in diastolic forces in our MCT RV cells.

Stones *et al.* (2013) reported increased microtubule proliferation in the MCT model which was reported to decreased the compliance of RV cells in a cat PAB model (Zile *et al.*, 1999). Under normal circumstances microtubules have a minimal contribution to stiffness in response to longitudinal stretch (Granzier & Irving, 1995), however they do seem to play an important role in shear stress (Nishimura *et al.*, 2005). Microtubule proliferation may have an important role *in vivo* where myocytes are in a three dimensional organisation in the ventricle wall and subject to different types of stresses.

6.4.2 Contraction-frequency relationship differs under load in failing and healthy myocytes

Our finding of enhanced or unchanged contractility in failing cells at low pacing frequencies has also been reported in isolated hearts and trabeculae from rat MCT (Lamberts *et al.*, 2007a; Lamberts *et al.*, 2007b) and cat pulmonary artery banding (Quaile *et al.*, 2007). In these studies, a negative force-frequency relationship was found in the failing RV which is likely due to the steeply negative Ca^{2+}-frequency relationship (Chapter 5).

Direct comparisons between tension developed by single cells, trabeculae and papillary muscles is complicated by factors such as attachment method, system compliance, variable geometry, extracellular volume, as well as paracrine and endocrine influences. Consequently the peak tension reported in trabeculae and papillary muscle studies can be as much as an order of magnitude higher than for single myocytes (Alvarez *et al.*, 1999). Conversely variable collagen content, particularly in heart failure, will influence the force of contraction in trabeculae and papillary muscle which is not an issue with isolated cells. Our data from single cells measured at resting length are comparable to the peak forces measured at resting length in isometrically contracting rat (2 $mN.mm^{-2}$) and rabbit myocytes (5.4 $mN.mm^{-2}$) (Bluhm *et al.*, 1995; Yasuda *et al.*, 2001). Shearing due to sarcomere shortening of the unattached surfaces of the cell, or compliance in the MyoTak, may lower the measured

force of contraction. This problem was elegantly and intricately tackled by Iribe *et al.* (2014) by attaching cells both top and bottom to carbon fibres to increase the surface area for attachment which increased the detachment force. We did not aim to record maximum twitch forces, however isometric forces in excess of 6.50 μN were recorded in the current investigation which is higher than the maximum previously reported (5.72 μN) (Nishimura *et al.*, 2004). Inaccuracies measuring cell width and the assumption of a constant cell width:depth ratio in pathological conditions may also lead to over- or underestimation of cell cross-sectional area (Wang & Gerdes, 1999; Natali *et al.*, 2002).

Changes in force with frequency were exaggerated compared to unloaded shortening, which was also found in failing and non-failing muscle strips and isolated cells from human heart failure (Brixius *et al.*, 2001). Only using unloaded cell shortening might lead one to conclude failing RV myocyte contractility at 5 Hz (a typical resting heart rate for a rat) was unchanged or enhanced, whereas if isometric force was measured contractility would clearly be depressed. This highlights the need for complementary functional measurements ideally across different levels of structural complexity.

The slopes of the unloaded shortening-frequency relationship were less steep than in Fura-4 loaded cells described in Chapter 5. The buffering effect of Ca^{2+} indicators will be non-linear under non-saturating conditions, therefore the relative buffering in failing cells at lower pacing frequencies (where Ca^{2+} transients are large) will be less than in control cells with smaller Ca^{2+} transients. The opposite effects of pacing frequency on Ca^{2+} transient amplitude in control and failing cells will exaggerate the effect of pacing on contraction.

6.4.3 Load-dependence of time course of contraction

The time to 50% peak contraction tended to be longer in failing cells, however this was less apparent at faster pacing frequencies. The rate of force development and shortening depends on synchronous Ca^{2+} entry through L-type Ca^{2+} channels in T-tubules during depolarisation. Loss of T-tubules in failing cells identified in Chapter 5 slowed the Ca^{2+} transient upstroke and hence is likely to contribute to the slower rate of isometric force development in these cells (Ferrantini *et al.*, 2014). The adult rat myocardium primarily expresses α-MHC however in heart failure there is a shift towards the fetal β-MHC (Ishikawa *et al.*, 1992b; Korstjens *et al.*, 2002). β-MHC has a lower ATPase activity and higher ADP affinity than α-MHC resulting in slower

crossbridge turnover and slower contraction velocity (Chung *et al.*, 2014). This may be exacerbated by the loss of CK described previously which could increase cytosolic ADP and slow the rate of crossbridge cycling (Sequeira *et al.*, 2015a).

The cytoskeleton imposes a viscous brake on shortening (Yamamoto *et al.*, 1998) and was investigated by Zile *et al.* (1998) and (1999), using a cat pulmonary artery banding model. They found the viscous dampening of RV cells embedded in an agarose matrix was increased and isotonic shortening velocity of papillary muscles was reduced by PAB, coinciding with increased β-tubulin expression in PAB muscles. Microtubule depolymerization with colchicine restored the velocity of shortening and normalized the viscous dampening in cells. Proliferation of microtubules in failing RV MCT cells was also found by Stones *et al.* (2013), however depolymerization did not normalize cell shortening velocity. A possible explanation for these discrepant findings could lie in microtubules playing a greater role in modulating shear stress which will be important in a three dimensional papillary muscle or gel matrix, but less so when shortening in a single axis (Nishimura *et al.*, 2005).

The timecourse of activation and relaxation in myocytes usually shows clear load-dependency, with force development faster and relaxation slower in isometric compared to isotonic conditions (Yasuda *et al.*, 2003; Iribe *et al.*, 2007; Iribe *et al.*, 2014). Myocyte shortening decreases the affinity of TnC for Ca^{2+}, whereas under isometric conditions myofilament affinity for Ca^{2+} remains high. Conversely, isometric stretch was shown to decrease the rate of force development and crossbridge cycling rate in intact human RV trabeculae, presumably due to crossbridges remaining in a high affinity bound state for longer (Milani-Nejad *et al.*, 2015). Shortening cells also contract against an internal load with both an elastic and a viscous component, the latter of which depends on shortening velocity. We found the time to relaxation was slower in CON cells under isometric compared to isotonic conditions as we expected, however the time to relaxation was not different in loaded or unloaded FAIL cells, and the time to 50% peak contraction was not different in different loading conditions in either group of cells. The analysis of instantaneous elastance also revealed a delayed time to peak elastance in failing cells, however there was no difference in the rate of relaxation using this method.

6.4.4 Ca^{2+} waves depend on resting sarcomere length

Umar *et al.* (2012) and Benoist *et al.* (2011) reported isolated hearts from MCT rats were more susceptible to spontaneous or pacing induced ventricular fibrillation, and there is a report of spontaneous ventricular fibrillation leading to the death of a conscious MCT rat implanted with telemetry (Liles *et al.*, 2012). We found increased frequency of Ca^{2+} waves in failing RV cells, which could be a trigger for ventricular arrhythmias. We have already identified elevated SR Ca^{2+} content as a possible mechanism behind increased Ca^{2+} waves in failing cells in Chapter 5 (Venetucci *et al.*, 2007). We also investigated a hypothesized link between RyR2 spacing and Ca^{2+} waves (Keizer *et al.*, 1998; Izu *et al.*, 2006). Sarcomere length was used as a proxy for RyR2 spacing as it has been shown to be preserved despite loss of t-tubules in heart failure (Heinzel *et al.*, 2008; Lenaerts *et al.*, 2009). The shorter SL in FAIL cells is expected to result in a smaller barrier for Ca^{2+} spark diffusion between RyR2 on neighbouring junctional SR and hence profoundly increase the probability of Ca^{2+} wave initiation.

6.4.4.1 Increasing sarcomere length with blebbistatin decreases waves

When resting SL was increased by blebbistatin there was a significant reduction in Ca^{2+} wave frequency as hypothesised, however there was also a reduction in Ca^{2+} transient amplitude due to reduced SR content. Fortuitously, a side-effect of measuring SR content was a reduction in SL probably due to a residual myofilament Ca^{2+} sensitising effect of caffeine. Following caffeine application blebbistatin no longer increased SL or reduced wave frequency. Therefore it can be said that after the same duration of 60-120 s exposure to blebbistatin (i.e. under equivalent SR Ca^{2+} loads) but with different resting SL, wave frequency only decreased when slack SL increased. This supports the predictions of Izu *et al.* (2006). Our results may be applicable in other cases of heart failure where resting SL is also shorter, such as diabetic and troponin-mutation related cardiomyopathies (Tardiff *et al.*, 1999; Flagg *et al.*, 2009). Conversely, Prosser *et al.* (2011) found mechanically stretching rat myocytes from 1.84 to 1.99 µm had the opposite effect and increased Ca^{2+} wave frequency, particularly in *mdx* dystrophic mouse ventricular myocytes. However this occurred due to stretch-induced cytoskeletal activation of NADPH oxidase 2 which generates reactive oxygen species sensitising RyR2 and promoting Ca^{2+} leak. This would not occur in our experiment due to passive rather than active lengthening.

Blebbistatin was chosen as it uncouples actin and myosin and lengthens resting SL, but reportedly has no effect on I_{CaL} or Ca^{2+} transient morphology (Dou *et al.*, 2007; Fedorov *et al.*, 2007; Farman *et al.*, 2008). We found blebbistatin significantly altered Ca^{2+} transient amplitude and SR content, possibly through promoting Ca^{2+} efflux from the cell. This was not due to rundown of the cells, as time matched control cells in normal Tyrode maintained normal contractions, Ca^{2+} transients and SR content. This discrepancy with the literature could be due to species differences in sensitivity to blebbistatin, for instance our data show contractions were <15% and <5% of initial amplitude after 1 and 3 min of blebbistatin, whereas after 5 min in the same concentration of blebbistatin mouse ventricular myocytes contracted ~20% of initial amplitude (Dou *et al.*, 2007). Alternatively, the higher concentration of blebbistatin used in this study (10 µM vs 0.5 µM) (Farman *et al.*, 2008), use of different Ca^{2+} indicators (Fedorov *et al.*, 2007), or a direct consequence of changes in heart failure (Venkataraman *et al.*, 2013) may account for the differences between reports.

Blebbistatin is the drug of choice in electrophysiological optical mapping studies compared to 2,3-BDM or cytochalasin D which have well known effects on Ca^{2+} handling and electrophysiology of the heart (Adams *et al.*, 1998; Howarth *et al.*, 1998; Fedorov *et al.*, 2007; Lou *et al.*, 2012). However, blebbistatin too was reported to alter action potential morphology in a rabbit optical mapping study (Brack *et al.*, 2013), increase spontaneous activity in rat atrium preparation (Kanlop & Sakai, 2010), and decrease the susceptibility to ventricular fibrillation in troponin T mutant mice with elevated myofilament Ca^{2+} sensitivity (Baudenbacher *et al.*, 2008). Further work should characterise the effects of blebbistatin on Ca^{2+} handling in relation to its use as a mechanical uncoupler in cardiac electrophysiology investigations.

The sarcomere lengthening effect of blebbistatin was less than we found using 2,3-BDM (see Fowler *et al.* (2015a)), which was surprising considering both work by blocking P_i release from the M•ADP•P_i complex. Blebbistatin binds with high affinity and irreversibly to the large 50 kDa cleft in the motor domain of myosin keeping it in an open state and preventing the power stroke (Allingham *et al.*, 2005; Farman *et al.*, 2008), whereas 2,3-BDM binds with low affinity. Blebbistatin may therefore stabilize the accumulation of weak AM•ADP•P_i crossbridges whereas 2,3-BDM prevents the powerstroke but can also dissociate and allow actin and myosin to dissociate. An alternative inhibitor with a different mode of action may be useful in dissecting whether

this is the case; N-benzyl-p-toluene sulphonamide (BTS) is another small molecule inhibitor which reversibly binds the same hydrophobic pocket as blebbistatin preventing P_i release and also reduces actin affinity in fast skeletal muscle myosin of rabbit and frog (Cheung *et al.*, 2002; Shaw *et al.*, 2003), and is 100x less potent in rat cardiac muscle meaning it may cause fewer weakly bound crossbridges.

6.4.4.2 Shortening sarcomere length with DNFB increases waves

The CK inhibitor DNFB shortened SL and promoted Ca^{2+} waves in healthy cells. CK inhibition results in a 'rigor-like' state of contracture in healthy myocytes due to local accumulation of ADP which slows crossbridge detachment and cycling (Sequeira *et al.*, 2015a). This is the same mechanism we believe is responsible for the shorter resting sarcomere length and steeper EDFLR in failing RV cells due to reduced CK expression (Fowler *et al.*, 2015a). Definitive conclusions on the importance of SL in this situation cannot be made as CK inhibition also impacted Ca^{2+} handling, increasing cytosolic and SR Ca^{2+}.

SERCA requires the highest free energy of ATP hydrolysis (~59 kJ/mol) to function normally compared to all other ATPases and therefore should be very sensitive to changes in ΔG_{ATP} resulting from CK inhibition (Shannon & Bers, 1997; Tian *et al.*, 1998). It was therefore surprising to find SERCA activity unchanged and SR content elevated in DNFB-treated cells. A different CK inhibitor, iodoacetamide, was reported to cause no change in Ca^{2+} transient amplitude but slow the rate of Ca^{2+} decay and raise diastolic Ca^{2+} in rat ventricular myocytes (Ren *et al.*, 2009; Sequeira *et al.*, 2015b).

Inhibition of CK coupled with Na^+/K^+-ATPase could raise $[Na^+]_i$ and promote Ca^{2+} retention or influx into the cell via NCX (Blum *et al.*, 1991). Alternatively, increased leak of Ca^{2+} from the SR could occur due to direct modification of sulfhydryl groups on RyR2 by DNFB (Hadad *et al.*, 1999). The elevated cytosolic Ca^{2+} may reduce the trans-SR Ca^{2+} gradient thereby lowering the free energy required for SERCA pump function, and cause CaMKII activation and phosphorylation of PLB thus reducing SERCA inhibition. Alternatively, glycolytic enzymes functionally coupled with SERCA may be sufficient to maintain Ca^{2+} uptake activity without a functioning CK system (Xu *et al.*, 1995). In a rat aortic banding model of congestive heart failure, De Sousa *et al.* (1999) showed a reduced efficiency of CK, but preserved ability of glycolytic enzymes,

to load the SR with Ca^{2+}. In MCT rats there is an overall shift towards greater glycolysis which may partially compensate for reduced energy flux through CK (Piao *et al.*, 2010).

Acute inhibition of CK caused a negative contraction- and Ca^{2+} transient-frequency relationship, reminiscent of failing RV cells which have reduced CK protein expression. More complete metabolic inhibition with cyanide, iodoacetate and 2,3-deoxyglucose results in a gradual decline in contraction and Ca^{2+} transient in cells contracting at 1 Hz (Lancaster & Harrison, 1998) likely due to shortening of the AP by activation of I_{KATP} (Nichols & Lederer, 1990). Metabolic acidosis could decrease myofilament sensitivity by influencing TnC Ca^{2+} binding which would reduce contraction (Orchard & Kentish, 1990); metabolic acidosis has also been reported in a rat MI model (Kemi *et al.*, 2006). This suggests alternative energy sources were sufficient to maintain contraction at low demand in our DNFB cells, but not at higher demand. CK inhibition with iodoacetamide was also found to impair contractile reserve in Langendorff-perfused hearts and cause systolic and diastolic dysfunction when infused directly into the coronary arteries of pigs (Hamman *et al.*, 1995; Korinek *et al.*, 2004). In contrast, cardiac overexpression of CK-M in mice with aortic banding pressure overload increased flux through CK, improved the inotropic response to adrenergic challenge by dobutamine and improved survival (Gupta *et al.*, 2012). In human left heart failure, low energy flux through CK was associated with worsening prognosis (Bottomley *et al.*, 2013), whereas inhibition of the ROS-producing enzyme xanthine oxidase with allopurinol increased flux through CK and improved cardiac work efficiency (Cappola *et al.*, 2001; Hirsch *et al.*, 2012). These data suggest reduced energy flux through the CK system be an important mediator of contractile dysfunction in both RV and LV failure and would thus make an ideal therapeutic target.

6.4.1 Exogenous CK lengthens the shorter failing sarcomere length

Work from the laboratories of Renée Ventura-Clapier and Theo Wallimann demonstrated dynamic binding of CK-M to the myofilaments of Triton skinned muscle fibres which was functionally equivalent to the native enzyme (Ventura-Clapier *et al.*, 1987b; Kraft *et al.*, 1995). Exchange of fluorescently labelled CK-M with non-fluorescent CK-M takes 7-10 min to fully equilibrate, however in the absence of exogeneous enzyme CK-M stays firmly bound for several hours indicating a high affinity association with myomesin (Kraft *et al.*, 1995). Incubating saponin permeabilized FAIL RV cells in a solution containing CK and PCr restored resting SL to

CON length, whereas if either CK or PCr was absent there was no change. This shows loss of CK-M activity from the myofilaments may allow local ADP to accumulate which would slow crossbridge detachment and result in a 'rigor-like' state of contraction.

It is not clear from this experiment whether loss or inactivation of CK is responsible, as the additional CK could attach to free binding sites or replace damaged CK. We reported a loss of CK-M protein in the RV of MCT rats which could mean there were more free binding sites (Fowler *et al.*, 2015a), however the high affinity of CK-M for the myomesin suggests it is unlikely there are unoccupied binding sites (Kraft *et al.*, 1995). Alternatively CK-M was shown to be vulnerable to oxidative inactivation by peroxynitrite in a MI model of heart failure in rat (Mihm & Bauer, 2002). If this were the case, and provided the modification was reversible, then antioxidants or reducing agents should improve CK activity. (Hirsch *et al.*, 2012) showed the xanthine oxidase inhibitor allopurinol increased flux through the CK reaction, lowered ADP and increased the free energy of ATP hydrolysis in human patients with non-ischaemic cardiomyopathy. In a similar patient population, Cappola *et al.* (2001) further showed this resulted in increased cardiac work efficiency. This suggests rescue of inactivated CK may be a feasible and beneficial therapeutic strategy to improve energetic derangement in heart failure.

6.5 Conclusion

RV contractile function is a primary prognostic indicator in PAH and also in left heart failure. We have identified systolic and diastolic dysfunction occurring in isolated RV myocytes from MCT rats suggesting they are a major source of dysfunction in the failing RV. Aspects of the failing phenotype, such as the negative contraction-frequency relationship, could be induced in healthy cells by inhibiting energy transfer through the creatine kinase pathway. Reduced energy transfer through the creatine kinase system and impaired cardiac reserve are predictors of mortality in left heart failure (Bottomley *et al.*, 2013), suggesting this may be a common feature of heart failure and a possible therapeutic target. Manipulating resting sarcomere length with blebbistatin in failing cells reduced the incidence of spontaneous Ca^{2+} waves (Izu *et al.*, 2006). These data show energetic dysfunction is a key contributor to both systolic and diastolic dysfunction and may further promote a pro-arrhythmogenic phenotype; restoring energy flux through the creatine kinase system either by increasing expression or activity could be beneficial to RV function in PAH.

Chapter 7 General discussion, conclusions and future perspectives

7.1 Introduction

This research investigated the controversial hypothesis that β_1-blockers confer a benefit to survival and RV function in PAH. This contradicts current PAH treatment guidelines and a study of the acute effects of non-selective β-blockers in PAH (Provencher *et al.*, 2006b; Galiè *et al.*, 2015b), but is supported by a small number of preclinical studies (Bogaard *et al.*, 2010; de Man *et al.*, 2011) and retrospective clinical studies (So *et al.*, 2012; Thenappan *et al.*, 2014; Bandyopadhyay *et al.*, 2015). The MCT model was used to induce severe PAH leading to RV failure in rats, and a regime was developed of chronic treatment with the β_1-selective AR blocker metoprolol. MCT+BB rats survived for significantly longer than placebo treated FAIL rats which appeared to be due to preserved RV function. The mechanisms contributing to RV dysfunction in FAIL and subsequent rescue in MCT+BB rats were investigated at the *in vivo*, tissue, single cell and molecular levels, with particular attention paid to the role of excitation-contraction coupling and metabolic derangement. The importance of altered energy metabolism in contractile dysfunction of FAIL hearts was a recurring theme and it is tempting to speculate some of the beneficial effects of metoprolol may have arisen due to reduced energy expenditure. This final chapter will summarize some of the key findings of this work, their possible role in RV dysfunction in PAH, new areas of research which may follow on as a result, and the potential clinical implications of this study. Table 7.1 highlights some of the changes which occurred in the RV of FAIL rats and whether or not this was improved in MCT+BB rats.

7.2 Survival and functional benefit of β_1 AR blockade in PAH

A β-blocker treatment regime was successfully developed which increased the survival of MCT treated rats by around 30%. Treatment with metoprolol was initiated once PAH was already present (see Chapter 3 and Jones *et al.* (2002)) as this more closely replicates the clinical situation in which PAH is often diagnosed late into the condition. The function of MCT+BB rats was assessed at two stages: the first was around the time placebo treated FAIL rats would normally develop heart failure thus allowing a comparison of function at temporally equivalent points, and the second was on the day heart failure symptoms developed. Using this approach we determined metoprolol slowed the deterioration of RV function but did not prevent it.

Repeated monitoring of *in vivo* RV function was made possible by establishing and validating echocardiography as a technique, which had not previously been available to the Cardiac Research group at the University of Leeds. Invasive right heart catheterisation was used alongside echocardiography to measure pulmonary vascular resistance and to characterise RV function using load-independent parameters of contractility. Early trends towards PAH were identified by day 15 in MCT treated rats using Doppler ultrasound to predict RV systolic pressure, in agreement with previous studies (Jones *et al.*, 2002). This progressed over the following days into severe PAH in both FAIL and MCT+BB rats. Increased systolic pressures were compensated for by increased RV wall thickness and weight measured *post mortem* in FAIL rats, which were slightly reduced in MCT+BB rats. This was reflected by increased width of single RV cells which was greatest in FAIL and reduced in MCT+BB. Resting RV cell length progressively shortened with increasing disease severity, indicating that at this stage hypertrophy is primarily concentric and driven by high systolic pressure (Tamura *et al.*, 1998).

The RV in FAIL rats was hypocontractile as shown by reduced ejection fraction and decreased cardiac output, whereas in MCT+BB rats cardiac output was intermediate between CON and FAIL due to a partial improvement in stroke volume. This occurred despite there being no change in RV systolic pressure or pulmonary vascular resistance, indicating RV contractility in MCT+BB rats was enhanced as shown by a partial normalization of ventriculo-arterial coupling. Poor RV systolic function was reflected at the level of single RV cells: the rate of force development and Ca^{2+} release was slower in FAIL cells than CON, likely due to spatially and temporally dyssynchronized systolic Ca^{2+} release which was associated with a disorganized t-tubule system. In contrast, Ca^{2+} release kinetics were restored in MCT+BB cells coinciding with complete normalization of t-tubule structures. Unloaded shortening and Ca^{2+} transient amplitude were initially greater in FAIL RV cells at low pacing frequencies, however when challenged by increasing pacing up to 7 Hz there was a steep fall in both Ca^{2+} and contraction. In contrast, CON cell contractility and Ca^{2+} transient amplitude increased with frequency, whereas in MCT+BB cells the relationship was intermediate between CON and FAIL. This indicates MCT+BB rats may be better able to cope when stressed, for instance during exercise. The SR of FAIL RV cells was overloaded, possibly due to decreased Ca^{2+} efflux from the cell via

NCX or a prolonged AP (Benoist *et al.*, 2012), whereas SR content and NCX activity were partially restored towards CON levels in MCT+BB cells.

In contrast to the large changes identified in RV function *in vivo* and *in vitro*, there were usually minor or no differences in LV structure and function. There was no change in LV wall thickness which concurred with no change in cellular hypertrophy in the LV of any group, indicating the combination of pressure overload and catecholamines are required for a maximal hypertrophic response (Kögler *et al.*, 2003). LV ejection fraction measured by echo was normal in all treatment groups, however in MCT-treated groups the septum bulged into the LV reducing its cavity size and thus preload. Isolated LV cells from FAIL and MCT+BB rats tended to show enhanced contractility and larger Ca^{2+} transients across the range of pacing frequencies suggesting the LV may have adapted to reduced filling by augmenting its contractility.

These data indicated metoprolol was primarily acting through direct protective effects on the RV myocardium rather than afterload reduction. Metoprolol delayed the progression of RV dysfunction and eventual failure although it did not prevent it, as RV function was similar in placebo and metoprolol treated rats at the point of failure. This is in agreement with clinical data highlighting the prognostic importance of RV function in PAH (van de Veerdonk *et al.*, 2011), and shows β_1AR blockers represent a viable therapeutic option to target the failing RV.

7.3 Role of creatine kinase in the failing phenotype

Diastolic function was severely impaired in FAIL rats as indexed by the load-independent EDPVR, whereas there was a partial improvement in MCT+BB rats. There was no change in fibrosis in the RV or LV of any group of rats measured using histology, suggesting collagen is not the primary source of ventricle stiffness in MCT rats. Diastolic dysfunction was present at the level of single FAIL RV cells which had a shorter resting SL, steeper EDFLR when stretched and slower rate of relaxation despite no dramatic changes in the rate of Ca^{2+} removal or myofilament Ca^{2+} sensitivity. This indicated mechanisms other than Ca^{2+} handling were responsible for impaired diastolic function. MCT treated rats had depressed total CK activity measured in RV homogenates, which concurs with reduced CK-M and CK-mt protein expression we reported in Fowler *et al.* (2015a). SL was shorter in FAIL than CON cells. The SL in CON cells was shorter following CK inhibition with DNFB, conversely incubating permeabilized FAIL RV cells with exogeneous CK and PCr restored SL. Inhibiting CK

in healthy cells caused a steep negative contraction- and Ca^{2+} transient amplitude frequency relationship remarkably similar to FAIL cells, suggesting the reduced CK activity may have pleiotropic effects on contraction. These data support the hypothesis that loss of CK in the failing RV cardiomyocytes slows crossbridge cycling and increases diastolic stiffness, but is partially restored in MCT+BB rats which corresponds to improved ventricle compliance.

7.4 Tissue hypoxia and metabolism in the failing RV

Using histology it was shown that the average area of RV myocardium supplied by each capillary was greater in MCT+BB and FAIL rats, although this may have occurred for different reasons: muscle fibre hypertrophy increased the diffusion distance from capillaries to the fibre cores in MCT+BB rats. This also occurred in FAIL rats as well as an additional trend for capillary rarefaction. Finite element calculations were used to predict myocardial PO_2 from capillary distribution which showed the majority of FAIL RV myocardium was hypoxic, whereas there was a partial improvement in tissue PO_2 in MCT+BB rats.

Mitochondrial mass was estimated by citrate synthase activity in RV homogenates, however this did not account for differences in survival or function as activity did not change between different treatment groups. Maximal respiration and individual activities of mitochondrial respiratory complexes were measured functionally *in situ* by supplying saponin permeabilized RV cells with different substrates and inhibitors, however none of the measured parameters differed between CON and FAIL, indicating the ETS was preserved at this stage of disease. In contrast the ability of the CK system to stimulate submaximal respiration was greatly reduced in FAIL, and to a lesser extent in MCT+BB, suggesting the hypertrophic myocardium may be less able to respond to a sudden increase in energy demand.

These data indicate O_2 availability, rather than loss of mitochondria or specific defects in the ETS, may limit oxidative ATP production in FAIL rats. Accordingly RV coronary perfusion was found to be inversely related to RV hypertrophy in human PAH (van Wolferen *et al.*, 2008). The improved myocardial oxygenation in MCT+BB rats may have contributed to the increased stroke work of the RV compared to FAIL rats (Khalafbeigui *et al.*, 1979). A further possible benefit could be reduced apoptosis, which may account for the significant reduction in cellular hypertrophy despite modest reductions in ventricular weight if there were more, but smaller, cardiomyocytes.

7.5 Proposed mechanism of protection by metoprolol

Identifying the cellular pathways responsible for the improvements in MCT+BB rats requires characterisation of molecular signalling events which was outwith the scope of this thesis but is work currently ongoing at the University of Leeds. It is however possible to speculate, based on the observed changes in cellular structure and function, where metoprolol may be exerting its influence:

Table 7.1 shows Ca^{2+} handling was subject to the greatest detrimental changes in function in FAIL cells and was also most likely to improve following metoprolol treatment, thus indicating a critical role in the pathophysiology of failing hearts (Figure 7.1A). Improved Ca^{2+} handling in MCT+BB cells may stem from preserved T-tubule structure due to increased expression of JP2, with or without increased BIN-1 expression (Figure 7.1B). This would tether T-tubules to the junctional SR preserving Ca^{2+} release kinetics and maintaining normal trans-sarcolemmal ion exchange. This would help prevent Ca^{2+} overload and reduce arrhythmogenic Ca^{2+} waves and activation of Ca^{2+}-dependent kinases (e.g. CaMKII), phosphatases (e.g. calcineurin) and proteases (e.g. calpain). Thus amelioration of the disruption to Ca^{2+} signalling may prevent excessive hypertrophy either directly by influencing gene transcription, or indirectly by prevention of apoptosis.

The specificity of metoprolol to β_1 receptors confined its actions primarily to the myocardium and did not alter pulmonary vascular resistance, therefore the remaining RV hypertrophy is likely attributable to mechanical stresses relayed to the nucleus via the cytoskeleton rather than circulating factors, as there was no detectable LV hypertrophy in any group. Reduced hypertrophy would enhance mitochondrial O_2 availability by reducing O_2 demand and facilitating delivery from capillaries. Improved O_2 availability could decrease the reliance on inefficient glycolysis as a source of energy (Piao *et al.*, 2010). Hepatic glycogenolysis is primarily promoted by β_2 receptors whereas lipolysis is mostly under the control of β_1AR (Arinze & Kawai, 1983). Koch *et al.* (1981) showed lipid, but not carbohydrate, mobilization was blunted by metoprolol during exercise in hypertensive patients, therefore β-blockers may result in an unfavourable blood lipid and glycaemic profile by increasing blood glucose levels and depressing fat utilization. Thus altered metabolism and reduced daily energy expenditure could account for slower weight loss in MCT+BB rats (Sharma *et al.*,

2001). Preservation of the CK energy shuttle would improve energy delivery to cytosolic ATPases and speed crossbridge kinetics thus improving diastolic function.

Metoprolol preserved β_1AR expression which would improve the ability of the RV to cope during periods of increased demand (R. Norman, personal communication); prevention of agonist binding and receptor phosphorylation may have prevented desensitization. The inverse agonism by metoprolol may also be clinically relevant as this provides additional survival benefits in severe heart failure independent of β_1AR desensitization (Harding *et al.*, 2001).

7.6 Sarcomere length-dependence of Ca^{2+} waves

We tested whether the shorter SL in RV FAIL cells increased Ca^{2+} wave frequency. There was a progressive increase in wave frequency from CON to MCT+BB to FAIL. When CK was inhibited by DNFB in CON cells the resting SL decreased and wave frequency increased, however off-target effects such as raised cytosolic and SR Ca^{2+} also occurred which were likely to influence wave frequency. Lengthening SL in FAIL RV cells with the crossbridge uncoupler blebbistatin reduced wave frequency, but also decreased SR Ca^{2+} load. Wave frequency was unchanged when blebbistatin failed to lengthen SL due to prior exposure of the cell to caffeine despite an identical duration exposure to blebbistatin (i.e. under equivalent SR Ca^{2+} loads). The velocity of waves also increased from MCT+BB to FAIL. This data supports an inverse relationship between SL and wave frequency, as proposed by Keizer and Smith (1998) and Chen-Izu *et al.* (2006). This may contribute to the greater proportion of waves triggering a global Ca^{2+} transient in FAIL RV cells, and therefore the risk of ventricular arrhythmias as a result of delayed afterdepolarizations.

7.7 Future directions

β-blockers could be incorporated into a therapeutic regime for PAH as an adjunctive therapy alongside traditional vasodilators which would target both the cause of PAH (excessive vasoconstriction and vascular remodelling) and the ultimate cause of death in the majority of patients (RV failure) (Delcroix & Naeije, 2010). Unintended drug interactions have contributed to the reluctance to use β-blockers in PAH in the past (Peacock & Ross, 2010), therefore it will be critical to firstly identify possible interactions between β-blockers and existing therapies, and also whether there is an additive effect on function and/or survival. A possible combination could be metoprolol

and sildenafil as these are metabolised by separate enzymes and are unlikely to cause systemic hypotension. This could be tested experimentally with a clinically relevant dose of sildenafil, such as used by Schermuly *et al.* (2004) in MCT rats from day 14 onwards, which slightly improves survival and significantly lowers pulmonary vascular resistance, without directly improving RV function (Andersen *et al.*, 2008).

Currently the effect of metoprolol on apoptosis in MCT+BB rats is mostly speculative although preliminary data indicates upregulation of caspase-3 in the RV of FAIL rats (R. Norman, personal communication). There is precedent for reduced apoptosis occurring with low dose metoprolol (2 mg/kg/day) in a canine coronary microembolism model of heart failure. Apoptosis occurs within a relatively narrow window of time and ideally complementary techniques which identify different steps in the apoptosis pathway should be used. A histological method to detect apoptotic signalling in nuclei, such as TUNEL staining or an enzyme assay using a fluorogenic substrate specific for the cleaved and activated form of caspase-3 such as Ac-DMQD-AMC, would be useful additions to this work and would provide further insight into the myocardium-specific effects of metoprolol (Kaur *et al.*, 2015).

Although not presented in this thesis, *ex vivo* passive pressure-volume measurements were recorded in Langendorff-perfused FAIL hearts to explore the effect loss of CK activity had on the diastolic properties of the RV. Using an inflatable PVC balloon connected to a pressure transducer we showed inhibiting CK increased the passive stiffness of the LV (these results are presented in Appendix B and Sequeira *et al.* (2015b)). Unfortunately, at low pressures the balloon conformed poorly to the complex RV geometry precluding accurate volume measurements (Suga & Sagawa, 1979; Goto *et al.*, 1988), therefore we could not measure stiffness using this method in FAIL hearts. Using a working RV configuration may circumvent the problem of RV geometry.

No studies to date have investigated titin in MCT PAH, although there is data showing hypophosphorylation of titin in the RV of human PAH (Rain *et al.*, 2013). We have clearly shown crossbridges play an important role in diastolic dysfunction in FAIL cells, however even 40 mM 2,3-BDM did not completely restore resting SL to CON length (Fowler *et al.*, 2015a), suggesting some additional non-crossbridge component may be present. Rats with a mutant giant isoform of titin (3.8 MDa) have been described which display reduced passive stiffness (Greaser *et al.*, 2008) and consequently shown

longer resting sarcomere length in skeletal muscle fibres (Greaser & Pleitner, 2014) and isolated cardiomyocytes (M. Helmes, personal communication), however I am unaware of any cases of the resting sarcomere length being shortened as a result of titin. Degradation of titin by proteases MMP-2 and Ca^{2+} activated calpain have been reported in human dilated cardiomyopathy which could reduce the resting SL and impair recoil during early diastole (Hein *et al.*, 1994).

We present the first empirical evidence of the SL-dependence of Ca^{2+} waves which was hypothesised over 15 years ago (Keizer *et al.*, 1998; Chen-Izu *et al.*, 2006). Wave frequency was also measured in a small number of cells subjected to isometric stretch to different SL in the presence of the antioxidant *n*-acetylcysteine (20 mM) (to counteract NADPH oxidase induced Ca^{2+} waves (Prosser *et al.*, 2011)), however time constraints of the laboratory visit to Amsterdam prevented collection of a complete dataset. Further work could build on these findings, perhaps by using saponin skinned cells to avoid the confounding influence of cytosolic Ca^{2+} or ROS induced Ca^{2+} leak on wave frequency. It should be possible to stretch saponin permeabilized cells using MyoTak which could open up new opportunities in studying the interaction between contraction and SR and mitochondrial function. Confocal analysis of wave velocity would add further support to our conclusions if wave velocity was negatively associated with SL.

Whether the change in SL is physiologically relevant ultimately depends on whether it also differs *in vivo*, however accurate measurement of SL in contracting hearts presents huge technical challenges and is therefore still somewhat elusive. Diastolic SL measured *in situ* in di-ANEPPS loaded mouse hearts ranges from 1.95 to 2.3 µm when intraventricular pressure is increased from 0 to 40 mmHg (Bub *et al.*, 2010; Nance *et al.*, 2015), however these may be overestimated due to oedema and use of Ca^{2+}-free buffers. Inspection of the images in Xie *et al.* (2012), who used the same method as above, appears to show a severity-dependent decrease in SL *in situ* in the RV of arrested MCT hearts. Recently, Aguirre *et al.* (2014) measured the *in vivo* SL of beating mouse LV and found it to be closer to 1.90 µm in diastole and 1.75 µm at end systole, presumably reflecting the contribution of Ca^{2+} activated crossbridges during diastole due to the high murine heart rate. This suggests crossbridge activation during diastole prevents excessive stretch and allows the heart to continually work on the ascending limb of the length-tension relationship. This could also mean the heart is

susceptible to SL-dependent Ca^{2+} wave initiation, as Ca^{2+} waves are known to occur in Langendorff-perfused hearts (Kaneko *et al.*, 2000).

We found a tendency for FAIL cells to have increased sensitivity to exogeneous ADP, similar to findings in rats with developing or deficient CK systems (Clark *et al.*, 1994; Anmann *et al.*, 2014). The MOM presents the greatest diffusion barrier for exogeneous ADP to mitochondria (Guzun *et al.*, 2009) due to the VDAC pore which in turn is regulated by free tubulin (Rostovtseva *et al.*, 2008). Stones *et al.* (2013) found free:total tubulin was reduced in the MCT RV suggesting this may be modifying mitochondrial permeability. It would be interesting to know whether this is indeed the cause, perhaps by using colchicine or paclitaxel to increase or decrease free tubulin, respectively as greater VDAC opening will increase respiratory flux and therefore ROS production potentially leading to mitochondrial damage (Maldonado *et al.*, 2015). Microtubules are also thought to be influential in internalizing and desensitizing β_1AR and are increased primarily in the pressure-overloaded RV rather than LV in the cat PAB model (Sato *et al.*, 1997), therefore it would be interesting to know whether this is responsible for the greater loss of β_1AR in the RV compared to LV of MCT rats (Seyfarth *et al.*, 2000; Leineweber *et al.*, 2003).

7.8 Clinical perspectives

The European Society of Cardiology guidelines on pulmonary hypertension consistently emphasise improvements in RV function and regression of remodelling as of utmost importance as treatment goals (McLaughlin *et al.*, 2013; Galiè *et al.*, 2015b), therefore it is astonishing that there are currently no therapies which specifically target the RV. Our work shows a salutary effect of metoprolol in PAH which acted primarily through direct effects on the RV and provides insight into potential mechanisms underlying improved RV function. We show what is true for the left is also true for right: namely that β-blockers do not represent a “cure” for heart failure but improve survival and slow the deterioration of function and remodelling which is critically important for quality of life and prognosis (Bristow, 2000; van de Veerdonk *et al.*, 2011).

Our data add to a small but growing number of preclinical studies demonstrating improved survival and/or RV function with selective and non-selective β-blockers (Bogaard *et al.*, 2010; de Man *et al.*, 2011; Perros *et al.*, 2015), and the next step clearly is translating this into small closely monitored clinical trials in human PAH. Such trials in NYHA class II and III PAH patients are currently underway in the

Netherlands and Virginia (Grinnan *et al.*, 2014; Van Campen *et al.*, 2014). In these single arm or crossover-design studies of 6-18 patients currently receiving PAH-specific therapy, adjunctive therapy with bisoprolol and carvedilol has generated promising results: after 3-6 months of treatment RV ejection fraction and stroke volume both increased with a trend towards improve exercise capacity. Importantly all patients tolerated β-blockers when they were introduced at a low dose and gradually uptitrated, as per recommendations (Bristow & Quaife, 2015). What is now needed is a larger scale clinical trial of β-blockers which is appropriately powered to detect persistent benefits over a longer period of time and with RV function as a primary endpoint. It is hoped our work will advance the understanding of the pathophysiology of RV failure in PAH and draw attention to the benefit of RV targeted therapies.

Table 7.1 Summary of changes in structure and function with metoprolol treatment

			MCT+BB	FAIL	MCT+BB vs FAIL P<0.05?
Biometrics	Survival		↓	↓↓	YES
	Heart rate		↓↓	↓	NO
	RV:BW		↑↑↑	↑↑↑	NO
	LV:BW		–	–	NO
	RV:LV+S		↑↑↑	↑↑↑	NO
In vivo RV function	Systolic pressure		↑	↑	NO
	Diastolic pressure		↑	↑	NO
	Wall thickness		↑↑	↑↑↑	YES
	Ejection fraction		↓	↓↓	NO
	Stroke volume		↓	↓↓↓	NO
	Cardiac output		↓	↓↓↓	NO
	EDPVR		–	↑	NO
	ESPVR/Ea		–	↓	NO
	PVR		↑↑↑	↑↑↑	NO
Metabolic function	Capillary density		↓	↓↓↓	NO
	Tissue hypoxia		–	↑	NO
	Fibrosis		–	–	NO
	Mitochondrial mass		–	–	NO
	ETS capacity		–	–	NO
	Reactive oxygen species		–	–	NO
	Total CK activity		↓↓↓	↓↓↓	NO
	CK-mt activity		–	↓	NO
	CK-mt expression[1]		↓	↓↓	NO
	CK-M expression[1]		↓	↓↓	NO
Calcium handling	Cellular hypertrophy		↑	↑↑↑	YES
	Sarcomere length		↓↓	↓↓↓	YES
	T-tubule organisation		–	↓↓↓	YES
	Ca^{2+} release kinetics		–	↓	YES
	Contraction:	low pacing	–	↑↑↑	YES
		response to faster pacing	flat	steep negative	YES
	Ca^{2+} transient:	low pacing	↑↑	↑↑↑	NO
		response to faster pacing	negative	steep negative	NO
	SR content		–	↑↑↑	YES
	Myofilament sensitivity		–	–	YES
	Spontaneous waves		↑↑	↑↑↑	YES

Arrows indicate direction of change relative to CON and the level of significance; single arrow P<0.05, double arrow P<0.01, triple arrow P<0.001 vs CON. [1]R. Stones, personal communication.

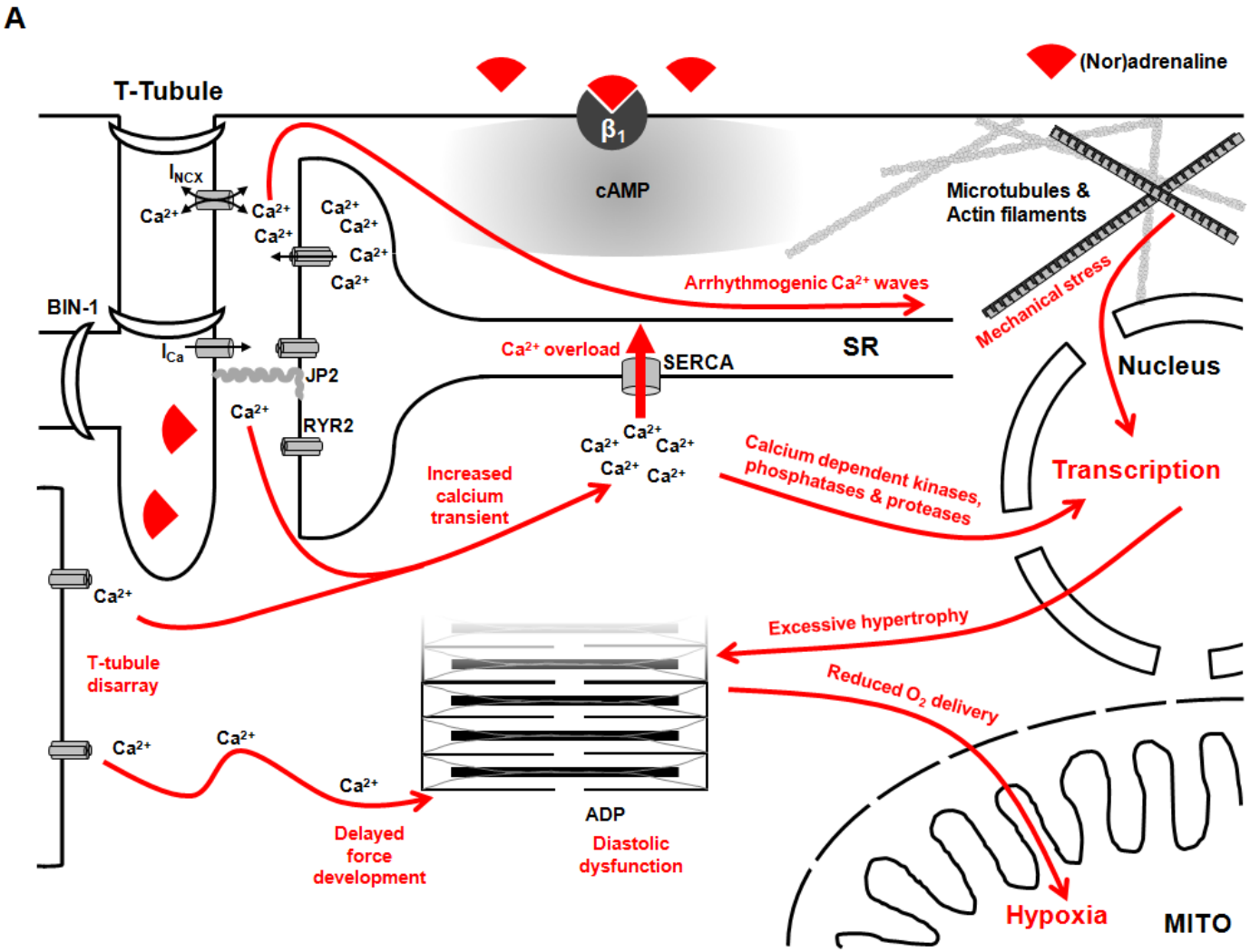
A
T-Tubule
(Nor)adrenaline
β1
cAMP
Microtubules &
Actin filaments
INCX
Ca2+
BIN-1
ICa
JP2
RYR2
Arrhythmogenic Ca2+ waves
Mechanical stress
Ca2+ overload
SERCA
SR
Nucleus
Transcription
Increased
calcium
transient
Calcium dependent kinases,
phosphatases & proteases
Excessive hypertrophy
T-tubule
disarray
Reduced O2 delivery
ADP
Delayed
force
development
Diastolic
dysfunction
Hypoxia
MITO

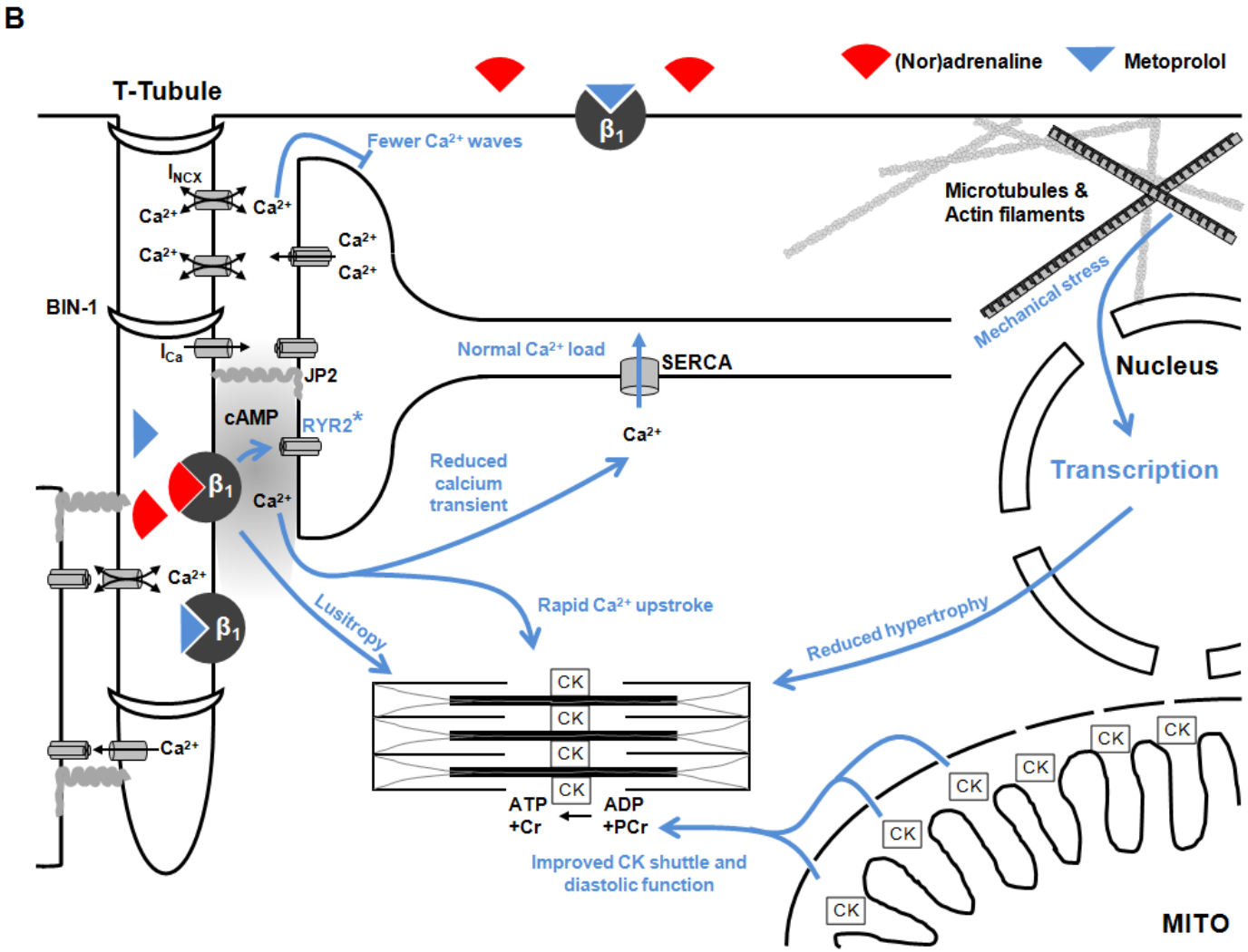
B
T-Tubule
(Nor)adrenaline
Metoprolol
β1
Fewer Ca2+ waves
INCX
Ca2+
Ca2+
Ca2+
Ca2+
Ca2+
BIN-1
ICa
JP2
cAMP
RYR2*
Normal Ca2+ load
SERCA
Ca2+
Reduced calcium transient
Microtubules & Actin filaments
Mechanical stress
Nucleus
Transcription
Rapid Ca2+ upstroke
Lusitropy
Reduced hypertrophy
CK
ATP +Cr
ADP +PCr
Improved CK shuttle and diastolic function
MITO

Figure 7.1 Postulated mechanisms underlying improved function with metoprolol

A Severe Ca^{2+} handling abnormalities underpinned the pathophysiology of FAIL cells. Loss of T-tubules orphans RYR2 on the junctional SR slowing the rise time of the Ca^{2+} transient and force development. Reduced NCX activity leads to Ca^{2+} overload, spontaneous Ca^{2+} waves, and activation of Ca^{2+}-dependent transcription pathways. Increased pulmonary afterload initiates hypertrophic remodelling and parallel sarcomere addition. Increased O_2 diffusion distance between capillaries and muscle fibre cores produces a compromised metabolic state, which is compounded by reduced CK function in mitochondria and at the myofilaments slowing crossbridge turnover. Chronic activation of β_1 receptors initiates pro-hypertrophic and pro-apoptotic pathways and causes desensitization and internalization of receptors. **B** Metoprolol greatly improved Ca^{2+} handling and restored T-tubule structure, perhaps through preserved JP2 expression. Increased NCX activity prevents Ca^{2+} overload and associated Ca^{2+} waves. Hypertrophy is partially reduced improving myocardial oxygenation, however persistent elevated pulmonary vascular resistance means hypertrophy is not completely avoided. Energy transfer around the cell is improved due to restored CK expression which aids crossbridge turnover and diastolic function. Metoprolol-treated cells retain β_1 receptor density thereby preserving the capacity for PKA-dependent phosphorylation of intracellular targets when the level of β-blockade is overcome during periods of increased sympathetic activity.

Appendix A

We attempted to replicate the treatment regime described by Bogaard *et al.* (2010), using a dose of 150 mg/kg/day metoprolol dissolved in drinking water. Despite extensive time and effort, we found no survival or functional benefit from using this supra-physiological dose (approximately equivalent to around 1.8 g metoprolol per day in humans (see Section 3.4.2.1 for discussion)). The concentration was tailored to each cage of rats according to their daily water consumption over the preceding 14 days, and ranged from 0.84 - 1.99 mg/mL, the average concentration was 1.33 mg/mL. Daily water intake remained fairly stable in CON and FAIL rats throughout the monitoring period (Figure 8.A). In contrast, water intake in MCT+BB_{150} rats dropped suddenly when metoprolol was introduced to the drinking water, and continued to fall for the remaining study time. The same reduction in fluid intake was also seen in 3 rats which began β-blocker treatment on day 21. As such, the calculated daily dose of metoprolol consumed in the drinking water varied between 28-94 mg/kg, or 18-63% of the target dose.

A possible reason for these discrepant findings in relation to Bogaard *et al.* (2010) is that the actual daily dose of metoprolol consumed differed greatly from the target dose (calculated based on water consumption). This is consistent with the findings of Prabhu *et al.* (2000) and Cherng *et al.* (1994) who found 2 mg/mL metoprolol in drinking water resulted in a variable intake between 71-157 mg/kg/day in Wistar and Sprague-Dawley rats with MI. Indeed, Yaoita *et al.* (2002) stopped treating rats with MI with 270 mg/kg/day metoprolol administered by gavage due to a higher rate of mortality. Water intake was not reported by Bogaard *et al.* (2010) therefore the actual daily dose of metoprolol consumed in that study is unknown, but is likely to be much lower than claimed.

Consistent with our finding in MCT+BB rats there was no change in PVR in FAIL+BB_{150} rats, however interestingly there was a trend for the EDPVR to be improved relative to FAIL rats (P=0.07) (Figure 8.). This suggests a key effect of β-blockers may lie in their positive effect on diastolic function.

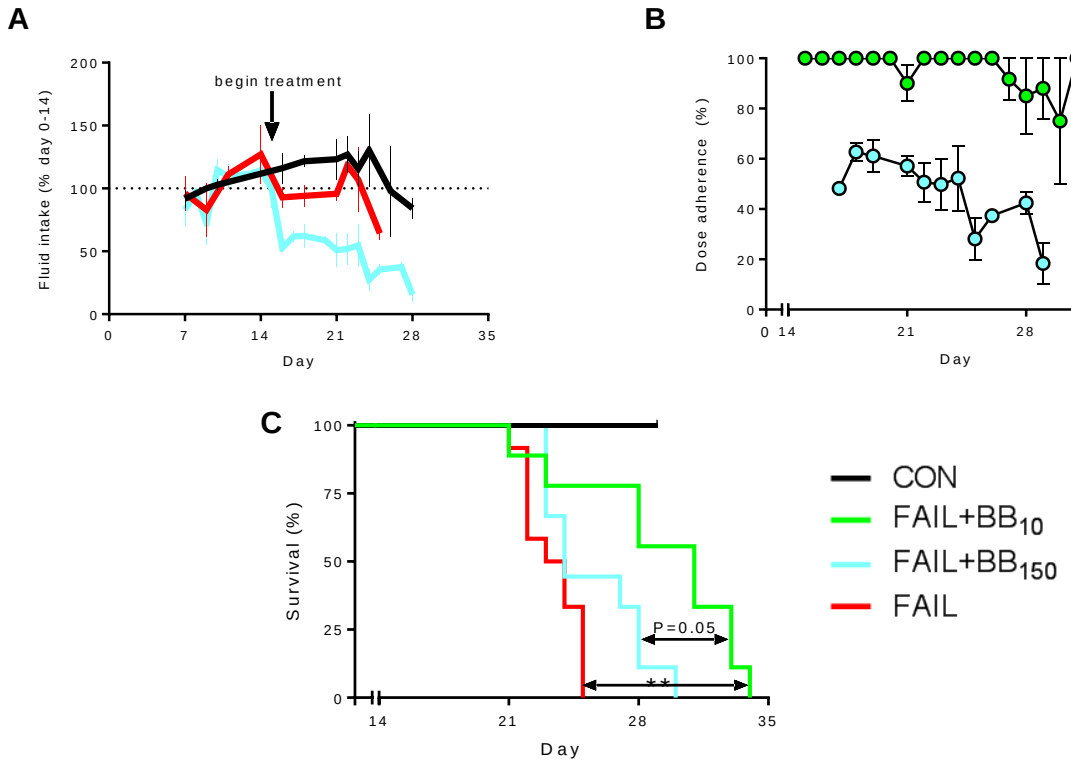

Figure 8.1 No survival benefit with high dose metoprolol

A Fluid intake was monitored before and after addition of metoprolol to drinking water at a concentration equivalent to 150 mg/kg/day. Water intake remained stable throughout the monitoring period in CON and FAIL, however when metoprolol was added (arrow) the daily water intake dropped suddenly and continued to fall. **B** Dose adherence was calculated based on the daily water intake. A target dose of 150 mg/kg metoprolol was not sustained due to taste aversion. **C** The median survival of FAIL+BB_{150} rats (day 24) was not significantly different to placebo treated FAIL (day 23), but tended to be worse than FAIL+BB_{10} (P=0.05). N=12 CON, 9 FAIL, 21 FAIL+150mg/kg Met rats

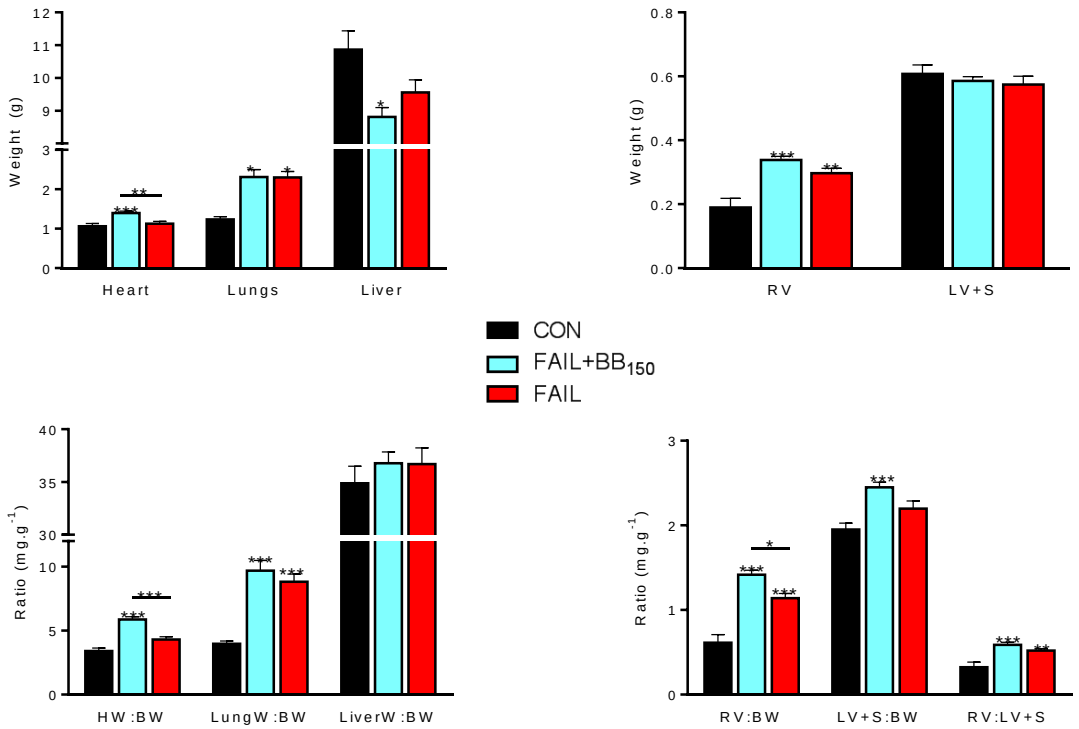

Figure 8.2 Organ weights following high dose metoprolol

A Organ weights, **B** ventricle weights, **C** organ ratios, and **D** ventricle ratios in CON (N=8), FAIL (N=10) and FAIL+BB_{150} (N=18) rats.

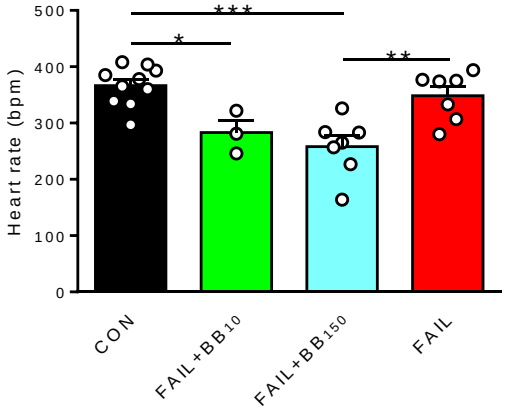
Heart rate (bpm)
500
400
300
200
100
0
***
*
**
CON
FAIL+BB10
FAIL+BB150
FAIL

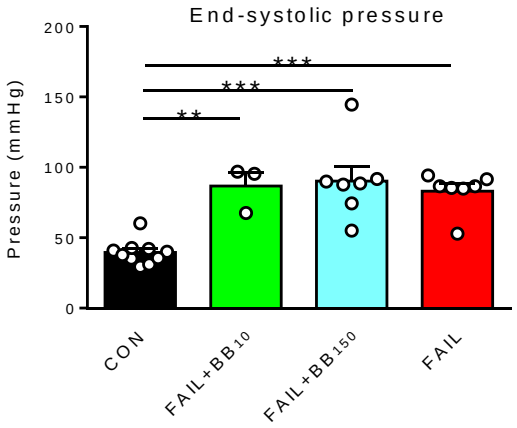
End-systolic pressure
Pressure (mmHg)
200
150
100
50
0
***
***
**
CON
FAIL+BB10
FAIL+BB150
FAIL

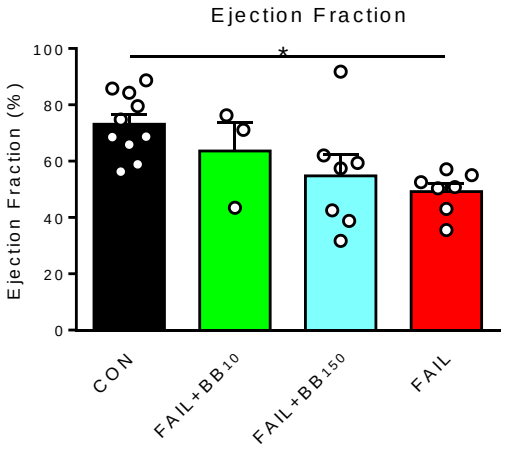
Ejection Fraction
Ejection Fraction (%)
100
80
60
40
20
0
*
CON
FAIL+BB10
FAIL+BB150
FAIL

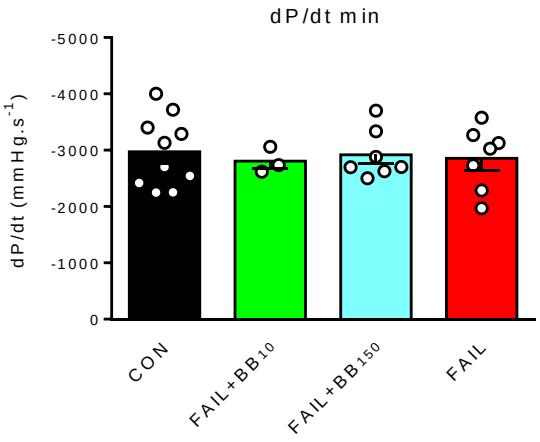
dP/dt min
dP/dt (mmHg.s-1)
-5000
-4000
-3000
-2000
-1000
0
CON
FAIL+BB10
FAIL+BB150
FAIL

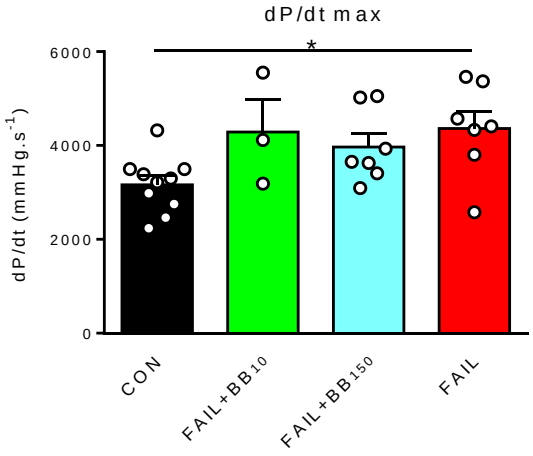
dP/dt max
dP/dt (mmHg.s-1)
6000
4000
2000
0
*
CON
FAIL+BB10
FAIL+BB150
FAIL

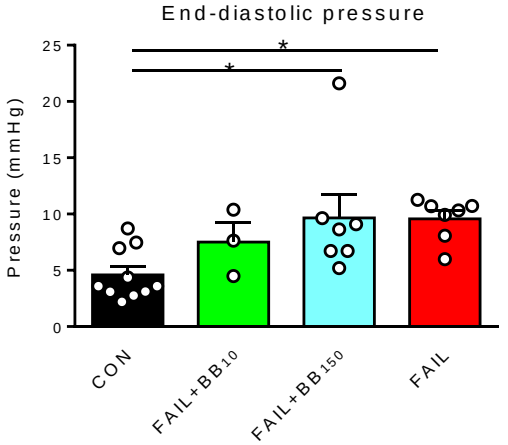
End-diastolic pressure
Pressure (mmHg)
25
20
15
10
5
0
*
*
CON
FAIL+BB10
FAIL+BB150
FAIL

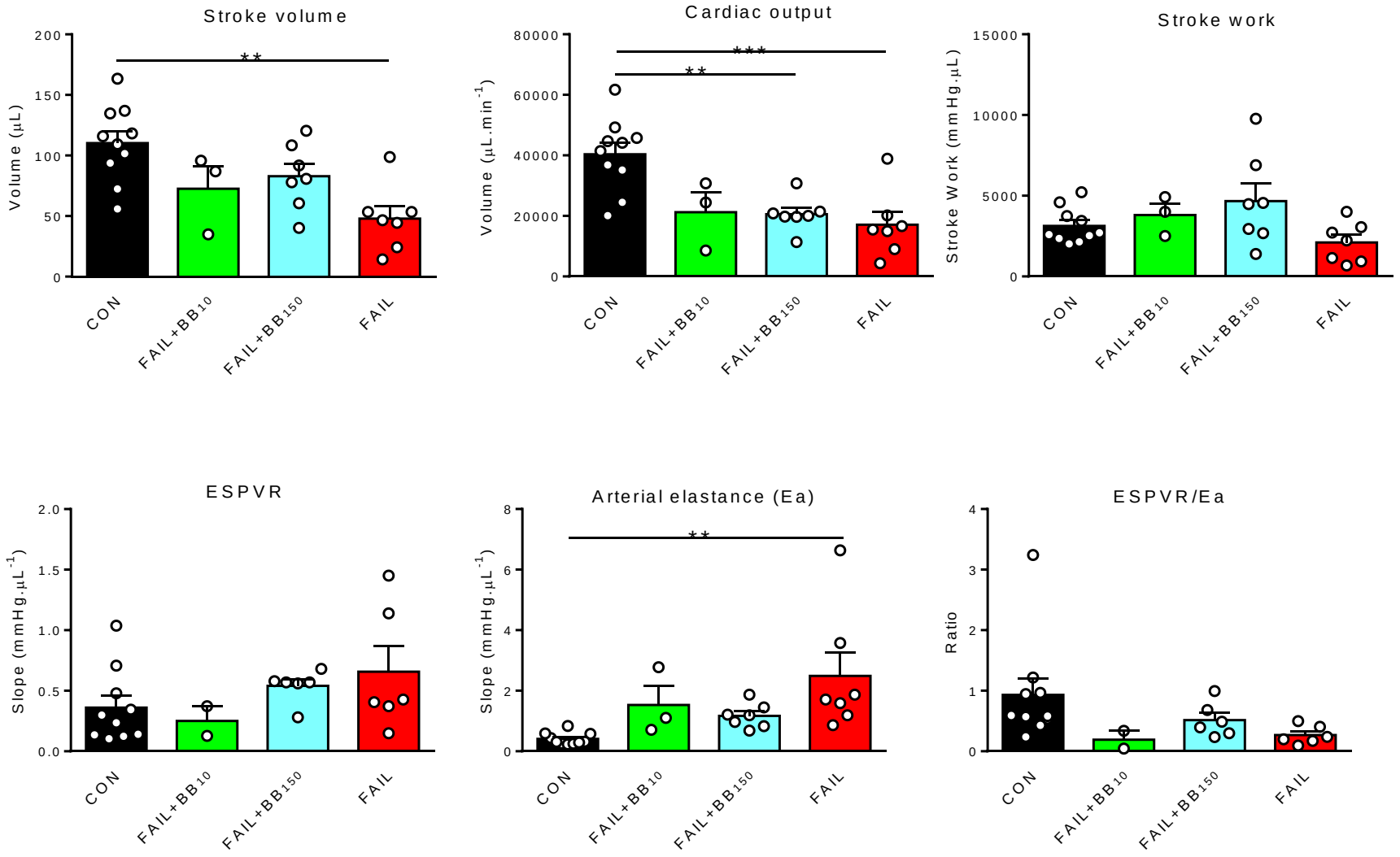
Stroke volume
Volume (µL)
200
150
100
50
0
**
CON
FAIL+BB10
FAIL+BB150
FAIL
Cardiac output
Volume (µL.min-1)
80000
60000
40000
20000
0
***
**
CON
FAIL+BB10
FAIL+BB150
FAIL
Stroke work
Stroke Work (mmHg.µL)
15000
10000
5000
0
CON
FAIL+BB10
FAIL+BB150
FAIL
ESPVR
Slope (mmHg.µL-1)
2.0
1.5
1.0
0.5
0.0
CON
FAIL+BB10
FAIL+BB150
FAIL
Arterial elastance (Ea)
Slope (mmHg.µL-1)
8
6
4
2
0
**
CON
FAIL+BB10
FAIL+BB150
FAIL
ESPVR/Ea
Ratio
4
3
2
1
0
CON
FAIL+BB10
FAIL+BB150
FAIL

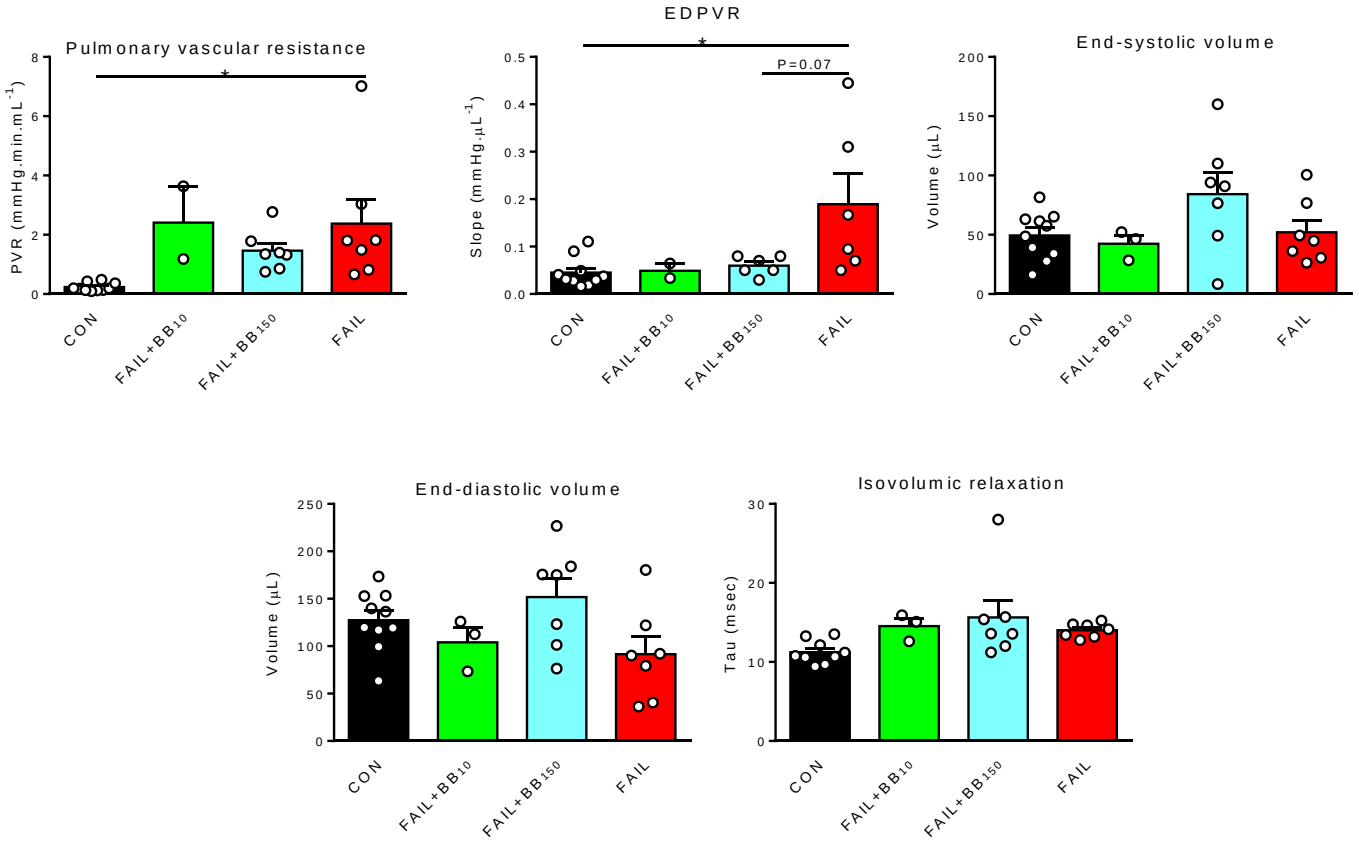

Figure 8.3 RV PV measurements in high dose metoprolol rats at onset of heart failure

MCT-treated rats were treated with either Ribena placebo, 10 mg/kg/day metoprolol (FAIL+BB_{10}), or 150 mg/kg/day metoprolol (FAIL+BB_{150}) and RV function assessed on the day heart failure symptoms developed.

Table 8.1 Doppler ultrasound measurements in high dose metoprolol rats at the onset of heart failure

	CON	FAIL+BB_{150}	FAIL
Heart rate (bpm)	409 ± 9	317 ± 15***	364 ± 12
PA acceleration time (ms)	35.9 ± 3.0	22.4 ± 2.1**	20.5 ± 1.5***
Velocity-time integral (cm)	5.96 ± 0.19	2.25 ± 0.27***	2.64 ± 0.41***
Peak velocity (m/s)	1.00 ± 0.03	0.57 ± 0.06***	0.67 ± 0.08***
Ejection time (ms)	0.12 ± 0.01	0.09 ± 0.01**	0.08 ± 0.01**
Systolic Pressure (mmHg)	51.5 ± 5.5	78.58 ± 5.08**	79.6 ± 2.8***
Stroke Volume (µL)	140 ± 13	55 ± 9***	52 ± 9***
Cardiac Output (mL/min)	57.7 ± 6.4	16.9 ± 3.0***	18.9 ± 3.4***
Cardiac Index ($\mu L/cm^2$)	129.0 ± 14.1	44.7 ± 8.0*	46.8 ± 8.2*

Data are mean±SEM. Measurements were recorded on the day heart failure symptoms developed (Failing columns) or on the median survival day of FAIL rats for CON. Calculated values are shown in italics. PA, pulmonary artery. N= 9 CON, 9 FAIL+BB_{150}, 7 FAIL. *P<0.05, **P<0.01, ***P<0.001 vs CON.

Table 8.2 M-mode ultrasound measurements in high dose metoprolol rats at the onset of heart failure

	CON	FAIL+BB_{150}	FAIL
RV thickness diastole (mm)	0.72 ± 0.04	1.21 ± 0.05***	1.43 ± 0.07***
RV thickness systole (mm)	0.87 ± 0.07	1.48 ± 0.07***	1.59 ± 0.10***
RV internal diameter diastole (mm	2.47 ± 0.26	5.42 ± 0.36*	5.00 ± 0.26*
RV internal diameter systole (mm)	1.43 ± 0.17	4.30 ± 0.23***	4.10 ± 0.24***
RV wall shortening (%)	39.5 ± 7.4	19.6 ± 3.4	18.1 ± 1.4
IVS thickness diastole (mm)	1.88 ± 0.14	2.17 ± 0.09	2.16 ± 0.10
IVS thickness systole (mm)	2.35 ± 0.15	2.41 ± 0.10	2.46 ± 0.17
LV thickness diastole (mm)	1.98 ± 0.14	2.11 ± 0.10	2.00 ± 0.15
LV thickness systole (mm)	2.90 ± 0.20	2.74 ± 0.13	2.45 ± 0.19
LV internal diameter diastole (mm	5.55 ± 0.30	4.98 ± 0.33	4.93 ± 0.34
LV internal diameter systole (mm)	3.02 ± 0.26	3.40 ± 0.38	2.98 ± 0.45
LV wall shortening (%)	46.2 ± 2.3	32.6 ± 5.2	39.4 ± 9.2

Data are mean±SEM. Measurements were recorded on the day heart failure symptoms developed (Failing columns) or on the median survival day of FAIL rats for CON. Calculated values are shown in italics. RV, right ventricle; IVS, interventricular septum; LV, left ventricle. N= 9 CON, 9 FAIL+BB_{150}, 7 FAIL rats. *P<0.05, **P<0.01, ***P<0.001 vs CON

Table 8.3 B-mode ultrasound measurements in high dose metoprolol rats at the onset of heart failure

	CON	FAIL+BB_{150}	FAIL
RV area diastole (cm^2)	0.11 ± 0.01	0.33 ± 0.03***	0.34 ± 0.04***
RV area systole (cm^2)	0.05 ± 0.01	0.24 ± 0.03***	0.25 ± 0.03***
RV area change (%)	52.0 ± 3.7	25.4 ± 3.9***	27.4 ± 3.1**
LV area diastole (cm^2)	0.25 ± 0.02	0.13 ± 0.01*	0.16 ± 0.02
LV area systole (cm^2)	0.09 ± 0.01	0.05 ± 0.01**	0.06 ± 0.01$^{\#}$
LV area change (%)	61.8 ± 2.6	59.2 ± 3.9	61.2 ± 7.4
LV systolic circularity (%)	87.0 ± 0.9	69.3 ± 3.6**	65.0 ± 2.2***

Data are mean±SEM. Measurements were recorded on the day heart failure symptoms developed (Failing columns) or on the median survival day of FAIL rats for CON. Calculated values are shown in italics. RV, right ventricle; LV, left ventricle. N= 9 CON, 9 FAIL+BB_{150}, 7 FAIL rats. *P<0.05, **P<0.01, ***P<0.001 vs CON, $^{\#}$P=0.06 vs CON

Appendix B

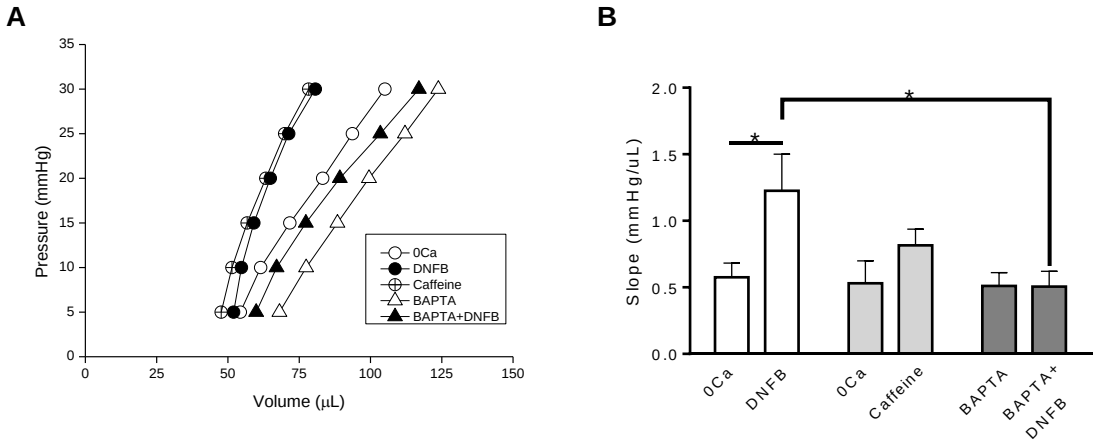

Figure 9.1 Passive LV pressure volume relationship

A fluid-filled balloon was passed into the LV of a Langendorff-perfused heart through the left atrium. Volume was controlled with a micropump dispensing at 400 µL.min^{-1} and pressure recorded continuously via a side port connected to a pressure transducer. The heart was arrested in diastole by perfusing 0 mM Ca^{2+} solution (0Ca) then balloon volume was adjusted in cycles to produce passive pressure-volume (PV) curves between 0-30 mmHg. Measurements were taken during inflation of the balloon. Measurements were taken after 60 min perfusion with 0Ca (N=6 hearts) or 20 µM BAPTA-AM (N=5 hearts). PV measurements were repeated following 30 min perfusion with DNFB (20 µM). In an additional two hearts , instead of DNFB a low dose of caffeine (200 µM) was used. **A** Mean PV relationships in different solutions (error bars are omitted for clarity) **B** Mean slopes of PV curves. DNFB significantly steepened the PV curve, however when intracellular Ca^{2+} was buffered there was no change in PV slope. Caffeine slightly reduced LV compliance but less so than DNFB. These data show elevated ADP in combination with diastolic Ca^{2+} significantly increases passive ventricle stiffness.

References

Abel FL & Waldhaus JA. (1967). Effects of alterations in pulmonary vascular resistance on right ventricular function. *J Thorac Cardiovasc Surg* **54,** 886-894.

Åblad B, Carlsson E & Ek L. (1973). Pharmacological studies of two new cardioselective adrenergic beta-receptor antagonists. *Life Sciences* **12,** 107-119.

Acsai K, Kun A, Farkas AS, Fülöp F, Nagy N, Balázs M, Szentandrássy N, Nánási PP, Papp JG, Varró A & Tóth A. (2007). Effect of partial blockade of the Na+/Ca2+-exchanger on Ca2+ handling in isolated rat ventricular myocytes. *European Journal of Pharmacology* **576,** 1-6.

Adams W, Trafford AW & Eisner DA. (1998). 2,3-Butanedione monoxime (BDM) decreases sarcoplasmic reticulum Ca content by stimulating Ca release in isolated rat ventricular myocytes. *Pflugers Arch* **436,** 776-781.

Aguirre AD, Vinegoni C, Sebas M & Weissleder R. (2014). Intravital imaging of cardiac function at the single-cell level. *Proceedings of the National Academy of Sciences* **111,** 11257-11262.

Akar FG & Rosenbaum DS. (2003). Transmural Electrophysiological Heterogeneities Underlying Arrhythmogenesis in Heart Failure. *Circulation Research* **93,** 638-645.

Akki A, Su J, Yano T, Gupta A, Wang Y, Leppo MK, Chacko VP, Steenbergen C & Weiss RG. (2012). Creatine Kinase Over-expression Improves ATP Kinetics and Contractile Function in Post-Ischemic Myocardium. *American Journal of Physiology - Heart and Circulatory Physiology*.

Al-Shammari AA, Gaffney EA & Egginton S. (2012). Re-evaluating the Use of Voronoi Tessellations in the Assessment of Oxygen Supply from Capillaries in Muscle. *Bull Math Biol* **74,** 2204-2231.

Al-Shammari AA, Gaffney EA & Egginton S. (2014). Modelling capillary oxygen supply capacity in mixed muscles: Capillary domains revisited. *Journal of Theoretical Biology* **356,** 47-61.

Allen DG & Kurihara S. (1982). The effects of muscle length on intracellular calcium transients in mammalian cardiac muscle. *The Journal of Physiology* **327,** 79-94.

Allingham JS, Smith R & Rayment I. (2005). The structural basis of blebbistatin inhibition and specificity for myosin II. *Nat Struct Mol Biol* **12,** 378-379.

Alvarez BV, Pérez NG, Ennis IL, Camilión de Hurtado MC & Cingolani HE. (1999). Mechanisms Underlying the Increase in Force and Ca2+

Transient That Follow Stretch of Cardiac Muscle : A Possible Explanation of the Anrep Effect. *Circulation Research* **85,** 716-722.

Andersen A, Nielsen JM, Peters CD, Schou UK, Sloth E & Nielsen-Kudsk JE. (2008). Effects of phosphodiesterase-5 inhibition by sildenafil in the pressure overloaded right heart. *European Journal of Heart Failure* **10,** 1158-1165.

Andersen GØ, Qvigstad E, Schiander I, Aass H, Osnes J-B & Skomedal T. (2002). α1-AR-induced positive inotropic response in heart is dependent on myosin light chain phosphorylation. *American Journal of Physiology - Heart and Circulatory Physiology* **283,** H1471-H1480.

Andersen S, Andersen A, de Man FS & Nielsen-Kudsk JE. (2015). Sympathetic nervous system activation and β-adrenoceptor blockade in right heart failure. *European Journal of Heart Failure* **17,** 358-366.

Andersen S, Schultz JG, Andersen A, Ringgaard S, Nielsen JM, Holmboe S, Vildbrad MD, de Man FS, Bogaard HJ, Vonk-Noordegraaf A & Nielsen-Kudsk JE. (2014). Effects of Bisoprolol and Losartan Treatment in the Hypertrophic and Failing Right Heart. *Journal of Cardiac Failure* **20,** 864-873.

Anker SD & Sharma R. (2002). The syndrome of cardiac cachexia. *International Journal of Cardiology* **85,** 51-66.

Anmann T, Varikmaa M, Timohhina N, Tepp K, Shevchuk I, Chekulayev V, Saks V & Kaambre T. (2014). Formation of highly organized intracellular structure and energy metabolism in cardiac muscle cells during postnatal development of rat heart. *Biochimica et Biophysica Acta (BBA) - Bioenergetics* **1837,** 1350-1361.

Apkon M & Nerbonne JM. (1991). Characterization of two distinct depolarization-activated K+ currents in isolated adult rat ventricular myocytes. *The Journal of General Physiology* **97,** 973-1011.

Arinze IJ & Kawai Y. (1983). Adrenergic regulation of glycogenolysis in isolated guinea-pig hepatocytes: Evidence that β2-receptors mediate catecholamine stimulation of glycogenolysis. *Archives of Biochemistry and Biophysics* **225,** 196-202.

Asghari P, Schulson M, Scriven DRL, Martens G & Moore EDW. (2009). Axial Tubules of Rat Ventricular Myocytes Form Multiple Junctions with the Sarcoplasmic Reticulum. *Biophysical journal* **96,** 4651-4660.

Association NYH. (1994). Nomenclature and Criteria for Diagnosis of Diseases of the Heart and Great Vessels., 9 edn, ed. Dolgin M. Little, Brown & Co., Boston.

Atkinson C, Stewart S, Upton PD, Machado R, Thomson JR, Trembath RC & Morrell NW. (2002). Primary Pulmonary Hypertension Is Associated With Reduced Pulmonary Vascular Expression of Type II Bone Morphogenetic Protein Receptor. *Circulation* **105,** 1672-1678.

Auerbach D, Bantle S, Keller S, Hinderling V, Leu M, Ehler E & Perriard J-C. (1999). Different Domains of the M-Band Protein Myomesin Are Involved in Myosin Binding and M-Band Targeting. *Molecular Biology of the Cell* **10,** 1297-1308.

Baan J, van der Velde ET, de Bruin HG, Smeenk GJ, Koops J, van Dijk AD, Temmerman D, Senden J & Buis B. (1984). Continuous measurement of left ventricular volume in animals and humans by conductance catheter. *Circulation* **70,** 812-823.

Baddeley D, Jayasinghe ID, Lam L, Rossberger S, Cannell MB & Soeller C. (2009). Optical single-channel resolution imaging of the ryanodine receptor distribution in rat cardiac myocytes. *Proceedings of the National Academy of Sciences*.

Badenhorst D, Maseko M, Tsotetsi OJ, Naidoo A, Brooksbank R, Norton GR & Woodiwiss AJ. (2003). Cross-linking influences the impact of quantitative changes in myocardial collagen on cardiac stiffness and remodelling in hypertension in rats. *Cardiovascular Research* **57,** 632-641.

Bal E, Ilgin S, Atli O, Ergun B & Sirmagul B. (2013). The effects of gender difference on monocrotaline-induced pulmonary hypertension in rats. *Human & Experimental Toxicology* **32,** 766-774.

Balaban RS, Kantor HL, Katz LA & Briggs RW. (1986). Relation between work and phosphate metabolite in the in vivo paced mammalian heart. *Science* **232,** 1121-1123.

Balestra GM, Mik EG, Eerbeek O, Specht PAC, van der Laarse WJ & Zuurbier CJ. (2015). Increased in vivo mitochondrial oxygenation with right ventricular failure induced by pulmonary arterial hypertension: mitochondrial inhibition as driver of cardiac failure? *Respiratory Research* **16,** 6.

Bandyopadhyay D, Bajaj NS, Zein J, Minai OA & Dweik RA. (2015). Outcomes of β-blocker use in pulmonary arterial hypertension: a propensity-matched analysis. *European Respiratory Journal* **46,** 750-760.

Banerjee I, Fuseler JW, Price RL, Borg TK & Baudino TA. (2007). Determination of cell types and numbers during cardiac development in the neonatal and adult rat and mouse. *American Journal of Physiology - Heart and Circulatory Physiology* **293,** H1883-H1891.

Bassani JW, Bassani RA & Bers DM. (1994). Relaxation in rabbit and rat cardiac cells: species-dependent differences in cellular mechanisms. *The Journal of Physiology* **476,** 279-293.

Bassani RA & Bers DM. (1994). Na-Ca Exchange is Required for Rest-decay but not for Rest-potential of Twitches in Rabbit and Rat Ventricular Myocytes. *Journal of Molecular and Cellular Cardiology* **26,** 1335-1347.

Baudenbacher F, Schober T, Pinto JR, Sidorov VY, Hilliard F, Solaro RJ, Potter JD & Knollmann BC. (2008). Myofilament Ca(2+) sensitization causes susceptibility to cardiac arrhythmia in mice. *The Journal of clinical investigation* **118,** 3893-3903.

Beard DA, Schenkman KA & Feigl EO. (2003). Myocardial oxygenation in isolated hearts predicted by an anatomically realistic microvascular transport model. *American Journal of Physiology - Heart and Circulatory Physiology* **285,** H1826-H1836.

Bella J, Eaton M, Brodsky B & Berman HM. (1994). Crystal and molecular structure of a collagen-like peptide at 1.9 A resolution. *Science (New York, NY)* **266,** 75-81.

Benitah J-P, Alvarez JL & Gómez AM. (2010). L-type Ca2+ current in ventricular cardiomyocytes. *Journal of Molecular and Cellular Cardiology* **48,** 26-36.

Bennett HJ, Davenport JB, Kitmitto A & Webb K. (2015). 172 Junctophilin-2 interacts with the cardiac L-Type voltage-gated calcium channel. *Heart* **101,** A98.

Benoist D, Stones R, Benson AP, Fowler ED, Drinkhill MJ, Hardy MEL, Saint DA, Cazorla O, Bernus O & White E. (2014). Systems approach to the study of stretch and arrhythmias in right ventricular failure induced in rats by monocrotaline. *Progress in Biophysics and Molecular Biology* **115,** 162-172.

Benoist D, Stones R, Drinkhill M, Bernus O & White E. (2011). Arrhythmogenic substrate in hearts of rats with monocrotaline-induced pulmonary hypertension and right ventricular hypertrophy. *Am J Physiol-Heart Circul Physiol* **300,** H2230-H2237.

Benoist D, Stones R, Drinkhill MJ, Benson AP, Yang Z, Cassan C, Gilbert SH, Saint DA, Cazorla O, Steele DS, Bernus O & White E. (2012). Cardiac arrhythmia mechanisms in rats with heart failure induced by pulmonary hypertension. *American Journal of Physiology - Heart and Circulatory Physiology* **302,** H2381-H2395.

Berlin JR, Cannell MB & Lederer WJ. (1989). Cellular origins of the transient inward current in cardiac myocytes. Role of fluctuations and waves of elevated intracellular calcium. *Circulation Research* **65,** 115-126.

Bers DM. (2001). *Excitation-Contraction Coupling and Cardiac Contractile Force*. Kluwer Academic, Dordrecht, The Netherlands.

Bers DM. (2002). Cardiac excitation-contraction coupling. *Nature* **415,** 198-205.

Bers DM, Lederer WJ & Berlin JR. (1990). Intracellular Ca transients in rat cardiac myocytes: role of Na-Ca exchange in excitation-contraction coupling. *American Journal of Physiology - Cell Physiology* **258,** C944-C954.

Bers DM, Li LI, Satoh H & McCall E. (1998). Factors That Control Sarcoplasmic Reticulum Calcium Release in Intact Ventricular Myocytesa. *Annals of the New York Academy of Sciences* **853,** 157-177.

Bessman SP & Fonyo A. (1966). The possible role of the mitochondrial bound creatine kinase in regulation of mitochondrial respiration. *Biochemical and Biophysical Research Communications* **22,** 597-602.

Bhatia RS, Tu JV, Lee DS, Austin PC, Fang J, Haouzi A, Gong Y & Liu PP. (2006). Outcome of Heart Failure with Preserved Ejection Fraction in a Population-Based Study. *New England Journal of Medicine* **355,** 260-269.

Bhatnagar P, Wickramasinghe K, Williams J, Rayner M & Townsend N. (2015). The epidemiology of cardiovascular disease in the UK 2014. *Heart*.

Birkedal R, Laasmaa M & Vendelin M. (2014). The location of energetic compartments affects energetic communication in cardiomyocytes. *Frontiers in Physiology* **5**.

Black JW, Crowther AF, Shanks RG, Smith LH & Dornhorst AC. (1964). A new adrenergic: beta-receptor antagonist. *The Lancet* **283,** 1080-1081.

Bluhm WF, McCulloch AD & Lew WYW. (1995). Active force in rabbit ventricular myocytes. *Journal of Biomechanics* **28,** 1119-1122.

Blum H, Balschi JA & Johnson RG. (1991). Coupled in vivo activity of creatine phosphokinase and the membrane-bound (Na+,K+)-ATPase in the resting and stimulated electric organ of the electric fish Narcine brasiliensis. *Journal of Biological Chemistry* **266,** 10254-10259.

Bogaard HJ, Natarajan R, Henderson SC, Long CS, Kraskauskas D, Smithson L, Ockaili R, McCord JM & Voelkel NF. (2009). Chronic Pulmonary Artery Pressure Elevation Is Insufficient to Explain Right Heart Failure. *Circulation* **120,** 1951-1960.

Bogaard HJ, Natarajan R, Mizuno S, Abbate A, Chang PJ, Chau VQ, Hoke NN, Kraskauskas D, Kasper M, Salloum FN & Voelkel NF. (2010). Adrenergic Receptor Blockade Reverses Right Heart Remodeling and Dysfunction in

Pulmonary Hypertensive Rats. *American Journal of Respiratory and Critical Care Medicine* **182,** 652-660.

Böhm M, Ettelbrück S, Flesch M, van Gilst WH, Knorr A, Maack C, Pinto YM, Paul M, Teisman ACH & Zolk O. (1998). β-Adrenergic signal transduction following carvedilol treatment in hypertensive cardiac hypertrophy. *Cardiovascular Research* **40,** 146-155.

Bollensdorff C, Lookin O & Kohl P. (2011). Assessment of contractility in intact ventricular cardiomyocytes using the dimensionless 'Frank–Starling Gain' index. *Pflugers Arch* **462,** 39-48.

Bond RA, Leff P, Johnson TD, Milano CA, Rockman HA, McMinn TR, Apparsundaram S, Hyek MF, Kenakin TP, Allen LF & Lefkowitz RJ. (1995). Physiological effects of inverse agonists in transgenic mice with myocardial overexpression of the [beta]2-adrenoceptor. *Nature* **374,** 272-276.

Borbély A, Falcao-Pires I, van Heerebeek L, Hamdani N, Édes I, Gavina C, Leite-Moreira AF, Bronzwaer JGF, Papp Z, van der Velden J, Stienen GJM & Paulus WJ. (2009). Hypophosphorylation of the Stiff N2B Titin Isoform Raises Cardiomyocyte Resting Tension in Failing Human Myocardium. *Circulation Research* **104,** 780-786.

Borgdorff MAJ, Bartelds B, Dickinson MG, Boersma B, Weij M, Zandvoort A, Silljé HHW, Steendijk P, de Vroomen M & Berger RMF. (2012). Sildenafil enhances systolic adaptation, but does not prevent diastolic dysfunction, in the pressure-loaded right ventricle. *European Journal of Heart Failure* **14,** 1067-1074.

Borgdorff MAJ, Bartelds B, Dickinson MG, Steendijk P, de Vroomen M & Berger RMF. (2013). Distinct loading conditions reveal various patterns of right ventricular adaptation. *American Journal of Physiology - Heart and Circulatory Physiology* **305,** H354-H364.

Bottomley PA, Panjrath GS, Lai S, Hirsch GA, Wu K, Najjar SS, Steinberg A, Gerstenblith G & Weiss RG. (2013). Metabolic Rates of ATP Transfer Through Creatine Kinase (CK Flux) Predict Clinical Heart Failure Events and Death. *Science Translational Medicine* **5,** 215re213.

Bouchard RA, Clark RB & Giles WR. (1995). Effects of Action Potential Duration on Excitation-Contraction Coupling in Rat Ventricular Myocytes: Action Potential Voltage-Clamp Measurements. *Circulation Research* **76,** 790-801.

Bovo E, de Tombe Pieter P & Zima Aleksey V. (2014). The Role of Dyadic Organization in Regulation of Sarcoplasmic Reticulum Ca2+ Handling during Rest in Rabbit Ventricular Myocytes. *Biophysical journal* **106,** 1902-1909.

Bovo E, Mazurek SR, Blatter LA & Zima AV. (2011). Regulation of sarcoplasmic reticulum Ca2+ leak by cytosolic Ca2+ in rabbit ventricular myocytes. *The Journal of Physiology* **589,** 6039-6050.

Boyman L, Williams GSB, Khananshvili D, Sekler I & Lederer WJ. (2013). NCLX: The mitochondrial sodium calcium exchanger. *Journal of Molecular and Cellular Cardiology* **59,** 205-213.

Brack KE, Narang R, Winter J & Ng GA. (2013). The mechanical uncoupler blebbistatin is associated with significant electrophysiological effects in the isolated rabbit heart. *Experimental Physiology* **98,** 1009-1027.

Brandstrom AE, Carlsson PAE, Carlsson SAI, Corrodi HR, Ek L & Ablad BAH. (1976). Phenoxy-hydroxypropylamines, their preparation, and method and pharmaceutical preparations for treating cardiovascular diseases. Google Patents.

Brimioulle S, Wauthy P, Ewalenko P, Rondelet Bt, Vermeulen F, Kerbaul F & Naeije R. (2003). Single-beat estimation of right ventricular end-systolic pressure-volume relationship. *American Journal of Physiology - Heart and Circulatory Physiology* **284,** H1625-H1630.

Brioschi M, Polvani G, Fratto P, Parolari A, Agostoni P, Tremoli E & Banfi C. (2012). Redox proteomics identification of oxidatively modified myocardial proteins in human heart failure: implications for protein function. *PloS one* **7,** e35841.

Bristow MR. (2000). β-Adrenergic Receptor Blockade in Chronic Heart Failure. *Circulation* **101,** 558-569.

Bristow MR & Quaife RA. (2015). The adrenergic system in pulmonary arterial hypertension: bench to bedside (2013 Grover Conference series). *Pulmonary Circulation* **5,** 415-423.

Brixius K, Hoischen S, Reuter H, Lasek K & Schwinger RHG. (2001). Force/shortening–frequency relationship in multicellular muscle strips and single cardiomyocytes of human failing and nonfailing hearts. *Journal of Cardiac Failure* **7,** 335-341.

Brock TG, McNish RW & Peters-Golden M. (1999). Arachidonic Acid Is Preferentially Metabolized by Cyclooxygenase-2 to Prostacyclin and Prostaglandin E2. *Journal of Biological Chemistry* **274,** 11660-11666.

Brooksby P, Levi AJ & Jones JV. (1993). Investigation of the mechanisms underlying the increased contraction of hypertrophied ventricular myocytes isolated from the spontaneously hypertensive rat. *Cardiovascular Research* **27,** 1268-1277.

Brown RE, Jarvis KL & Hyland KJ. (1989). Protein measurement using bicinchoninic acid: elimination of interfering substances. *Analytical Biochemistry* **180,** 136-139.

Bryant S, Kimura TE, Kong CHT, Watson JJ, Chase A, Suleiman MS, James AF & Orchard CH. (2014). Stimulation of ICa by basal PKA activity is facilitated by caveolin-3 in cardiac ventricular myocytes. *Journal of Molecular and Cellular Cardiology* **68,** 47-55.

Bryant SM, Kong CHT, Watson J, Cannell MB, James AF & Orchard CH. (2015). Altered distribution of ICa impairs Ca release at the t-tubules of ventricular myocytes from failing hearts. *Journal of Molecular and Cellular Cardiology* **86,** 23-31.

Bub G, Camelliti P, Bollensdorff C, Stuckey DJ, Picton G, Burton RAB, Clarke K & Kohl P. (2010). Measurement and analysis of sarcomere length in rat cardiomyocytes in situ and in vitro. *American Journal of Physiology - Heart and Circulatory Physiology* **298,** H1616-H1625.

Burkhoff D, Kronenberg MW, Yue DT, Maughan WL, Hunter WC & Sagawa K. (1987). Quantitative comparison of canine right and left ventricular isovolumic pressure waves. *American Journal of Physiology - Heart and Circulatory Physiology* **253,** H475-H479.

Burkhoff D & Sagawa K. (1986). Ventricular efficiency predicted by an analytical model. *American Journal of Physiology - Regulatory, Integrative and Comparative Physiology* **250,** R1021-R1027.

Calaghan S & White E. (2004). Activation of Na+–H+ exchange and stretch-activated channels underlies the slow inotropic response to stretch in myocytes and muscle from the rat heart. *The Journal of Physiology* **559,** 205-214.

Caldwell JL, Smith CE, Taylor RF, Kitmitto A, Eisner DA, Dibb KM & Trafford AW. (2014). Dependence of Cardiac Transverse Tubules on the BAR Domain Protein Amphiphysin II (BIN-1). *Circulation Research*.

Callahan LA & Supinski GS. (2007). Diaphragm and cardiac mitochondrial creatine kinases are impaired in sepsis. *Journal of Applied Physiology* **102,** 44-53.

Campian ME, Verberne HJ, Hardziyenka M, de Bruin K, Selwaness M, van den Hoff MJB, Ruijter JM, van Eck-Smit BLF, de Bakker JMT & Tan HL. (2009). Serial Noninvasive Assessment of Apoptosis During Right Ventricular Disease Progression in Rats. *Journal of Nuclear Medicine* **50,** 1371-1377.

Candasamy AJ, Haworth RS, Cuello F, Ibrahim M, Aravamudhan S, Krüger M, Holt MR, Terracciano CMN, Mayr M, Gautel M & Avkiran M. (2014).

Phosphoregulation of the Titin-cap Protein Telethonin in Cardiac Myocytes. *Journal of Biological Chemistry* **289,** 1282-1293.

Cappola TP, Kass DA, Nelson GS, Berger RD, Rosas GO, Kobeissi ZA, Marbán E & Hare JM. (2001). Allopurinol Improves Myocardial Efficiency in Patients With Idiopathic Dilated Cardiomyopathy. *Circulation* **104,** 2407-2411.

Cardozo RHL, de Vroomen M, van Bel F, Baan J & Steendijk P. (2003). Simultaneous measurement of right and left ventricular volume by the conductance catheter technique in the newborn lamb. *Netherlands Heart Journal* **11,** 203-209.

Cazorla O, Freiburg A, Helmes M, Centner T, McNabb M, Wu Y, Trombitás K, Labeit S & Granzier H. (2000a). Differential Expression of Cardiac Titin Isoforms and Modulation of Cellular Stiffness. *Circulation Research* **86,** 59-67.

Cazorla O, Le Guennec J-Y & White E. (2000b). Length–Tension Relationships of Sub-epicardial and Sub-endocardial Single Ventricular Myocytes from Rat and Ferret Hearts. *Journal of Molecular and Cellular Cardiology* **32,** 735-744.

Center for Drug Evaluation and Research CfBEaR. (2002). Estimating the safe starting dose in clinical trials for therapeutics in adult healthy volunteers. *US Food and Drug Administration, Rockville, Maryland*.

Champion HC, Michelakis ED & Hassoun PM. (2009). Comprehensive Invasive and Noninvasive Approach to the Right Ventricle–Pulmonary Circulation Unit: State of the Art and Clinical and Research Implications. *Circulation* **120,** 992-1007.

Chance B & Williams GR. (1955). Respiratory enzymes in oxidative phosphorylation: I. Kinetics of oxygen utilization. *Journal of Biological Chemistry* **217,** 383-394.

Chase A & Orchard CH. (2011). Ca efflux via the sarcolemmal Ca ATPase occurs only in the t-tubules of rat ventricular myocytes. *Journal of Molecular and Cellular Cardiology* **50,** 187-193.

Chaturvedi RR, Herron T, Simmons R, Shore D, Kumar P, Sethia B, Chua F, Vassiliadis E & Kentish JC. (2010). Passive Stiffness of Myocardium From Congenital Heart Disease and Implications for Diastole. *Circulation (Baltimore)* **121,** 979-988.

Chemla D, Castelain V, Hervé P, Lecarpentier Y & Brimioulle S. (2002). Haemodynamic evaluation of pulmonary hypertension. *European Respiratory Journal* **20,** 1314-1331.

Chen-Izu Y, McCulle SL, Ward CW, Soeller C, Allen BM, Rabang C, Cannell MB, Balke CW & Izu LT. (2006). Three-Dimensional Distribution of Ryanodine Receptor Clusters in Cardiac Myocytes. *Biophysical journal* **91,** 1-13.

Chen B, Guo A, Zhang C, Chen R, Zhu Y, Hong J, Kutschke W, Zimmerman K, Weiss RM, Zingman L, Anderson ME, Wehrens XHT & Song L-S. (2013). Critical roles of junctophilin-2 in T-tubule and excitation–contraction coupling maturation during postnatal development. *Cardiovascular Research* **100,** 54-62.

Chen B, Li Y, Jiang S, Xie Y-P, Guo A, Kutschke W, Zimmerman K, Weiss RM, Miller FJ, Anderson ME & Song L-S. (2012). β-Adrenergic receptor antagonists ameliorate myocyte T-tubule remodeling following myocardial infarction. *The FASEB Journal* **26,** 2531-2537.

Cheng G, Kasiganesan H, Baicu CF, Wallenborn JG, Kuppuswamy D & Cooper G. (2012). Cytoskeletal role in protection of the failing heart by β-adrenergic blockade. *American Journal of Physiology - Heart and Circulatory Physiology* **302,** H675-H687.

Cheng H, Lederer WJ & Cannell MB. (1993). Calcium Sparks: Elementary Events Underlying Excitation-Contraction Coupling in Heart Muscle. *Science* **262,** 740-744.

Chepelev NL, Bennitz JD, Wright JS, Smith JC & Willmore WG. (2009). Oxidative modification of citrate synthase by peroxyl radicals and protection with novel antioxidants. *Journal of Enzyme Inhibition and Medicinal Chemistry* **24,** 1319-1331.

Cherng WJ, Liang CS & Hood WB. (1994). Effects of metoprolol on left ventricular function in rats with myocardial infarction. *American Journal of Physiology - Heart and Circulatory Physiology* **266,** H787-H794.

Cheung A, Dantzig JA, Hollingworth S, Baylor SM, Goldman YE, Mitchison TJ & Straight AF. (2002). A small-molecule inhibitor of skeletal muscle myosin II. *Nat Cell Biol* **4,** 83-88.

Chu C, Thai K, Park KW, Wang P, Makwana O, Lovett DH, Simpson PC & Baker AJ. (2013). Intraventricular and interventricular cellular heterogeneity of inotropic responses to α1-adrenergic stimulation. *American Journal of Physiology - Heart and Circulatory Physiology* **304,** H946-H953.

Chung CS & Granzier HL. (2011). Contribution of titin and extracellular matrix to passive pressure and measurement of sarcomere length in the mouse left ventricle. *Journal of Molecular and Cellular Cardiology* **50,** 731-739.

Chung CS, Mitov MI, Callahan LA & Campbell KS. (2014). Increased myocardial short-range forces in a rodent model of diabetes reflect

elevated content of β myosin heavy chain. *Archives of Biochemistry and Biophysics* **552–553,** 92-99.

Cingolani HE, Chiappe GE, Ennis IL, Morgan PG, Alvarez BV, Casey JR, Dulce RA, Pérez NG & Camilión de Hurtado MC. (2003). Influence of Na+-Independent Cl−-HCO3− Exchange on the Slow Force Response to Myocardial Stretch. *Circulation Research* **93,** 1082-1088.

Cingolani OH, Yang X-P, Liu Y-H, Villanueva M, Rhaleb N-E & Carretero OA. (2004). Reduction of Cardiac Fibrosis Decreases Systolic Performance Without Affecting Diastolic Function in Hypertensive Rats. *Hypertension* **43,** 1067-1073.

Clark JF, Khuchua Z, Kuznetsov AV, Vassil'eva E, Boehm E, Radda GK & Saks V. (1994). Actions of the creatine analogue beta-guanidinopropionic acid on rat heart mitochondria. *Biochemical Journal* **300,** 211-216.

Colegrave M & Peckham M. (2014). Structural Implications of β-Cardiac Myosin Heavy Chain Mutations in Human Disease. *The Anatomical Record* **297,** 1670-1680.

Communal C, Singh K, Sawyer DB & Colucci WS. (1999). Opposing Effects of β1- and β2-Adrenergic Receptors on Cardiac Myocyte Apoptosis : Role of a Pertussis Toxin–Sensitive G Protein. *Circulation* **100,** 2210-2212.

Copple BL, Ganey PE & Roth RA. (2003). Liver inflammation during monocrotaline hepatotoxicity. *Toxicology* **190,** 155-169.

Cordero-Reyes AM, Gupte AA, Youker KA, Loebe M, Hsueh WA, Torre-Amione G, Taegtmeyer H & Hamilton DJ. (2014). Freshly isolated mitochondria from failing human hearts exhibit preserved respiratory function. *Journal of Molecular and Cellular Cardiology* **68,** 98-105.

Correia-Pinto J, Henriques-Coelho T, Roncon-Albuquerque R, Jr., Lourenço A, Melo-Rocha G, Vasques-Nóvoa F, Gillebert T & Leite-Moreira A. (2009). Time course and mechanisms of left ventricular systolic and diastolic dysfunction in monocrotaline-induced pulmonary hypertension. *Basic Research in Cardiology* **104,** 535-545.

Courand P-Y, Pina Jomir G, Khouatra C, Scheiber C, Turquier S, Glérant J-C, Mastroianni B, Gentil B, Blanchet-Legens A-S, Dib A, Derumeaux G, Humbert M, Mornex J-F, Cordier J-F & Cottin V. (2015). Prognostic value of right ventricular ejection fraction in pulmonary arterial hypertension. *European Respiratory Journal* **45,** 139-149.

Cowley PM, Wang G, Chang AN, Makwana O, Swigart PM, Lovett DH, Stull JT, Simpson PC & Baker AJ. (2015). The α1A-adrenergic receptor subtype mediates increased contraction of failing right ventricular myocardium. *American Journal of Physiology - Heart and Circulatory Physiology* **309,** H888-H896.

Crawford RM, RANKI HJ, BOTTING CH, BUDAS GR & JOVANOVIC A. (2002). Creatine kinase is physically associated with the cardiac ATP-sensitive K+ channel in vivo. *The FASEB Journal* **16,** 102-104.

D'Alonzo GE, Barst RJ, Ayres SM, Bergofsky EH, Brundage BH, Detre KM, Fishman AP, Goldring RM, Groves BM, Kernis JT, Levy PS, Pietra GG, Reid LM, Reeves JT, Rich S, Vreim CE, Williams GW & Wu M. (1991). Survival in Patients with Primary Pulmonary HypertensionResults from a National Prospective Registry. *Annals of Internal Medicine* **115,** 343-349.

Dabestani A, Mahan G, Gardin JM, Takenaka K, Burn C, Allfie A & Henry WL. (1987). Evaluation of pulmonary artery pressure and resistance by pulsed Doppler echocardiography. *The American Journal of Cardiology* **59,** 662-668.

Daicho T, Yagi T, Abe Y, Ohara M, Marunouchi T, Takeo S & Tanonaka K. (2009). Possible Involvement of Mitochondrial Energy-Producing Ability in the Development of Right Ventricular Failure in Monocrotaline-Induced Pulmonary Hypertensive Rats. *Journal of Pharmacological Sciences* **111,** 33-43.

Darmansjah I, Wong E, Setiawati A, Moeloek D, Irawati D, Siagian M & Muchtar A. (1990). Pharmacokinetic and Pharmacodynamic Properties of Controlled Release (CR/ZOK) Metoprolol in Healthy Oriental Subjects: A Comparison with Conventional Formulations of Metoprolol and Atenolol. *The Journal of Clinical Pharmacology* **30,** S39-S45.

Dass S, Holloway CJ, Cochlin LE, Rider OJ, Mahmod M, Robson M, Sever E, Clarke K, Watkins H, Ashrafian H, Karamitsos TD & Neubauer S. (2015). No Evidence of Myocardial Oxygen Deprivation in Non-Ischemic Heart Failure. *Circulation: Heart Failure*.

de Man FS, Handoko ML, van Ballegoij JJM, Schalij I, Bogaards SJP, Postmus PE, van der Velden J, Westerhof N, Paulus WJ & Vonk-Noordegraaf A. (2011). Bisoprolol Delays Progression Towards Right Heart Failure in Experimental Pulmonary Hypertension. *Circulation: Heart Failure*.

De Sousa E, Lechêne P, Fortin D, N'Guessan Bt, Belmadani S, Bigard X, Veksler V & Ventura-Clapier R. (2002). Cardiac and skeletal muscle energy metabolism in heart failure: beneficial effects of voluntary activity. *Cardiovascular Research* **56,** 260-268.

De Sousa E, Veksler V, Minajeva A, Kaasik A, Mateo P, Mayoux E, Hoerter J, Bigard X, Serrurier B & Ventura-Clapier R. (1999). Subcellular Creatine Kinase Alterations. *Circulation Research* **85,** 68-76.

de Tombe PP. (2003). Cardiac myofilaments: mechanics and regulation. *Journal of Biomechanics* **36,** 721-730.

Delbridge LM, Satoh H, Yuan W, Bassani JW, Qi M, Ginsburg KS, Samarel AM & Bers DM. (1997). Cardiac myocyte volume, Ca2+ fluxes, and sarcoplasmic reticulum loading in pressure-overload hypertrophy. *American Journal of Physiology - Heart and Circulatory Physiology* **272,** H2425-H2435.

Delcroix M & Naeije R. (2010). Optimising the management of pulmonary arterial hypertension patients: emergency treatments. *European Respiratory Review* **19,** 204-211.

Dell'Italia LJ. (1991). The right ventricle: anatomy, physiology, and clinical importance. *Current Problems in Cardiology* **16,** 658-720.

Deng Z, Morse JH, Slager SL, Cuervo N, Moore KJ, Venetos G, Kalachikov S, Cayanis E, Fischer SG, Barst RJ, Hodge SE & Knowles JA. (2000). Familial Primary Pulmonary Hypertension (Gene PPH1) Is Caused by Mutations in the Bone Morphogenetic Protein Receptor–II Gene. *The American Journal of Human Genetics* **67,** 737-744.

Des Tombe AL, Van Beek-Harmsen BJ, Lee-De Groot MBE & Van Der Laarse WJ. (2002). Calibrated histochemistry applied to oxygen supply and demand in hypertrophied rat myocardium. *Microscopy Research and Technique* **58,** 412-420.

Despa S, Brette F, Orchard CH & Bers DM. (2003). Na/Ca Exchange and Na/K-ATPase Function Are Equally Concentrated in Transverse Tubules of Rat Ventricular Myocytes. *Biophysical journal* **85,** 3388-3396.

Dhamoon AS & Jalife J. (2005). The inward rectifier current (IK1) controls cardiac excitability and is involved in arrhythmogenesis. *Heart Rhythm* **2,** 316-324.

Di Lenarda A, Remme WJ, Charlesworth A, Cleland JGF, Lutiger B, Metra M, Komajda M, Torp-Pedersen C, Scherhag A, Swedberg K, Poole-Wilson PA & for the Ci. (2005). Exchange of β-blockers in heart failure patients. Experiences from the poststudy phase of COMET (the Carvedilol or Metoprolol European Trial). *European Journal of Heart Failure* **7,** 640-649.

Díaz ME, Graham HK & Trafford AW. (2004). Enhanced sarcolemmal Ca2+ efflux reduces sarcoplasmic reticulum Ca2+ content and systolic Ca2+ in cardiac hypertrophy. *Cardiovascular Research* **62,** 538-547.

Dibb KM, Clarke JD, Eisner DA, Richards MA & Trafford AW. (2013). A functional role for transverse (t-) tubules in the atria. *Journal of Molecular and Cellular Cardiology* **58,** 84-91.

Dibb KM, Eisner DA & Trafford AW. (2007). Regulation of systolic [Ca2+]i and cellular Ca2+ flux balance in rat ventricular myocytes by SR Ca2+, L-type

Ca2+ current and diastolic [Ca2+]i. *The Journal of Physiology* **585,** 579-592.

Dou Y, Arlock P & Arner A. (2007). Blebbistatin specifically inhibits actin-myosin interaction in mouse cardiac muscle. *American Journal of Physiology - Cell Physiology* **293,** C1148-C1153.

Drake JI, Gomez-Arroyo J, Dumur CI, Kraskauskas D, Natarajan R, Bogaard HJ, Fawcett P & Voelkel NF. (2013). Chronic carvedilol treatment partially reverses the right ventricular failure transcriptional profile in experimental pulmonary hypertension. *Physiological Genomics* **45,** 449-461.

Dries E, Bito V, Lenaerts I, Antoons G, Sipido KR & Macquaide N. (2013). Selective Modulation of Coupled Ryanodine Receptors During Microdomain Activation of Calcium/Calmodulin-Dependent Kinase II in the Dyadic Cleft. *Circulation Research* **113,** 1242-1252.

Eisner DA, Li Y & O'Neill S. (2012). Do calcium waves propagate between cells and synchronize alternating calcium release in rat ventricular myocytes? *The Journal of Physiology*.

Enache I, Charles A-L, Bouitbir J, Favret F, Zoll J, Metzger D, Oswald-Mammosser M, Geny B & Charloux A. (2013). Skeletal muscle mitochondrial dysfunction precedes right ventricular impairment in experimental pulmonary hypertension. *Molecular and Cellular Biochemistry* **373,** 161-170.

Endoh M. (2004). Force–frequency relationship in intact mammalian ventricular myocardium: physiological and pathophysiological relevance. *European Journal of Pharmacology* **500,** 73-86.

Engelhardt S, Hein L, Wiesmann F & Lohse MJ. (1999). Progressive hypertrophy and heart failure in β1-adrenergic receptor transgenic mice. *Proceedings of the National Academy of Sciences* **96,** 7059-7064.

Eschenhagen T. (2010). Is ryanodine receptor phosphorylation key to the fight or flight response and heart failure? *The Journal of Clinical Investigation* **120,** 4197-4203.

Faber JE, Szymeczek CL, Salvi SS & Zhang H. (2006a). Enhanced α1-adrenergic trophic activity in pulmonary artery of hypoxic pulmonary hypertensive rats. *American Journal of Physiology - Heart and Circulatory Physiology* **291,** H2272-H2281.

Faber MJ, Dalinghaus M, Lankhuizen IM, Steendijk P, Hop WC, Schoemaker RG, Duncker DJ, Lamers JMJ & Helbing WA. (2006b). Right and left ventricular function after chronic pulmonary artery banding in rats assessed with biventricular pressure-volume loops. *American Journal of Physiology - Heart and Circulatory Physiology* **291,** H1580-H1586.

Fabiato A. (1985). Time and calcium dependence of activation and inactivation of calcium-induced release of calcium from the sarcoplasmic reticulum of a skinned canine cardiac Purkinje cell. *The Journal of general physiology* **85,** 247-289.

Fabiato A & Fabiato F. (1975). Contractions induced by a calcium-triggered release of calcium from the sarcoplasmic reticulum of single skinned cardiac cells. *The Journal of Physiology* **249,** 469-495.

Fan D, Wannenburg T & de Tombe PP. (1997). Decreased Myocyte Tension Development and Calcium Responsiveness in Rat Right Ventricular Pressure Overload. *Circulation* **95,** 2312-2317.

Farman G, Tachampa K, Mateja R, Cazorla O, Lacampagne A & Tombe P. (2008). Blebbistatin: use as inhibitor of muscle contraction. *Pflugers Arch - Eur J Physiol* **455,** 995-1005.

Fedorov VV, Lozinsky IT, Sosunov EA, Anyukhovsky EP, Rosen MR, Balke CW & Efimov IR. (2007). Application of blebbistatin as an excitation–contraction uncoupler for electrophysiologic study of rat and rabbit hearts. *Heart Rhythm* **4,** 619-626.

Feigenbaum H. (2004). *Feigenbaum's Echocardiography*. Lippincott Williams & Wilkins.

Ferrantini C, Coppini R, Sacconi L, Tosi B, Zhang ML, Wang GL, de Vries E, Hoppenbrouwers E, Pavone F, Cerbai E, Tesi C, Poggesi C & ter Keurs HEDJ. (2014). Impact of detubulation on force and kinetics of cardiac muscle contraction. *The Journal of general physiology* **143,** 783-797.

Ferrari R, Cargnoni A & Ceconi C. (2006). Anti-ischaemic effect of ivabradine. *Pharmacological Research* **53,** 435-439.

Flagg TP, Cazorla O, Remedi MS, Haim TE, Tones MA, Bahinski A, Numann RE, Kovacs A, Schaffer JE, Nichols CG & Nerbonne JM. (2009). Ca2+-Independent Alterations in Diastolic Sarcomere Length and Relaxation Kinetics in a Mouse Model of Lipotoxic Diabetic Cardiomyopathy. *Circulation Research* **104,** 95-103.

Fowler ED, Benoist D, Drinkhill MJ, Stones R, Helmes M, Wüst RCI, Stienen GJM, Steele DS & White E. (2015a). Decreased creatine kinase is linked to diastolic dysfunction in rats with right heart failure induced by pulmonary artery hypertension. *Journal of Molecular and Cellular Cardiology* **86,** 1-8.

Fowler ED, Norman R, Steer E, Pervolaraki E, Stones R, Drinkhill M, Calaghan SC, Steele DS & White E. (2015b). The β1 adrenergic receptor blocker metoprolol improves survival and partially restores Ca2+ handling

abnormalities in rat pulmonary artery hypertension. *Proc Physiol Soc* **34,** C03.

Frank JS & Langer GA. (1974). THE MYOCARDIAL INTERSTITIUM: ITS STRUCTURE AND ITS ROLE IN IONIC EXCHANGE. *The Journal of Cell Biology* **60,** 586-601.

Friebe A & Koesling D. (2003). Regulation of Nitric Oxide-Sensitive Guanylyl Cyclase. *Circulation Research* **93,** 96-105.

Fröhlich H, Zhao J, Täger T, Cebola R, Schellberg D, Katus HA, Grundtvig M, Hole T, Atar D, Agewall S & Frankenstein L. (2015). Carvedilol Compared With Metoprolol Succinate in the Treatment and Prognosis of Patients With Stable Chronic Heart Failure: Carvedilol or Metoprolol Evaluation Study. *Circulation: Heart Failure* **8,** 887-896.

Fuchs F & Wang Y-P. (1996). Sarcomere Length Versus Interfilament Spacing as Determinants of Cardiac Myofilament Ca2+Sensitivity and Ca2+Binding. *Journal of Molecular and Cellular Cardiology* **28,** 1375-1383.

Fujiwara K, Tanaka H, Mani H, Nakagami T & Takamatsu T. (2008). Burst Emergence of Intracellular Ca2+ Waves Evokes Arrhythmogenic Oscillatory Depolarization via the Na+–Ca2+ Exchanger: Simultaneous Confocal Recording of Membrane Potential and Intracellular Ca2+ in the Heart. *Circulation Research* **103,** 509-518.

Fukuda N, Kajiwara H, Ishiwata Si & Kurihara S. (2000). Effects of MgADP on Length Dependence of Tension Generation in Skinned Rat Cardiac Muscle. *Circulation Research* **86,** e1-e6.

Fukumoto K, Kobayashi T, Tachibana K, Kato R, Tanaka K, Komamura K, Kamakura S, Kitakaze M & Ueno K. (2006). Effect of Amiodarone on the Serum Concentration/Dose Ratio of Metoprolol in Patients with Cardiac Arrhythmia. *Drug Metabolism and Pharmacokinetics* **21,** 501-505.

Fuller MD, Emrick MA, Sadilek M, Scheuer T & Catterall WA. (2010). Molecular Mechanism of Calcium Channel Regulation in the Fight-or-Flight Response. *Science Signaling* **3,** ra70-ra70.

Furberg CD, Psaty BM, Pahor M & Alderman MH. (2001). Clinical Implications of Recent Findings from the Antihypertensive and Lipid-Lowering Treatment To Prevent Heart Attack Trial (ALLHAT) and Other Studies of Hypertension. *Annals of Internal Medicine* **135,** 1074-1078.

Gadeberg HC, Bryant SM, James AF & Orchard CH. (2015). Altered distribution of Na-Ca exchange in ventricular myocytes from failing rat hearts. *Proc Physiol Soc* **34,** PC038.

Galiè N, Barberà JA, Frost AE, Ghofrani H-A, Hoeper MM, McLaughlin VV, Peacock AJ, Simonneau G, Vachiery J-L, Grünig E, Oudiz RJ, Vonk-Noordegraaf A, White RJ, Blair C, Gillies H, Miller KL, Harris JHN, Langley J & Rubin LJ. (2015a). Initial Use of Ambrisentan plus Tadalafil in Pulmonary Arterial Hypertension. *New England Journal of Medicine* **373,** 834-844.

Galiè N, Humbert M, Vachiery J-L, Gibbs S, Lang I, Torbicki A, Simonneau G, Peacock A, Vonk Noordegraaf A, Beghetti M, Ghofrani A, Gomez Sanchez MA, Hansmann G, Klepetko W, Lancellotti P, Matucci M, McDonagh T, Pierard LA, Trindade PT, Zompatori M & Hoeper M. (2015b). 2015 ESC/ERS Guidelines for the diagnosis and treatment of pulmonary hypertension. *European Heart Journal*.

Galiè N, Manes A, Negro L, Palazzini M, Bacchi-Reggiani ML & Branzi A. (2009). A meta-analysis of randomized controlled trials in pulmonary arterial hypertension. *European Heart Journal* **30,** 394-403.

Gardner LA, Santos NMD, Matta SG, Whitt MA & Bahouth SW. (2004). Role of the Cyclic AMP-dependent Protein Kinase in Homologous Resensitization of the β1-Adrenergic Receptor. *Journal of Biological Chemistry* **279,** 21135-21143.

Garnier A, Fortin D, Deloménie C, Momken I, Veksler V & Ventura-Clapier R. (2003). Depressed mitochondrial transcription factors and oxidative capacity in rat failing cardiac and skeletal muscles. *The Journal of Physiology* **551,** 491-501.

Garnier D. (1994). Attachment procedures for mechanical manipulation of isolated cardiac myocytes: a challenge. *Cardiovascular Research* **28,** 1758-1764.

Gauthier C, Leblais V, Kobzik L, Trochu JN, Khandoudi N, Bril A, Balligand JL & Le Marec H. (1998). The negative inotropic effect of beta3-adrenoceptor stimulation is mediated by activation of a nitric oxide synthase pathway in human ventricle. *Journal of Clinical Investigation* **102,** 1377-1384.

Gauthier C, Tavernier G, Charpentier F, Langin D & Le Marec H. (1996). Functional beta3-adrenoceptor in the human heart. *Journal of Clinical Investigation* **98,** 556-562.

Gercken G & Schlette U. (1968). *Metabolite status of the heart in acute insufficiency due to 1-fluoro-2,4-dinitrobenzene*, vol. 24.

Gerdes AM. (2015). How to improve the overall quality of cardiac morphometric data. *American Journal of Physiology - Heart and Circulatory Physiology* **309,** H9-H14.

Gerdes AM, Callas G & Kasten FH. (1979). Differences in regional capillary distribution and myocyte sizes in normal and hypertrophic rat hearts. *American Journal of Anatomy* **156,** 523-531.

Gerdes AM & Capasso JM. (1995). Structural remodeling and mechanical dysfunction of cardiac myocytes in heart failure. *Journal of Molecular and Cellular Cardiology* **27,** 849-856.

Gerdes AM, Kellerman SE, Moore JA, Muffly KE, Clark LC, Reaves PY, Malec KB, McKeown PP & Schocken DD. (1992). Structural remodeling of cardiac myocytes in patients with ischemic cardiomyopathy. *Circulation* **86,** 426-430.

Gerdes AM, Onodera T, Wang X & McCune SA. (1996). Myocyte Remodeling During the Progression to Failure in Rats With Hypertension. *Hypertension* **28,** 609-614.

Ghio S, Klersy C, Magrini G, D'Armini AM, Scelsi L, Raineri C, Pasotti M, Serio A, Campana C & Viganò M. (2010). Prognostic relevance of the echocardiographic assessment of right ventricular function in patients with idiopathic pulmonary arterial hypertension. *International Journal of Cardiology* **140,** 272-278.

Ghio S, Pazzano AS, Klersy C, Scelsi L, Raineri C, Camporotondo R, D'Armini A & Visconti LO. (2011). Clinical and Prognostic Relevance of Echocardiographic Evaluation of Right Ventricular Geometry in Patients With Idiopathic Pulmonary Arterial Hypertension. *The American Journal of Cardiology* **107,** 628-632.

Ghio S, Temporelli PL, Klersy C, Simioniuc A, Girardi B, Scelsi L, Rossi A, Cicoira M, Genta FT & Dini FL. (2013). Prognostic relevance of a non-invasive evaluation of right ventricular function and pulmonary artery pressure in patients with chronic heart failure. *European Journal of Heart Failure* **15,** 408-414.

Ghofrani H-A, Galiè N, Grimminger F, Grünig E, Humbert M, Jing Z-C, Keogh AM, Langleben D, Kilama MO, Fritsch A, Neuser D & Rubin LJ. (2013). Riociguat for the Treatment of Pulmonary Arterial Hypertension. *New England Journal of Medicine* **369,** 330-340.

Ghofrani HA, Rose F, Schermuly RT, Olschewski H, Wiedemann R, Kreckel A, Weissmann N, Ghofrani S, Enke B, Seeger W & Grimminger F. (2003). Oral sildenafil as long-term adjunct therapy to inhaled iloprost in severe pulmonary arterial hypertension. *Journal of the American College of Cardiology* **42,** 158-164.

Giaid A & Saleh D. (1995). Reduced Expression of Endothelial Nitric Oxide Synthase in the Lungs of Patients with Pulmonary Hypertension. *New England Journal of Medicine* **333,** 214-221.

Gilbert EM, Abraham WT, Olsen S, Hattler B, White M, Mealy P, Larrabee P & Bristow MR. (1996). Comparative Hemodynamic, Left Ventricular Functional, and Antiadrenergic Effects of Chronic Treatment With Metoprolol Versus Carvedilol in the Failing Heart. *Circulation* **94,** 2817-2825.

Gleason WL & Braunwald E. (1962). STUDIES ON THE FIRST DERIVATIVE OF THE VENTRICULAR PRESSURE PULSE IN MAN. *Journal of Clinical Investigation* **41,** 80-91.

Goldman D. (2008). Theoretical Models of Microvascular Oxygen Transport to Tissue. *Microcirculation* **15,** 795-811.

Goldman Y & Brenner B. (1987). Special Topic: Molecular Mechanism of Muscle Contraction. *Annu Rev Physiol* **49,** 629-636.

Gomez-Arroyo JG, Farkas L, Alhussaini AA, Farkas D, Kraskauskas D, Voelkel NF & Bogaard HJ. (2011). The Monocrotaline Model of Pulmonary Hypertension In Perspective. *American Journal of Physiology - Lung Cellular and Molecular Physiology*.

Gomez-Arroyo JG, Farkas L, Alhussaini AA, Farkas D, Kraskauskas D, Voelkel NF & Bogaard HJ. (2012). The monocrotaline model of pulmonary hypertension in perspective. *Am J Physiol-Lung Cell Mol Physiol* **302,** L363-L369.

Gopalan SM, Flaim C, Bhatia SN, Hoshijima M, Knoell R, Chien KR, Omens JH & McCulloch AD. (2003). Anisotropic stretch-induced hypertrophy in neonatal ventricular myocytes micropatterned on deformable elastomers. *Biotechnology and Bioengineering* **81,** 578-587.

Gordon AM, Huxley AF & Julian FJ. (1966). The variation in isometric tension with sarcomere length in vertebrate muscle fibres. *The Journal of Physiology* **184,** 170-192.

Gorelik J, Wright PT, Lyon AR & Harding SE. (2013). Spatial control of the βAR system in heart failure: the transverse tubule and beyond. *Cardiovascular Research* **98,** 216-224.

Goto Y, Slinker BK & LeWinter MM. (1988). Accuracy of volume measurement of rabbit left ventricle by balloon method. *American Journal of Physiology - Heart and Circulatory Physiology* **255,** H394-H396.

Gouma E, Simos Y, Verginadis I, Lykoudis E, Evangelou A & Karkabounas S. (2012). A simple procedure for estimation of total body surface area and determination of a new value of Meeh's constant in rats. *Laboratory Animals* **46,** 40-45.

Grantham CJ & Cannell MB. (1996). Ca2+ Influx During the Cardiac Action Potential in Guinea Pig Ventricular Myocytes. *Circulation Research* **79,** 194-200.

Granzier HL & Irving TC. (1995). Passive tension in cardiac muscle: contribution of collagen, titin, microtubules, and intermediate filaments. *Biophysical journal* **68,** 1027-1044.

Greaser ML & Pleitner JM. (2014). Titin Isoform Size is Not Correlated with Thin Filament Length in Rat Skeletal Muscle. *Frontiers in Physiology* **5**.

Greaser ML, Warren CM, Esbona K, Guo W, Duan Y, Parrish AM, Krzesinski PR, Norman HS, Dunning S, Fitzsimons DP & Moss RL. (2008). Mutation that dramatically alters rat titin isoform expression and cardiomyocyte passive tension. *Journal of Molecular and Cellular Cardiology* **44,** 983-991.

Gresham KS & Stelzer JE. (2015). The contributions of MyBP-C and TnI phosphorylation to β-adrenergic enhancement of in vivo cardiac function. *The Journal of Physiology***,** n/a-n/a.

Grimm AF & Whitehorn WV. (1968). Myocardial length-tension sarcomere relationships. *American Journal of Physiology* **214,** 1378-&.

Grinnan D, Bogaard H-J, Grizzard J, Van Tassell B, Abbate A, DeWilde C, Priday A & Voelkel NF. (2014). Treatment of Group I Pulmonary Arterial Hypertension with Carvedilol Is Safe. *American Journal of Respiratory and Critical Care Medicine* **189,** 1562-1564.

Groepenhoff H, Westerhof N, Jacobs W, Boonstra A, Postmus PE & Vonk-Noordegraaf A. (2010). Exercise stroke volume and heart rate response differ in right and left heart failure. *European Journal of Heart Failure* **12,** 716-720.

Grosse R, Spitzer E, Kupriyanov VV, Saks VA & Repke KRH. (1980). Coordinate interplay between (Na+ + K+)-ATPase and creatine phosphokinase optimizes (Na+/K+)-antiport across the membrane of vesicles formed from the plasma membrane of cardiac muscle cell. *Biochimica et Biophysica Acta (BBA) - Biomembranes* **603,** 142-156.

Grossman W, Jones D & McLaurin LP. (1975). Wall stress and patterns of hypertrophy in the human left ventricle. *Journal of Clinical Investigation* **56,** 56-64.

Grünig E, Tiede H, Enyimayew EO, Ehlken N, Seyfarth H-J, Bossone E, D'Andrea A, Naeije R, Olschewski H, Ulrich S, Nagel C, Halank M & Fischer C. (2013). Assessment and Prognostic Relevance of Right Ventricular Contractile Reserve in Patients With Severe Pulmonary Hypertension. *Circulation* **128,** 2005-2015.

Grutzner A, Garcia-Manyes S, Kotter S, Badilla CL, Fernandez JM & Linke WA. (2009). Modulation of Titin-Based Stiffness by Disulfide Bonding in the Cardiac Titin N2-B Unique Sequence. *Biophysical Journal* **97,** 825-834.

Guazzi M & Borlaug BA. (2012). Pulmonary Hypertension Due to Left Heart Disease. *Circulation* **126,** 975-990.

Guo A, Zhang X, Iyer VR, Chen B, Zhang C, Kutschke WJ, Weiss RM, Franzini-Armstrong C & Song L-S. (2014). Overexpression of junctophilin-2 does not enhance baseline function but attenuates heart failure development after cardiac stress. *Proceedings of the National Academy of Sciences* **111,** 12240-12245.

Gupta A, Akki A, Wang Y, Leppo MK, Chacko VP, Foster DB, Caceres V, Shi S, Kirk JA, Su J, Lai S, Paolocci N, Steenbergen C, Gerstenblith G & Weiss RG. (2012). Creatine kinase-mediated improvement of function in failing mouse hearts provides causal evidence the failing heart is energy starved. *The Journal of clinical investigation* **122,** 291-302.

Guzun R, Timohhina N, Tepp K, Monge C, Kaambre T, Sikk P, Kuznetsov AV, Pison C & Saks V. (2009). Regulation of respiration controlled by mitochondrial creatine kinase in permeabilized cardiac cells in situ: Importance of system level properties. *Biochimica et Biophysica Acta (BBA) - Bioenergetics* **1787,** 1089-1105.

Hadad N, Feng W & Shoshan-Barmatz V. (1999). Modification of ryanodine receptor/Ca2+ release channel with dinitrofluorobenzene. *Biochemical Journal* **342,** 239-248.

Haddad F, Doyle R, Murphy DJ & Hunt SA. (2008a). Right Ventricular Function in Cardiovascular Disease, Part II: Pathophysiology, Clinical Importance, and Management of Right Ventricular Failure. *Circulation* **117,** 1717-1731.

Haddad F, Hunt SA, Rosenthal DN & Murphy DJ. (2008b). Right Ventricular Function in Cardiovascular Disease, Part I. *Circulation* **117,** 1436-1448.

Hales PW, Schneider JE, Burton RAB, Wright BJ, Bollensdorff C & Kohl P. (2012). Histo-anatomical structure of the living isolated rat heart in two contraction states assessed by diffusion tensor MRI. *Progress in Biophysics and Molecular Biology* **110,** 319-330.

Hamman BL, Bittl JA, Jacobus WE, Allen PD, Spencer RS, Tian R & Ingwall JS. (1995). Inhibition of the creatine kinase reaction decreases the contractile reserve of isolated rat hearts. *American Journal of Physiology - Heart and Circulatory Physiology* **269,** H1030-H1036.

Hammerschmidt S, Bell M, Büchler N, Wahn H, Remkes H, Lohse MJ & Neubauer S. (2000). Acute changes of myocardial creatine kinase gene

expression under β-adrenergic stimulation. *Biochimica et Biophysica Acta (BBA) - Molecular Basis of Disease* **1502,** 471-480.

Han JC, Taberner AJ, Tran K, Nickerson DP, Nash MP, Nielsen PMF, Crampin EJ & Loiselle DS. (2012). Relating components of pressure-volume area in Suga's formulation of cardiac energetics to components of the stress-time integral. *Journal of Applied Physiology* **113,** 988-995.

Handoko ML, de Man FS, Allaart CP, Paulus WJ, Westerhof N & Vonk-Noordegraaf A. (2010). Perspectives on novel therapeutic strategies for right heart failure in pulmonary arterial hypertension: lessons from the left heart. *European Respiratory Review* **19,** 72-82.

Harding VB, Jones LR, Lefkowitz RJ, Koch WJ & Rockman HA. (2001). Cardiac βARK1 inhibition prolongs survival and augments β blocker therapy in a mouse model of severe heart failure. *Proceedings of the National Academy of Sciences* **98,** 5809-5814.

Harrison SM & Boyett MR. (1995). The role of the Na(+)-Ca2+ exchanger in the rate-dependent increase in contraction in guinea-pig ventricular myocytes. *The Journal of Physiology* **482,** 555-566.

Hasenfuss G, Reinecke H, Studer R, Meyer M, Pieske B, Holtz J, Holubarsch C, Posival H, Just H & Drexler H. (1994). Relation between myocardial function and expression of sarcoplasmic reticulum Ca(2+)-ATPase in failing and nonfailing human myocardium. *Circulation Research* **75,** 434-442.

Hauton D, Winter J, Al-Shammari AA, Gaffney EA, Evans RD & Egginton S. (2015). Changes to both cardiac metabolism and performance accompany acute reductions in functional capillary supply. *Biochimica et Biophysica Acta (BBA) - General Subjects* **1850,** 681-690.

Hein S, Scholz D, Fujitani N, Rennollet H, Brand T, Friedl A & Schaper J. (1994). Altered Expression of Titin and Contractile Proteins in Failing Human Myocardium. *Journal of Molecular and Cellular Cardiology* **26,** 1291-1306.

Heinzel FR, Bito V, Biesmans L, Wu M, Detre E, von Wegner F, Claus P, Dymarkowski S, Maes F, Bogaert J, Rademakers F, D'hooge J & Sipido K. (2008). Remodeling of T-Tubules and Reduced Synchrony of Ca2+ Release in Myocytes From Chronically Ischemic Myocardium. *Circulation Research* **102,** 338-346.

Heinzel FR, MacQuaide N, Biesmans L & Sipido K. (2011). Dyssynchrony of Ca2+ release from the sarcoplasmic reticulum as subcellular mechanism of cardiac contractile dysfunction. *Journal of Molecular and Cellular Cardiology* **50,** 390-400.

Helmes M, Breel EJ, Iannuzzi D & van der Velden J. Measuring Work Loops in Intact Isolated Cardiac Myocytes by Controlling Pre- and Afterload using a New Generation Force Transducer. *Biophysical journal* **106,** 564a.

Helmes M, Trombita´s Kr & Granzier H. (1996). Titin Develops Restoring Force in Rat Cardiac Myocytes. *Circulation Research* **79,** 619-626.

Hess P, Clozel M & Clozel JP. (1996). Telemetry monitoring of pulmonary arterial pressure in freely moving rats. *Journal of Applied Physiology* **81,** 1027-1032.

Hidalgo CG, Chung CS, Saripalli C, Methawasin M, Hutchinson KR, Tsaprailis G, Labeit S, Mattiazzi A & Granzier HL. (2013). The multifunctional Ca(2+)/calmodulin-dependent protein kinase II delta (CaMKIIδ) phosphorylates cardiac titin's spring elements. *Journal of Molecular and Cellular Cardiology* **54,** 90-97.

Hirsch GA, Bottomley PA, Gerstenblith G & Weiss RG. (2012). Allopurinol Acutely Increases Adenosine Triphospate Energy Delivery in Failing Human Hearts. *Journal of the American College of Cardiology* **59,** 802-808.

Hjalmarson Å, Goldstein S, Fagerberg B & et al. (2000). Effects of controlled-release metoprolol on total mortality, hospitalizations, and well-being in patients with heart failure: The metoprolol cr/xl randomized intervention trial in congestive heart failure (merit-hf). *JAMA* **283,** 1295-1302.

Hobai IA & O'Rourke B. (2001). Decreased Sarcoplasmic Reticulum Calcium Content Is Responsible for Defective Excitation-Contraction Coupling in Canine Heart Failure. *Circulation* **103,** 1577-1584.

Hoeper MM, Bogaard HJ, Condliffe R, Frantz R, Khanna D, Kurzyna M, Langleben D, Manes A, Satoh T, Torres F, Wilkins MR & Badesch DB. (2013). Definitions and Diagnosis of Pulmonary Hypertension. *Journal of the American College of Cardiology* **62,** D42-D50.

Holubarsch C, Ruf T, Goldstein DJ, Ashton RC, Nickl W, Pieske B, Pioch K, Lu¨demann J, Wiesner S, Hasenfuss G, Posival H, Just Hr & Burkhoff D. (1996). Existence of the Frank-Starling Mechanism in the Failing Human Heart: Investigations on the Organ, Tissue, and Sarcomere Levels. *Circulation* **94,** 683-689.

Hong T-T, Smyth JW, Chu KY, Vogan JM, Fong TS, Jensen BC, Fang K, Halushka MK, Russell SD, Colecraft H, Hoopes CW, Ocorr K, Chi NC & Shaw RM. (2012). BIN1 is reduced and Cav1.2 trafficking is impaired in human failing cardiomyocytes. *Heart Rhythm* **9,** 812-820.

Hong T-T, Smyth JW, Gao D, Chu KY, Vogan JM, Fong TS, Jensen BC, Colecraft HM & Shaw RM. (2010). BIN1 Localizes the L-Type Calcium Channel to Cardiac T-Tubules. *PLoS Biol* **8,** e1000312.

Hong T, Yang H, Zhang S-S, Cho HC, Kalashnikova M, Sun B, Zhang H, Bhargava A, Grabe M, Olgin J, Gorelik J, Marban E, Jan LY & Shaw RM. (2014). Cardiac BIN1 folds T-tubule membrane, controlling ion flux and limiting arrhythmia. *Nat Med* **20,** 624-632.

Honjo H, Inada S, Lancaster MK, Yamamoto M, Niwa R, Jones SA, Shibata N, Mitsui K, Horiuchi T, Kamiya K, Kodama I & Boyett MR. (2003). Sarcoplasmic Reticulum Ca2+ Release Is Not a Dominating Factor in Sinoatrial Node Pacemaker Activity. *Circulation Research* **92,** e41-e44.

Horan LG, Flowers NC & Havelda CJ. (1981). Relation between right ventricular mass and cavity size: an analysis of 1500 human hearts. *Circulation* **64,** 135-138.

Hornemann T, Kempa S, Himmel M, Hayeß K, Fürst DO & Wallimann T. (2003). Muscle-type Creatine Kinase Interacts with Central Domains of the M-band Proteins Myomesin and M-protein. *Journal of Molecular Biology* **332,** 877-887.

Howarth FC, Boyett MR & White E. (1998). Rapid effects of cytochalasin-D on contraction and intracellular calcium in single rat ventricular myocytes. *Pflugers Arch* **436,** 804-806.

Huang J, Wolk JH, Gewitz MH & Mathew R. (2010). Progressive endothelial cell damage in an inflammatory model of pulmonary hypertension. *Experimental Lung Research* **36,** 57-66.

Humbert M, Morrell NW, Archer SL, Stenmark KR, MacLean MR, Lang IM, Christman BW, Weir EK, Eickelberg O, Voelkel NF & Rabinovitch M. (2004). Cellular and molecular pathobiology of pulmonary arterial hypertension. *Journal of the American College of Cardiology* **43,** S13-S24.

Humbert M, Sitbon O, Chaouat A, Bertocchi M, Habib G, Gressin V, Yaïci A, Weitzenblum E, Cordier J-F, Chabot F, Dromer C, Pison C, Reynaud-Gaubert M, Haloun A, Laurent M, Hachulla E, Cottin V, Degano B, Jaïs X, Montani D, Souza R & Simonneau G. (2010). Survival in Patients With Idiopathic, Familial, and Anorexigen-Associated Pulmonary Arterial Hypertension in the Modern Management Era. *Circulation* **122,** 156-163.

Ibrahim M, Navaratnarajah M, Siedlecka U, Rao C, Dias P, Moshkov AV, Gorelik J, Yacoub MH & Terracciano CM. (2012). Mechanical unloading reverses transverse tubule remodelling and normalizes local Ca(2+)-induced Ca(2+)release in a rodent model of heart failure. *European Journal of Heart Failure* **14,** 571-580.

Ide T, Tsutsui H, Kinugawa S, Utsumi H, Kang D, Hattori N, Uchida K, Arimura K-i, Egashira K & Takeshita A. (1999). Mitochondrial Electron Transport

Complex I Is a Potential Source of Oxygen Free Radicals in the Failing Myocardium. *Circulation Research* **85,** 357-363.

Ingwall JS. (1984). The hypertrophied myocardium accumulates the MB-creatine kinase isozyme. *European Heart Journal* **5,** 129-139.

Ingwall JS & Weiss RG. (2004). Is the Failing Heart Energy Starved? *Circulation Research* **95,** 135-145.

Iribe G, Helmes M & Kohl P. (2007). *Force-length relations in isolated intact cardiomyocytes subjected to dynamic changes in mechanical load*, vol. 292.

Iribe G, Kaneko T, Yamaguchi Y & Naruse K. (2014). Load dependency in force–length relations in isolated single cardiomyocytes. *Progress in Biophysics and Molecular Biology* **115,** 103-114.

Ishikawa K, Hashimoto H, Mitani S, Toki Y, Okumura K & Ito T. (1995). Enalapril improves heart failure induced by monocrotaline without reducing pulmonary hypertension in rats: roles of preserved myocardial creatine kinase and lactate dehydrogenase isoenzymes. *International Journal of Cardiology* **47,** 225-233.

Ishikawa S, Honda M, Yamada S, Goto Y, Ishikawa S, Yoshikane H, Ishinaga Y, Kuzuo H, Morioka S & Moriyama K. (1992a). Biochemical and structural remodeling of collagen in the right ventricular hypertrophy induced by monocrotaline. *Japanese Circulation Journal* **56,** 392-403.

Ishikawa S, Honda M, Yamada S, Goto Y, Morioka S, Ishinaga Y, Murakami Y, Masumura S & Moriyama K. (1992b). Different biventricular remodelling of myosin and collagen in pulmonary hypertension. *Clinical and Experimental Pharmacology and Physiology* **19,** 723-732.

Ishikawa S, Honda M, Yamada S, Morioka S & Moriyama K. (1991). Biventricular down-regulation of beta-adrenergic receptors in right ventricular hypertrophy induced by monocrotaline. *Japanese Circulation Journal* **55,** 1077-1085.

Israeli-Rosenberg S, Chen C, Li R, Deussen DN, Niesman IR, Okada H, Patel HH, Roth DM & Ross RS. (2015). Caveolin modulates integrin function and mechanical activation in the cardiomyocyte. *The FASEB Journal* **29,** 374-384.

Izu LT, Means SA, Shadid JN, Chen-Izu Y & Balke CW. (2006). Interplay of Ryanodine Receptor Distribution and Calcium Dynamics. *Biophysical journal* **91,** 95-112.

Jacobs H, Heldt HW & Klingenberg M. (1964). High activity of creatine kinase in mitochondria from muscle + brain + evidence for separate mitochondrial

isoenzyme of creatine kinase. *Biochemical and Biophysical Research Communications* **16,** 516-&.

Jacobs W, van de Veerdonk MC, Trip P, de Man F, Heymans MW, Marcus JT, Kawut SM, Bogaard H-J, Boonstra A & Vonk Noordegraaf A. (2014). THe right ventricle explains sex differences in survival in idiopathic pulmonary arterial hypertension. *Chest* **145,** 1230-1236.

Janse MJ. (2004). Electrophysiological changes in heart failure and their relationship to arrhythmogenesis. *Cardiovascular Research* **61,** 208-217.

Janssen PM & de Tombe PP. (1997). Uncontrolled sarcomere shortening increases intracellular Ca2+ transient in rat cardiac trabeculae. *American Journal of Physiology - Heart and Circulatory Physiology* **272,** H1892-H1897.

Jiang Y, Pandya K, Smithies O & Hsu EW. (2004). Three-dimensional diffusion tensor microscopy of fixed mouse hearts. *Magnetic Resonance in Medicine* **52,** 453-460.

Johnson JA & Burlew BS. (1996). Metoprolol metabolism via cytochrome P4502D6 in ethnic populations. *Drug Metabolism and Disposition* **24,** 350-355.

Jones JE, Mendes L, Rudd MA, Russo G, Loscalzo J & Zhang Y-Y. (2002). Serial noninvasive assessment of progressive pulmonary hypertension in a rat model. *American Journal of Physiology - Heart and Circulatory Physiology* **283,** H364-H371.

Junqueira LCU, Bignolas G & Brentani RR. (1979). Picrosirius staining plus polarization microscopy, a specific method for collagen detection in tissue sections. *Histochem J* **11,** 447-455.

Kääb S, Nuss HB, Chiamvimonvat N, O'Rourke B, Pak PH, Kass DA, Marban E & Tomaselli GF. (1996). Ionic Mechanism of Action Potential Prolongation in Ventricular Myocytes From Dogs With Pacing-Induced Heart Failure. *Circulation Research* **78,** 262-273.

Kaasik A, Minajeva A, De Sousa E, Ventura-Clapier R & Veksler V. (1999). Nitric oxide inhibits cardiac energy production via inhibition of mitochondrial creatine kinase. *FEBS Letters* **444,** 75-77.

Kaasik A, Veksler V, Boehm E, Novotova M, Minajeva A & Ventura-Clapier R. (2001). Energetic Crosstalk Between Organelles: Architectural Integration of Energy Production and Utilization. *Circulation Research* **89,** 153-159.

Kanai A & Salama G. (1995). Optical Mapping Reveals That Repolarization Spreads Anisotropically and Is Guided by Fiber Orientation in Guinea Pig Hearts. *Circulation Research* **77,** 784-802.

Kaneko T, Tanaka H, Oyamada M, Kawata S & Takamatsu T. (2000). Three Distinct Types of Ca2+ Waves in Langendorff-Perfused Rat Heart Revealed by Real-Time Confocal Microscopy. *Circulation Research* **86,** 1093-1099.

Kanlop N & Sakai T. (2010). Optical mapping study of blebbistatin-induced chaotic electrical activities in isolated rat atrium preparations. *J Physiol Sci* **60,** 109-117.

Karamitsos TD, Dass S, Suttie J, Sever E, Birks J, Holloway CJ, Robson MD, Jerosch-Herold M, Watkins H & Neubauer S. (2013). Blunted Myocardial Oxygenation Response During Vasodilator Stress in Patients With Hypertrophic Cardiomyopathy. *Journal of the American College of Cardiology* **61,** 1169-1176.

Kasahara Y, Kiyatake K, Tatsumi K, Sugito K, Kakusaka I, Yamagata S-i, Ohmori S, Kitada M & Kuriyama T. (1997). Bioactivation of Monocrotaline by P-450 3A in Rat Liver. *Journal of Cardiovascular Pharmacology* **30,** 124-129.

Kassiri Z, Myers R, Kaprielian R, Banijamali HS & Backx PH. (2000). Rate-dependent changes of twitch force duration in rat cardiac trabeculae: a property of the contractile system. *The Journal of Physiology* **524,** 221-231.

Katz WE, Gasior TA, Quinlan JJ, Lazar JM, Firestone L, Griffith BP & Gorcsan IIIJ. (1996). Immediate effects of lung transplantation on right ventricular morphology and function in patients with variable degrees of pulmonary hypertension. *Journal of the American College of Cardiology* **27,** 384-391.

Kaur G, Singh N, Lingeshwar P, Siddiqui HH & Hanif K. (2015). Poly (ADP-ribose) polymerase-1: An emerging target in right ventricle dysfunction associated with pulmonary hypertension. *Pulmonary Pharmacology & Therapeutics* **30,** 66-79.

Kawai M, Hussain M & Orchard CH. (1999). Excitation-contraction coupling in rat ventricular myocytes after formamide-induced detubulation. *American Journal of Physiology - Heart and Circulatory Physiology* **277,** H603-H609.

Keizer J & Smith GD. (1998). Spark-to-wave transition: saltatory transmission of calcium waves in cardiac myocytes. *Biophysical Chemistry* **72,** 87-100.

Keizer J, Smith GD, Ponce-Dawson S & Pearson JE. (1998). Saltatory Propagation of Ca2+ Waves by Ca2+ Sparks. *Biophysical journal* **75,** 595-600.

Kemi OJ, Arbo I, Høydal MA, Loennechen JP, Wisløff U, Smith GL & Ellingsen Ø. (2006). Reduced pH and contractility in failing rat cardiomyocytes. *Acta Physiologica* **188,** 185-193.

Kendall M, Akhlaghi S, Hughes B & Lewis H. (1990). Is Metoprolol CR/ZOK More Selective Than Conventional Metoprolol and Atenolol? *The Journal of Clinical Pharmacology* **30,** S98-S102.

Kentish JC, McCloskey DT, Layland J, Palmer S, Leiden JM, Martin AF & Solaro RJ. (2001). Phosphorylation of Troponin I by Protein Kinase A Accelerates Relaxation and Crossbridge Cycle Kinetics in Mouse Ventricular Muscle. *Circulation Research* **88,** 1059-1065.

Kerckhoffs RCP, Omens J & McCulloch AD. (2012). A single strain-based growth law predicts concentric and eccentric cardiac growth during pressure and volume overload. *Mechanics research communications* **42,** 40-50.

Khalafbeigui F, Suga H & Sagawa K. (1979). Left ventricular systolic pressure-volume area correlates with oxygen consumption. *American Journal of Physiology - Heart and Circulatory Physiology* **237,** H566-H569.

Khuchua ZA, Qin W, Boero J, Cheng J, Payne RM, Saks VA & Strauss AW. (1998). Octamer Formation and Coupling of Cardiac Sarcomeric Mitochondrial Creatine Kinase Are Mediated by Charged N-terminal Residues. *Journal of Biological Chemistry* **273,** 22990-22996.

Kilbaugh TJ, Karlsson M, Byro M, Bebee A, Ralston J, Sullivan S, Duhaime A-C, Hansson MJ, Elmér E & Margulies SS. (2015). Mitochondrial bioenergetic alterations after focal traumatic brain injury in the immature brain. *Experimental Neurology* **271,** 136-144.

Kindo M, GERELLI S, BOUITBIR J, CHARLES A-L, ZOLL J, HOANG MINH T, MONASSIER L, FAVRET F, PIQUARD F & GENY B. (2012). Pressure overload-induced mild cardiac hypertrophy reduces left ventricular transmural differences in mitochondrial respiratory chain activity and increases oxidative stress. *Frontiers in Physiology* **3**.

King NM, Methawasin M, Nedrud J, Harrell N, Chung CS, Helmes M & Granzier H. (2011). Mouse intact cardiac myocyte mechanics: cross-bridge and titin-based stress in unactivated cells. *The Journal of general physiology* **137,** 81-91.

Kiriazis H, Wang K, Xu Q, Gao XM, Ming Z, Su Y, Moore XL, Lambert G, Gibbs ME, Dart AM & Du XJ. (2008). Knockout of β(1)- and β(2)-adrenoceptors attenuates pressure overload-induced cardiac hypertrophy and fibrosis. *British Journal of Pharmacology* **153,** 684-692.

Kitabatake A, Inoue M, Asao M, Masuyama T, Tanouchi J, Morita T, Mishima M, Uematsu M, Shimazu T, Hori M & Abe H. (1983). Noninvasive

evaluation of pulmonary hypertension by a pulsed Doppler technique. *Circulation* **68,** 302-309.

Kjaergaard J, Akkan D, Iversen KK, Køber L, Torp-Pedersen C & Hassager C. (2007). Right ventricular dysfunction as an independent predictor of short- and long-term mortality in patients with heart failure. *European Journal of Heart Failure* **9,** 610-616.

Knöll R, Hoshijima M, Hoffman HM, Person V, Lorenzen-Schmidt I, Bang M-L, Hayashi T, Shiga N, Yasukawa H, Schaper W, McKenna W, Yokoyama M, Schork NJ, Omens JH, McCulloch AD, Kimura A, Gregorio CC, Poller W, Schaper J, Schultheiss HP & Chien KR. (2002). The Cardiac Mechanical Stretch Sensor Machinery Involves a Z Disc Complex that Is Defective in a Subset of Human Dilated Cardiomyopathy. *Cell* **111,** 943-955.

Kobayashi H, Yoshimura Y, Suzuki H & Hosoda Y. (1994). Regional difference of capillary-to-fiber ratio in the heart of monocrotaline-treated rats. *Basic Research in Cardiology* **89,** 118-127.

Kobayashi T, Jin L & de Tombe PP. (2008). Cardiac thin filament regulation. *Pflugers Archiv : European journal of physiology* **457,** 37-46.

Koch G, Franz I-W & Lohmann FW. (1981). Effects of Short-Term and Long-Term Treatment with Cardio-Selective and non-Selective β-Receptor Blockade on Carbohydrate and Lipid Metabolism and on Plasma Catecholamines at Rest and during Exercise. *Clinical Science* **61,** 433s-435s.

Kockskämper J, von Lewinski D, Khafaga M, Elgner A, Grimm M, Eschenhagen T, Gottlieb PA, Sachs F & Pieske B. (2008). The slow force response to stretch in atrial and ventricular myocardium from human heart: Functional relevance and subcellular mechanisms. *Progress in Biophysics and Molecular Biology* **97,** 250-267.

Kögler H, Hartmann O, Leineweber K, Nguyen van P, Schott P, Brodde O-E & Hasenfuss G. (2003). Mechanical Load-Dependent Regulation of Gene Expression in Monocrotaline-Induced Right Ventricular Hypertrophy in the Rat. *Circulation Research* **93,** 230-237.

Kohl P, Nesbitt AD, Cooper PJ & Lei M. (2001). Sudden cardiac death by Commotio cordis: role of mechano—electric feedback. *Cardiovascular Research* **50,** 280-289.

Kolega J. (2004). Phototoxicity and photoinactivation of blebbistatin in UV and visible light. *Biochemical and Biophysical Research Communications* **320,** 1020-1025.

Konhilas JP, Irving TC & de Tombe PP. (2002). Myofilament Calcium Sensitivity in Skinned Rat Cardiac Trabeculae: Role of Interfilament Spacing. *Circulation Research* **90,** 59-65.

Konorev EA, Hogg N & Kalyanaraman B. (1998). Rapid and irreversible inhibition of creatine kinase by peroxynitrite. *FEBS Letters* **427,** 171-174.

Kooij V, Boontje N, Zaremba R, Jaquet K, dos Remedios C, Stienen GM & van der Velden J. (2010). Protein kinase C α and ε phosphorylation of troponin and myosin binding protein C reduce Ca2+ sensitivity in human myocardium. *Basic Research in Cardiology* **105,** 289-300.

Korinek J, Anagnostopoulos PC, Pislaru C, Dzeja P, Seward JB, Terzic A & Belohlavek M. (2004). Both systolic and diastolic dysfunction characterize nonischemic inhibition of myocardial energy metabolism: An experimental strain rate echocardiographic study. *Journal of the American Society of Echocardiography* **17,** 1239-1244.

Korn ED. (1969). Cell membranes: structure and synthesis. *Annu Rev Biochem* **38,** 263-288.

Korstjens IJM, Rouws CHFC, Van Der Laarse WJ, Van Der Zee L & Stienen GJM. (2002). Myocardial force development and structural changes associated with monocrotaline induced cardiac hypertrophy and heart failure. *Journal of Muscle Research and Cell Motility* **23,** 93-102.

Kosanovic D, Kojonazarov B, Luitel H, Dahal B, Sydykov A, Cornitescu T, Janssen W, Brandes R, Davie N, Ghofrani H, Weissmann N, Grimminger F, Seeger W & Schermuly R. (2011). Therapeutic efficacy of TBC3711 in monocrotaline-induced pulmonary hypertension. *Respiratory Research* **12,** 87.

Kovács M, Tóth J, Hetényi C, Málnási-Csizmadia A & Sellers JR. (2004). Mechanism of Blebbistatin Inhibition of Myosin II. *Journal of Biological Chemistry* **279,** 35557-35563.

Kraft T, Hornemann T, Stolz M, Nier V & Wallimann T. (2000). Coupling of creatine kinase to glycolytic enzymes at the sarcomeric I-band of skeletal muscle: a biochemical study in situ. *Journal of Muscle Research and Cell Motility* **21,** 691-703.

Kraft T, Messerli M, Rothen-Rutishauser B, Perriard JC, Wallimann T & Brenner B. (1995). Equilibration and exchange of fluorescently labeled molecules in skinned skeletal muscle fibers visualized by confocal microscopy. *Biophysical journal* **69,** 1246-1258.

Krogh A. (1919). The number and distribution of capillaries in muscles with calculations of the oxygen pressure head necessary for supplying the tissue. *The Journal of Physiology* **52,** 409-415.

Kurihara S, Saeki Y, Hongo K, Tanaka E & Sudo N. (1990). Effects of Length Change on Intracellular Ca²⁺ Transients in Ferret Ventricular Muscle Treated with 2,3-Buranedione Monoxime (BDM). *The Japanese Journal of Physiology* **40,** 915-920.

Kurzyna M & Torbicki A. (2007). Neurohormonal modulation in right ventricular failure. *European Heart Journal Supplements* **9,** H35-H40.

Kuschel M, Zhou Y-Y, Cheng H, Zhang S-J, Chen Y, Lakatta EG & Xiao R-P. (1999). Gi Protein-mediated Functional Compartmentalization of Cardiac β2-Adrenergic Signaling. *Journal of Biological Chemistry* **274,** 22048-22052.

Kuum M, Kaasik A, Joubert F, Ventura-Clapier R & Veksler V. (2009). Energetic state is a strong regulator of sarcoplasmic reticulum Ca^{2+} loss in cardiac muscle: different efficiencies of different energy sources. *Cardiovascular Research* **83,** 89-96.

Kuznetsov AV, Khuchua ZA, Vassil'eva EV, Medved'eva NV & Saks VA. (1989). Heart mitochondrial creatine kinase revisited: The outer mitochondrial membrane is not important for coupling of phosphocreatine production to oxidative phosphorylation. *Archives of Biochemistry and Biophysics* **268,** 176-190.

Kuznetsov AV, Schneeberger S, Seiler R, Brandacher G, Mark W, Steurer W, Saks V, Usson Y, Margreiter R & Gnaiger E. (2004). *Mitochondrial defects and heterogeneous cytochrome c release after cardiac cold ischemia and reperfusion*, vol. 286.

Kuznetsov AV, Veksler V, Gellerich FN, Saks V, Margreiter R & Kunz WS. (2008). Analysis of mitochondrial function in situ in permeabilized muscle fibers, tissues and cells. *Nat Protocols* **3,** 965-976.

Lakatta EG, Maltsev VA & Vinogradova TM. (2010). A Coupled SYSTEM of Intracellular Ca2+ Clocks and Surface Membrane Voltage Clocks Controls the Timekeeping Mechanism of the Heart's Pacemaker. *Circulation Research* **106,** 659-673.

Lamberts RR, Hamdani N, Soekhoe TW, Boontje NM, Zaremba R, Walker LA, de Tombe PP, van der Velden J & Stienen GJM. (2007a). Frequency-dependent myofilament Ca^{2+} desensitization in failing rat myocardium. *The Journal of Physiology* **582,** 695-709.

Lamberts RR, Vaessen RJ, Westerhof N & Stienen GJM. (2007b). Right ventricular hypertrophy causes impairment of left ventricular diastolic function in the rat. *Basic Research in Cardiology* **102,** 19-27.

Lancaster MK & Harrison SM. (1998). Changes in contraction, cytosolic Ca2+ and pH during metabolic inhibition and upon restoration of mitochondrial

respiration in rat ventricular myocytes. *Experimental Physiology* **83,** 349-360.

Landmesser U, Dikalov S, Price SR, McCann L, Fukai T, Holland SM, Mitch WE & Harrison DG. (2003). Oxidation of tetrahydrobiopterin leads to uncoupling of endothelial cell nitric oxide synthase in hypertension. *The Journal of Clinical Investigation* **111,** 1201-1209.

Larsen S, Nielsen J, Hansen CN, Nielsen LB, Wibrand F, Stride N, Schroder HD, Boushel R, Helge JW, Dela F & Hey-Mogensen M. (2012). Biomarkers of mitochondrial content in skeletal muscle of healthy young human subjects. *The Journal of Physiology* **590,** 3349-3360.

Laser A, Neubauer S, Tian R, Hu K, Gaudron P, Ingwall JS & Ertl G. (1996). Long-term beta-blocker treatment prevents chronic creatine kinase and lactate dehydrogenase system changes in rat hearts after myocardial infarction. *Journal of the American College of Cardiology* **27,** 487-493.

Le Guennec JY, Peineau N, Argibay JA, Mongo KG & Garnier D. (1990). A new method of attachment of isolated mammalian ventricular myocytes for tension recording: Length dependence of passive and active tension. *Journal of Molecular and Cellular Cardiology* **22,** 1083-1093.

Lee JK, Kodama I, Honjo H, Anno T, Kamiya K & Toyama J. (1997). Stage-dependent changes in membrane currents in rats with monocrotaline-induced right ventricular hypertrophy. *American Journal of Physiology - Heart and Circulatory Physiology* **272,** H2833-H2842.

Lee U, Lee I, Lee BK & Kang HE. (2013). Faster non-renal clearance of metoprolol in streptozotocin-induced diabetes mellitus rats. *European Journal of Pharmaceutical Sciences* **50,** 447-453.

Leineweber K, Brandt K, Wludyka B, Beilfuß A, Pönicke K, Heinroth-Hoffmann I & Brodde O-E. (2002). Ventricular Hypertrophy Plus Neurohumoral Activation Is Necessary to Alter the Cardiac β-Adrenoceptor System in Experimental Heart Failure. *Circulation Research* **91,** 1056-1062.

Leineweber K, Seyfarth T, Abraham G, Gerbershagen H-P, Heinroth-Hoffmann I, Pönicke K & Brodde O-E. (2003). Cardiac β-Adrenoceptor Changes in Monocrotaline-Treated Rats: Differences Between Membrane Preparations From Whole Ventricles and Isolated Ventricular Cardiomyocytes. *Journal of Cardiovascular Pharmacology* **41,** 333-342.

Lemieux H, Semsroth S, Antretter H, Höfer D & Gnaiger E. (2011a). Mitochondrial respiratory control and early defects of oxidative phosphorylation in the failing human heart. *The International Journal of Biochemistry & Cell Biology* **43,** 1729-1738.

Lemieux H, Votion MD & Gnaiger E. (2011b). Mitochondrial respiration in permeabilized fibres: needle biopsies from horse skeletal muscle. *Mitochondrial Physiology Network* **12,** 1-4.

Lemke T, Welling A, Christel CJ, Blaich A, Bernhard D, Lenhardt P, Hofmann F & Moosmang S. (2008). Unchanged β-Adrenergic Stimulation of Cardiac L-type Calcium Channels in Cav1.2 Phosphorylation Site S1928A Mutant Mice. *Journal of Biological Chemistry* **283,** 34738-34744.

Lenaerts I, Bito V, Heinzel FR, Driesen RB, Holemans P, D'hooge J, Heidbüchel H, Sipido KR & Willems R. (2009). Ultrastructural and Functional Remodeling of the Coupling Between Ca2+ Influx and Sarcoplasmic Reticulum Ca2+ Release in Right Atrial Myocytes From Experimental Persistent Atrial Fibrillation. *Circulation Research* **105,** 876-885.

Lewis JF, Kuo LC, Nelson JG, Limacher MC & Quinones MA. (1984). Pulsed Doppler echocardiographic determination of stroke volume and cardiac output: clinical validation of two new methods using the apical window. *Circulation* **70,** 425-431.

Li K-L, Rieck D, Solaro RJ & Dong W. (2014). In Situ Time-Resolved FRET Reveals Effects of Sarcomere Length on Cardiac Thin-Filament Activation. *Biophysical journal* **107,** 682-693.

Liao Z, Lockhead D, Larson ED & Proenza C. (2010). Phosphorylation and modulation of hyperpolarization-activated HCN4 channels by protein kinase A in the mouse sinoatrial node. *The Journal of General Physiology* **136,** 247-258.

Liguo C, John L, Maria A, Jason O, Arvinder D & Luiz B. (2013). Direct Evidence Of Unprovoked Arrhythmias In Telemetered, Conscious Rats With Chronic Pulmonary Artery Hypertension. In *C64 EXPERIMENTAL MODELS OF PULMONARY VASCULAR DISEASE II*, pp. A4648-A4648. American Thoracic Society.

Liles J, Oliver J, Chi L, Dhalla A & Belardinelli L. (2012). Ranolazine Reduces Monocrotaline-induced Pulmonary Hypertension when Administered Following Disease Induction. *Circulation* **126,** A11990.

Limas CJ & Limas C. (1990). Effects of xamoterol on the reversible cycling of cardiac beta-adrenoceptors. *Journal of Cardiovascular Pharmacology* **16,** 945-951.

Ling Y, Johnson MK, Kiely DG, Condliffe R, Elliot CA, Gibbs JSR, Howard LS, Pepke-Zaba J, Sheares KKK, Corris PA, Fisher AJ, Lordan JL, Gaine S, Coghlan JG, Wort SJ, Gatzoulis MA & Peacock AJ. (2012). Changing Demographics, Epidemiology, and Survival of Incident Pulmonary Arterial Hypertension. *American Journal of Respiratory and Critical Care Medicine* **186,** 790-796.

Liu R, Ramani B, Soto D, De Arcangelis V & Xiang Y. (2009). Agonist Dose-dependent Phosphorylation by Protein Kinase A and G Protein-coupled Receptor Kinase Regulates β2 Adrenoceptor Coupling to Gi Proteins in Cardiomyocytes. *Journal of Biological Chemistry* **284,** 32279-32287.

Lohmann K. (1934). Uber die enzymatische aufspaltung der kreatinphosphorsaure; Zugleich ein beitrag zum chemismus der muskelkontraktion. *Biochem Z* **271,** 264-277.

López-Sendó J, Swedberg K, McMurray J, Tamargo J, Maggioni AP, Dargie H, Tendera M, Waagstein F, Kjekshus J, Lechat P, Pedersen CT, Priori SG, Alonso García MA, Blanc J-J, Budaj A, Cowie M, Dean V, Deckers J, Fernandez Burgos E, Lekakis J, Lindahl B, Mazzotta G, McGregor K, Morais J, Oto A, Smiseth OA, Ardissino D, Avendano C, Lundqvist CB, ment DC, Drexler H, Ferrari R, Fox KA, Julian D, Kearney P, Klein W, ber LK, Mancia G, Nieminen M, Ruzyllo W, Simoons M, Thygesen K, Tognoni G, Tritto I & Wallentin L. (2004). Expert consensus document on β-adrenergic receptor blockers. *The Task Force on Beta-Blockers of the European Society of Cardiology* **25,** 1341-1362.

Lorentzon M, Råmunddal T, Bollano E, Soussi B, Waagstein F & Omerovic E. (2007). In Vivo Effects of Myocardial Creatine Depletion on Left Ventricular Function, Morphology, and Energy Metabolism—Consequences in Acute Myocardial Infarction. *Journal of Cardiac Failure* **13,** 230-237.

Lorenz CH, Walker ES, Morgan VL, Klein SS & Graham TP. (1999). Normal human right and left ventricular mass, systolic function, and gender differences by cine magnetic resonance imaging. *J Cardiov Magn Reson* **1,** 7-21.

Lou Q, Li W & Efimov IR. (2012). The role of dynamic instability and wavelength in arrhythmia maintenance as revealed by panoramic imaging with blebbistatin vs. 2,3-butanedione monoxime. *American Journal of Physiology - Heart and Circulatory Physiology* **302,** H262-H269.

Louch WE, Bito V, Heinzel FR, Macianskiene R, Vanhaecke J, Flameng W, Mubagwa K & Sipido KR. (2004). Reduced synchrony of Ca2+ release with loss of T-tubules—a comparison to Ca2+ release in human failing cardiomyocytes. *Cardiovascular Research* **62,** 63-73.

Louch WE, Mørk HK, Sexton J, Strømme TA, Laake P, Sjaastad I & Sejersted OM. (2006). T-tubule disorganization and reduced synchrony of Ca2+ release in murine cardiomyocytes following myocardial infarction. *The Journal of Physiology* **574,** 519-533.

Loughrey CM, Seidler T, Miller SLW, Prestle J, MacEachern KE, Reynolds DF, Hasenfuss G & Smith GL. (2004). Over-expression of FK506-binding protein FKBP12.6 alters excitation-contraction coupling in adult rabbit cardiomyocytes. *J Physiol-London* **556,** 919-934.

Lourenço AP, Roncon-Albuquerque R, Brás-Silva C, Faria B, Wieland J, Henriques-Coelho T, Correia-Pinto J & Leite-Moreira AF. (2006). Myocardial dysfunction and neurohumoral activation without remodeling in left ventricle of monocrotaline-induced pulmonary hypertensive rats. *American Journal of Physiology - Heart and Circulatory Physiology* **291,** H1587-H1594.

Lowensohn HS, Khouri EM, Gregg DE, Pyle RL & Patterson RE. (1976). Phasic right coronary artery blood flow in conscious dogs with normal and elevated right ventricular pressures. *Circulation Research* **39,** 760-766.

Lu X, Ginsburg KS, Kettlewell S, Bossuyt J, Smith GL & Bers DM. (2013). Measuring Local Gradients of Intramitochondrial [Ca2+] in Cardiac Myocytes During Sarcoplasmic Reticulum Ca2+ Release. *Circulation Research* **112,** 424-431.

Luers C, Fialka F, Elgner A, Zhu D, Kockskämper J, von Lewinski D & Pieske B. (2005). Stretch-dependent modulation of [Na+]i, [Ca2+]i, and pHi in rabbit myocardium–a mechanism for the slow force response. *Cardiovascular Research* **68,** 454-463.

Lukyanenko V & Györke S. (1999). Ca2+ sparks and Ca2+ waves in saponin-permeabilized rat ventricular myocytes. *The Journal of Physiology* **521,** 575-585.

Luttrell LM & Lefkowitz RJ. (2002). The role of β-arrestins in the termination and transduction of G-protein-coupled receptor signals. *Journal of Cell Science* **115,** 455-465.

Lyon AR, Nikolaev VO, Miragoli M, Sikkel MB, Paur H, Benard L, Hulot J-S, Kohlbrenner E, Hajjar RJ, Peters NS, Korchev YE, Macleod KT, Harding SE & Gorelik J. (2012). Plasticity of Surface Structures and β2-Adrenergic Receptor Localization in Failing Ventricular Cardiomyocytes During Recovery From Heart Failure. *Circulation: Heart Failure* **5,** 357-365.

Maack C, Cremers B, Flesch M, Höper A, Südkamp M & Böhm M. (2000). Different intrinsic activities of bucindolol, carvedilol and metoprolol in human failing myocardium. *British Journal of Pharmacology* **130,** 1131-1139.

MacDonald JR, Oellermann M, Rynbeck S, Chang G, Ruggiero K, Cooper GJS & Hickey AJR. (2011). *Transmural differences in respiratory capacity across the rat left ventricle in health, aging, and streptozotocin-induced diabetes mellitus: evidence that mitochondrial dysfunction begins in the subepicardium*, vol. 300.

MacDougall DA, Agarwal SR, Stopford EA, Chu H, Collins JA, Longster AL, Colyer J, Harvey RD & Calaghan S. (2012). Caveolae compartmentalise

β2-adrenoceptor signals by curtailing cAMP production and maintaining phosphatase activity in the sarcoplasmic reticulum of the adult ventricular myocyte. *Journal of Molecular and Cellular Cardiology* **52,** 388-400.

Maier LS & Bers DM. (2007). Role of Ca2+/calmodulin-dependent protein kinase (CaMK) in excitation–contraction coupling in the heart. *Cardiovascular Research* **73,** 631-640.

Maier LS, Bers DM & Pieske B. (2000). Differences in Ca2+-Handling and Sarcoplasmic Reticulum Ca2+-Content in Isolated Rat and Rabbit Myocardium. *Journal of Molecular and Cellular Cardiology* **32,** 2249-2258.

Maldonado EN, Gooz M, DeHart DN & Lemasters JJ. (2015). VDAC Opening Drugs to Induce Mitochondrial Dysfunction and Cell Death. *Biophysical journal* **108,** 369a.

Maldonado EN, Patnaik J, Mullins MR & Lemasters JJ. (2010). Free Tubulin Modulates Mitochondrial Membrane Potential in Cancer Cells. *Cancer research* **70,** 10192-10201.

Marchese A & Trejo J. (2013). Ubiquitin-dependent regulation of G protein-coupled receptor trafficking and signaling. *Cellular Signalling* **25,** 707-716.

Maron BA & Leopold JA. (2015). Emerging Concepts in the Molecular Basis of Pulmonary Arterial Hypertension: Part II: Neurohormonal Signaling Contributes to the Pulmonary Vascular and Right Ventricular Pathophenotype of Pulmonary Arterial Hypertension. *Circulation* **131,** 2079-2091.

Martini FH. (2006). *Fundamentals of Anatomy & Physiology*. Pearson.

Marx SO, Reiken S, Hisamatsu Y, Jayaraman T, Burkhoff D, Rosemblit N & Marks AR. (2000). PKA Phosphorylation Dissociates FKBP12.6 from the Calcium Release Channel (Ryanodine Receptor): Defective Regulation in Failing Hearts. *Cell* **101,** 365-376.

Matthews JC & McLaughlin V. (2008). Acute Right Ventricular Failure in the Setting of Acute Pulmonary Embolism or Chronic Pulmonary Hypertension: A Detailed Review of the Pathophysiology, Diagnosis, and Management. *Current Cardiology Reviews* **4,** 49-59.

Mattiazzi A, Mundiña-Weilenmann C, Guoxiang C, Vittone L & Kranias E. (2005). Role of phospholamban phosphorylation on Thr17 in cardiac physiological and pathological conditions. *Cardiovascular Research* **68,** 366-375.

Mattocks AR, Legg RF & Jukes R. (1990). Trapping of short-lived electrophilic metabolites of pyrrolizidine alkaloids escaping from perfused rat liver. *Toxicology Letters* **54,** 93-99.

McCormack JG, Halestrap AP & Denton RM. (1990). Role of calcium ions in regulation of mammalian intramitochondrial metabolism. *Physiological Reviews* **70,** 391-425.

McCrossan ZA, Billeter R & White E. (2004). Transmural changes in size, contractile and electrical properties of SHR left ventricular myocytes during compensated hypertrophy. *Cardiovascular Research* **63,** 283-292.

McKee PA, Castelli WP, McNamara PM & Kannel WB. (1971). The Natural History of Congestive Heart Failure: The Framingham Study. *New England Journal of Medicine* **285,** 1441-1446.

McLaughlin V, Channick R, Ghofrani H-A, LeMarie J-C, Naeije R, Packer M, Souza R, Tapson V, Tolson J & Hoeper M. (2014). Effect of bosentan and sildenafil combination therapy on morbidity and mortality in pulmonary arterial hypertension (pah): Results from the compass-2 study. *Chest* **146,** 860A-860A.

McLaughlin VV, Channick R, Chin K, Frey A, Gaine S, Ghofrani A, Hoeper M, Lang I, Preiss R, Rubin LJ, Simonneau G, Sitbon O, Stefani M, Tapson V & Galiè N. (2015). Effect of selexipag on morbidity/mortality in pulmonary arterial hypertension: results of the GRIPHON study. *Journal of the American College of Cardiology* **65**.

McLaughlin VV, Gaine SP, Howard LS, Leuchte HH, Mathier MA, Mehta S, Palazzini M, Park MH, Tapson VF & Sitbon O. (2013). Treatment Goals of Pulmonary Hypertension. *Journal of the American College of Cardiology* **62,** D73-D81.

McMartin L & Summers RJ. (1999). Functional analysis of desensitization of the β-adrenoceptor signalling pathway in rat cardiac tissues following chronic isoprenaline infusion. *British Journal of Pharmacology* **127,** 1012-1020.

Medugorac I. (1982). Characterization of intramuscular collagen in the mammalian left ventricle. *Basic Research in Cardiology* **77,** 589-598.

Méry PF, Lohmann SM, Walter U & Fischmeister R. (1991). Ca2+ current is regulated by cyclic GMP-dependent protein kinase in mammalian cardiac myocytes. *Proceedings of the National Academy of Sciences* **88,** 1197-1201.

Méry PF, Pavoine C, Belhassen L, Pecker F & Fischmeister R. (1993). Nitric oxide regulates cardiac Ca2+ current. Involvement of cGMP-inhibited and cGMP-stimulated phosphodiesterases through guanylyl cyclase activation. *Journal of Biological Chemistry* **268,** 26286-26295.

Meyrick B & Reid L. (1980). Hypoxia-induced structural changes in the media and adventitia of the rat hilar pulmonary artery and their regression. *The American Journal of Pathology* **100,** 151-178.

Mihm Michael J & Bauer John A. (2002). Peroxynitrite-induced inhibition and nitration of cardiac myofibrillar creatine kinase. *Biochimie* **84,** 1013-1019.

Mik EG, Ince C, Eerbeek O, Heinen A, Stap J, Hooibrink B, Schumacher CA, Balestra GM, Johannes T, Beek JF, Nieuwenhuis AF, van Horssen P, Spaan JA & Zuurbier CJ. (2009). Mitochondrial oxygen tension within the heart. *Journal of Molecular and Cellular Cardiology* **46,** 943-951.

Mik EG, Johannes T, Zuurbier CJ, Heinen A, Houben-Weerts JHPM, Balestra GM, Stap J, Beek JF & Ince C. (2008). In Vivo Mitochondrial Oxygen Tension Measured by a Delayed Fluorescence Lifetime Technique. *Biophysical journal* **95,** 3977-3990.

Milani-Nejad N, Canan BD, Elnakish MT, Davis JP, Chung J-H, Fedorov V, Binkley PF, Higgins RSD, Kilic A, Mohler PJ & Janssen PML. (2015). The Frank-Starling Mechanism Involves Deceleration of Cross-Bridge Kinetics and is Preserved in Failing Human Right Ventricular Myocardium. *American Journal of Physiology - Heart and Circulatory Physiology*.

Minamikawa T, Cody SH & Williams DA. (1997). In situ visualization of spontaneous calcium waves within perfused whole rat heart by confocal imaging. *American Journal of Physiology - Heart and Circulatory Physiology* **272,** H236-H243.

Miura M, Hirose M, Endoh H, Wakayama Y, Sugai Y, Nakano M, Fukuda K, Shindoh C, Shirato K & Shimokawa H. (2011). Acceleration of Ca^{2+} Waves in Monocrotaline-Induced Right Ventricular Hypertrophy in the Rat. *Circulation Journal* **75,** 1343-1349.

Miura M, Ishide N, Oda H, Sakurai M, Shinozaki T & Takishima T. (1993). Spatial features of calcium transients during early and delayed afterdepolarizations. *American Journal of Physiology - Heart and Circulatory Physiology* **265,** H439-H444.

Monfredi O, Maltsev VA & Lakatta EG. (2013). Modern Concepts Concerning the Origin of the Heartbeat. *Physiology* **28,** 74-92.

Montani D, Savale L, Natali D, Jaïs X, Herve P, Garcia G, Humbert M, Simonneau G & Sitbon O. (2010). Long-term response to calcium-channel blockers in non-idiopathic pulmonary arterial hypertension. *European Heart Journal* **31,** 1898-1907.

Morimoto S-i, Shimizu K, Yamada K, Hiramitsu S & Hishida H. (1999). Can β-blocker therapy be withdrawn from patients with dilated cardiomyopathy? *American Heart Journal* **138,** 456-459.

Mørk HK, Sjaastad I, Sande JB, Periasamy M, Sejersted OM & Louch WE. (2007). Increased cardiomyocyte function and Ca2+ transients in mice during early congestive heart failure. *Journal of Molecular and Cellular Cardiology* **43,** 177-186.

Mouchaers KTB, Schalij I, Versteilen AMG, Hadi AM, van Nieuw Amerongen GP, van Hinsbergh VWM, Postmus PE, van der Laarse WJ & Vonk-Noordegraaf A. (2009). Endothelin receptor blockade combined with phosphodiesterase-5 inhibition increases right ventricular mitochondrial capacity in pulmonary arterial hypertension. *American Journal of Physiology - Heart and Circulatory Physiology* **297,** H200-H207.

Mulieri LA, Barnes W, Leavitt BJ, Ittleman FP, LeWinter MM, Alpert NR & Maughan DW. (2002). Alterations of Myocardial Dynamic Stiffness Implicating Abnormal Crossbridge Function in Human Mitral Regurgitation Heart Failure. *Circulation Research* **90,** 66-72.

Muller AJ, Baker JF, DuHadaway JB, Ge K, Farmer G, Donover PS, Meade R, Reid C, Grzanna R, Roach AH, Shah N, Soler AP & Prendergast GC. (2003). Targeted Disruption of the Murine Bin1/Amphiphysin II Gene Does Not Disable Endocytosis but Results in Embryonic Cardiomyopathy with Aberrant Myofibril Formation. *Molecular and Cellular Biology* **23,** 4295-4306.

Naeije R. (2010). Treatment of right heart failure on pulmonary arterial hypertension: is going left a step in the right direction? *European Respiratory Review* **19,** 4-6.

Naeije R & Manes A. (2014). The right ventricle in pulmonary arterial hypertension. *European Respiratory Review* **23,** 476-487.

Naeije R & Torbicki A. (1995). More on the noninvasive diagnosis of pulmonary hypertension: Doppler echocardiography revisited. *European Respiratory Journal* **8,** 1445-1449.

Nag AC. (1980). Study of non-muscle cells of the adult mammalian heart - a fine-structural analysis and distribution. *Cytobios* **28,** 41-61.

Nagatsu M, Spinale FG, Koide M, Tagawa H, DeFreitas G, Cooper G & Carabello BA. (2000). Bradycardia and the Role of β-Blockade in the Amelioration of Left Ventricular Dysfunction. *Circulation* **101,** 653-659.

Nakayama Y, Nakanishi N, Sugimachi M, Takaki H, Kyotani S, Satoh T, Okano Y, Kunieda T & Sunagawa K. (1997). Characteristics of Pulmonary Artery Pressure Waveform for Differential Diagnosis of Chronic Pulmonary Thromboembolism and Primary Pulmonary Hypertension. *Journal of the American College of Cardiology* **29,** 1311-1316.

Nance ME, Whitfield JT, Zhu Y, Gibson AK, Hanft LM, Campbell KS, Meininger GA, McDonald KS, Segal SS & Domeier TL. (2015). Attenuated sarcomere lengthening of the aged murine left ventricle observed using two-photon fluorescence microscopy. *American Journal of Physiology - Heart and Circulatory Physiology* **309,** H918-H925.

Nascimben L, Ingwall JS, Pauletto P, Friedrich J, Gwathmey JK, Saks V, Pessina AC & Allen PD. (1996). Creatine Kinase System in Failing and Nonfailing Human Myocardium. *Circulation* **94,** 1894-1901.

Natali AJ, Fowler ED, Calaghan S & White E. (2015). Voluntary exercise delays heart failure onset in rats with pulmonary artery hypertension. *Am J Physiol Heart Circ Physiol* **309,** 421-424.

Natali AJ, Wilson LA, Peckham M, Turner DL, Harrison SM & White E. (2002). Different regional effects of voluntary exercise on the mechanical and electrical properties of rat ventricular myocytes. *The Journal of Physiology* **541,** 863-875.

Nedrud J, Labeit S, Gotthardt M & Granzier H. (2011). Mechanics on Myocardium Deficient in the N2B Region of Titin: The Cardiac-Unique Spring Element Improves Efficiency of the Cardiac Cycle. *Biophysical Journal* **101,** 1385-1392.

Neely JR & Morgan HE. (1974). Relationship between carbohydrate and lipid-metabolism and energy-balance of heart-muscle. *Annu Rev Physiol* **36,** 413-459.

Negretti N, O'Neill SC & Eisner DA. (1993). The relative contributions of different intracellular and sarcolemmal systems to relaxation in rat ventricular myocytes. *Cardiovascular Research* **27,** 1826-1830.

Nerbonne JM. (2000). Molecular basis of functional voltage-gated K+ channel diversity in the mammalian myocardium. *The Journal of Physiology* **525,** 285-298.

Nerbonne JM & Kass RS. (2005). Molecular Physiology of Cardiac Repolarization. *Physiological Reviews* **85,** 1205-1253.

Neubauer S, Horn M, Cramer M, Harre K, Newell JB, Peters W, Pabst T, Ertl G, Hahn D, Ingwall JS & Kochsiek K. (1997). Myocardial Phosphocreatine-to-ATP Ratio Is a Predictor of Mortality in Patients With Dilated Cardiomyopathy. *Circulation* **96,** 2190-2196.

Nichols CG & Lederer WJ. (1990). The regulation of ATP-sensitive K+ channel activity in intact and permeabilized rat ventricular myocytes. *The Journal of Physiology* **423,** 91-110.

Nicholson DW, Ali A, Thornberry NA, Vaillancourt JP, Ding CK, Gallant M, Gareau Y, Griffin PR, Labelle M, Lazebnik YA, Munday NA, Raju SM,

Smulson ME, Yamin T-T, Yu VL & Miller DK. (1995). Identification and inhibition of the ICE/CED-3 protease necessary for mammalian apoptosis. *Nature* **376,** 37-43.

Nikolaev VO, Moshkov A, Lyon AR, Miragoli M, Novak P, Paur H, Lohse MJ, Korchev YE, Harding SE & Gorelik J. (2010). β2-Adrenergic Receptor Redistribution in Heart Failure Changes cAMP Compartmentation. *Science* **327,** 1653-1657.

Nishimura S, Nagai S, Katoh M, Yamashita H, Saeki Y, Okada J-i, Hisada T, Nagai R & Sugiura S. (2005). Microtubules Modulate the Stiffness of Cardiomyocytes Against Shear Stress. *Circulation Research*.

Nishimura S, Yasuda S-i, Katoh M, Yamada KP, Yamashita H, Saeki Y, Sunagawa K, Nagai R, Hisada T & Sugiura S. (2004). Single cell mechanics of rat cardiomyocytes under isometric, unloaded, and physiologically loaded conditions. *American Journal of Physiology - Heart and Circulatory Physiology* **287,** H196-H202.

Nootens M, Kaufmann E, Rector T, Toher C, Judd D, Francis GS & Rich S. (1995). Neurohormonal activation in patients with right ventricular failure from pulmonary hypertension: Relation to hemodynamic variables and endothelin levels. *Journal of the American College of Cardiology* **26,** 1581-1585.

O'Donnell SR & Wanstall JC. (1981). Demonstration of both beta 1- and beta 2-adrenoceptors mediating relaxation of isolated ring preparations of rat pulmonary artery. *British Journal of Pharmacology* **74,** 547-552.

Oikawa M, Kagaya Y, Otani H, Sakuma M, Demachi J, Suzuki J, Takahashi T, Nawata J, Ido T, Watanabe J & Shirato K. (2005). Increased [18F]Fluorodeoxyglucose Accumulation in Right Ventricular Free Wall in Patients With Pulmonary Hypertension and the Effect of Epoprostenol. *Journal of the American College of Cardiology* **45,** 1849-1855.

Okumura K, Kato H, Honjo O, Breitling S, Kuebler W, Sun M & Friedberg M. (2015). Carvedilol improves biventricular fibrosis and function in experimental pulmonary hypertension. *J Mol Med***,** 1-12.

Oldham HG & Clarke SE. (1997). In vitro Identification of the Human Cytochrome P450 Enzymes Involved in the Metabolism of R(+)- and S(−)-Carvedilol. *Drug Metabolism and Disposition* **25,** 970-977.

Omori K & Kotera J. (2007). Overview of PDEs and Their Regulation. *Circulation Research* **100,** 309-327.

Orchard CH & Kentish JC. (1990). Effects of changes of pH on the contractile function of cardiac muscle. *American Journal of Physiology - Cell Physiology* **258,** C967-C981.

Owan TE, Hodge DO, Herges RM, Jacobsen SJ, Roger VL & Redfield MM. (2006). Trends in Prevalence and Outcome of Heart Failure with Preserved Ejection Fraction. *New England Journal of Medicine* **355,** 251-259.

Pacher P, Nagayama T, Mukhopadhyay P, Batkai S & Kass DA. (2008). Measurement of cardiac function using pressure-volume conductance catheter technique in mice and rats. *Nat Protocols* **3,** 1422-1434.

Packer M. (1993). How should physicians view heart failure? The philosophical and physiological evolution of three conceptual models of the disease. *The American Journal of Cardiology* **71,** C3-C11.

Packer M, Medina N & Yushak M. (1984). Hemodynamic and clinical limitations of long-term inotropic therapy with amrinone in patients with severe chronic heart failure. *Circulation* **70,** 1038-1047.

Page E, McCallister LP & Power B. (1971). Stereological Measurements of Cardiac Ultrastructures Implicated in Excitation-Contraction Coupling. *Proceedings of the National Academy of Sciences of the United States of America* **68,** 1465-1466.

Palmer JW, Tandler B & Hoppel CL. (1977). Biochemical properties of subsarcolemmal and interfibrillar mitochondria isolated from rat cardiac muscle. *Journal of Biological Chemistry* **252,** 8731-8739.

Pan LC, Wilson DW, Lame MW, Jones AD & Segall HJ. (1993). COR Pulmonale Is Caused by Monocrotaline and Dehydromonocrotaline, but Not by Glutathione or Cysteine Conjugates of Dihydropyrrolizine. *Toxicology and Applied Pharmacology* **118,** 87-97.

Parikh SS, Zou SZ & Tung L. (1993). Contraction and relaxation of isolated cardiac myocytes of the frog under varying mechanical loads. *Circulation Research* **72,** 297-311.

Park SJ, Zhang J, Ye Y, Ormaza S, Liang P, Bank AJ, Miller LW & Bache RJ. (2002). Myocardial creatine kinase expression after left ventricular assist device support. *Journal of the American College of Cardiology* **39,** 1773-1779.

Parton RG, Way M, Zorzi N & Stang E. (1997). Caveolin-3 Associates with Developing T-tubules during Muscle Differentiation. *The Journal of Cell Biology* **136,** 137-154.

Patel JR, Pleitner JM, Moss RL & Greaser ML. (2012). Magnitude of length-dependent changes in contractile properties varies with titin isoform in rat ventricles. *American Journal of Physiology - Heart and Circulatory Physiology* **302,** H697-H708.

Paulin R & Michelakis ED. (2014). The Metabolic Theory of Pulmonary Arterial Hypertension. *Circulation Research* **115,** 148-164.

Paulin R, Sutendra G, Gurtu V, Dromparis P, Haromy A, Provencher S, Bonnet S & Michelakis ED. (2015). A miR-208–Mef2 Axis Drives the Decompensation of Right Ventricular Function in Pulmonary Hypertension. *Circulation Research* **116,** 56-69.

Peacock A & Ross K. (2010). Pulmonary hypertension: a contraindication to the use of β-adrenoceptor blocking agents. *Thorax* **65,** 454-455.

Perrin S, Chaumais M-C, O'Connell C, Amar D, Savale L, Jaïs X, Montani D, Humbert M, Simonneau G & Sitbon O. (2015). New pharmacotherapy options for pulmonary arterial hypertension. *Expert Opinion on Pharmacotherapy* **16,** 2113-2131.

Perros F, Ranchoux B, Izikki M, Bentebbal S, Happé C, Antigny F, Jourdon P, Dorfmüller P, Lecerf F, Fadel E, Simonneau G, Humbert M, Bogaard HJ & Eddahibi S. (2015). Nebivolol for Improving Endothelial Dysfunction, Pulmonary Vascular Remodeling, and Right Heart Function in Pulmonary Hypertension. *Journal of the American College of Cardiology* **65,** 668-680.

Pesta D & Gnaiger E. (2012). High-Resolution Respirometry: OXPHOS Protocols for Human Cells and Permeabilized Fibers from Small Biopsies of Human Muscle #. In *T Mitochondrial Bioenergetics*, pp. 25-58.

Peter BJ, Kent HM, Mills IG, Vallis Y, Butler PJG, Evans PR & McMahon HT. (2004). BAR Domains as Sensors of Membrane Curvature: The Amphiphysin BAR Structure. *Science* **303,** 495-499.

Pett K & Hauton D. (2012). The effects of asymmetric ventricular filling on left–right ventricular interaction in the normal rat heart. *Pflugers Arch - Eur J Physiol* **464,** 523-534.

Piao L, Fang Y-H, Cadete VJ, Wietholt C, Urboniene D, Toth P, Marsboom G, Zhang H, Haber I, Rehman J, Lopaschuk G & Archer S. (2010). The inhibition of pyruvate dehydrogenase kinase improves impaired cardiac function and electrical remodeling in two models of right ventricular hypertrophy: resuscitating the hibernating right ventricle. *J Mol Med* **88,** 47-60.

Piao L, Fang Y-H, Parikh KS, Ryan JJ, D'Souza KM, Theccanat T, Toth PT, Pogoriler J, Paul J, Blaxall BC, Akhter SA & Archer SL. (2012). GRK2-Mediated Inhibition of Adrenergic and Dopaminergic Signaling in Right Ventricular Hypertrophy: Therapeutic Implications in Pulmonary Hypertension. *Circulation* **126,** 2859-2869.

Pieske B, Maier LS, Bers DM & Hasenfuss G. (1999). Ca2+ Handling and Sarcoplasmic Reticulum Ca2+ Content in Isolated Failing and Nonfailing Human Myocardium. *Circulation Research* **85,** 38-46.

Plante E, Lachance D, Roussel É, Drolet M-C, Arsenault M & Couet J. (2006). Impact of Anesthesia on Echocardiographic Evaluation of Systolic and Diastolic Function in Rats. *Journal of the American Society of Echocardiography* **19,** 1520-1525.

Pleština R & Stoner HB. (1972). Pulmonary oedema in rats given monocrotaline pyrrole. *The Journal of Pathology* **106,** 235-249.

Poláková E, Illaste A, Niggli E & Sobie EA. (2015). Maximal acceleration of Ca2+ release refractoriness by β-adrenergic stimulation requires dual activation of kinases PKA and CaMKII in mouse ventricular myocytes. *The Journal of Physiology* **593,** 1495-1507.

Poole-Wilson PA, Swedberg K, Cleland JGF, Di Lenarda A, Hanrath P, Komajda M, Lubsen J, Lutiger B, Metra M, Remme WJ, Torp-Pedersen C, Scherhag A & Skene A. (2003). Comparison of carvedilol and metoprolol on clinical outcomes in patients with chronic heart failure in the Carvedilol Or Metoprolol European Trial (COMET): randomised controlled trial. *The Lancet* **362,** 7-13.

Popovich M, Kostin S, Branishte T, Kobets V & Kapelko V. (1995). Cellular hypertrophy in cardiomyopathic patients is associated with lower creatine-stimulated mitochondrial respiration. *Molecular and Cellular Biochemistry* **143,** 1-5.

Portman MA, Bhat AM, Cohen MH & Jacobstein MD. (1987). Left ventricular systolic circular index: An echocardiographic measure of transseptal pressure ratio. *American Heart Journal* **114,** 1178-1182.

Powell T & Twist VW. (1976). A rapid technique for the isolation and purification of adult cardiac muscle cells having respiratory control and a tolerance to calcium. *Biochemical and Biophysical Research Communications* **72,** 327-333.

Prabhu SD, Chandrasekar B, Murray DR & Freeman GL. (2000). β-Adrenergic Blockade in Developing Heart Failure: Effects on Myocardial Inflammatory Cytokines, Nitric Oxide, and Remodeling. *Circulation* **101,** 2103-2109.

Price LC, Wort SJ, Perros F, Dorfmüller P, Huertas A, Montani D, Cohen-Kaminsky S & Humbert M. (2012). INflammation in pulmonary arterial hypertension. *Chest* **141,** 210-221.

Prosser BL, Ward CW & Lederer WJ. (2011). X-ROS Signaling: Rapid Mechano-Chemo Transduction in Heart. *Science* **333,** 1440-1445.

Provencher S, Chemla D, Hervé P, Sitbon O, Humbert M & Simonneau G. (2006a). Heart rate responses during the 6-minute walk test in pulmonary arterial hypertension. *European Respiratory Journal* **27,** 114-120.

Provencher S, Herve P, Jais X, Lebrec D, Humbert M, Simonneau G & Sitbon O. (2006b). Deleterious Effects of β-Blockers on Exercise Capacity and Hemodynamics in Patients With Portopulmonary Hypertension. *Gastroenterology* **130,** 120-126.

Puchner EM, Alexandrovich A, Kho AL, Hensen U, Schäfer LV, Brandmeier B, Gräter F, Grubmüller H, Gaub HE & Gautel M. (2008). Mechanoenzymatics of titin kinase. *Proceedings of the National Academy of Sciences* **105,** 13385-13390.

Quaife RA, Chen MY, Lynch D, Badesch DB, Groves BM, Wolfel E, Robertson AD, Bristow MR & Voelkel NF. (2006). Importance of right ventricular end-systolic regional wall stress in idiopathic pulmonary arterial hypertension: A new method for estimation of right ventricular wall stress. *European Journal of Medical Research* **11,** 214-220.

Quaile MP, Rossman EI, Berretta RM, Bratinov G, Kubo H, Houser SR & Margulies KB. (2007). Reduced sarcoplasmic reticulum Ca2+ load mediates impaired contractile reserve in right ventricular pressure overload. *Journal of Molecular and Cellular Cardiology* **43,** 552-563.

Rain S, Handoko ML, Trip P, Gan CT-J, Westerhof N, Stienen GJ, Paulus WJ, Ottenheijm CAC, Marcus JT, Dorfmüller P, Guignabert C, Humbert M, MacDonald P, dos Remedios C, Postmus PE, Saripalli C, Hidalgo CG, Granzier HL, Vonk-Noordegraaf A, van der Velden J & de Man FS. (2013). Right Ventricular Diastolic Impairment in Patients With Pulmonary Arterial Hypertension. *Circulation* **128,** 2016-2025.

Ramos M, Lamé MW, Segall HJ & Wilson DW. (2007). Monocrotaline pyrrole induces Smad Nuclear Accumulation and Altered Signaling Expression in Human Pulmonary Arterial Endothelial Cells. *Vascular pharmacology* **46,** 439-448.

Reagan-Shaw S, Nihal M & Ahmad N. (2008). Dose translation from animal to human studies revisited. *The FASEB Journal* **22,** 659-661.

Redington AN, Gray HH, Hodson ME, Rigby ML & Oldershaw PJ. (1988). Characterisation of the normal right ventricular pressure-volume relation by biplane angiography and simultaneous micromanometer pressure measurements. *British Heart Journal* **59,** 23-30.

Redington AN, Rigby ML, Shinebourne EA & Oldershaw PJ. (1990). Changes in the pressure-volume relation of the right ventricle when its loading conditions are modified. *British Heart Journal* **63,** 45-49.

Redout EM, Wagner MJ, Zuidwijk MJ, Boer C, Musters RJP, van Hardeveld C, Paulus WJ & Simonides WS. (2007). Right-ventricular failure is associated with increased mitochondrial complex II activity and production of reactive oxygen species. *Cardiovascular Research* **75,** 770-781.

Reid MJ, Lamé MW, Morin D, Wilson DW & Segall HJ. (1998). Involvement of cytochrome P450 3A in the metabolism and covalent binding of 14C-monocrotaline in rat liver microsomes. *Journal of Biochemical and Molecular Toxicology* **12,** 157-166.

Reilly AM, Petrou S, Panchal RG & Williams DA. (2001). Restoration of calcium handling properties of adult cardiac myocytes from hypertrophied hearts. *Cell Calcium* **30,** 59-66.

Ren J, Davidoff AJ & Ingwall JS. (2009). Creatine kinase inhibitor iodoacetamide antagonizes calcium-stimulated inotropy in cardiomyocytes. *Clinical and Experimental Pharmacology and Physiology* **36,** 141-145.

Respress JL, van Oort RJ, Li N, Rolim N, Dixit SS, deAlmeida A, Voigt N, Lawrence WS, Skapura DG, Skårdal K, Wisløff U, Wieland T, Ai X, Pogwizd SM, Dobrev D & Wehrens XHT. (2012). Role of RyR2 Phosphorylation at S2814 During Heart Failure Progression. *Circulation Research* **110,** 1474-1483.

Rey M, Weber EW & Hess PD. (2012). Simultaneous Pulmonary and Systemic Blood Pressure and ECG Interval Measurement in Conscious, Freely Moving Rats. *Journal of the American Association for Laboratory Animal Science* **51,** 231-238.

Roberts JT & Wearn JT. (1941). Quantitative changes in the capillary-muscle relationship in human hearts during normal growth and hypertrophy. *American Heart Journal* **21,** 617-633.

Rockman HA, Koch WJ & Lefkowitz RJ. (2002). Seven-transmembrane-spanning receptors and heart function. *Nature* **415,** 206-212.

Rogers SL & Gelfand VI. (2000). Membrane trafficking, organelle transport, and the cytoskeleton. *Current Opinion in Cell Biology* **12,** 57-62.

Rognmo Ø, Moholdt T, Bakken H, Hole T, Mølstad P, Myhr NE, Grimsmo J & Wisløff U. (2012). Cardiovascular Risk of High- Versus Moderate-Intensity Aerobic Exercise in Coronary Heart Disease Patients. *Circulation* **126,** 1436-1440.

Roosimaa M, Põdramägi T, Kadaja L, Ruusalepp A, Paju K, Puhke R, Eimre M, Orlova E, Piirsoo A, Peet N, Gellerich FN & Seppet E. (2013). Dilation of human atria: Increased diffusion restrictions for ADP, overexpression of

hexokinase 2 and its coupling to oxidative phosphorylation in cardiomyocytes. *Mitochondrion* **13,** 399-409.

Rosalki SB. (1967). An improved procedure for serum creatine phosphokinase determination. *J Lab Clin Med* **69,** 696-&.

Rosca MG, Vazquez EJ, Kerner J, Parland W, Chandler MP, Stanley W, Sabbah HN & Hoppel CL. (2008). Cardiac mitochondria in heart failure: decrease in respirasomes and oxidative phosphorylation. *Cardiovascular Research* **80,** 30-39.

Rosenbaum DS, Jackson LE, Smith JM, Garan H, Ruskin JN & Cohen RJ. (1994). Electrical Alternans and Vulnerability to Ventricular Arrhythmias. *New England Journal of Medicine* **330,** 235-241.

Ross PJ, Lewis MJ, Sheridan DJ & Henderson AH. (1981). Adrenergic hypersensitivity after beta-blocker withdrawal. *British Heart Journal* **45,** 637-642.

Rostovtseva TK, Sheldon KL, Hassanzadeh E, Monge C, Saks V, Bezrukov SM & Sackett DL. (2008). Tubulin binding blocks mitochondrial voltage-dependent anion channel and regulates respiration. *Proceedings of the National Academy of Sciences of the United States of America* **105,** 18746-18751.

Roth RA, Dotzlaf LA, Baranyi B, Kuo CH & Hook JB. (1981). Effect of monocrotaline ingestion on liver, kidney, and lung of rats. *Toxicology and Applied Pharmacology* **60,** 193-203.

Rubin LJ, Badesch DB, Barst RJ, Galiè N, Black CM, Keogh A, Pulido T, Frost A, Roux S, Leconte I, Landzberg M & Simonneau G. (2002). Bosentan Therapy for Pulmonary Arterial Hypertension. *New England Journal of Medicine* **346,** 896-903.

Rubin LJ, Mendoza J, Hood M, McGoon M, Barst R, Williams WB, Diehl JH, Crow J & Long W. (1990). Treatment of Primary Pulmonary Hypertension with Continuous Intravenous Prostacyclin (Epoprostenol)Results of a Randomized Trial. *Annals of Internal Medicine* **112,** 485-491.

Rudski LG, Lai WW, Afilalo J, Hua L, Handschumacher MD, Chandrasekaran K, Solomon SD, Louie EK & Schiller NB. (2010). Guidelines for the Echocardiographic Assessment of the Right Heart in Adults: A Report from the American Society of Echocardiography: Endorsed by the European Association of Echocardiography, a registered branch of the European Society of Cardiology, and the Canadian Society of Echocardiography. *Journal of the American Society of Echocardiography* **23,** 685-713.

Ruiter G, de Man FS, Schalij I, Sairras S, Grünberg K, Westerhof N, van der Laarse WJ & Vonk-Noordegraaf A. (2013). Reversibility of the

monocrotaline pulmonary hypertension rat model. *European Respiratory Journal* **42,** 553-556.

Ryan JJ & Archer SL. (2014). The Right Ventricle in Pulmonary Arterial Hypertension: Disorders of Metabolism, Angiogenesis and Adrenergic Signaling in Right Ventricular Failure. *Circulation Research* **115,** 176-188.

Rybin VO, Xu X, Lisanti MP & Steinberg SF. (2000). Differential Targeting of β-Adrenergic Receptor Subtypes and Adenylyl Cyclase to Cardiomyocyte Caveolae: A mechanism to functionally regulate the camp signaling pathway. *Journal of Biological Chemistry* **275,** 41447-41457.

Sabbah H, Sharov V, Lesch M & Goldstein S. (1995). Progression of heart failure: A role for interstitial fibrosis. *Molecular and Cellular Biochemistry* **147,** 29-34.

Sabbah HN, Sharov VG, Gupta RC, Todor A, Singh V & Goldstein S. (2000). Chronic therapy with metoprolol attenuates cardiomyocyte apoptosis in dogs with heart failure. *Journal of the American College of Cardiology* **36,** 1698-1705.

Sahara M, Sata M, Morita T, Nakamura K, Hirata Y & Nagai R. (2007). Diverse Contribution of Bone Marrow–Derived Cells to Vascular Remodeling Associated With Pulmonary Arterial Hypertension and Arterial Neointimal Formation. *Circulation* **115,** 509-517.

Sakamoto T, Limouze J, Combs CA, Straight AF & Sellers JR. (2004). Blebbistatin, a Myosin II Inhibitor, Is Photoinactivated by Blue Light. *Biochemistry* **44,** 584-588.

Sande JB, Sjaastad I, Hoen IB, Bøkenes J, Tønnessen T, Holt E, Lunde PK & Christensen G. (2002). Reduced level of serine16 phosphorylated phospholamban in the failing rat myocardium: a major contributor to reduced SERCA2 activity. *Cardiovascular Research* **53,** 382-391.

Sanguinetti MC & Jurkiewicz NK. (1990). Two components of cardiac delayed rectifier K+ current. Differential sensitivity to block by class III antiarrhythmic agents. *The Journal of General Physiology* **96,** 195-215.

Sano M, Minamino T, Toko H, Miyauchi H, Orimo M, Qin Y, Akazawa H, Tateno K, Kayama Y, Harada M, Shimizu I, Asahara T, Hamada H, Tomita S, Molkentin JD, Zou Y & Komuro I. (2007). p53-induced inhibition of Hif-1 causes cardiac dysfunction during pressure overload. *Nature* **446,** 444-448.

Sato H, Nagai T, Kuppuswamy D, Narishige T, Koide M, Menick DR & Cooper G. (1997). Microtubule Stabilization in Pressure Overload Cardiac Hypertrophy. *The Journal of Cell Biology* **139,** 963-973.

Sato PY, Chuprun JK, Schwartz M & Koch WJ. (2015). The Evolving Impact of G Protein-Coupled Receptor Kinases in Cardiac Health and Disease. *Physiological Reviews* **95,** 377-404.

Satoh H, Delbridge LM, Blatter LA & Bers DM. (1996). Surface:volume relationship in cardiac myocytes studied with confocal microscopy and membrane capacitance measurements: species-dependence and developmental effects. *Biophysical journal* **70,** 1494-1504.

Schäfer S, Ellinghaus P, Janssen W, Kramer F, Lustig K, Milting H, Kast R & Klein M. (2009). Chronic inhibition of phosphodiesterase 5 does not prevent pressure-overload-induced right-ventricular remodelling. *Cardiovascular Research* **82,** 30-39.

Scheffler IE. (2008). *Mitochondria*. Wiley.

Schermuly RT, Kreisselmeier KP, Ghofrani HA, Yilmaz H, Butrous G, Ermert L, Ermert M, Weissmann N, Rose F, Guenther A, Walmrath D, Seeger W & Grimminger F. (2004). Chronic Sildenafil Treatment Inhibits Monocrotaline-induced Pulmonary Hypertension in Rats. *American Journal of Respiratory and Critical Care Medicine* **169,** 39-45.

Schlattner U, Tokarska-Schlattner M & Wallimann T. (2006). Mitochondrial creatine kinase in human health and disease. *Biochimica et Biophysica Acta (BBA) - Molecular Basis of Disease* **1762,** 164-180.

Schott P, Singer SS, Kögler H, Neddermeier D, Leineweber K, Brodde O-E, Regitz-Zagrosek V, Schmidt B, Dihazi H & Hasenfuss G. (2005). Pressure overload and neurohumoral activation differentially affect the myocardial proteome. *PROTEOMICS* **5,** 1372-1381.

Schram G, Pourrier M, Melnyk P & Nattel S. (2002). Differential Distribution of Cardiac Ion Channel Expression as a Basis for Regional Specialization in Electrical Function. *Circulation Research* **90,** 939-950.

Schröder F, Klein G, Fiedler B, Bastein M, Schnasse N, Hillmer A, Ames S, Gambaryan S, Drexler H, Walter U, Lohmann SM & Wollert KC. (2003). Single L-type Ca2+ channel regulation by cGMP-dependent protein kinase type I in adult cardiomyocytes from PKG I transgenic mice. *Cardiovascular Research* **60,** 268-277.

Schwinger RH, Böhm M, Koch A, Schmidt U, Morano I, Eissner HJ, Uberfuhr P, Reichart B & Erdmann E. (1994). The failing human heart is unable to use the Frank-Starling mechanism. *Circulation Research* **74,** 959-969.

Scriven DR, Dan P & Moore ED. (2000). Distribution of proteins implicated in excitation-contraction coupling in rat ventricular myocytes. *Biophysical Journal* **79,** 2682-2691.

Sengupta PP, Tajik AJ, Chandrasekaran K & Khandheria BK. (2008). Twist Mechanics of the Left Ventricle: Principles and Application. *JACC: Cardiovascular Imaging* **1,** 366-376.

Sequeira V, Najafi A, McConnell M, Fowler ED, Bollen IAE, Wüst RCI, dos Remedios C, Helmes M, White E, Stienen GJM, Tardiff J, Kuster DWD & van der Velden J. (2015a). Synergistic role of ADP and Ca2+ in diastolic myocardial stiffness. *The Journal of Physiology* **593,** 3899-3916.

Sequeira V, Najafi A, McConnell M, Fowler ED, Bollen IAE, Wüst RCI, Remedios Cd, Helmes M, White E, Stienen GJM, Tardiff J, Kuster DWD & van der Velden J. (2015b). Synergistic role of ADP and Ca2+ in diastolic myocardial stiffness. *The Journal of Physiology***,** n/a-n/a.

Severinghaus J & Astrup P. (1986). History of blood gas analysis. IV. Leland Clark's oxygen electrode. *J Clin Monitor Comput* **2,** 125-139.

Seyfarth T, Gerbershagen H-P, Giessler C, Leineweber K, Heinroth-Hoffmann I, Pönicke K & Brodde O-E. (2000). The Cardiac β -Adrenoceptor-G-protein(s)-adenylyl Cyclase System in Monocrotaline-treated Rats. *Journal of Molecular and Cellular Cardiology* **32,** 2315-2326.

Shah AM, Spurgeon HA, Sollott SJ, Talo A & Lakatta EG. (1994). 8-bromo-cGMP reduces the myofilament response to Ca2+ in intact cardiac myocytes. *Circulation Research* **74,** 970-978.

Sham JSK, Song L-S, Chen Y, Deng L-H, Stern MD, Lakatta EG & Cheng H. (1998). Termination of Ca2+ release by a local inactivation of ryanodine receptors in cardiac myocytes. *Proceedings of the National Academy of Sciences* **95,** 15096-15101.

Shang W, Lu F, Sun T, Xu J, Li L-L, Wang Y, Wang G, Chen L, Wang X, Cannell MB, Wang S-Q & Cheng H. (2014). Imaging Ca2+ Nanosparks in Heart With a New Targeted Biosensor. *Circulation Research* **114,** 412-420.

Shannon TR & Bers DM. (1997). Assessment of intra-SR free [Ca] and buffering in rat heart. *Biophysical journal* **73,** 1524-1531.

Shannon TR, Ginsburg KS & Bers DM. (2000). Potentiation of Fractional Sarcoplasmic Reticulum Calcium Release by Total and Free Intra-Sarcoplasmic Reticulum Calcium Concentration. *Biophysical journal* **78,** 334-343.

Sharma AM, Pischon T, Hardt S, Kunz I & Luft FC. (2001). Hypothesis: β-Adrenergic Receptor Blockers and Weight Gain : A Systematic Analysis. *Hypertension* **37,** 250-254.

Sharov VG, Todor AV, Silverman N, Goldstein S & Sabbah HN. (2000). Abnormal Mitochondrial Respiration in Failed Human Myocardium. *Journal of Molecular and Cellular Cardiology* **32,** 2361-2367.

Shaw MA, Ostap EM & Goldman YE. (2003). Mechanism of Inhibition of Skeletal Muscle Actomyosin by N-Benzyl-p-toluenesulfonamide†. *Biochemistry* **42,** 6128-6135.

Shen W, Spindler M, Higgins MA, Jin N, Gill RM, Bloem LJ, Ryan TP & Ingwall JS. (2005). The fall in creatine levels and creatine kinase isozyme changes in the failing heart are reversible: Complex post-transcriptional regulation of the components of the CK system. *Journal of Molecular and Cellular Cardiology* **39,** 537-544.

Shiels HA & White E. (2008). The Frank–Starling mechanism in vertebrate cardiac myocytes. *Journal of Experimental Biology* **211,** 2005-2013.

Shiina Y, Funabashi N, Lee K, Daimon M, Sekine T, Kawakubo M, Sekine Y, Takahashi M, Yajima R, Wakatsuki Y, Tanabe N, Kuriyama T & Komuro I. (2009a). Doppler imaging predicts cardiac events in chronic pulmonary thromboembolism. *International Journal of Cardiology* **133,** 167-172.

Shiina Y, Funabashi N, Lee K, Daimon M, Sekine T, Kawakubo M, Takahashi M, Yajima R, Tanabe N, Kuriyama T & Komuro I. (2009b). Right atrium contractility and right ventricular diastolic function assessed by pulsed Tissue Doppler Imaging can predict brain natriuretic peptide in adults with acquired pulmonary hypertension. *International Journal of Cardiology* **135,** 53-59.

Shipley RA, Shipley LJ & Wearn JT. (1937). The capillary supply in normal and hypertrophied hearts of rabbits. *The Journal of Experimental Medicine* **65,** 29-42.

Simonneau G, Robbins IM, Beghetti M, Channick RN, Delcroix M, Denton CP, Elliott CG, Gaine SP, Gladwin MT, Jing Z-C, Krowka MJ, Langleben D, Nakanishi N & Souza R. (2009). Updated Clinical Classification of Pulmonary Hypertension. *Journal of the American College of Cardiology* **54,** S43-S54.

Sitbon O, Humbert M, Jaïs X, Ioos V, Hamid AM, Provencher S, Garcia G, Parent F, Hervé P & Simonneau G. (2005). Long-Term Response to Calcium Channel Blockers in Idiopathic Pulmonary Arterial Hypertension. *Circulation* **111,** 3105-3111.

Sitbon O, Jaïs X, Savale L, Cottin V, Bergot E, Macari EA, Bouvaist H, Dauphin C, Picard F, Bulifon S, Montani D, Humbert M & Simonneau G. (2014). Upfront triple combination therapy in pulmonary arterial hypertension: a pilot study. *European Respiratory Journal* **43,** 1691-1697.

Smith PK, Krohn RI, Hermanson GT, Mallia AK, Gartner FH, Provenzano MD, Fujimoto EK, Goeke NM, Olson BJ & Klenk DC. (1985). Measurement of protein using bicinchoninic acid. *Analytical Biochemistry* **150,** 76-85.

So PP-S, Davies RA, Chandy G, Stewart D, Beanlands RSB, Haddad H, Pugliese C & Mielniczuk LM. (2012). Usefulness of Beta-Blocker Therapy and Outcomes in Patients With Pulmonary Arterial Hypertension. *The American Journal of Cardiology* **109,** 1504-1509.

Soeller C & Baddeley D. (2013). Super-resolution imaging of EC coupling protein distribution in the heart. *Journal of Molecular and Cellular Cardiology* **58,** 32-40.

Soeller C, Crossman D, Gilbert R & Cannell MB. (2007). Analysis of ryanodine receptor clusters in rat and human cardiac myocytes. *Proceedings of the National Academy of Sciences* **104,** 14958-14963.

Söhl G & Willecke K. (2004). Gap junctions and the connexin protein family. *Cardiovascular Research* **62,** 228-232.

Sokolova N, Vendelin M & Birkedal R. (2009). Intracellular diffusion restrictions in isolated cardiomyocytes from rainbow trout. *BMC Cell Biology* **10,** 90.

Souders CA, Bowers SLK & Baudino TA. (2009). Cardiac Fibroblast: The Renaissance Cell. *Circulation Research* **105,** 1164-1176.

Spurgeon HA, duBell WH, Stern MD, Sollott SJ, Ziman BD, Silverman HS, Capogrossi MC, Talo A & Lakatta EG. (1992). Cytosolic calcium and myofilaments in single rat cardiac myocytes achieve a dynamic equilibrium during twitch relaxation. *The Journal of Physiology* **447,** 83-102.

Srere PA. (1969). [1] Citrate synthase: [EC 4.1.3.7. Citrate oxaloacetate-lyase (CoA-acetylating)]. In *Methods in Enzymology*, ed. John ML, pp. 3-11. Academic Press.

Stacher E, Graham BB, Hunt JM, Gandjeva A, Groshong SD, McLaughlin VV, Jessup M, Grizzle WE, Aldred MA, Cool CD & Tuder RM. (2012). Modern Age Pathology of Pulmonary Arterial Hypertension. *American Journal of Respiratory and Critical Care Medicine* **186,** 261-272.

Stachowiak O, Dolder M, Wallimann T & Richter C. (1998). Mitochondrial Creatine Kinase Is a Prime Target of Peroxynitrite-induced Modification and Inactivation. *Journal of Biological Chemistry* **273,** 16694-16699.

Stamler JS, Loh E, Roddy MA, Currie KE & Creager MA. (1994). Nitric oxide regulates basal systemic and pulmonary vascular resistance in healthy humans. *Circulation* **89,** 2035-2040.

Starling MR. (1993). Left ventricular-arterial coupling relations in the normal human heart. *American Heart Journal* **125,** 1659-1666.

Starr I, Jeffers WA & Meade Jr RH. (1943). The absence of conspicuous increments of venous pressure after severe damage to the right ventricle of the dog, with a discussion of the relation between clinical congestive failure and heart disease. *American Heart Journal* **26,** 291-301.

Steele DS & Smith GL. (1993). Effects of 2,3-butanedione monoxime on sarcoplasmic reticulum of saponin-treated rat cardiac muscle. *American Journal of Physiology - Heart and Circulatory Physiology* **265,** H1493-H1500.

Steinberg SF & Brunton LL. (2001). Compartmentation of g protein-coupled signaling pathways in cardiac myocytes. *Annual Review of Pharmacology and Toxicology* **41,** 751-773.

Stolz M & Wallimann T. (1998). Myofibrillar interaction of cytosolic creatine kinase (CK) isoenzymes: allocation of N-terminal binding epitope in MM-CK and BB-CK. *Journal of Cell Science* **111,** 1207-1216.

Stones R, Benoist D, Peckham M & White E. (2013). Microtubule proliferation in right ventricular myocytes of rats with monocrotaline-induced pulmonary hypertension. *Journal of Molecular and Cellular Cardiology* **56,** 91-96.

Stride N, Larsen S, Hey-Mogensen M, Sander K, Lund JT, Gustafsson F, Køber L & Dela F. (2013). Decreased mitochondrial oxidative phosphorylation capacity in the human heart with left ventricular systolic dysfunction. *European Journal of Heart Failure* **15,** 150-157.

Suga H & Sagawa K. (1974). Instantaneous Pressure-Volume Relationships and Their Ratio in the Excised, Supported Canine Left Ventricle. *Circulation Research* **35,** 117-126.

Suga H & Sagawa K. (1979). Accuracy of ventricular lumen volume measurement by intraventricular balloon method. *American Journal of Physiology - Heart and Circulatory Physiology* **236,** H506-H507.

Suga H, SAGAWA K & SHOUKAS AA. (1973). Load Independence of the Instantaneous Pressure-Volume Ratio of the Canine Left Ventricle and Effects of Epinephrine and Heart Rate on the Ratio. *Circulation Research* **32,** 314-322.

Sutendra G, Dromparis P, Paulin R, Zervopoulos S, Haromy A, Nagendran J & Michelakis E. (2013). A metabolic remodeling in right ventricular hypertrophy is associated with decreased angiogenesis and a transition from a compensated to a decompensated state in pulmonary hypertension. *J Mol Med* **91,** 1315-1327.

Szwejkowski BR, Elder DHJ, Shearer F, Jack D, Choy AMJ, Pringle SD, Struthers AD, George J & Lang CC. (2012). Pulmonary hypertension predicts all-cause mortality in patients with heart failure: a retrospective cohort study. *European Journal of Heart Failure* **14,** 162-167.

Takeshima H, Komazaki S, Nishi M, Lino M & Kangawa K. (2000). Junctophilins: A novel family of junctional membrane complex proteins. *Mol Cell* **6,** 11-22.

Tamura T, Onodera T, Said S & Gerdes AM. (1998). Correlation of Myocyte Lengthening to Chamber Dilation in the Spontaneously Hypertensive Heart Failure (SHHF) Rat. *Journal of Molecular and Cellular Cardiology* **30,** 2175-2181.

Tang WHW, Militello M & Francis GS. (2003). In heart failure, all beta-blockers are not necessarily equal. *Cleveland Clinic Journal of Medicine* **70,** 1081-1087.

Taraseviciene-Stewart L, Kasahara Y, Alger L, Hirth P, Mc Mahon G, Waltenberger J, Voelkel NF & Tuder RM. (2001). Inhibition of the VEGF receptor 2 combined with chronic hypoxia causes cell death-dependent pulmonary endothelial cell proliferation and severe pulmonary hypertension. *The FASEB Journal* **15,** 427-438.

Tardiff JC, Hewett TE, Palmer BM, Olsson C, Factor SM, Moore RL, Robbins J & Leinwand LA. (1999). Cardiac troponin T mutations result in allele-specific phenotypes in a mouse model for hypertrophic cardiomyopathy. *The Journal of clinical investigation* **104,** 469-481.

Tasche C, Meyhöfer E & Brenner B. (1999). A force transducer for measuring mechanical properties of single cardiac myocytes. *American Journal of Physiology - Heart and Circulatory Physiology* **277,** H2400-H2408.

ter Veld F, Jeneson JAL & Nicolay K. (2005). Mitochondrial affinity for ADP is twofold lower in creatine kinase knock-out muscles. *FEBS Journal* **272,** 956-965.

Terentyev D, Györke I, Belevych AE, Terentyeva R, Sridhar A, Nishijima Y, Carcache de Blanco E, Khanna S, Sen CK, Cardounel AJ, Carnes CA & Györke S. (2008). Redox Modification of Ryanodine Receptors Contributes to Sarcoplasmic Reticulum Ca2+ Leak in Chronic Heart Failure. *Circulation Research* **103,** 1466-1472.

Thenappan T, Roy SS, Duval S, Glassner-Kolmin C & Gomberg-Maitland M. (2014). β-Blocker Therapy Is Not Associated With Adverse Outcomes in Patients With Pulmonary Arterial Hypertension: A Propensity Score Analysis. *Circulation: Heart Failure* **7,** 903-910.

Tian R, Halow JM, Meyer M, Dillmann WH, Figueredo VM, Ingwall JS & Camacho SA. (1998). Thermodynamic limitation for Ca2+ handling

contributes to decreased contractile reserve in rat hearts. *American Journal of Physiology - Heart and Circulatory Physiology* **275,** H2064-H2071.

Tofovic SP, Salah EM, Mady HH, Jackson EK & Melhem MF. (2005). Estradiol Metabolites Attenuate Monocrotaline-Induced Pulmonary Hypertension in Rats. *Journal of Cardiovascular Pharmacology* **46,** 430-437.

Tomaselli GF & Marbán E. (1999). Electrophysiological remodeling in hypertrophy and heart failure. *Cardiovascular Research* **42,** 270-283.

Tsien RY. (1981). A non-disruptive technique for loading calcium buffers and indicators into cells. *Nature* **290,** 527-528.

Turrens JF & Boveris A. (1980). Generation of superoxide anion by the NADH dehydrogenase of bovine heart mitochondria. *Biochemical Journal* **191,** 421-427.

Tzagoloff A. (1982). *Mitochondria*. Plenum Press.

Uchida T, Yashima M, Gotoh M, Qu Z, Garfinkel A, Weiss JN, Fishbein MC, Mandel WJ, Chen P-S & Karagueuzian HS. (1999). Mechanism of Acceleration of Functional Reentry in the Ventricle: Effects of ATP-Sensitive Potassium Channel Opener. *Circulation* **99,** 704-712.

Ueda H, Kawagishi K, Terasawa F, Nakamura A & Moriizumi T. (2004). Caveolin-3 at the T-tubule Colocalizes with α-actinin in the Adult Murine Cardiac Muscle. *ACTA HISTOCHEMICA ET CYTOCHEMICA* **37,** 373-378.

Ujwal R, Cascio D, Colletier J-P, Faham S, Zhang J, Toro L, Ping P & Abramson J. (2008). The crystal structure of mouse VDAC1 at 2.3 Å resolution reveals mechanistic insights into metabolite gating. *Proceedings of the National Academy of Sciences of the United States of America* **105,** 17742-17747.

Umar S, Lee J-H, de Lange E, Iorga A, Partow-Navid R, Bapat A, van der Laarse A, Saggar R, Saggar R, Ypey DL, Karagueuzian HS & Eghbali M. (2012). Spontaneous Ventricular Fibrillation in Right Ventricular Failure Secondary to Chronic Pulmonary Hypertension / Clinical Perspective. *Circulation: Arrhythmia and Electrophysiology* **5,** 181-190.

Urboniene D, Haber I, Fang Y-H, Thenappan T & Archer SL. (2010). Validation of high-resolution echocardiography and magnetic resonance imaging vs. high-fidelity catheterization in experimental pulmonary hypertension. *American Journal of Physiology - Lung Cellular and Molecular Physiology* **299,** L401-L412.

Van Campen JSJA, Karin De B, Martha W, Handoko ML, Cor PA, Frances SDM, Harm JB & Anton Vonk N. (2014). Beta-Blocker Therapy In

Patients With Idiopathic Pulmonary Arterial Hypertension: A Randomized Controlled Trial. In *A19 LATE BREAKING ABSTRACTS IN CLINICAL TRIALS*, pp. A6569-A6569. American Thoracic Society.

van de Veerdonk MC, Kind T, Marcus JT, Mauritz G-J, Heymans MW, Bogaard H-J, Boonstra A, Marques KMJ, Westerhof N & Vonk-Noordegraaf A. (2011). Progressive Right Ventricular Dysfunction in Patients With Pulmonary Arterial Hypertension Responding to Therapy. *Journal of the American College of Cardiology* **58,** 2511-2519.

van Wolferen SA, Marcus JT, Boonstra A, Marques KMJ, Bronzwaer JGF, Spreeuwenberg MD, Postmus PE & Vonk-Noordegraaf A. (2007). Prognostic value of right ventricular mass, volume, and function in idiopathic pulmonary arterial hypertension. *European Heart Journal* **28,** 1250-1257.

van Wolferen SA, Marcus JT, Westerhof N, Spreeuwenberg MD, Marques KMJ, Bronzwaer JGF, Henkens IR, Gan CT-J, Boonstra A, Postmus PE & Vonk-Noordegraaf A. (2008). Right coronary artery flow impairment in patients with pulmonary hypertension. *European Heart Journal* **29,** 120-127.

Vangheluwe P, Louch WE, Ver Heyen M, Sipido K, Raeymaekers L & Wuytack F. (2003). Ca2+ transport ATPase isoforms SERCA2a and SERCA2b are targeted to the same sites in the murine heart. *Cell Calcium* **34,** 457-464.

Varikmaa M, Bagur R, Kaambre T, Grichine A, Timohhina N, Tepp K, Shevchuk I, Chekulayev V, Metsis M, Boucher F, Saks V, Kuznetsov AV & Guzun R. (2014). Role of mitochondria–cytoskeleton interactions in respiration regulation and mitochondrial organization in striated muscles. *Biochimica et Biophysica Acta (BBA) - Bioenergetics* **1837,** 232-245.

Varro A, Negretti N, Hester SB & Eisner DA. (1993). An estimate of the calcium content of the sarcoplasmic reticulum in rat ventricular myocytes. *Pflugers Arch* **423,** 158-160.

Vatner SF, Park M, Yan L, Lee GJ, Lai L, Iwatsubo K, Ishikawa Y, Pessin J & Vatner DE. (2013). Adenylyl cyclase type 5 in cardiac disease, metabolism, and aging. *American Journal of Physiology - Heart and Circulatory Physiology* **305,** H1-H8.

Vazquez EJ, Berthiaume JM, Kamath V, Achike O, Buchanan E, Montano MM, Chandler MP, Miyagi M & Rosca MG. (2015). Mitochondrial complex I defect and increased fatty acid oxidation enhance protein lysine acetylation in the diabetic heart. *Cardiovascular Research* **107,** 453-465.

Veeraraghavan R, Poelzing S & Gourdie RG. (2014). Intercellular Electrical Communication in the Heart: A New, Active Role for the Intercalated Disk. *Cell Communication & Adhesion* **21,** 161-167.

Veksler VI, Kuznetsov AV, Anflous K, Mateo P, van Deursen J, Wieringa B & Ventura-Clapier R. (1995). Muscle Creatine Kinase-deficient Mice: II. Cardiac and skeletal muscles exhibit tissue-specific adaptation of the mitochondrial function. *Journal of Biological Chemistry* **270,** 19921-19929.

Veksler VI, Ventur-Clapier R, Lechene P & Vassort G. (1988). Functional state of myofibrils, mitochondria and bound creatine kinase in skinned ventricular fibers of cardiomyopathic hamsters. *Journal of Molecular and Cellular Cardiology* **20,** 329-342.

Venetucci LA, Trafford AW & Eisner DA. (2007). Increasing Ryanodine Receptor Open Probability Alone Does Not Produce Arrhythmogenic Calcium Waves: Threshold Sarcoplasmic Reticulum Calcium Content Is Required. *Circulation Research* **100,** 105-111.

Venkataraman R, Baldo MP, Hwang HS, Veltri T, Pinto JR, Baudenbacher FJ & Knollmann BC. (2013). Myofilament calcium de-sensitization and contractile uncoupling prevent pause-triggered ventricular tachycardia in mouse hearts with chronic myocardial infarction. *Journal of Molecular and Cellular Cardiology* **60,** 8-15.

Ventura-Clapier R, Mekhfi H & Vassort G. (1987a). Role of creatine kinase in force development in chemically skinned rat cardiac muscle. *The Journal of general physiology* **89,** 815-837.

Ventura-Clapier R, Saks VA, Vassort G, Lauer C & Elizarova GV. (1987b). Reversible MM-creatine kinase binding to cardiac myofibrils. *American Journal of Physiology - Cell Physiology* **253,** C444-C455.

Vermeulen JT, McGuire MA, Opthof T, Coronel R, De Bakker JMT, Klöpping C & Janse MJ. (1994). Triggered activity and automaticity in ventricular trabeculae of failing human and rabbit hearts. *Cardiovascular Research* **28,** 1547-1554.

Vescovo G, Jones SM, Harding SE & Poole-Wilson PA. (1989). Isoproterenol sensitivity of isolated cardiac myocytes from rats with monocrotaline-induced right-sided hypertrophy and heart failure. *Journal of Molecular and Cellular Cardiology* **21,** 1047-1061.

Voelkel NF, Quaife RA, Leinwand LA, Barst RJ, McGoon MD, Meldrum DR, Dupuis J, Long CS, Rubin LJ, Smart FW, Suzuki YJ, Gladwin M, Denholm EM & Gail DB. (2006). Right ventricular function and failure - Report of a National Heart, lung, and Blood Institute working group on cellular and molecular mechanisms of right heart failure. *Circulation* **114,** 1883-1891.

von Haehling S, Doehner W & Anker SD. (2007). Nutrition, metabolism, and the complex pathophysiology of cachexia in chronic heart failure. *Cardiovascular Research* **73,** 298-309.

von Lewinski D, Kockskämper J, Zhu D, Post H, Elgner A & Pieske B. (2009). Reduced Stretch-Induced Force Response in Failing Human Myocardium Caused by Impaired Na+-Contraction Coupling. *Circulation: Heart Failure* **2,** 47-55.

von Ludinghausen M. (2003). The venous drainage of the human myocardium. *Venous Drainage of the Human Myocardium* **168,** 1-+.

Vonk-Noordegraaf A, Haddad F, Chin KM, Forfia PR, Kawut SM, Lumens J, Naeije R, Newman J, Oudiz RJ, Provencher S, Torbicki A, Voelkel NF & Hassoun PM. (2013). Right Heart Adaptation to Pulmonary Arterial Hypertension: Physiology and Pathobiology. *Journal of the American College of Cardiology* **62,** D22-D33.

Waagstein F, Caidahl K, Wallentin I, Bergh CH & Hjalmarson A. (1989). Long-term beta-blockade in dilated cardiomyopathy. Effects of short- and long-term metoprolol treatment followed by withdrawal and readministration of metoprolol. *Circulation* **80,** 551-563.

Waagstein F, Hjalmarson A, Swedberg K, Bristow MR, Gilbert EM, Camerini F, Fowler MB, Silver MA, Johnson MR & Goss FG. (1993). Beneficial effects of metoprolol in idiopathic dilated cardiomyopathy. *The Lancet* **342,** 1441-1446.

Wagner-Mann C & Sturek M. (1991). Endothelin mediates Ca influx and release in porcine coronary smooth muscle cells. *American Journal of Physiology - Cell Physiology* **260,** C771-C777.

Wagner E, Lauterbach MA, Kohl T, Westphal V, Williams GSB, Steinbrecher JH, Streich J-H, Korff B, Tuan H-TM, Hagen B, Luther S, Hasenfuss G, Parlitz U, Jafri MS, Hell SW, Lederer WJ & Lehnart SE. (2012). Stimulated Emission Depletion Live-Cell Super-Resolution Imaging Shows Proliferative Remodeling of T-Tubule Membrane Structures After Myocardial Infarction. *Circulation Research* **111,** 402-414.

Walker JS, Walker LA, Margulies K, Buttrick P & de Tombe P. (2011a). Protein kinase A changes calcium sensitivity but not crossbridge kinetics in human cardiac myofibrils. *American Journal of Physiology - Heart and Circulatory Physiology* **301,** H138-H146.

Walker LA, Walker JS, Glazier A, Brown DR, Stenmark KR & Buttrick PM. (2011b). Biochemical and myofilament responses of the right ventricle to severe pulmonary hypertension. *American Journal of Physiology - Heart and Circulatory Physiology* **301,** H832-H840.

Wang X & Gerdes AM. (1999). Chronic Pressure Overload Cardiac Hypertrophy and Failure in Guinea Pigs: III. Intercalated Disc Remodeling. *Journal of Molecular and Cellular Cardiology* **31,** 333-343.

Watanabe K, Nair P, Labeit D, Kellermayer MSZ, Greaser M, Labeit S & Granzier H. (2002). Molecular Mechanics of Cardiac Titin's PEVK and N2B Spring Elements. *Journal of Biological Chemistry* **277,** 11549-11558.

Wei S, Guo A, Chen B, Kutschke W, Xie Y-P, Zimmerman K, Weiss RM, Anderson ME, Cheng H & Song L-S. (2010). T-Tubule Remodeling During Transition From Hypertrophy to Heart Failure. *Circulation Research* **107,** 520-531.

Weinstein AA, Chin LMK, Keyser RE, Kennedy M, Nathan SD, Woolstenhulme JG, Connors G & Chan L. (2013). Effect of aerobic exercise training on fatigue and physical activity in patients with pulmonary arterial hypertension. *Respiratory Medicine* **107,** 778-784.

Weiss RG, Gerstenblith G & Bottomley PA. (2005). ATP flux through creatine kinase in the normal, stressed, and failing human heart. *Proceedings of the National Academy of Sciences of the United States of America* **102,** 808-813.

Weiss S, Oz S, Benmocha A & Dascal N. (2013). Regulation of Cardiac L-Type Ca2+ Channel CaV1.2 Via the β-Adrenergic-cAMP-Protein Kinase A Pathway: Old Dogmas, Advances, and New Uncertainties. *Circulation Research* **113,** 617-631.

White E, Le Guennec JY, Nigretto JM, Gannier F, Argibay JA & Garnier D. (1993). The effects of increasing cell length on auxotonic contractions; membrane potential and intracellular calcium transients in single guinea-pig ventricular myocytes. *Experimental Physiology* **78,** 65-78.

Whittaker P, Kloner RA, Boughner DR & Pickering JG. (1994). Quantitative assessment of myocardial collagen with picrosirius red staining and circularly-polarized light. *Basic Research in Cardiology* **89,** 397-410.

Wikstrand J, Hjalmarson Åk, Waagstein F, Fagerberg Bj, Goldstein S, Kjekshus J & Wedel H. (2002). Dose of metoprolol CR/XL and clinical outcomes in patients with heart failure: Analysis of the experience in metoprolol CR/XL randomized intervention trial in chronic heart failure (MERIT-HF). *Journal of the American College of Cardiology* **40,** 491-498.

Williams GSB, Boyman L & Lederer WJ. (2015). Mitochondrial calcium and the regulation of metabolism in the heart. *Journal of Molecular and Cellular Cardiology* **78,** 35-45.

Wisler JW, DeWire SM, Whalen EJ, Violin JD, Drake MT, Ahn S, Shenoy SK & Lefkowitz RJ. (2007). A unique mechanism of β-blocker action:

Carvedilol stimulates β-arrestin signaling. *Proceedings of the National Academy of Sciences* **104,** 16657-16662.

Wojtczak A, Wojtczak M & Skrętkowicz J. (2014). The relationship between plasma concentration of metoprolol and CYP2D6 genotype in patients with ischemic heart disease. *Pharmacological Reports* **66,** 511-514.

Wong YY, Handoko ML, Mouchaers KTB, de Man FS, Vonk-Noordegraaf A & van der Laarse WJ. (2010). Reduced mechanical efficiency of rat papillary muscle related to degree of hypertrophy of cardiomyocytes. *American Journal of Physiology - Heart and Circulatory Physiology* **298,** H1190-H1197.

Wong YY, Ruiter G, Lubberink M, Raijmakers PG, Knaapen P, Marcus JT, Boonstra A, Lammertsma AA, Westerhof N, van der Laarse WJ & Vonk-Noordegraaf A. (2011a). Right Ventricular Failure in Idiopathic Pulmonary Arterial Hypertension Is Associated With Inefficient Myocardial Oxygen Utilization. *Circulation: Heart Failure* **4,** 700-706.

Wong YY, Westerhof N, Ruiter G, Lubberink M, Raijmakers P, Knaapen P, Marcus JT, Boonstra A, Lammertsma AA, van der Laarse WJ & Vonk-Noordegraaf A. (2011b). Systolic pulmonary artery pressure and heart rate are main determinants of oxygen consumption in the right ventricular myocardium of patients with idiopathic pulmonary arterial hypertension. *European Journal of Heart Failure* **13,** 1290-1295.

Workman AJ, Kane KA, Russell JA, Norrie J & Rankin AC. (2003). Chronic beta-adrenoceptor blockade and human atrial cell electrophysiology: evidence of pharmacological remodelling. *Cardiovascular Research* **58,** 518-525.

Wright CD, Chen Q, Baye NL, Huang Y, Healy CL, Kasinathan S & O'Connell TD. (2008). Nuclear α1-Adrenergic Receptors Signal Activated ERK Localization to Caveolae in Adult Cardiac Myocytes. *Circulation Research* **103,** 992-1000.

Wu Y, Cazorla O, Labeit D, Labeit S & Granzier H. (2000). Changes in Titin and Collagen Underlie Diastolic Stiffness Diversity of Cardiac Muscle. *Journal of Molecular and Cellular Cardiology* **32,** 2151-2161.

Wüst RCI, Myers DS, Stones R, Benoist D, Robinson PA, Boyle JP, Peers C, White E & Rossiter HB. (2012). Regional skeletal muscle remodeling and mitochondrial dysfunction in right ventricular heart failure. *American Journal of Physiology - Heart and Circulatory Physiology* **302,** H402-H411.

Xiao B, Sutherland C, Walsh MP & Chen SRW. (2004). Protein Kinase A Phosphorylation at Serine-2808 of the Cardiac Ca2+-Release Channel (Ryanodine Receptor) Does Not Dissociate 12.6-kDa FK506-Binding Protein (FKBP12.6). *Circulation Research* **94,** 487-495.

Xiao B, Zhong G, Obayashi M, Yang D, Chen K, Walsh Michael P, Shimoni Y, Cheng H, ter Keurs H & Chen S R W. (2006). Ser-2030, but not Ser-2808, is the major phosphorylation site in cardiac ryanodine receptors responding to protein kinase A activation upon β-adrenergic stimulation in normal and failing hearts. *Biochemical Journal* **396,** 7-16.

Xie Y-P, Chen B, Sanders P, Guo A, Li Y, Zimmerman K, Wang L-C, Weiss RM, Grumbach IM, Anderson ME & Song L-S. (2012). Sildenafil Prevents and Reverses Transverse-Tubule Remodeling and Ca^{2+} Handling Dysfunction in Right Ventricle Failure Induced by Pulmonary Artery Hypertension. *Hypertension* **59,** 355-362.

Xu KY, Zweier JL & Becker LC. (1995). Functional Coupling Between Glycolysis and Sarcoplasmic Reticulum Ca2+ Transport. *Circulation Research* **77,** 88-97.

Yamamoto S, Tsutsui H, Takahashi M, Ishibashi Y, Tagawa H, Imanaka-Yoshida K, Saeki Y & Takeshita A. (1998). Role of Microtubules in the Viscoelastic Properties of Isolated Cardiac Muscle. *Journal of Molecular and Cellular Cardiology* **30,** 1841-1853.

Yang X, Long L, Southwood M, Rudarakanchana N, Upton PD, Jeffery TK, Atkinson C, Chen H, Trembath RC & Morrell NW. (2005). Dysfunctional Smad Signaling Contributes to Abnormal Smooth Muscle Cell Proliferation in Familial Pulmonary Arterial Hypertension. *Circulation Research* **96,** 1053-1063.

Yang Z, Pascarel C, Steele DS, Komukai K, Brette F & Orchard CH. (2002). Na+-Ca2+ Exchange Activity Is Localized in the T-Tubules of Rat Ventricular Myocytes. *Circulation Research* **91,** 315-322.

Yaoita H, Sakabe A, Maehara K & Maruyama Y. (2002). Different Effects of Carvedilol, Metoprolol, and Propranolol on Left Ventricular Remodeling After Coronary Stenosis or After Permanent Coronary Occlusion in Rats. *Circulation* **105,** 975-980.

Yasuda S-I, Sugiura S, Kobayakawa N, Fujita H, Yamashita H, Katoh K, Saeki Y, Kaneko H, Suda Y, Nagai R & Sugi H. (2001). A novel method to study contraction characteristics of a single cardiac myocyte using carbon fibers. *American Journal of Physiology - Heart and Circulatory Physiology* **281,** H1442-H1446.

Yasuda S-i, Sugiura S, Yamashita H, Nishimura S, Saeki Y, Momomura S-i, Katoh K, Nagai R & Sugi H. (2003). Unloaded shortening increases peak of Ca2+ transients but accelerates their decay in rat single cardiac myocytes. *American Journal of Physiology - Heart and Circulatory Physiology* **285,** H470-H475.

Yin FC, Spurgeon HA, Rakusan K, Weisfeldt ML & Lakatta EG. (1982). Use of tibial length to quantify cardiac hypertrophy: application in the aging rat. *American Journal of Physiology - Heart and Circulatory Physiology* **243,** H941-H947.

Yoon I-S, Choi M-K, Kim JS, Shim C-K, Chung S-J & Kim D-D. (2010). Pharmacokinetics and first-pass elimination of metoprolol in rats: contribution of intestinal first-pass extraction to low bioavailability of metoprolol. *Xenobiotica* **41,** 243-251.

Yoshikawa WS, Nakamura K, Miura D, Shimizu J, Hashimoto K, Kataoka N, Toyota H, Okuyama H, Miyoshi T, Morita H, Fukushima Kusano K, Matsuo T, Takaki M, Kajiya F, Yagi N, Ohe T & Ito H. (2013). Increased Passive Stiffness of Cardiomyocytes in the Transverse Direction and Residual Actin and Myosin Cross-Bridge Formation in Hypertrophied Rat Hearts Induced by Chronic β-Adrenergic Stimulation. *Circulation Journal* **77,** 741-748.

Younes A, Schneider JM, Bercovici J & Swynghedauw B. (1985). Redistribution of creatine kinase isoenzymes in chronically overloaded myocardium. *Cardiovascular Research* **19,** 15-19.

Yuan P, Wu W-H, Gao L, Zheng Z-Q, Liu D, Mei H-Y, Zhang Z-L & Jing Z-C. (2013). Oestradiol ameliorates monocrotaline pulmonary hypertension via NO, prostacyclin and endothelin-1 pathways. *European Respiratory Journal* **41,** 1116-1125.

Zak R. (1974). Development and proliferative capacity of cardiac-muscle cells. *Circulation Research* **35,** 17-26.

Zebrack JS, Munger M, MacGregor J, Lombardi WL, Stoddard GP & Gilbert EM. (2009). β-Receptor Selectivity of Carvedilol and Metoprolol Succinate in Patients with Heart Failure (SELECT Trial): A Randomized Dose-Ranging Trial. *Pharmacotherapy: The Journal of Human Pharmacology and Drug Therapy* **29,** 883-890.

Zhang C, Chen B, Guo A, Zhu Y, Miller JD, Gao S, Yuan C, Kutschke W, Zimmerman K, Weiss RM, Wehrens XHT, Hong J, Johnson FL, Santana LF, Anderson ME & Song L-S. (2014). Microtubule-Mediated Defects in Junctophilin-2 Trafficking Contribute to Myocyte Transverse-Tubule Remodeling and Ca2+ Handling Dysfunction in Heart Failure. *Circulation* **129,** 1742-1750.

Zhang J, Barak LS, Winkler KE, Caron MG & Ferguson SSG. (1997). A Central Role for β-Arrestins and Clathrin-coated Vesicle-mediated Endocytosis in β2-Adrenergic Receptor Resensitization: Differential regulation of receptor resensitization in two distinct cell types. *Journal of Biological Chemistry* **272,** 27005-27014.

Zile MR, Baicu CF, S. Ikonomidis J, Stroud RE, Nietert PJ, Bradshaw AD, Slater R, Palmer BM, Van Buren P, Meyer M, M. Redfield M, A. Bull D, L. Granzier H & LeWinter MM. (2015). Myocardial Stiffness in Patients With Heart Failure and a Preserved Ejection Fraction: Contributions of Collagen and Titin. *Circulation* **131,** 1247-1259.

Zile MR, Koide M, Sato H, Ishiguro Y, Conrad CH, Buckley JM, Morgan JP & Cooper G. (1999). Role of microtubules in the contractile dysfunction of hypertrophied myocardium. *Journal of the American College of Cardiology* **33,** 250-260.

Zile MR, Richardson K, Cowles MK, Buckley JM, Koide M, Cowles BA, Gharpuray V & Cooper G. (1998). Constitutive Properties of Adult Mammalian Cardiac Muscle Cells. *Circulation* **98,** 567-579.

Zima AV & Blatter LA. (2006). Redox regulation of cardiac calcium channels and transporters. *Cardiovascular Research* **71,** 310-321.

Zima AV, Bovo E, Bers DM & Blatter LA. (2010). Ca2+ spark-dependent and -independent sarcoplasmic reticulum Ca2+ leak in normal and failing rabbit ventricular myocytes. *The Journal of Physiology* **588,** 4743-4757.

Zimmer H-G. (2002). Who Discovered the Frank-Starling Mechanism? *Physiology* **17,** 181-184.

Zong P, Tune JD & Downey HF. (2005). Mechanisms of Oxygen Demand/Supply Balance in the Right Ventricle. *Experimental Biology and Medicine* **230,** 507-519.